Drivers of coastal sea level variability along the east and south of South Africa

Bernardino João Nhantumbo

Submitted in accordance with the requirements for the degree of

Doctor of Philosophy in Physical Oceanography

Department of Oceanography

UNIVERSITY OF CAPE TOWN
IYUNIVESITHI YASEKAPA • UNIVERSITEIT VAN KAAPSTAD

Supervisors: Prof. Frank Shillington
Dr. Björn Backeberg
Dr. Jan Even Nilsen
Prof. Chris Reason

November 2018

Abstract

Sea level rise and variability is of great concern in the coastal areas where a significant part of the global population is settled. Therefore, understanding regional and local long-term sea level variability as well as its trend is critical. On the other hand, quantifying how the sea level has varied on different timescales and why, is critical for understanding sea level changes, and crucial for improving future global, regional, and local projections. In this study, monthly mean sea level records of seven individual tide gauges, from the east and south coast of South Africa were used to analyse the embedded timescales of variability. These timescales were separated through the Empirical Mode Decomposition (EMD) method. This is the first time that the EMD method has been applied to southern African tide gauge records. The sensitivity of the EMD method when dealing with data gaps was tested on artificially created gaps in monthly mean synthetic altimetry sea level records, representing the seven individual tide gauges under consideration. The missing values were filled by linear interpolation, average value and linear trend value. The results suggested that whichever gap filling method is applied, the separated EMD timescales will display a distorted temporal structure of the continuous time series. As a consequence, monthly mean tide gauge sea level records were optimised by filling the gaps as best as possible using satellite altimetry data and the adjacent tide gauge records where possible, and then the oscillatory timescales of variability were separated using the EMD method with the intent to determine their physical drivers. However, identifying a single driver for each separated timescale is challenging due to our limited knowledge of how sea level is linked to the various forcing mechanisms. Therefore, the timescales of sea level variability extracted using the EMD were grouped into sub-annual and interannual timescales, and their relationship to possible driving mechanisms was investigated. The sub-annual timescale indicates how sea level responds to the mesoscale and synoptic weather systems in the annual cycle, including seasonal and annual large-scale wind and atmospheric pressure pattern changes. The interannual timescale indicates an association with the climate indices including El Niño-Southern Oscillation, Indian Ocean Dipole and Southern Annular Mode through large-scale

sea surface temperature patterns and large-scale pressure and wind patterns. In addition, the results have suggested that the studied coastal sea level has an association with the Agulhas Current at both sub-annual and interannual timescale through absolute dynamic topography variations at the Agulhas Current core locations. However, due to limitations in Agulhas Current data, the study was limited to East London and Port Elizabeth and the results suggested that the Agulhas Current contribution is responsible for over 62% of the monthly sea level variability at East London. However, the results were not sufficiently consistent to suggest a firm conclusion at Port Elizabeth.

Contents

Declaration

"I know the meaning of Plagiarism and declare that all of the work in the document, save for that which is properly acknowledged, is my own"

Signature: Signed by candidate

Date: 01/11/2018

Acknowledgments

First and foremost, I would like to thank the Nansen-Tutu Centre for Marine Environmental Research for fully sponsoring my PhD studies, through funds sourced from the Nansen Scientific Society and from the Applied Centre for Climate and Earth Systems Science (ACCESS). I would also like to thank my employer, National Institute of Meteorology – Mozambique for grating me a study leave to continue with my studying advancement.

I would like to express my sincere gratitude to my supervisors, Prof. Frank Shillington, Dr. Björn Backeberg, Dr. Jan Even Nilsen and Prof. Chris Reason, for giving me sufficient freedom in my research and at the same time for guiding me towards the right direction. Special thanks go to Dr. Björn Backeberg and Dr. Jan Even Nilsen for agreeing to be my supervisor and for bringing a new vibe to the project. I would also like to thank Dr. Jan Even Nilsen for his patience, pedagogic skills and his knowledge in the sea level science; I will miss our Skype sessions.

My sincere thanks also go to the Nansen Scientific Society who provided me with an opportunity to travel to Bergen, Norway, and the Nansen Environmental and Remote Sensing Center (NERSC) who gave access to the research facilities. Without their precious support, it would not be possible to successfully conduct this research. My special thanks go to all data providers/suppliers used in this PhD work, especially for providing/supplying them free of charge which is crucial in this part of the globe where skills and resources are scarce. Moreover, I am particularly grateful to Prof. John Field for revising my manuscripts; his interest and patience helped me in spotting and correcting inconsistencies.

My thanks go to everyone who has contributed to the development of my research, and I deny to list names because the list is long, may God bless you all. I thank my fellow post-graduate students, visiting scientists and staff in the Department for a very interesting relationship. I would also like to take this opportunity to thanks my Precious's friends (P. Mongwe and P. Mahlalela) for the life chats, may God bless you.

Last but not least, I would like to thank my family: my wife, daughters and son for helping me to enjoy research and study, for keeping me grounded and loved. *Este trabalho é vosso tanto quanto é meu…*

List of Figures

List of Tables

Acronyms

ADT	Absolute dynamic topography
AC	Agulhas Current
ACT	Agulhas Current Time-Series Experiment
ARC	Agulhas Retroflection Current
AR5	Fifth Assessment Report
AVISO	Archiving, Validation and Interpretation of Satellite Oceanographic Data
CIRES	Cooperative Institute for Research in Environmental Sciences
CMEMS	Copernicus Marine and Environment Monitoring Service
CTW	Coastal Trapped Wave
ERSST	Extended reconstructed sea surface temperature
GIA	Glacial isostatic adjustment
GDR	Geophysical Data Records
GPS	Global positioning system
IB	Inverse barometer
IOC	Intergovernmental oceanographic commission
IPCC	Intergovernmental Panel on Climate Change
HYCOM	Hybrid Coordinate Ocean Model
MSL	Mean Sea Level
NCAR	National Centre for Atmospheric Research
NCEP	National Centre for Environmental Prediction
NOAA	National Oceanic and Atmospheric Administration
RCP	Representative Concentration Pathway
RSL	Relative sea level
SLA	Sea Level Anomaly
SLP	Sea Level Pressure

SODA Simple Ocean Data Assimilation

SST Sea surface temperature

TG Tide gauge

VLM Vertical land movement

CHAPTER 1

Introduction

1.1 Sea level variability and rise

From ancient to modern times, sea level variability and rise, especially changes in local mean sea level have been a concern for most of the coastal and inland communities (IOC, 1985; Pugh, 1987; Emery and Thomson, 2004). The concern arose due to the effects of the tidal cycles and highlighted the need to develop a basic understanding of it. Early time communities made remarkable developments in understanding the matter by associating sea level variations with the movements of the moon and sun, and so explain the produced regular tidal variations. However, the modern understanding of the tidal variations was through the Newtonian theory of gravitational attraction, paving the way for the sea level research field, which initially focused on understanding and further analysing the features that could not be explained by the gravitational attraction theory (Pugh, 1987).

It is now known that, at any given time, sea level variability and rise is a result of sea – air interactions (from weather to climate timescales), ocean and topography dynamics (White et al., 2005; Miller and Douglas, 2007; Church and Write, 2011; Zhang and Church, 2012). Sea level variability and rise is also a result of storage in the cryosphere, inland waters and soil. On climate scales the cryosphere contribution (mass contribution due to melting of ice sheets) dominates. On shorter scales it is possible for the global sea level to change because of changes in land storage (Fasullo et al, 2013; Cazenave et al, 2018).

Fig. 1 portrays the processes and components that contribute to sea level variability and rise. Remarkable advances in knowing the processes and components that contribute to sea level

variability and rise have been achieved over recent years, however many aspects are as yet debatable, due to the challenges: (i) in precisely quantifying the contribution of all single processes and components to local, regional and global sea level change, the so called closing of the sea level budget (Church et al., 2013b; Gregory et al., 2013); (ii) imposed by the fact that these processes and components interact with each other whilst driving sea level changes (Church et al., 2013b); (iii) to disentangle internal sea level variability from anthropogenic climate change signals (Church et al., 2010); In fact, the rising of sea level is the most certain impact of climate change (Church et al., 2010; Church et al., 2013b) that is known so far.

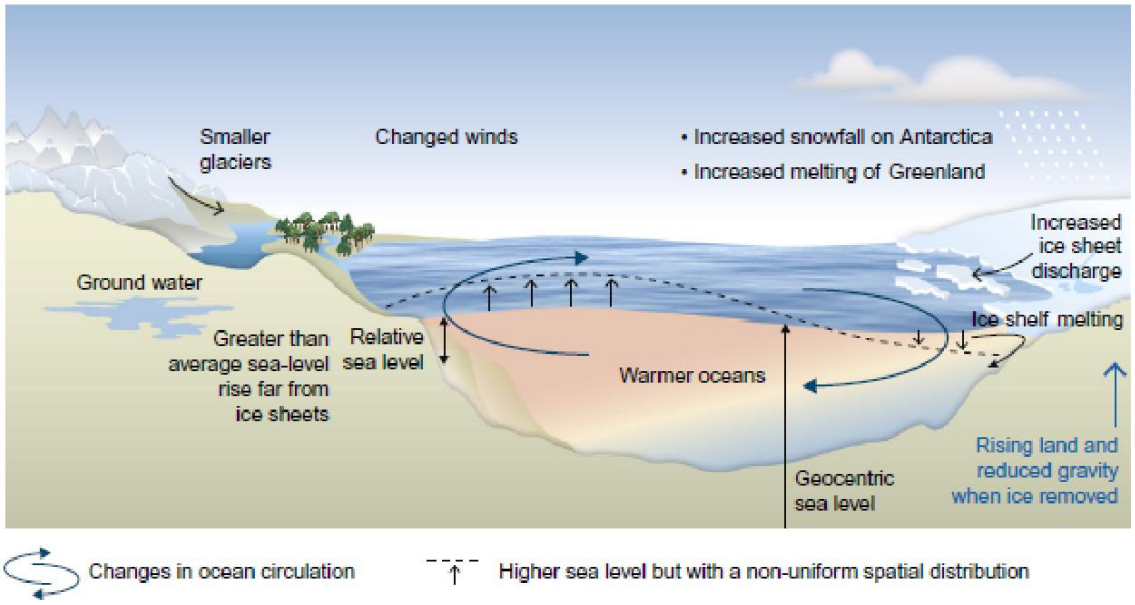

Fig. 1.1: Contributing processes to sea level change at global and regional scales from short to longer timescales (Church et al., 2013a). Note that the shape of the geoid is not shown.

Addressing these challenges is not as simple as it may look due to: first, the limitation in the data availability; second, poor quality of the existing data in most of the coastal areas; third, the interpretation of the physical meaning of the analysed data which remain questionable despite the fact that the mathematical concepts underpinning the analyses are correct. Moreover, the issue of variability is still puzzling given the difficulty to link it to various known driving mechanisms and to assess whether observed changes are due to natural or anthropogenic causes. This thesis aims to contribute to the understanding of regional sea level variability by

studying the driving mechanisms of the variability in tide gauge records along the east and south coast of South Africa.

1.1.1 Global sea level variability and rise

Thanks to paleo indicators (salt-marsh is the most used amongst others) an overview of the patterns of sea level changes over the last few millennia is now possible. Observations have suggested that within the intertidal zone, distinct assemblages of salt-marsh foraminifera appeared to characterise different height intervals that can be used as sea level indicators (e. g. Scott and Medioli, 1978, 1980). On the other hand, notable advances in understanding the observed twentieth-century global sea level variability and rise have been made thanks to numerous studies being carried out worldwide to calculate the rates of sea level rise (e.g. Cazenave et al, 2018).

The global sea level variability and rise is driven mainly by ocean-thermal expansion/contraction, land ice changes and changes in terrestrial water storage, with the latter being an independent contribution from ice-melt, as it is driven by hydrology changes (e.g. precipitation over land), water impoundment behind dams and/or groundwater depletion(Church et al., 2013a). The ocean-thermal expansion/contraction is known to be associated with variations in temperature leading to changes in water density. As the glaciers and ice sheets melt, they induce changes in ocean water mass and hence, ocean's volume. The latter is also associated with losses in land water storage, to explain 50% of the observed changes (Church et al., 2013b). However, our understanding of the observed twentieth-century global sea level variability and rise rely on sea level reconstructed proxies, which are a product of several different techniques (e.g. Ray and Douglas, 2011; Church and Write, 2011; Jevrejeva et al., 2014; Hay et al., 2015; Dangendorf et al., 2017). Fig. 1.2 illustrates the evolution of the observed twentieth-century global sea level variability and rise according to one of the techniques before mentioned.

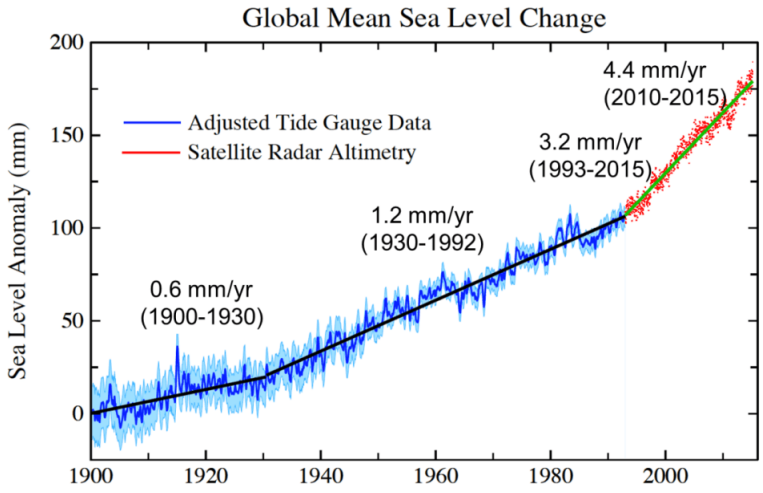

Fig. 1.2: The observed rates of 20th-century global mean sea level rise (http://climateadaptation.hawaii.gov/sea-level-rise/ - accessed 10 September 2018).

As can be seen in Fig. 2, the global sea level has not been rising steadily at the same rates over the twentieth-century, being faster in the most recent decades. A number of studies agree on this unprecedentedly fast global mean sea level rise in the most recent decades. However, despite the consensus in the refinements to be applied leading to more accurate rates, the differences in the estimation of the processes and components portrayed in Fig. 1 explain the rates suggested in various studies (Hay et al., 2015). To reconstruct the past sea level variability and rise, paleo indicators and instrumental data (tide gauges records and satellite altimetry observations) are employed. This is the reason for the spread noted over the first half of the century which is associated with uncertainties due to a limited number of instrumental data over this time span. Moreover, reconstructions of the sea level records provide reasonable representations of the Northern Hemisphere record but poor representations of the Southern Hemisphere record due to the limited number of tide gauges with long-term, high quality records.

Therefore, an improvement in estimating and accounting for the historical 20th-century global mean sea level rise will contribute to the reduction of the uncertainties associated with future sea level rise projections leading to reliable forecasts of current and future sea level changes,

and of course, to better coastal planning, management and engineering. Fig. 1.3 portrays the projected rates of global mean sea level rise under different greenhouse gas emissions scenarios, according to the Fifth Assessment Report (AR5) of the Intergovernmental Panel on Climate Change (IPCC) (Church et al., 2013b). The rates are compared to present day sea levels and as can be seen, global mean sea level will rise by 0.26 to 0.98 metre by the year 2100. However, we are currently following the representative concentration pathway (RCP8.5) scenario in terms of CO_2 emissions and this is also visible in sea levels, which are rising faster than anticipated by AR5 mainly due to larger contributions from the two ice-sheets in Antarctica and Greenland (Kopp et al., 2014; DeConto and Pollard, 2016; Jevrejeva et al., 2016; Le Bars et al., 2017).

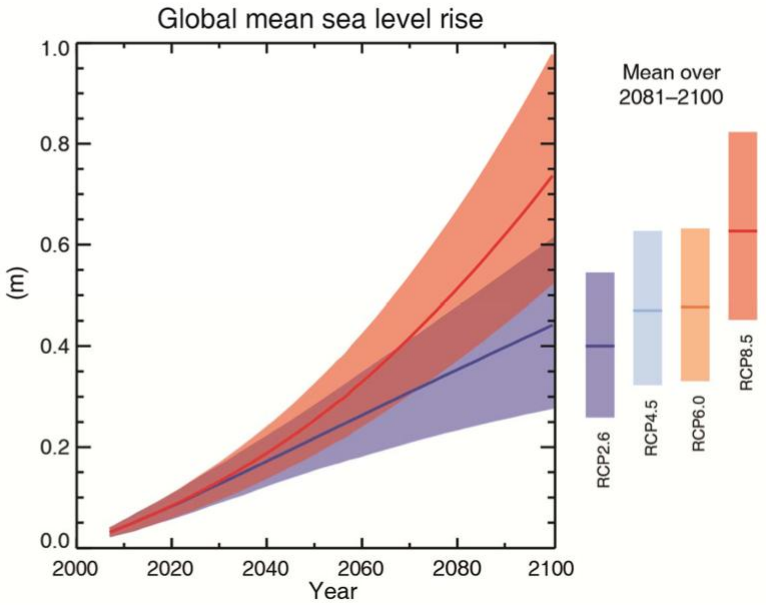

Fig. 1.3: The projected rate of global mean sea level rise under different greenhouse gas emissions scenarios (Church et al., 2013b).

At global scale, studies focus on improving the understanding of the processes and components that contribute to sea level variability and rise, due to persistent challenges in accurately resolving their contribution as well as characterising the variability on decadal and multi-decadal timescales. The changes in the processes and components that contribute to global sea

level variability and rise are observed locally, however their magnitudes differ regionally. In fact, studies have shown that although sea level is rising, it is not uniform, with some regions experiencing noticeable rises while others fall, due to several local phenomena. Therefore, the sea level rise rates and accelerations at specific places or regions must be understood, as well as the forcing mechanisms behind the changes.

1.1.2 Regional sea level variability and rise

Several studies have pointed out the urgency for understanding regional sea level variability and rise due to its direct socioeconomic impacts (Milne et al., 2009). Thus investigations focusing on the regional scale are being conducted particularly for improving the future sea level rise projections and coastal planning, management and engineering. Satellite altimetry observations have revealed important features of regional sea level variability and rise. Patterns of regional mean sea level trends over the period of satellite altimetry observations are displayed in Fig. 1.4. It is important to note that southern Africa has experienced a rise of 0 to 5 mm/year over this period. It should be noted however that the features displayed in Fig. 1.4 are subjected to variability i.e., are not stationary, and are dependent on the altimetry data corrections (e.g. Watson et al., 2015; Chambers et al., 2016) being carried out by several satellite altimetry research groups and the time span under consideration. Additionally, the features displayed in Fig. 1.4 are associated with natural or anthropogenic climate modes, including processes such as a dynamical redistribution of water masses and a change of water mass properties caused by changes in winds and air pressure, air–sea heat and freshwater fluxes and ocean currents (e.g. Church et al., 2013a; Stammer et al., 2013; Kopp et al., 2015).

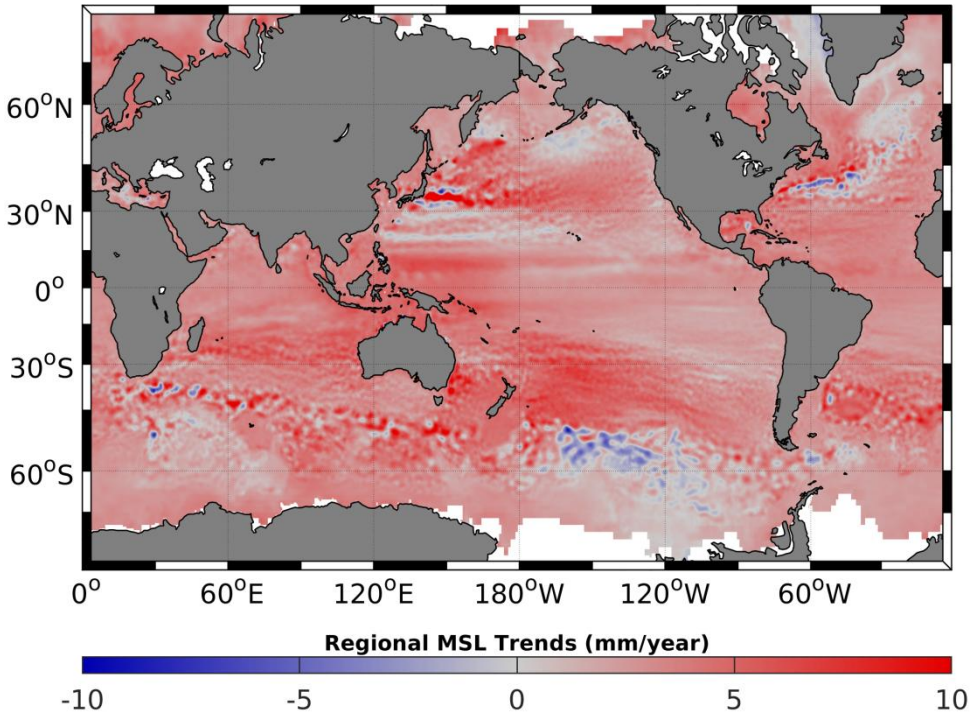

Fig. 1.4: The observed rates of regional sea level rise during the era of satellite altimetry. The altimetry data are gridded multi-mission altimetry observations, produced under the ESA Sea Level Climate Change Initiative (SL_cci v2.0) from January 1993 to December 2015, and obtained from Copernicus Marine and Environment Monitoring Service (CMEMS; http://www.marine.copernicus.eu).

Therefore, at regional scale, most of the current variations in sea level are driven by ocean dynamics (i.e. ocean circulation and wind forcing), gravitational changes related to any mass changes in land-locked ice and terrestrial water storage, inverse barometer changes, etc (e.g. Milne et al., 2009; Church et al., 2013b). Changes in ocean circulation are associated with changes in ocean currents due to surface winds variations, warming ocean temperatures and melting land ice (Church et al., 2010). Changes in wind forcing are associated with mesoscale and synoptic weather systems which are known to be modulated by natural or anthropogenic modes of climate variability. However, in some regions land uplift is observed due to recent loss of continental ice sheet, resulting in an apparent sea level fall. As a result, different drivers of regional sea level variability and rise may be found to be dependent on the timescales under consideration (e.g. Church et al., 2013a; Stammer et al., 2013; Kopp et al., 2015). The timescales of sea level variability are highly dependent on the record length and quality. Hence, understanding the historical sea level variability and rise is of critical importance.

Han et al. (2010) studied the patterns of Indian Ocean sea-level changing under a warming climate. They found that sea level has decreased substantially in the southern tropical Indian Ocean whereas it has increased almost everywhere in the southern African region. The aforementioned pattern is driven by changes in surface winds associated with a combined invigoration of the Indian Ocean Hadley and Walker Cells, patterns of atmospheric overturning circulation in the north-south and east-west direction, respectively, which is partly attributable to rising levels of atmospheric greenhouse gases. They also concluded that if ongoing anthropogenic warming dominates natural variability, the pattern they detected is likely to persist and to increase the environmental stress on some coasts and islands in the Indian Ocean.

Thus, understanding southern African sea level variability and rise is critical for all forms of coastal development. With a major migration of populations to coastal cities and both urban and peri-urban sprawl, it is imperative to understand the nature of the sea level changes at sensitive low lying areas. In addition to this, because of the likely increased storminess of the Southern Ocean (a major wave generation area for southern Africa), and the impact of tropical disturbances on the low lying areas such as Mozambique, combined impact of storm surges and wind waves, increased saltwater intrusion of farmlands, and coastal erosion are likely to affect many of the local resident populations (e.g. Singleton and Reason, 2007; INGC, 2009; Mavume et al., 2009). On the other hand, southern Africa is the host region for the western boundary current of the South Indian Ocean, the Agulhas Current. The Agulhas Current is part of the greater Agulhas System in the south-western Indian Ocean, which is believed to play an important role on global climate change (Beal et al., 2011). To what extent the Agulhas Current has been affecting coastal sea level still needs to be investigated.

1.2 Sea level records

Sea level records are crucial to advance our understanding of historical sea level variability and rise. Basically, paleo indicators (proxy records are no measurements per se, see also section 1.1.1), tide gauges and satellite altimetry have been the main measuring systems responsible

for the current understanding of the historical sea level changes, either separately or combined (Church et al., 2010; Church et al., 2013b). The challenge is always in how to combine records from different measuring systems given that each systems measure the sea level related to a specific benchmark (Church and Write, 2011). Paleo proxies give indications of how sea level has varied in the past decades to tens of thousands of years. Tide gauges give indications of how sea level has varied in the past minutes to centuries, including changes related to weather and tides. Satellite altimetry gives indications of how sea level has varied over the past 20 days to 25 years. Although their accuracy can be questionable, paleo indicators either natural (raised beaches and wave cut notches, fossil shells and vegetable matter, and submerged salt marshes) or man-made (ancient Roman fish tanks, Crusader wells in the Palestine, etc) provide useful indications of how sea level has varied prior to tide gauge records. Results of salt marshes collected from Kariega River estuary in the east coast of South Africa suggest that from 1100 to approximately 300 cal years BP, sea levels oscillated (approximately 0.5m amplitudes) but remained consistently lower than present day mean sea level. The lowest recorded sea level of −1±0.2 m was reached between 800 and 600 cal years BP. After 300 cal years BP, relative sea level has remained relatively stable (Strachan et al., 2014).

1.2.1 Tide gauge records

Tide gauge measurements are useful to advance the understanding of how oceanographic and climate processes might affect of the coastal zone (Komar et al, 2011; Prandi et al., 2009). Because of the fact that tide gauges are installed in harbours or in other regions close to the coast, it is difficult to relate their measurements to large scale oceanographic and climate signals given that their signals are affected by a host of different processes that cannot easily be accounted for by the relatively coarse resolution oceanographic and climate data available (Brundrit et al., 1984; Emery and Aubrey, 1991; Komar et al, 2011). Additionally, tide gauge data provide the sea level relative to the level of the continental crust, also known as relative sea level (RSL; Emery and Aubrey, 1991), and in order to relate tide gauge data to the large scale oceanography and climate, they need to be corrected to become absolute. Hence, relative

sea level changes include crustal movements due to a number of different processes, e.g. local processes such as groundwater or gas withdrawal, earthquakes, etc; and larger scale signals such as crustal deformations due to glacial isostatic adjustment (GIA), present day mass changes (ice melt and terrestrial water storage). Changes in groundwater storage induce local land subsidence. Local land subsidence is part of the process known as the vertical land movement, which is a small fraction over many coastal regions (Church et al., 2010). The most known and well modelled component of the vertical land movement is the GIA (Prandi et al., 2009). More details in the necessary corrections are found in Chapter 3. The quality of the RSL record is, however, questionable due to the presence of gaps and changes in the datum, and these often occur after gaps (Brundrit, 1984; Becker et al., 2009). A datum is a mathematical model that approximates the shape of the earth to enable accurate position, length and area calculations. Some natural or anthropogenic processes are responsible for these shifts (Becker et al., 2009), for example, instrumentation change or failure (Emery and Aubrey, 1991), ground water extraction (Rodolfo and Siringan, 2006), earthquakes (Fujii and Nakane, 1997), river discharges (Goodbred and Kuehl, 2000).

1.2.1 Satellite Altimetry observations

Great insights into the last 25 years sea level variability and rise are provided by satellite altimetry measurements. Thanks to satellite altimetry observations huge progress has been made in understanding the open ocean and regional sea level variability and rise differences. Satellite altimetry measurements are spatially advantageous, consequently easy to relate to large scale oceanographic and climate signals. In addition to this advantage is fact that they measure sea level relative to the geoid, hence the absolute sea level. The geoid is a model of global mean sea level that is used to measure precise surface elevations. Nevertheless, a number of corrections are necessary to be carried out so that satellite altimetry measurements are useful, which can be grouped as atmospheric propagation, tidal and sea surface corrections (e.g. Mertz et al., 2017). However, along the coast satellite altimetry fail to accurately measure important features of the coastal processes. As a result, satellite altimetry measurements are

flagged as unreliable (Birol and Niño, 2015; Cipollini et al., 2017) in the coastal zone (Roblou et al., 2007; Cipollini et al., 2010; Vignudelli et al., 2011; Stammer and Cazenave, 2017). Satellite altimetry observations are also disadvantageous regarding the temporal sampling frequency. The highest frequency sampling is around 10 days, where TOPEX/Poseidon (launched August, 1992), Jason-1 (launched December, 2001), Jason-2 (launched June, 2008) and Jason-3 (launched January 2016) satellite missions repeat the same ground track very closely (within about 1 kilometre). Satellites altimetry have been specifically designed to measure sea surface height with the highest possible accuracy and the presence of data gaps is due to the limitations concerning to appropriate corrections in the current science knowledge. More details in the necessary corrections are found in Chapter 3.

1.3 Thesis objectives and structure

The overall aim of this thesis is to determine the timescales of sea level variability around the east and south coast of South Africa and identify the corresponding drivers. The possible driving mechanisms being linked to the determined timescales include mesoscale and synoptic weather systems, different modes of climate variability as well as the Agulhas Current. Therefore, specifically this thesis aims to discover whether the Agulhas Current has a measurable impact on coastal sea level around the south and east coast of South Africa; and if so, how does this process operate?

Hence, the following research questions have been formulated:

1. What are the timescales of sea level variability measured by the tide gauges?

2. What are the driving mechanisms of the determined variability?
    a) Are regional and global drivers responsible for part of the observed changes in sea level records?

    b) Is the coastal sea level related to the offshore position and transport of Agulhas Current?

The basic literature of the research is presented in this introductory chapter, including the motivation and objectives. The main results of the research are presented in four separate chapters, Chapter 2 to 5, which have been written in a “pseudo paper” format, to facilitate publication in a scientific journal at a later date. Consequently each main chapter present its own introduction, data and methods, results, discussion and conclusions sections that may seem recurring. Despite this stand alone format of the chapters, the aim is to answer the research questions presented above. The overview about the context of these main chapters is briefly given next:

- **Chapter 2**

  This chapter aims to explain how the Empirical Mode Decomposition (EMD) method works, to compare it with other methods, and ultimately to test the impact of data gaps on the determined modes of variability. The EMD method is useful for non-stationary and nonlinear time series, such as sea level tide gauge records, as it separates oscillatory timescales from nonlinear long-term trend. The method is first applied to a continuous “synthetically created” data series, and the results are then compared to other methods. Secondly, the method is applied to the same data but with artificially created gaps to quantify their impact in terms of how they distorted the expected results. Various gap filling methods are also tested although only the results of three are presented. This approach provides insight into how the separated oscillatory modes are affected by different gap filling methods.

  Historical sea level records in southern Africa have many gaps of differing length, making it difficult to use analyses that require a continuous record. Additionally, it is difficult to find in sea level research the best data processing technique that can better handle the existing data sets. Reliable conclusions as to how sea level has varied and what has been behind the changes can be drawn only when the existing data sets are handled correctly. In this study, the EMD method is extensively used, given that no sea level timescale was pre-determined to be studied. However, the EMD method has the

limitation of not being able to handle the data gaps. Thus, Chapter 2 paved the way for optimising the tide gauge records by filling the gaps as best as possible.

- **Chapter 3**

The analyses in Chapter 2 suggest that all data gap filling methods tested adversely affect the results. Hence, this chapter uses satellite altimetry observations to help fill gaps in the tide gauge time series, aiming to create a fuller tide gauge time series. In order for this to be successful, a validation of concurrent tide gauge data and altimetry data at the nearest grid point was undertaken. Prior to satellite altimetry era, the gaps at one location are filled by the adjacent tide gauge records. This is done after a dedicated comparison analysis in regard to the correlations and coherence. Hence, Chapter 3 paves the way for separating the oscillatory timescales of sea level variability to answer to the first research question.

- **Chapter 4**

This chapter focuses on separating the oscillatory timescales of the improved monthly tide gauge records generated in Chapter 3, using the Empirical Mode Decomposition method. Then, the relationship between the separated sea level timescales and the possible driving mechanisms is investigated. The investigation is carried out by comparing and correlating the separated sea level timescales to atmospheric forcing and known climate indices as well as their input data. Additionally, composite average differences between positive and negative events, according to a specific standard deviation threshold are used to explain the mechanism by which the driving processes induce sea level variability and rise, as well as to account for the magnitude of the sea level changes during the events. As a result, Chapter 4 responds to the first research question and a significant part of the second.

- **Chapter 5**

  This chapter addresses the last part of the second research question and thus, aims to determine how variations in Agulhas Current transport and its offshore displacements impacts the coastal sea level. This is achieved by determining the Agulhas Current path and core position relative to the coast by using an Absolute Dynamic Topography gradient approach. Then, the possible connection between the Agulhas Current core location and volume transport is investigated. And finally, the investigation on how variations in volume transport and position of the Agulhas Current induce coastal sea level variability and rise is carried out.

- **Chapter 6**

  In this concluding chapter the main findings and suggested further research activities are presented. This chapter is important as it brings all the pieces together allowing judging the success or otherwise according to the aims and the research questions posed above.

CHAPTER 2

The Empirical Mode Decomposition/Hilbert - Huang Transformation (EMD): a method description and a sensitivity analysis

2.1. Introduction

Sea level rise is of great concern in coastal areas, where a significant part of the population is settled in many countries around the world (Rakodi and Treloar, 1997; Anthoff et al., 2006). As a consequence, sea level variability and rise is a crucial topic in the context of coastal vulnerability and management. Its importance has increased with the worldwide awareness caused by the rising of sea level due to natural variability and anthropogenic forcing (e.g. Meehl et al., 1998; Alexander, 2010; Church and White, 2011; Liu, 2012). Therefore, understanding regional and local long-term sea level variability as well as its trend is critical (White et al., 2014; Clark et al, 2015; Strassburg et al, 2015). It is also important to find out how these regional and local long-term sea level rise (SLR) rates corroborate the global mean SLR rates which have been shown to be higher over the last two decades (Church and White, 2011).

This chapter is devoted to discussing a modern method of data analysis, and how it can be applied to separate the oscillatory timescales embedded in the sea level tide gauge records along the coast of southern Africa. Tide gauge measurements are unique as they measure important features of coastal processes (Prandi et al., 2009). Unfortunately, historical sea level records in southern Africa have many gaps of differing length, making it difficult to use analyses that require a continuous record. This study uses the Empirical Mode Decomposition (EMD;

Huang et al., 1998) method, and is the first time that this method has been applied to southern African sea level records.

The EMD is a new method for analysing sea level records, applied by Feng et al. (2011) to study satellite altimetry sea level trends and their global distribution. Using sea level records along the east coast of the USA, Ezer and Corlett (2012) successfully tested the confidence levels of the EMD-separated trends. Additionally, they demonstrated that EMD is suitable for separating modes of variability in sea level data. Ezer et al. (2013) applied this method to study the impact of the Gulf Stream on coastal sea level along the United States mid-Atlantic coast. Currently EMD is being applied in a number of geophysical studies in addition to sea level research (e.g. Huang et al, 2003; Wu and Huang, 2009; Franzke, 2011; Chen et al., 2012; Ezer and Corlett, 2012; Ezer et al, 2011; 2013; 2016; Alberti et al., 2014; Chen et al., 2014; Park and Sweet, 2015).

The method is innovative as it brings, through the Hilbert transform, the ability to deal with the "instantaneous frequencies" (Huang et al., 1998). These instantaneous frequencies are an intrinsic aspect of the local nonlinearity within the data set. The instantaneous frequencies are the main constraint for existing nonlinear and non-stationary data processing methods and will be discussed below. In order to process nonlinear and non-stationary time series, the existing Fourier spectrum-based methods create artificial harmonics which, although mathematically acceptable, often have little physical meaning. The Hilbert transform generates intrinsic mode functions (IMFs) from the frequencies of the embedded timescales of the time series and then creates an energy-frequency-time distribution (Huang et al., 1998). It thus turns the EMD method into an effective filter (Huang et al, 2003; Ezer et al, 2016), as the filtering process is done with no pre-conditions unlike most of the traditional filtering methods, as discussed below.

In order to test its sensitivity when dealing with data gaps, a choice was made to apply the EMD method to synthetic sea level data. This is because the EMD has the limitation of not being able to handle the data gaps unlike, for instance, wavelet analysis which can deal with gaps (Torrence and Compo, 1998). Hence, the timescales of variability within synthetic sea level records were separated in order to determine and study their characteristics as part of the EMD

sensitivity experiment. Separating these timescales is one of the great challenges in sea level research (e.g. Emery and Aubrey, 1991; Gornitz, 1995; Bart et al., 2012), due to the absence of a consensus as to the most suitable method to be applied (e.g. Bart et al., 2012).

This chapter explains how the EMD method works, compares it with other methods, and ultimately test the effects of data gaps. The method is first applied to a continuous "synthetic" data series, and the results are then compared to other methods. Secondly, the method is applied to the same data but with artificially created gaps to quantify their impact in terms of how they distort the expected results. Various gap filling methods are also tested. This approach provides insight into how the separated oscillatory modes are affected by different gap filling methods.

This Chapter is structured as follows: a broad description of the EMD method is presented in Section 2, the synthetic data is described in Section 3, the Results and Discussion are presented in Section 4, and the Summary and Conclusion are offered in Section 5.

2.2. Methods

2.2.1 The Hilbert - Huang Transformation

Traditionally, Fourier spectral analysis has dominated quasi-periodic data analyses for many reasons, including both the lack of suitable alternatives and its simplicity. Since its introduction, Fourier spectral analysis has become the obvious way to determine the energy-frequency distribution within data. Although it is well accepted in the research community, to obtain results which are physically meaningful, the data must be linear, periodic or stationary (see Huang et al, 1998 for more details).

The data are considered as linear if:

$$\left.\begin{aligned} x_{(t)} &= ax_{1(t)} + bx_{2(t)} + cx_{3(t)} + \cdots \\ y_{(t)} &= ay_{1(t)} + by_{2(t)} + cy_{3(t)} + \cdots \end{aligned}\right\} \quad (2.1)$$

Where $x_{(t)}$ and $y_{(t)}$ are the input and output time series, respectively. x_1, x_2,…x_n, and y_1, y_2,…y_n, are the measured input and output, respectively.

The same time series $x_{(t)}$ is considered stationary, in general, if for all t:

$$\left.\begin{aligned} E\left(\left|x_{(t)}^2\right|\right) &< \infty, \\ E\left(x_{(t)}\right) &= m, \\ C\left(x_{(t_1)}, x_{(t_2)}\right) = C\left(x_{(t_1+\tau)}, x_{(t_2+\tau)}\right) &= C(t_1 - t_2) \end{aligned}\right\} \quad (2.2)$$

Where $E(.)$, is the expected value defined as the ensemble average of the quantity and $C(.)$ is the covariance function.

The Fourier spectral analysis has limitations when dealing with local non-linearity within the time series without significant energy spreading. In its first analysis of the data, the Fourier spectral analysis attributes the overall uniform harmonic components. When the data deviates significantly from a sine or cosine wave functions it produces more harmonic components, resulting in energy dispersion. The excessive presence of harmonics leads to erroneous energy-frequency distributions in nonlinear and non-stationary data. This is why, for instance, in power spectrum density and wavelet spectra, the results are fitted at higher frequencies with good confidence levels (Huang et al., 1998).

Many attempts have been made to design statistical methods taking into account the nonlinearity and non-stationarity of data (Huang et al., 1998). The EMD is close to wavelet analysis in that they are both suitable for time series spectral analysis. However, wavelet analysis is not adaptive, meaning that there are many pre-requisites for the analysis to be considered successful (Torrence and Compo, 1998). Furthermore, it is only useful if one understands and applies the main essential statistical tests (e.g. pre-whitening, stationarity,

etc). To overcome this need, the Morlet wavelet has become very popular amongst the other basic wavelet functions (Huang et al., 1998; Torrence and Compo, 1998).

To overcome the limitation faced by Fourier spectral analysis when dealing with nonlinear and non-stationary data, the Hilbert - Huang Transformation (HHT) defines $y_{(t)}$ for a time series $x_{(t)}$ as follow:

$$y_{(t)} = \frac{1}{\pi} P \int_{-\infty}^{\infty} \frac{\mathrm{x}_{(\mathrm{t}')}}{\mathrm{t} - \mathrm{t}'} \mathrm{dt}' \tag{2.3}$$

Where, P indicates the Cauchy principal value[1]. When conjugated, $x_{(t)}$ and $y_{(t)}$ gives:

$$z_{(t)} = x_{(t)} + iy_{(t)} = a_{(t)} e^{i\theta_{(t)}} \tag{2.4}$$

In which:

$$a_{(t)} = \left[x_{(t)}^2 + y_{(t)}^2\right]^{\frac{1}{2}}$$
$$\theta_{(t)} = arctan\left(\frac{y_{(t)}}{x_{(t)}}\right) \tag{2.5}$$

The Hilbert transform defines the instantaneous frequency as:

$$\omega = \frac{d\theta_{(t)}}{dt} \tag{2.6}$$

The instantaneous frequency is defined as a scalar, and therefore is a monocomponent, i.e. there is just one frequency value at a particular time (Huang et al., 1998). However, there is no

[1] In Mathematics, the Cauchy principal value is a method of assigning values to certain indeterminate improper integrals. The Cauchy principal value plays a fundamental role in the study of the Hilbert Transforms.

precise definition of the monocomponent signal. One should interpret it as a localized frequency within a narrow band. The concept of bandwidth has proven to be crucial, thus it gives rise to the definition of the number of zero crossings per unit time as follow:

$$N_0 = \frac{1}{\pi}\left(\frac{m_2}{m_0}\right)^{\frac{1}{2}} \tag{2.7}$$

At given time, the expected number of extrema is given by:

$$N_1 = \frac{1}{\pi}\left(\frac{m_4}{m_2}\right)^{\frac{1}{2}} \tag{2.8}$$

In which m_i is the i-th moment of the spectrum[2].

Hence, a standard bandwidth measure, although in global sense, can be defined as:

$$v^2 = \pi^2(N_1^2 - N_0^2) \tag{2.9}$$

If the HHT only dealt with local properties of the data using a global concept it would not be innovative. However, the HHT introduces IMFs to deal with instantaneous frequencies within the data. The HHT avoids IMFs which are physically meaningless by imposing on them two restrictive conditions: "*(1) in the whole data set, the number of extrema and the number of zero crossings must either be equal or differ at most by one; and (2) at any point, the mean value of the envelope defined by the local maxima and the envelope defined by the local minima is zero*" (Huang et al., 1998). Therefore, the IMFs represent the embedded oscillatory modes within the data.

At any given time, the data may have more than one mode of variability (Huang et al., 1998). Therefore, EMD was introduced to identify the IMFs under certain conditions.

[2] The i-th moment of the spectrum can be viewed as a way to use statistics to analyse the power spectrum.

2.2.2 Empirical Mode Decomposition

EMD (Huang et al., 1998; Wu and Huang, 2009) is designed for use in non-stationary and nonlinear time series. Using this method, any time series data can be decomposed into a finite number of oscillatory modes, the IMFs, with time-variable amplitudes and frequencies. The following three assumptions are required for a satisfactory decomposition to proceed: "*(1) the signal has at least two extrema, i.e. one maximum and one minimum; (2) the characteristic time scale is defined by the time lapse between the extrema; and (3) if the data were totally devoid of extrema but contained only inflection points, then it can be differentiated once or more times to reveal the extrema. Final results can be obtained by integration(s) of the components*" (Huang et al., 1998).

The Hilbert - Huang Transformation (HHT) identifies each IMF, and then the EMD decomposes them via the sifting process (Huang et al., 1998; 1999) following the equation:

$$x_{(t)} = \sum_{j=1}^{N} C_{j(t)} + R_{(t)} \tag{2.10}$$

In which $x_{(t)}$is the original time series, $C_{j(t)}$ is the number of IMFs (hereinafter modes) within the original time series and $R_{(t)}$ the residual. As a result, (i) the first mode j=1-1 (i.e., mode zero (0)), is always the raw time series and is the mode with the highest frequency at that stage; (ii) the residue is then considered as a new time series, and manipulated under the same sifting process to obtain the second mode j=2-1, which is the mode with next highest frequency; and (iii) The previous step (ii) is repeated continuously until there is no more signal to process. Thus, the last mode j=N-1 ($R_{(t)}$) is the lowest frequency oscillatory mode, i.e. has only one extremum and is considered to be the trend.

The number of cycles or modes is determined by the record length. The shape of each separated mode and, hence, the trend cannot be known in advance as the method is non-

parametric (Ezer and Corlett, 2012; Ezer et al., 2013). Consequently, the trend is neither linear nor quadratic but it is intrinsic to the analysed data (Huang et al., 1998; 1999).

The EMD analysis has advantages over spectral analysis because it can identify oscillatory modes with lower frequencies. Unlike typical Fourier analyses, the EMD allows one to derive sea level modes with periods twice as long as the record length (Ezer and Corlett, 2012). Thus neither Fourier spectral analysis nor wavelet analysis is well suited for studying long-term sea level variations, given that they can detect modes with periods up to approximately 5 years or a bit longer depending on the time series length (Ezer et al., 2013). Therefore, EMD overcomes some of the limitations of spectral and wavelet analyses (Huang et al., 1998; Alberti et al., 2014).

As with other statistical methods, the EMD technique does not identify the forcing behind the modes of variability. However, it does give a good indication of the dominant time-scales of variability needed to identify suitable forcing mechanisms. Thus, for many tide gauge locations, when the assessment is done and they show a trend of similar shape, it implies that these locations are likely to be governed by the same drivers (Ezer et al., 2013). To confirm a relationship with a driver, one can apply the same method to different known drivers. If one or more drivers show a shape similar to the sea level variations, it suggests that they may be the drivers of the sea level changes (Ezer et al., 2013).

Although the EMD analysis is a quick and simple way to determine the timescales of sea level variability, Chambers (2015) advises caution when interpreting each separated mode. This is because there is no good phase resonance between some oscillatory modes and the possible physical forcing. There is also a debate about the reliability of the EMD method to detect long-term sea level rise rates and so, detach the sea level rise accelerations (Kenigson and Han, 2014; Chambers, 2015). However, this reservation is not only related to the EMD method as pointed out by Visser et al. (2015), it applies mainly to short sea level records. Ezer et al. (2016) applied the method to approximately 100-200 year long tide gauge records from the United Kingdom and western European coasts. Their results were comparable with the sea level acceleration calculated using the standard quadratic regression method.

2.3. The synthetic data

The synthetic data sets are based on the monthly gridded altimetry sea level observations averaged from daily means. Hence, the synthetic monthly altimetry sea level data were chosen from a grid point closest to one tide gauge location. The altimetry data were based on the gridded multi-mission AVISO (Archiving, Validation and Interpretation of Satellite Oceanographic Data; http://www.aviso.altimetry.fr/) altimetry observations from January 1993 to December, 2015. The data are currently distributed by the Copernicus Marine and Environment Monitoring Service (CMEMS; http://www.marine.copernicus.eu). It was motivated by the fact that such data may better reflect some of the local coastal dynamics, particularly those occurring at high frequency. Given the time span of the altimetry observations, the data were repeated backwards to obtain a length similar to tide gauge records. As a consequence, depending on the record length, some features that are apparent during satellite era are also repeated prior to 1993. The trend of the repeated records was replaced by the linear trend of the data during satellite period so that the data may present a trend close to the definition for EMD analysis, i. e. it should have only one extremum (Huang et al., 1998).

As mentioned above, the EMD method was utilised to obtain the oscillatory timescales and the trend in the records. For reasons that will be explained below, wavelet spectral analysis was employed to determine the periodicity of separated modes and understand each temporal structure. Furthermore, each separated mode was analysed visually to ensure that frequencies displayed in the wavelet analysis are “real”.

Two synthetic monthly altimetry sea level data types were created, representing seven tide gauge sites. The locations are Richards Bay, Durban, East London, Port Elizabeth, Knysna, Mossel Bay and Simon’s Bay, all located in the east and south coast of South Africa, see Fig. 2.1 and Table 2.1, for more details. For a better interpretation of the results, the location are henceforth termed quasi-Richards Bay, quasi-Durban, quasi-East London, quasi-Port Elizabeth, quasi-Knysna, quasi-Mossel Bay and quasi-Simons Bay.

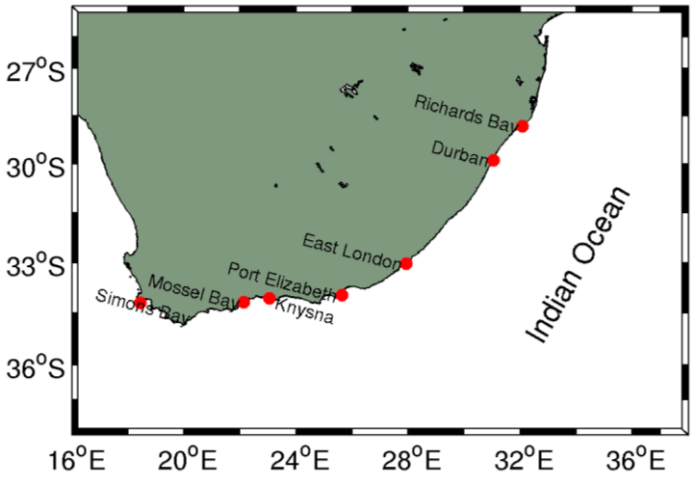

Fig. 2.1: Tide gauge locations used to create synthetic data.

The first synthetic dataset consisted of a set of continuous synthetic monthly altimetry sea level data with no gaps. Then, artificial gaps were introduced by removing data values where there are missing values in the tide gauge records, to obtain the second file. The EMD analysis was applied to both sets of data. As a result, the oscillatory modes representing the same periodicity were compared. This allowed quantifying the influence of data gaps in terms of how they distorted expected results. In other words, these assessments were done to ensure that gaps do not have any major impact in the time evolution of each mode. As part of the assessment, the wavelet spectral analysis helps to identify the differences in the modes of variability throughout the time spans studied.

Table 2.1: Characteristics based on which the synthetic data were built, where the end date is December, 2015 at all studied sites.

station	ID	Data coverage (%)	Starting date	Longest gap period (months)
Richards Bay	RB	55	Jun-77	73
Durban	D	69	Jan-71	28
East London	EL	53	Jan-67	75
Port Elizabeth	PE	78	Jan-78	18
Knysna	K	71	Aug-60	60
Mossel Bay	MB	79	Jul-58	24
Simons Bay	SB	79	Oct-57	49

Different gap filling methods are likely to have impacts on the shape of the modes separated. To examine these impacts, three gap filling methods were tested. (1) The commonly used linear interpolation method (henceforth linear interpolation), in which missing values are filled using adjacent values. This method is recommended when short gaps are observed (Thomson and Emery, 2014). The length of gap to which it can be applied for monthly mean sea level records is still not clear. (2) The gaps are filled by the average value of the entire synthetic sea level records (e.g. Cheng et al, 2015; hereinafter average value). (3) The missing values are replaced by the value of the linear trend of the existing data sets (e.g. Ezer et al, 2016; hereinafter linear trend value). Hence, three datasets with gaps were created at each studied site. Then, the sensitivity of each gap filling method was addressed.

The results of the three gap filling methods were compared to those from using data without gaps, the latter assumed to be the truth. Thus, the sensitivity experiment to test the impact of the gaps together with the gap filling methods was performed according to the gap locations in the records at each of the seven sites mentioned above. As a result of this analysis, it is anticipated that the modes of the EMD analysis decomposed from the data with gaps can then be used with more confidence.

2.4. Data analysis and comparison

2.4.1 Continuous and consistent synthetic data sets

The continuous synthetic monthly altimetry sea level time series were used to examine the ability of the EMD method to separate the timescales within the data and the results were then compared to other methods, e.g., power spectral analysis and wavelet analysis. Modes of quasi-Durban sea level records when decomposed with the EMD method are shown in Fig. 2.2. It illustrates that from the data without gaps, the sifting process produced 9 modes. The estimated period of each mode is also shown. The period estimation was done through visual

examination of the separated modes and wavelet analysis (figure not shown). The way the period estimation was done will be explained when the wavelet analysis results are discussed.

As can be seen in Fig. 2.2, mode 1 is characterised by an approximately 3-month cycle. Mode 2 represents a roughly 6-month cycle. Mode 3 is approximately a 12-month cycle. Together these modes comprise the sub-seasonal and seasonal components of the variability. Mode 4, 5 and 6 comprise the interannual component of sea level variability. For example, mode 4 occurs at a roughly 22-month cycle. Mode 7 has a periodicity of about 19 years. Modes 7 and 8 represent the multi-decadal or low-frequency component of the variability. Mode 9 reflects the trend and it should be emphasised that it is non-linear.

The modes 1 to 8 show de-trended time series with the variability centred on the local mean. The change of variability over the time is also noticeable; the change of amplitude makes this clear. However, it reflects the frequency variation over the each separated oscillatory mode.

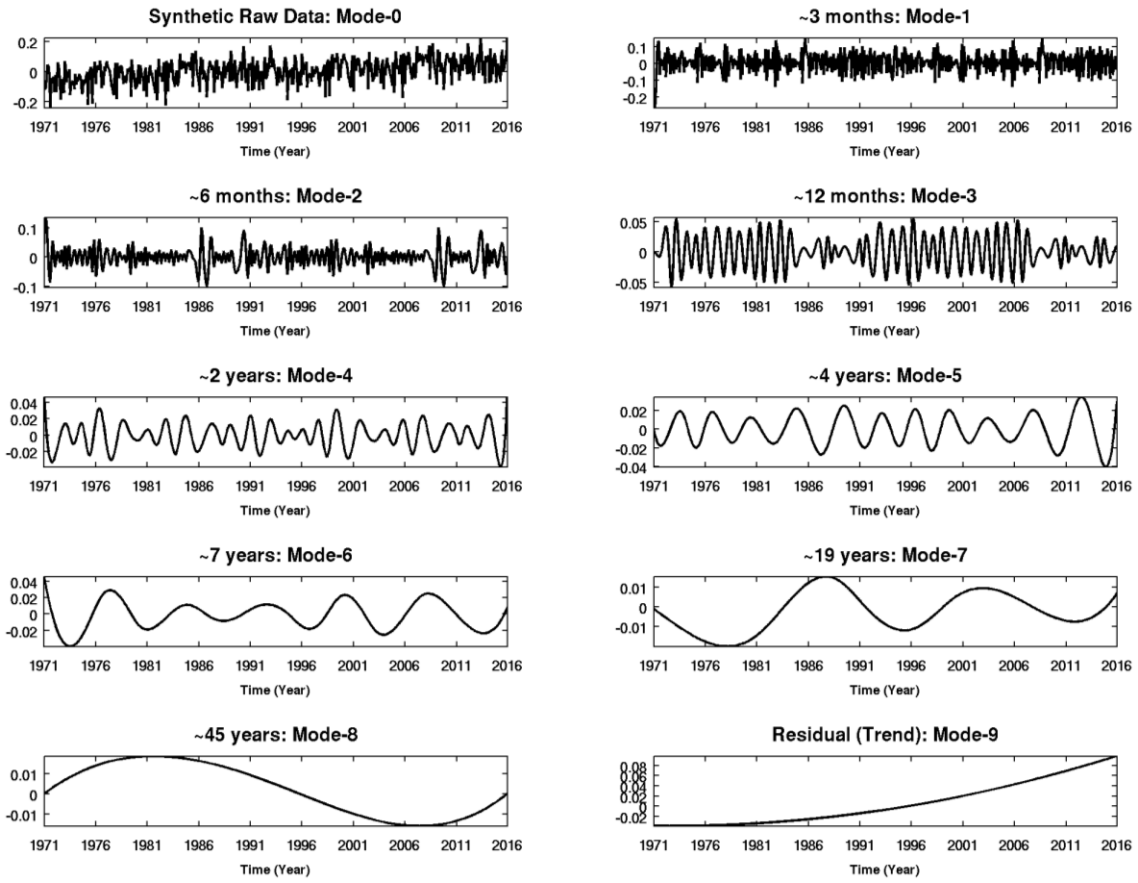

Fig. 2. 2: Quasi-Durban monthly continuous and consistent sea level height (in m) when decomposed with the EMD analysis, into nine modes; mode 0 is the raw data; modes 1 - 8 are the oscillating modes; mode 9 is the remaining residual mode and is the trend. The periodicity of each mode represents the average frequency since the modes do not exhibit a constant frequency in time.

Wavelet and power spectral analyses were undertaken to investigate their ability to distinguish longer period oscillatory modes at a high confidence level, for instance at 95% confidence level. Both methods are commonly used in physical oceanography for time series analysis (Thomson and Emery, 2014). As can be seen in Fig. 2.3, the power spectrum density depicts significant peaks between around 2.5-10 months (0.4 and 0.09 cycle/month). The wavelet spectrum portrays dominant modes of variability with a similar period of approximately 3-12 months. The 12 month period peak in the power density spectrum is just slightly higher than the error bar. It should be noted that the same peak appears as a sporadic dominant mode in the wavelet spectrum. As mentioned above, the presence of several harmonics is a limitation of these

methods (Huang et al., 1998). As a consequence, wavelet and power spectral analyses give reliable results at higher frequencies (Huang et al., 1998; Ezer et al., 2013). To locate low frequency oscillatory modes through either wavelet or power spectrum, one should reduce the confidence level. For example, at approximately 50 % confidence level it was possible to locate low frequencies. Of course, at such low confidence level the interpretation of the results is dubious.

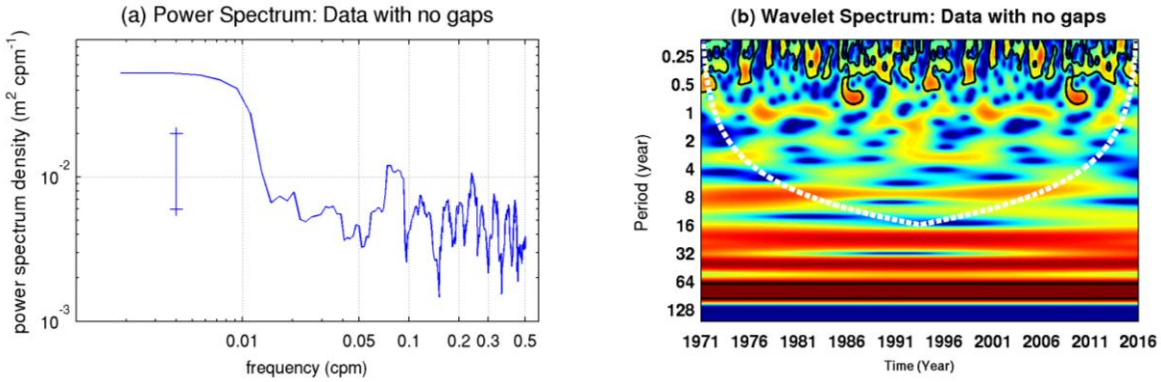

Fig. 2.3: (a) Power spectral analysis for the quasi-Durban continuous data. A multi-taper method with adaptive weighting (e. g. Percival and Walden, 1993) and 95% confidence (limit) plot is presented. (b) Wavelet analysis for the same data (Torrence and Compo, 1998). Colour shades show the wavelet spectral power (units: base 2 logarithm of sea level variance in m^2). The black contour denotes the 95% confidence level. The white dotted line is the cone of influence, meaning that any longer periods are insignificant.

The capacity of wavelet analysis to give high frequency variability with 95% confidence was used to study the periodicity of each separated mode. Applying wavelet analysis to each mode is useful for determining the average frequency of modes of variability. This is possible because the frequency of the analysed mode is considered to be the only frequency at each step. Thus the wavelet will show the dominant modes of variability at frequencies that match with the mode studied. The average frequencies of the oscillatory modes were also determined visually.

Due to its ability to separate the oscillatory modes within the data set, EMD can be used as a filter. Fig. 2.4 illustrates the reconstruction of the quasi-Durban data from the last mode, the residual, to the first mode, i.e. mode 0. Mode 9 shows the evolution of the trend over the time

span. The usefulness of such a trend will be discussed in Chapters 4 and 5. Here, it should be stated that nonlinear trends are useful to understand the processes behind the changes (as also mentioned in section 2.2.2). The sum of modes 8 and 9 (Fig. 2.4 (b)), gives the smoothed version of the trend and it represents the longest frequency in the time series. The difference between mode 9 and the sum of the separated modes starts to be clearer from the ensemble of the modes 7 to 9 (Fig. 2.4 (c)). The variations are much clearer from the sum of modes 6 to 9 (Fig. 2.4 (d)). After adding all the modes, the result is the match between the original data and the sum of the separated modes.

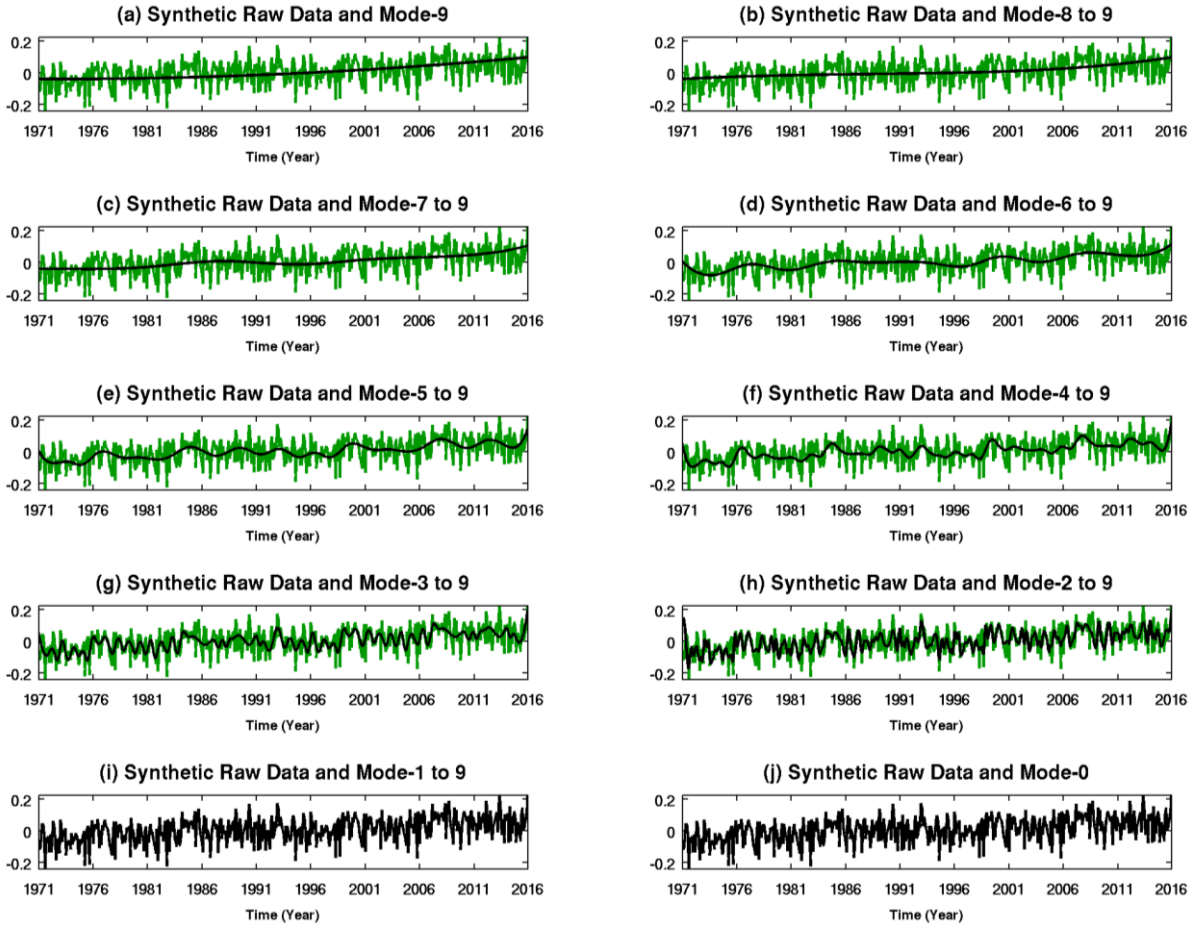

Fig. 2.4: The reconstruction of the quasi-Durban data (in m) through the oscillatory modes decomposed by the EMD method. In each panel, the original data (green line) is superposed on the added modes, plotted in black.

The example in Fig. 2.4 exhibits the ability of the EMD method to act as a low-pass filter. No pre-determined frequency was required. Also, the process is completely nonlinear. The EMD method can also be applied as a high pass filter. To do so, it is only necessary to add the modes from the high to low frequency, i.e. the opposite to that illustrated in Fig. 2.4. Either of these filtering processes can be used to obtain the sum of the modes of variability. The objective of the filtering process will define at which step one should stop. The combined modes yield different timescales that may be depicted as sub-annual, inter-annual, decadal and multi-decadal components of variability according to the data span (45 years in this example). This is particularly important when studying the forcing mechanisms behind the changes. The latter will be also discussed in Chapters 4 and 5 where actual *in situ* data will be analysed.

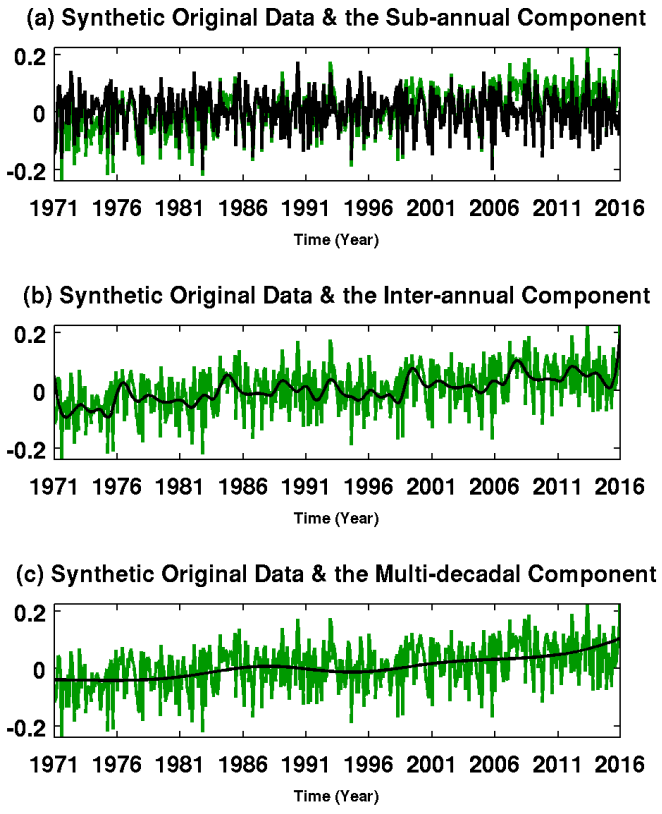

Fig. 2.5: EMD separated oscillatory modes of quasi-Durban records when combined, in black. The original synthetic monthly altimetry sea level data (in m) is presented in green.

The ensemble of the separated oscillatory modes of the studied data is shown in Fig. 2.5. The figure depicts three components. The sub-annual component represents all the modes with a periodicity of up to a year and a half. All the oscillatory modes with a periodicity between a 18 months and seven years are defined as part of the inter-annual component. When the periodicity is longer than seven up to 20 years, the modes of variability are defined as the decadal component. Lastly, the modes of variability longer than a 20-year period are defined as the multi-decadal component, i. e. the low frequency component of the data. In this study, the decadal and multi-decadal components were merged to avoid analysing one oscillatory mode (Chambers, 2015) in some locations due to the short sea level record length. Modes 1-3 comprise the sub-annual component of variability. Modes 4-6, modes 7-8, compose the inter-annual, decadal and multi-decadal component of variability, respectively.

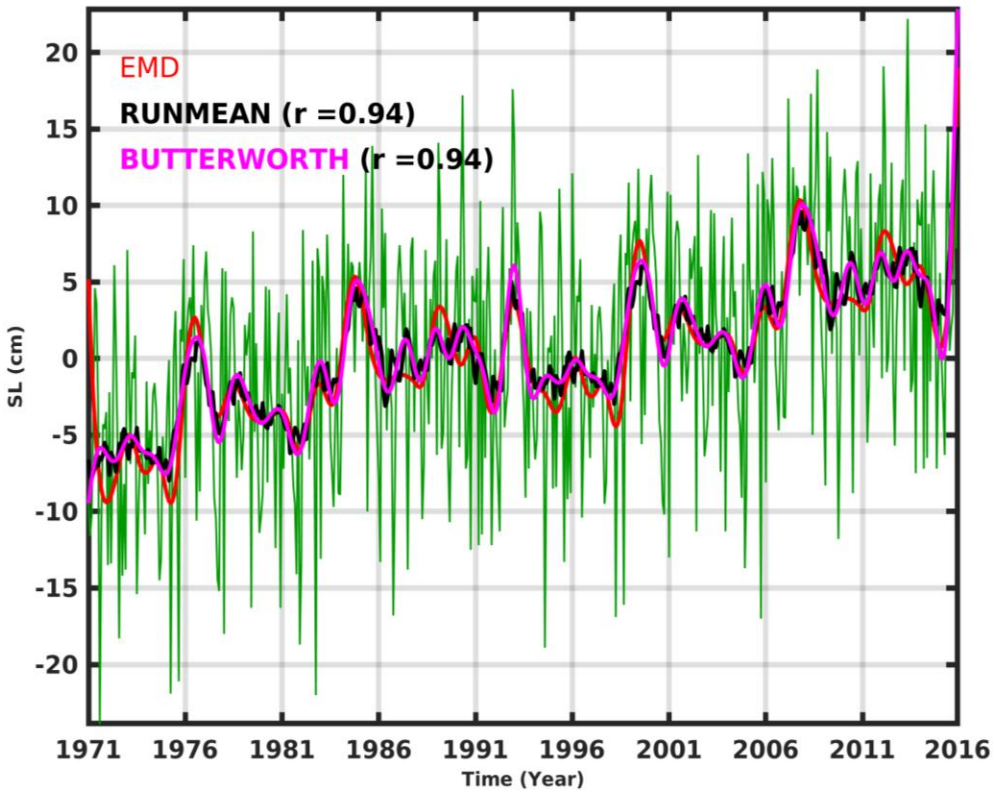

Fig. 2.6: The inter-annual component of variability of quasi-Durban records filtered through EMD (red line), running mean (black line) and Butterworth (magenta line). The original synthetic monthly altimetry sea level data is presented in green. Correlations coefficients are for correlations with the EMD filtered series.

As an example, the inter-annual component of variability of quasi-Durban records displayed in Fig. 2.5 was compared to the results of most used low-pass filters in physical oceanography (Thomson and Emery, 2014) and hence, in sea level research, the 13-month running mean and the Butterworth low pass filter of order 5 with cut off frequency of 1.5 years (Butterworth, 1930), Fig. 2.6. As can be seen, the EMD inter-annual component is comparable to the results of running mean and Butterworth filters, at 95 % confidence level. Note that the values at the ends are not physically meaningful. Having explored the EMD technique in a dataset with no gaps, the next section is dedicated to address the question of the influence of data gaps.

2.4.2 Synthetic data sets with artificial gaps

The synthetic monthly altimetry sea level time series with artificial gaps were also used to examine the ability of the EMD method to separate the timescales within the data and the results were then compared to other methods e.g., power spectral analysis and wavelet analysis. The missing values were created at the same positions as those found in the tide gauge records. As in the previous quasi-Durban sea level records analysis, when decomposed, the data with gaps yielded nine modes under the sifting process. The results are shown in Fig. 2.7. All previous steps were taken for a later comparison. Where the data were replaced by any of the gap filling methods, the resulting modes fail to show good temporal structure of the variability. The gaps in the data were linearly interpolated. This method showed poor results, particularly creating unreliable high mode amplitudes. The results of different gap filling methods will be compared and discussed below.

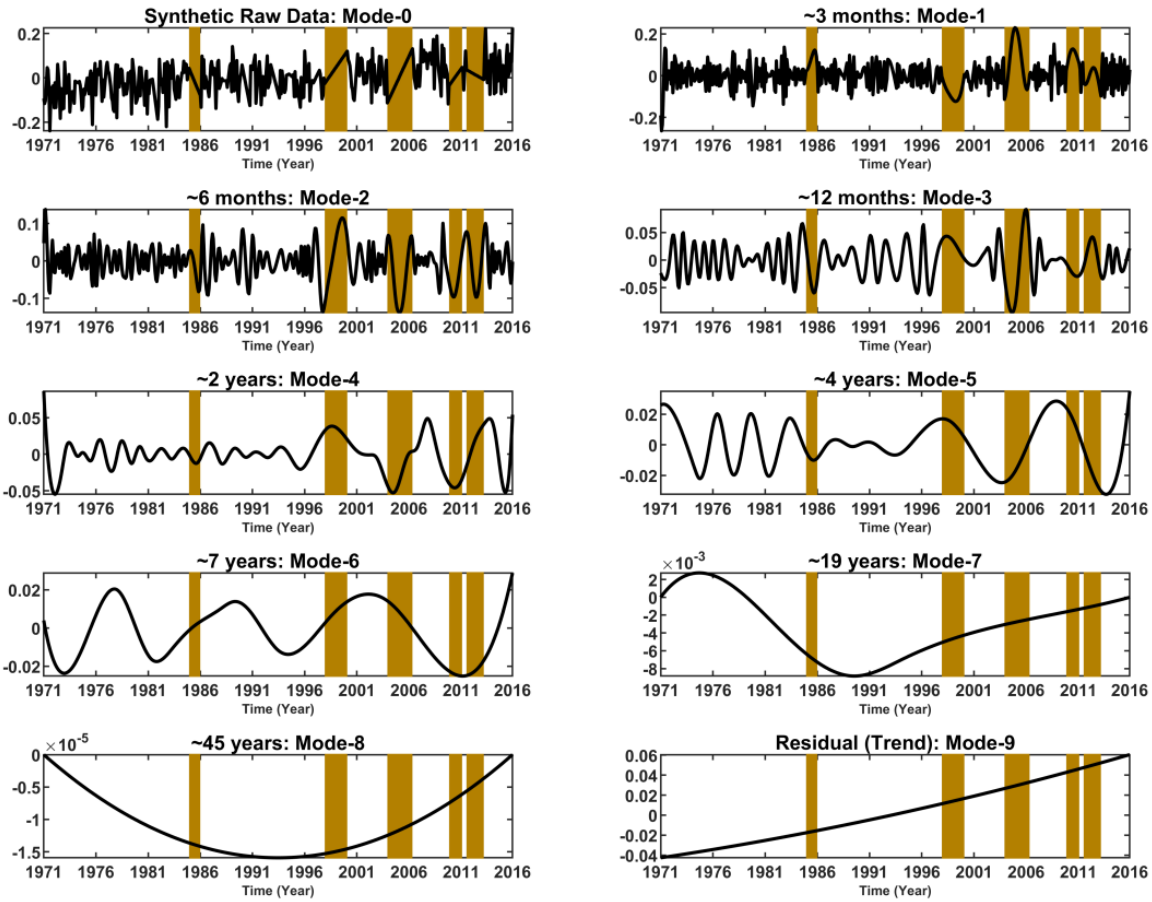

Fig. 2.7: Quasi-Durban monthly data with gaps filled by linear interpolation (in m) when decomposed with EMD analysis. As a result, nine modes were found, mode 0 is the raw data, modes 1-8 are the oscillating modes, the remaining residual mode is the trend (mode-9). Note that the periodicity of each mode represents the average frequency since they do not have a constant frequency. Brown shadings indicate where data gaps, from 12 consecutive months, are located in the raw time series.

Gaps randomly located and up to 10 years in duration were also tested with no significant differences in the results presented here. Power spectral density and wavelet analyses were undertaken to have some insight into how the modes of variability behave, as illustrated in Fig. 2.8. In the depicted figure, the records are for quasi-Durban sea level monthly means with the missing values replaced by linear interpolation. Although the peaks are still located at the same frequencies, their significance is reduced. It is noticeable in Fig. 2.8 (b) that some dominant modes of the variability are absent from previously seen data with no gaps.

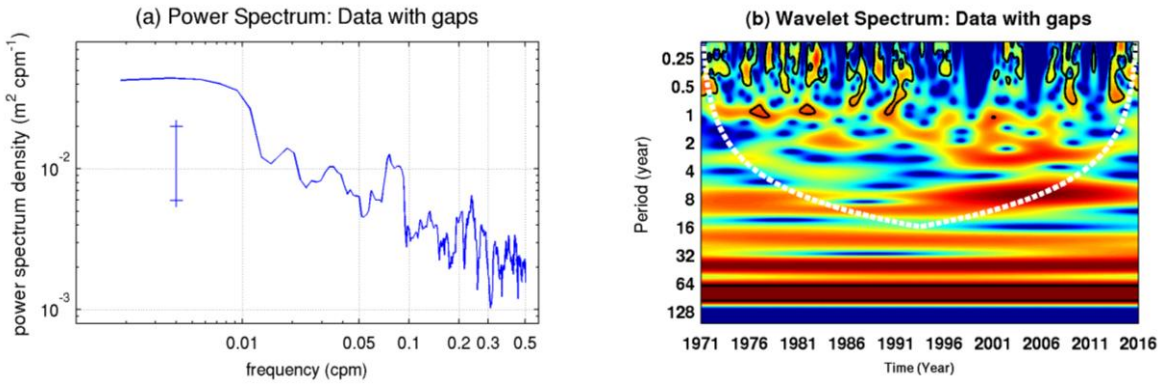

Fig. 2.8: (a) Power spectrum analysis for the quasi-Durban with artificial gaps added. There were filled by linear interpolation. It is using the multi-taper method with adaptive weighting (e.g. Percival and Walden, 1993) and 95% confidence (limit) plot is represented. (b) Wavelet analysis for the same data (Torrence and Compo, 1998). Colour shades show the wavelet spectral power (units: base 2 logarithm of sea level variance in m^2). The black contour denotes the 95% confidence level. White dotted line is the cone of influence, meaning that any longer periods are dubious.

It should be also noted, in Fig. 2.8 (b), that the filled values yielded results with false dominant modes. The dominant mode of variability at 12 months period is more obvious (see Fig. 2.3, for a comparison). The influence of the gaps in the data has been tested. As might be expected, results suggest that gaps have a varying effect according to their location and length. Nevertheless, there is a need to understand the magnitude of such impacts.

2.4.3 Comparison of the different gap filling methods

To quantify the impact of data gaps, investigation in terms of how they distorted the results of continuous synthetic monthly altimetry sea level time series was carried out as a sensitivity experiment. Thus, various gap filling methods are also tested. This approach provides insight into how the separated oscillatory modes are affected by different gap filling methods. In order to examine the similarity of the oscillatory modes for data with and without gaps, the modes were correlated according to their periodicity. Unless stated otherwise all correlations undertaken in this study were at 95 % confidence level. The correlation mode by mode, taking into account their average frequency is depicted in Fig. 2.9. As can be seen, there is a phase

mismatch between both sets of data as the frequency reduces. There is an appearance of sporadic higher amplitude in the EMD modes of the data with gaps, compared to its counterpart at same time location (Fig. 2.9). The magnitude of these higher amplitudes depends on the gap filling method. However, the average and the linear trend value filling methods usually give comparable results.

For mode 0 (i. e. the raw data), all gap filling methods show results that are statistically similar. The correlation coefficient value decreases consistently from mode 1 to mode 5. Then, the subsequent modes show low correlation coefficient values. The lowest frequency mode, which is considered to be the trend, shows a strong correlation. This suggests that, although the data may have gaps, EMD can still be used in the determination of the long-term trend. Nevertheless, correlation is not that revealing for the lowest frequency mode containing the trend. Thus, when it comes to the trend, it is not just the correlation that counts but also the trend shape. In this way, it is noticeable how the data with missing values may lead to underestimated, quasi-linear rather than non-linear trend results (in the cases presented here). The trend shapes will be discussed below.

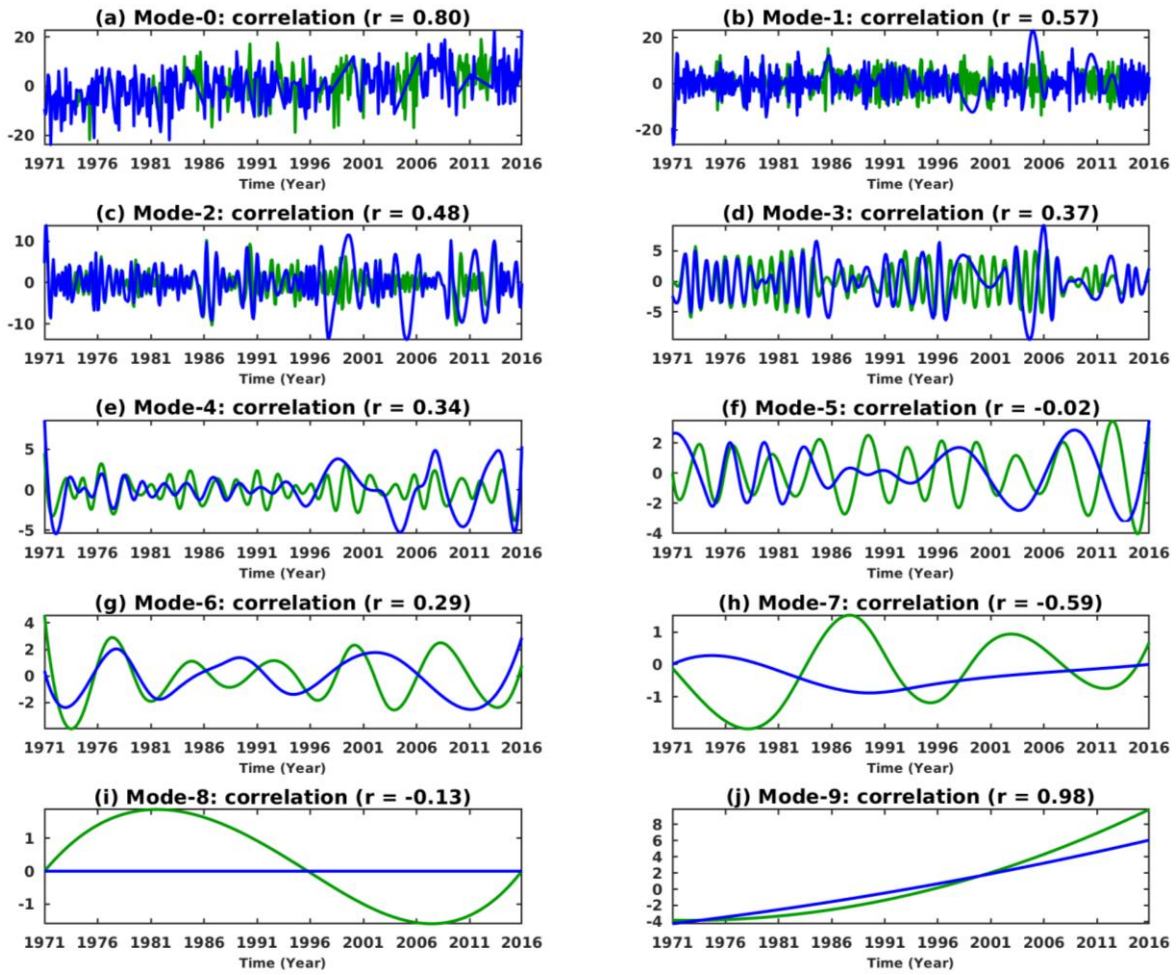

Fig. 2.9: The comparison between the no gaps quasi-Durban data (green line; in cm) versus data at same location but with gaps (blue line). The separated modes of variability are compared one by one. The missing values were replaced by the linear interpolation method.

The effect of the gaps on the time evolution of the modes of variability depends on their location in the time series. At all sites studied, changes on the mode shapes were found to be influenced by gaps in the data. The changes also depend on the method by which the gaps were filled. This leads to a conclusion that in its first sifting process, the EMD handles filled values as a bridge between the real records. The difficulty comes when sifting the residuals, where it seems like the EMD has lost the memory in regard to the replaced values. As a result, the subsequent modes exhibit, in some time locations, frequencies higher than the average frequency of the entire mode.

It may suggest that the interpolated values produce some sort of mode mixing, as mentioned above. In other words, the frequency at that location may be lower than the average frequency of the mode leading to a high period, when connecting data sets pierces. The latter is observed in all three gaps filling methods but with more emphasis in the linear interpolation method. The phenomenon is noticeable when the missing values are, as long as at least two consecutive years.

Results suggest that when missing values last for at least two consecutive years, it should be defined as a long gap. When two long data gaps are separated by at most a year consecutive values, a big "jump" is observed in all gap filling method (Fig. 2.9). The absence of a lowest or highest value at particular period, also forces changes in the mode shapes. Probably because the subsequent sea level variation is also part of the restoration force.

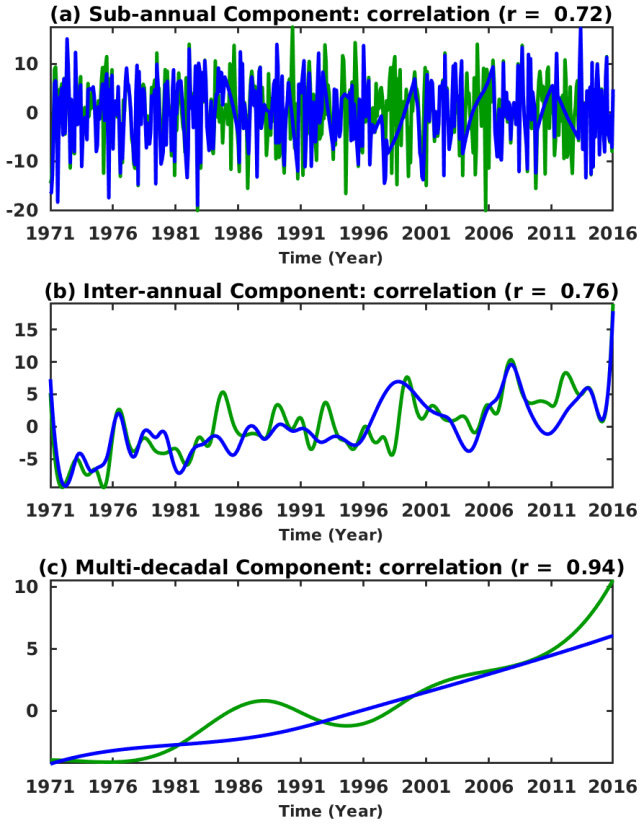

Fig. 2.10: The continuous quasi-Durban data (green line) versus data with gaps (blue line; linear interpolation method). The comparison in regard to the corresponding combined of the modes of variability (in cm).

The modes of variability were combined, and then the correlations were conducted, as illustrated in Fig. 2.10. The results when the gaps were linearly interpolated suggest that when combined, the oscillatory modes correlate well with each other. For quasi-Durban data, the correlation value is higher (0.94) for the multi-decadal component. The sub-annual and the inter-annual components yielded 0.72 and 0.76 correlations values, respectively. For this particular case of the multi-decadal component, the aforementioned correlation value was statistically similar to the linear trend method (see Table 2.2). Overall, the linear interpolation method yielded lower correlation values when compared to the two other methods.

Table 2.2: The correlation values between the combined modes of the data without and with gaps at all studied sites.

Tide gauge	gap filling method			
	linear interpolation	Average value	linear trend value	ensemble mean mode of variability
Richards Bay	0.77	0.75	0.99	sub-annual
	0.74	0.78	0.97	interannual
	0.86	0.99	0.97	multi-decadal
Durban	0.72	0.78	0.78	sub-annual
	0.76	0.84	0.85	interannual
	0.94	0.86	0.95	multi-decadal
East London	0.54	0.73	0.73	sub-annual
	0.70	0.65	0.61	interannual
	0.93	0.82	0.84	multi-decadal
Port Elizabeth	0.71	0.88	0.88	sub-annual
	0.74	0.84	0.78	interannual
	0.91	0.97	0.89	multi-decadal
Knysna	0.78	0.84	0.85	sub-annual
	0.80	0.93	0.95	interannual
	0.91	0.99	0.98	multi-decadal
Mossel Bay	0.82	0.86	0.87	sub-annual
	0.81	0.88	0.89	interannual
	0.97	0.97	0.97	multi-decadal
Simons Bay	0.84	0.87	0.88	sub-annual
	0.93	0.86	0.91	interannual
	0.97	0.92	0.98	multi-decadal

To improve the understanding of the effects of each gap filling method, Taylor diagrams (Taylor, 2001) were used to summarise the statistical comparisons. These diagrams may improve the ability to choose a specific method over others. In general for the interannual component of sea level variability, the linear interpolation method shows the worst results (Fig. 2.11), with the exception of quasi-East London and quasi-Simons Bay data (Fig. 2.11C and G), where the linear interpolation method shows better results. While for quasi-East London, the high value of the sea level standard deviation and root-mean-square (RMS) error is behind this noticeable difference, the same cannot be said for quasi-Simons Bay.

A closer look at the records of both sites revealed that they do not show similar gap structure. At East London, the longest gap period observed is 6 years after installation of the tide gauge (see also Table 2.1). At Simons Bay, there is a 19 month gap almost at the end of the time series. It appears that the linear interpolation method yields stronger correlation values when long missing values are located at the beginning or the end of the data time span. The other two methods seem to perform better in the opposite way. This aspect will be discussed later when comparing the shapes of the ensemble mode.

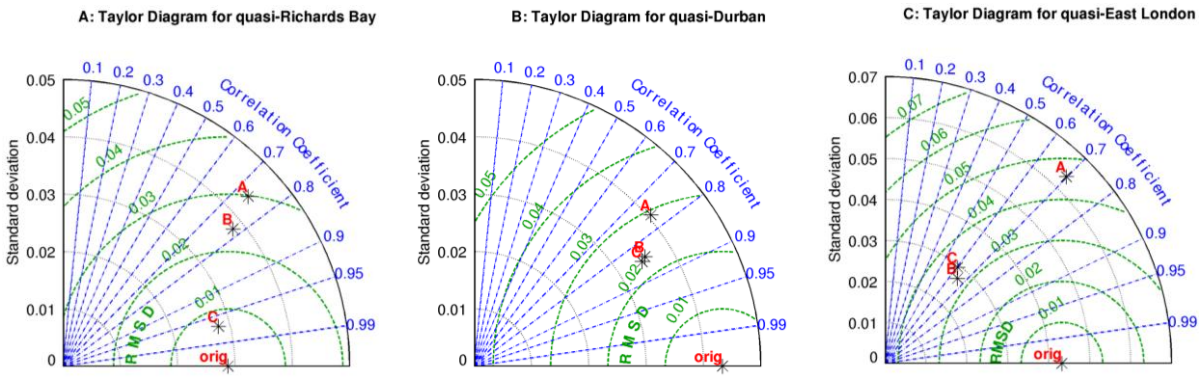

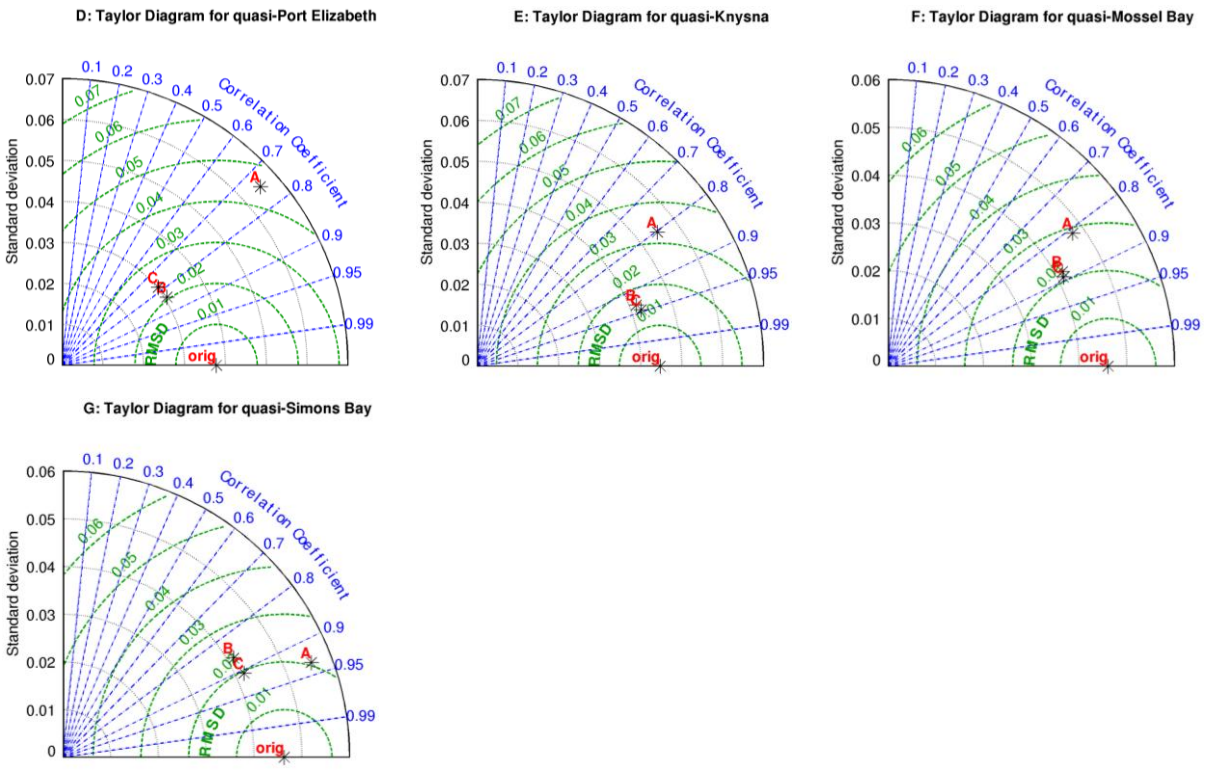

Fig. 2.11: Taylor diagrams for the synthetic monthly altimetry sea level data (in m) representing all studied sites. Statistics are related to the performance of the interannual component of each gap filling method. Orig indicates the original data without gaps; A, the linear interpolation method; B, the average value was used to replace the missing values; C, the missing values were filled with the value of the linear trend of the entire existing records.

The correlation between the multi-decadal components does not seem to be affected by the gap filling method applied (Fig. 2.12) except for quasi-Richards Bay, quasi-Durban and quasi-East London records (Fig. 2.12A, B and C), where correlation coefficients are not statistically similar. For quasi-Richards Bay and quasi-Durban, 0.86 is the lowest value and the data were filled by linear interpolation and the average value, respectively. For quasi-Mossel Bay (Fig. 2.12F), all gap filling methods show a similar correlation value of 0.97. This result may be due to the fact that the location has the second shortest gap period and the second longest time series record. This explanation seems to make sense when compared to the Port Elizabeth data set results (Fig. 2.12D). The Port Elizabeth records are the shortest (only 37 years) but they are compensated by the shortest gap period (18 consecutive months; see Tables 2.1 and 2.2 for more details).

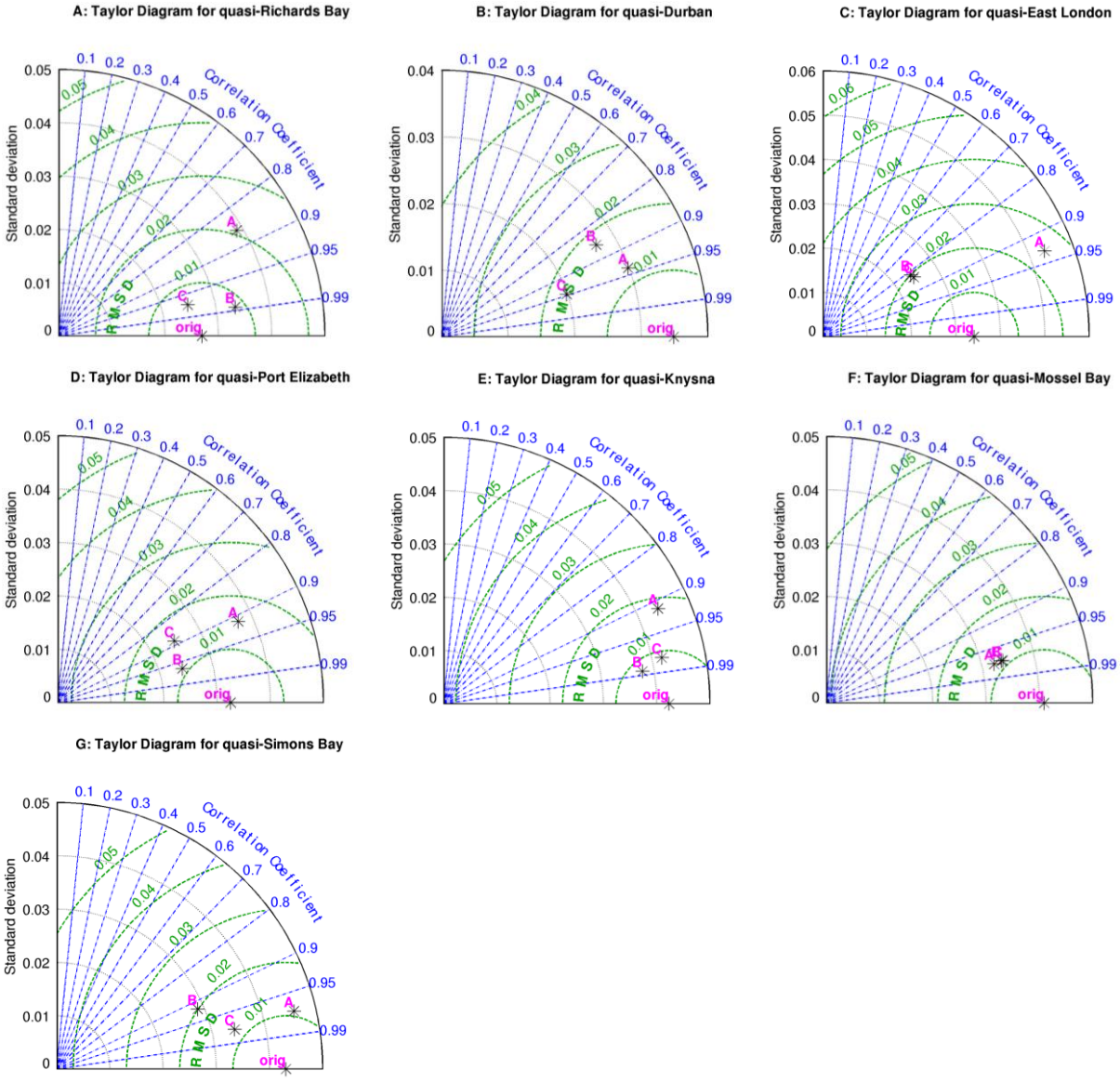

Fig. 2.12: Taylor diagrams for the synthetic monthly altimetry sea level data (in m) representing all studied sites. Statistics are in regard to the performance of multi-decadal component of sea level variability using each gap filling method. Orig indicates the data without gaps; A, the linear interpolation method; B, the average value was used to replace the missing values; C, the missing values were filled with the value of the linear trend of the entire existing records.

Fig. 2.13 illustrates the statistics for the trend using the Taylor diagrams for all studied locations. Overall, all gap filling methods give correlation coefficients higher than 0.95. Quasi-Richards Bay is an exception, where completely different results are found (Fig. 2.13A). For

quasi-Port Elizabeth, although the correlation and RMS difference values are numerically very close, the standard deviation values lead to noticeable differences (Fig. 2.13D). This suggests that for trend analysis the gap filling method does not significantly influence the result. In this regard, comparing the trend values seems to be the best approach. The latter is in agreement to the results from Ezer et al. (2016). The comparison with respect to the trend shape will be discussed below.

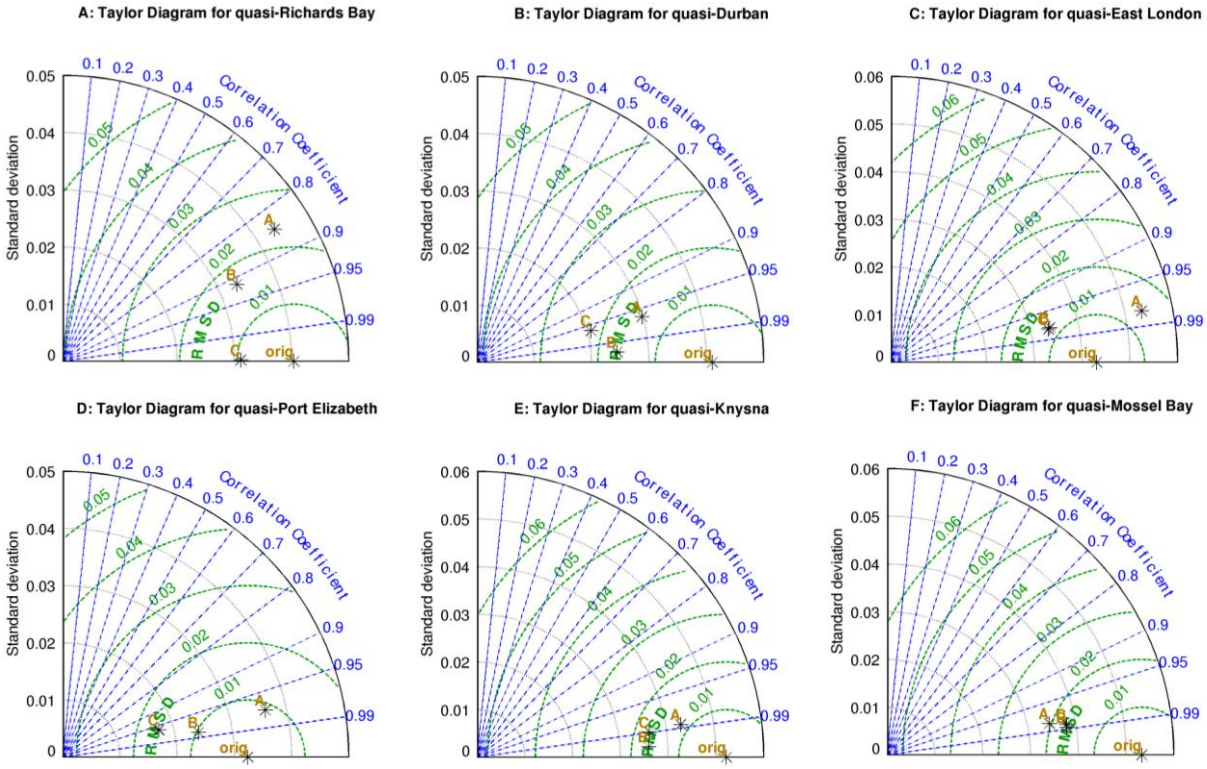

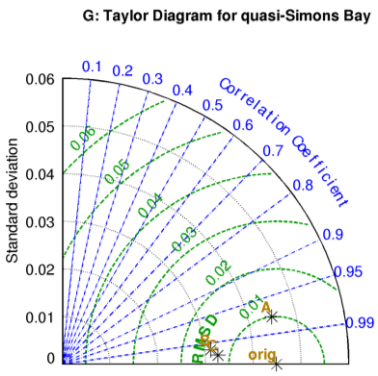

Fig. 2.13: Taylor diagram for the trends in synthetic monthly altimetry sea level records at all studied sites (in m). Orig indicates the data without gaps; A, the linear interpolation method; B, the average value was used to replace the missing values; C, the missing values were filled with the value of the linear trend of the entire existing records.

The same data were used to assess the impact of the gaps according to the tide gauge stations they represent. As mentioned above, it was decided that instead of producing subjective gaps, they should reflect the reality at sites to be discussed in Chapters 4 and 5. The results illustrated in Fig. 2.14 are an example of the results of such sensitivity experiments. When discussing sea level variations, correlation is sometimes not very meaningful. For example, two records can be considered as correlated if they show coherent variability. In order words, there is a need to assess the physical meaning of the results. This can be investigated using lag-correlation. Lagged correction coefficients tell you whether there is a temporal shift between two variables. Nevertheless, the correlations undertaken in this study are equivalent to lag-correlations at lag zero i.e. without lag.

The sub-annual components of sea level variability results are overall statistically similar (Table 2.2), i.e. there are no significant differences in the resulted correlation coefficients. In Fig. 2.14, the interannual components of sea level variability from the data representing all sites are shown. Overall, there is a good similarity in the variability of the original data and the data with gaps filled using the linear trend value (black line in Fig. 2.14) of the existing data sets. The results are comparable to the ones in which the gaps were filled by the mean value of the existing data sets (in red line, in Fig. 2.14). In fact, the linear trend value and the average value gap filling methods differ in terms of the magnitude of the amplitude. However, the linear

method value usually depicts variability of smaller amplitude. The linear interpolation method has the tendency of overestimating the amplitude. Disagreements with respect to the amplitude of the variability are observed over the time series.

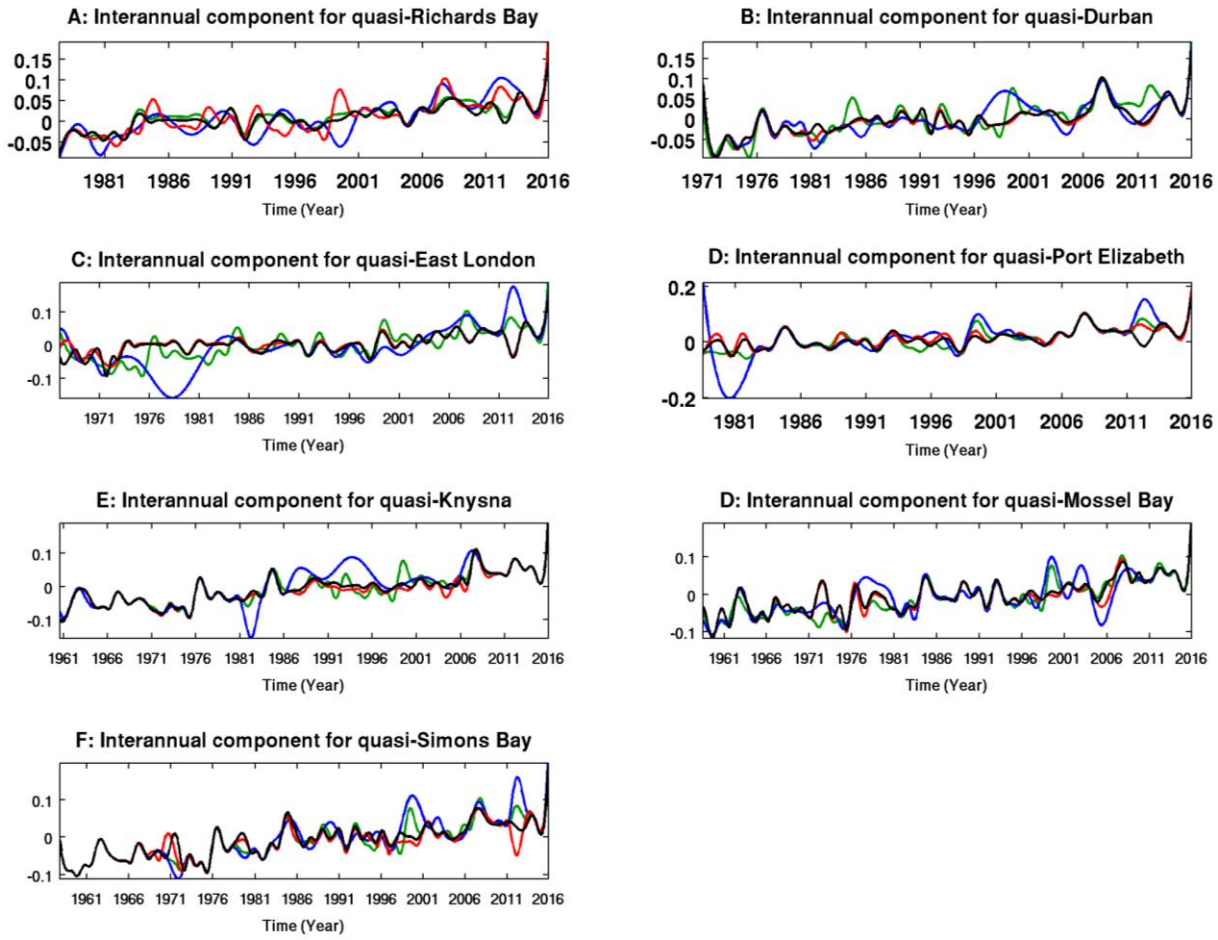

Fig. 2.14: A comparison between the synthetic monthly altimetry sea level data without gaps (green line) and the gap filled ones, by linear interpolation (blue line), by average value (red line) and by linear trend value (black line). In all panels the data are in metre. The comparison is only at the interannual component of sea level variability.

Fig. 2.15 depicts the variability of the multi-decadal components at all locations. In general, the component shapes are similar. All the gap filling methods seem to be robust enough to be used. For the multi-decadal component of variability, the disagreements are less pronounced. The drivers at this time scale may be more stable. On the other hand, the length of the records may not be long enough to capture profound changes. Examining method by method, it may be said

that the linear trend value filling exhibits better variability when compared with the original data. Studying the impact of the gaps in the ensemble of the low-frequency modes, Ezer et al. (2016) came to a similar conclusion. They conducted a sensitivity experiment where the created missing values represented 6 to 30% of the original records.

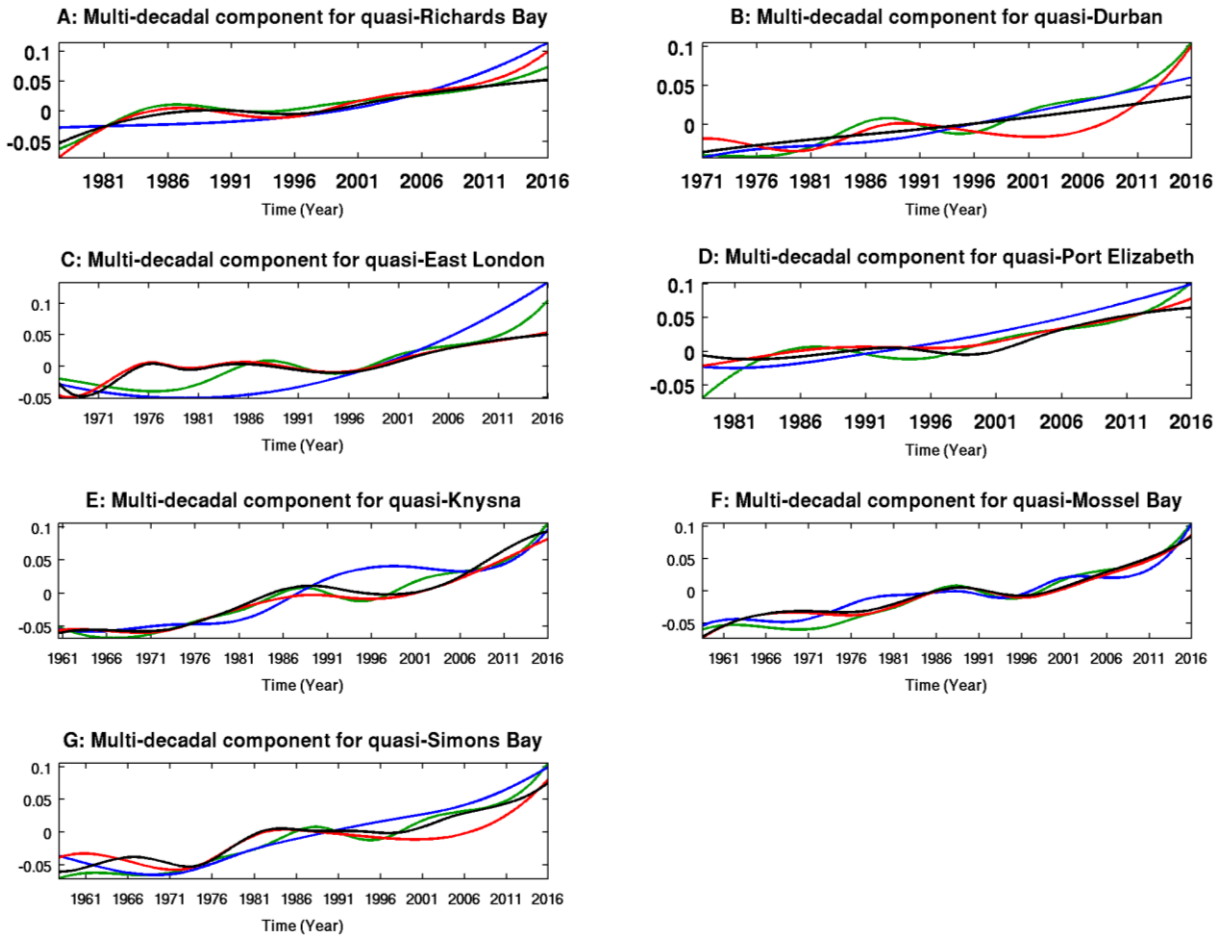

Fig. 2.15: A comparison at the multi-decadal component of sea level variability. In green is the synthetic monthly altimetry sea level data without gaps and the gap filled ones are represented by the blue line for the linear interpolation, red line for the average value and black line for the linear trend value, respectively. In all panels the data are in metre.

Different sea level EMD trend shapes are illustrated in Fig. 2.16. Despite the similarity observed, there is no gap filling method that may yield a result without error. It is noticeable that, in general, whichever method is used, underestimates occur. Moreover, filling the gaps with the

value of the linear trend seems to be the best method to be applied. The latter is consistent with results by Ezer et al. (2016). When they located five random gaps between 2 to 10 years with no overlap in the raw data without missing values, the estimated long-term trend exhibited quite similar results. This study suggests that although the ensemble of the modes differ in respect to the shape, data with gaps are reliable to draw consistent conclusion concerning to historical sea level variability and rise. Each gap filling method has its merit and its applicability will depend on factors such as gap length and time scale of variability in question.

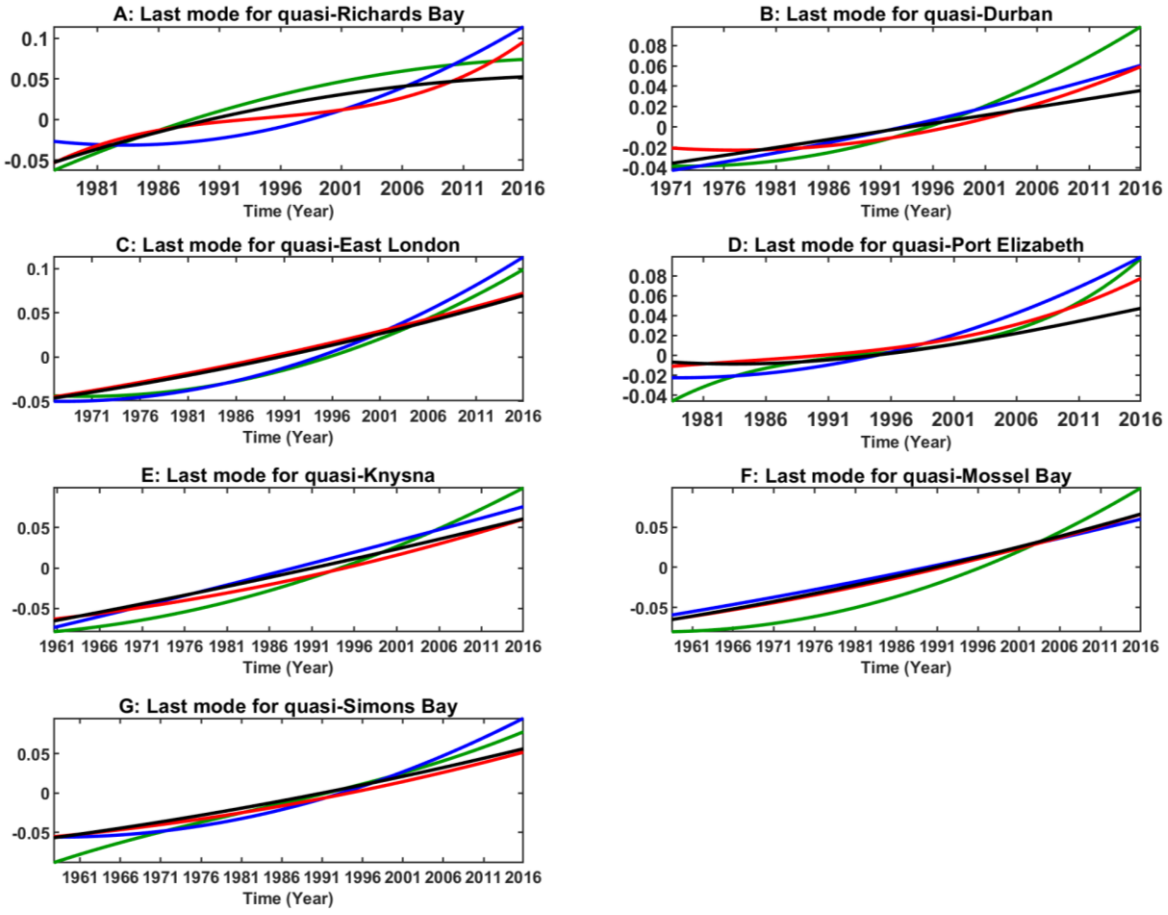

Fig. 2.16: The impact of the three gap filling methods on the residual mode, considered as the trend. The green line represents the synthetic monthly altimetry sea level data without gaps; the blue line indicates the linearly interpolated data; the red line represents the data filled by average value; the black line indicates the data filled by linear trend value. All the data are in metre.

Furthermore, the results suggest that when analysing data with gaps, the equation (2.10) should be defined as follows:

$$x_{(t)} = \sum_{j=1}^{N} C_{j(t)} + R_{(t)} + \varepsilon \tag{2.11}$$

Where ε represents all possible errors, for instance the error due to data gaps. A similar equation was suggested by Ezer et al. (2016). The determination of the trend rate is one of the main objectives in sea level research. With the challenge imposed by the data gaps, the trend rate for SLR estimation becomes problematic. Nevertheless, the mean sea level rise rate (MSLR, usually in mm/yr) for a time series $x_{(t)}$should be defined as follows:

$$MSLR = \frac{1}{\Delta t(M-1)} \sum_{i=1}^{M-1} (\mathrm{R_{i+1}} - \mathrm{R_i}) \tag{2.12}$$

In which $\Delta t = \frac{1}{12} y$, is the time in y; M is the number of monthly records, including the months with missing values. In this way, the mean acceleration of the observed sea level (ACC, in mm/yr^2) should be detected as follow:

$$ACC = \frac{1}{\Delta t^2(M-2)} \sum_{i=2}^{M-1} (\mathrm{R_{i-1}} - 2\mathrm{R_i} + \mathrm{R_{i+1}}) \tag{2.13}$$

Equations (2.12) and (2.13) give more insights into the sea level variability. As mentioned above, there is considerable debate regarding the trend and acceleration detection methods (Kenigson and Han, 2014; Chambers, 2015). The debate is allied to whether or not the derived trend from short records is part or not of a 60-year oscillation cycle (Chambers et at., 2012). Studies suggest that, at regional and local scale, focusing on separating and understanding the interannual and multi-decadal time scales within the sea level records may be wise before any attempt to calculate the acceleration (e. g. Woodworth, 1990; Douglas, 1992; Haigh et al., 2014). This happens because the possible underlying acceleration due to anthropogenic forcing

plays a major role on decadal and multi-decadal variability (Calafat and Chambers, 2013). Thus, the absence of an advanced understanding of this variability leads to a large uncertainty in the estimated acceleration over a short sea level record (Calafat and Chambers, 2013).

So far, it is still not clear which analysis method is suitable for estimation of the sea level rise acceleration (Visser et al., 2015) or which record length should be considered long enough for such a study. However, some studies point out that at least 50 years records are enough for estimating the acceleration (e. g. Douglas, 1992). It is argued that for a record length shorter than 50 years, decadal variability has a major impact on the acceleration rate. Nevertheless, due to the shortness of the studied data here, the trend and coefficient of acceleration values were not calculated in this study. However, the ability of the EMD method to separate the sea level data timescales was widely considered.

2.5. Summary and Conclusion

Monthly mean synthetic sea level records, representing seven individual tide gauges, from the south and east coast of South Africa were used to obtain the embedded timescales of variability. The Empirical Mode Decomposition method was used to separate the oscillating modes. The EMD method is an efficient and relatively simple method to obtain the timescales of variability within any sea level record.

It was shown that the other existing spectral analysis methods yield reliable results at high frequencies at 95 % confidence level. The EMD method is advantageous as it fragments the time series into a set of embedded frequency-dependent sub-time series, called Intrinsic Mode Functions. This capacity to display the energy-frequency-time distribution in such way made a huge difference for the objective of this study.

The study also served to test the sensitivity of the method when dealing with data gaps. The missing values were filled by linear interpolation, the average value and linear trend value. For a deeper understanding of the effects of data gaps, the timescales found were grouped as sub-annual, interannual and low-frequency components of sea level variability. As a result, the

correlation between the combined modes improved noticeably. However, whichever gap filling method is applied, results with some error should be expected.

Results suggest that, despite minor exceptions, filling the gaps with the linear trend value is the best way to obtain mode shapes similar to the ones from the data without gaps. The method is far better when the modes are combined. The sensitivity experiment may help, in future to draw better conclusions from data with certain gaps. Quadratic and cubic interpolations were also tested (not shown), having resulted in less accurate results when compared to linear interpolation. Given that the results for the various gap filling methods were not very convincing, it would be better exploring the possibility of eliminating or at least reduce the presence of the gaps by coupling other sea level data types in tide gauge records gaps prior to any further analyses of the tide gauge records.

CHAPTER 3

Creating a fuller time series of tide gauge records

3.1. Introduction

In Chapter 2, three gap filling methods were tested on synthetic monthly altimetry sea level (SL) records with artificial gaps created at the same locations as in the tide gauge SL measurements. (1) The commonly used linear interpolation method, in which missing values are filled by adjacent values. This method is recommended when short gaps are observed (Thomson and Emery, 2014). The length of gap to which it can be applied for monthly mean SL records is still not clear. (2) The gaps were filled by the average value of the entire synthetic SL records (e.g. Cheng et al, 2015). (3) The missing values were replaced by the value of the linear trend of the existing data sets (e.g. Ezer et al, 2016). The analyses suggest that no matter which gap filling method is applied, error should be expected in the results when applying the EMD method, indicating the need to embark on a journey of filling the gaps with independent observations whenever possible.

Tide gauges (TGs) measure important features of coastal processes (Prandi et al., 2009). However, their results are often questioned due to the occurrence of data gaps (Brundrit, 1984; Becker et al., 2009). Concern is usually increased due to the length and frequency of gaps in specific time series. Even when the data processing tools are designed to deal with data gaps, the presence of long gaps may cause doubt about the reliability of the conclusions. Thus efforts should be made to compare different SL data types, filling the gaps and hence improving their usefulness. Therefore, developing methods for coupling satellite altimetry observations to tide gauge records gaps is worth exploring (e.g. Becker et al., 2012; Meyssignac et al., 2012).

Satellite altimetry observations covering almost the entire globe (Church and White, 2011; White et al., 2014) have provided consistent and continuous data sets since the early 1990s (Fu and Le Traon, 2006; Church and White, 2011; Valladeau et al., 2012; Birol and Niño, 2015; Ablain et al., 2016). However, close to the coastline these data sets are flagged as unreliable (Birol and Niño, 2015; Cipollini et al., 2017) due to the complexity of the coastal dynamics allied to low sampling frequency compared to the tide gauges (Roblou et al., 2007, Passaro et al., 2014). As a result, several groups in different research institutions are investigating ways to improve their accuracy in the coastal zone (Roblou et al., 2007; Cipollini et al., 2010, Vignudelli et al., 2011; Stammer and Cazenave, 2017).

There are two main aspects to improving their accuracy: (i) the geophysical corrections and (ii) retracking the waveforms. The geophysical corrections include wet and dry troposphere corrections, ionosphere corrections and coastal tide and other coastal high-frequency signal corrections. These corrections must be applied everywhere, but they are particularly difficult in the coastal zone (Cipollini et al, 2010, Birol et al., 2016). The retracking of waveforms consists of retrieving the geometry of the waveforms when degradations are evident at the edge of the coastal waters, i.e. 10 km of the coastline (Cipollini et al., 2010; Passaro et al., 2014).

The accuracy of altimetry data close to the coast is continuously improving (Cipollini et al., 2010; Cipollini et al., 2017). This is being achieved due to a new generation of radars; ka-band (e.g. Vincent et al., 2006) and synthetic aperture altimeter (SRAL altimeter) also known as delay Doppler altimeter (e.g. Raney, 1998), together with the improved geophysical corrections and new re-tracking techniques (Cipollini et al., 2017).

There is a need to explore the possibility of filling the missing values at specific locations taking advantage of the adjacent tide gauge records (e.g. Brundrit, 1995; White et al., 2014). This is not particularly new along the coast of southern Africa. Brundrit (1995) filled tide gauge records gaps by interpolating the neighbouring station data sets. This procedure has been motivated by previous studies suggesting that the west and south coasts of southern Africa are dominated by the same mesoscale and synoptic weather systems (e.g. de Cueva et al., 1986). The question that always arises has to do with the maximum distance over which the interpolation can be

done; this is related to the need of two tide gauges to be well correlated and show coherent variability prior to any gap filling process.

The objective of this chapter is to create a fuller time series of tide gauge records. It was done by filling the data gaps with satellite altimetry observations. Before the era of satellite altimetry observations, gaps were filled in with the records of the adjacent tide gauge site, where possible.

This Chapter is structured as follows: the data and the analysis method are described in Section 2, the Results and Discussion are presented in Section 3, and the Summary and Conclusion are given in Section 4.

3.2. Data and Methods

3.2.1. Data

3.2.1.1 Tide gauge records

Tide gauge records from seven sites along the east and south coast of South Africa were used in this study (Fig. 3.1). The data consisted of all available monthly means obtained from Permanent Service for Mean Sea Level (PSMSL; Holgate et al., 2013; PSMSL, 2017; http://www.psmsl.org/) until December 2015. Monthly means of sea level data are suitable for determining changes ranging from months to years (Brundrit, 1984). This may reveal, depending on the record length, seasonal to decadal and/or multi-decadal signals linked to different local, regional and/or large scale drivers.

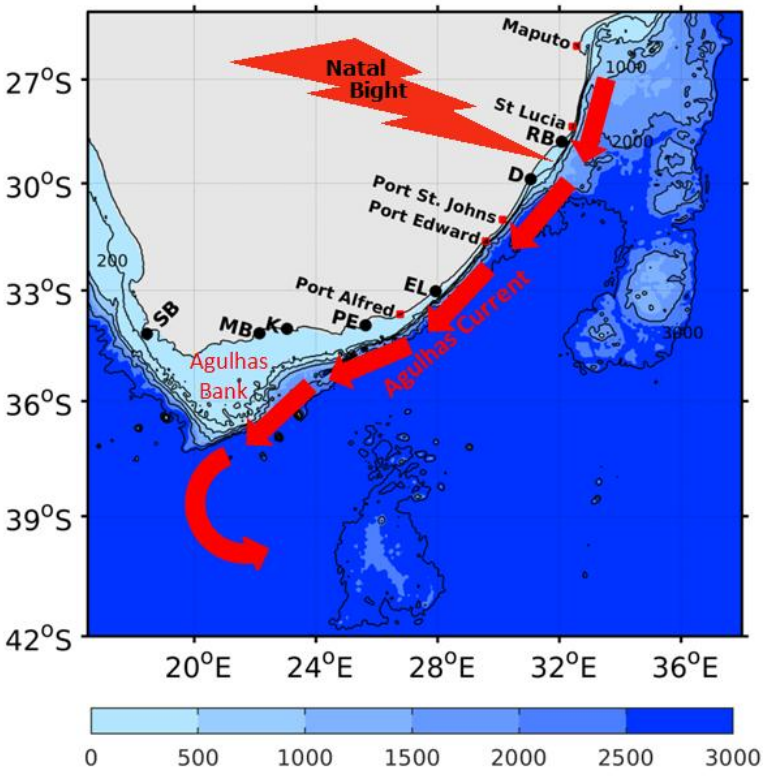

Fig. 3.1: Bathymetric map (m) and tide gauges locations (solid black dotes). RB, D, EL, PE, K, MB and SB indicate Richards Bay, Durban, East London, Port Elizabeth, Knysna, Mossel Bay and Simons Bay tide gauges sites, respectively.

However, TGs provide the sea level relative to the level of the continental crust, also known as relative sea level (RSL; Emery and Aubrey, 1991). The relative sea level contain the vertical motion of either the sea or land surface due to contributors such as glacial isostatic adjustment (GIA), earthquakes, groundwater depletion, sediment compaction and present day land ice melt (in a similar fashion as GIA) (e.g. Prandi et al., 2009). While satellite altimetry measures the sea level with respect to the geoid, and hence it is also known as the absolute sea level (Peltier, 1998; Tamisiea, 2011; Tamisiea and Mitrovica, 2011). As a consequence, the raw monthly TG sea level records need to be corrected for the effects of the meteorological forcing and the land motion so that can be comparable with satellite altimetry observations, as demonstrated by many studies (Cazenave et al., 1999; Nerem and Mitchell, 2002). Indeed, atmospheric corrections should also be conducted out on satellite altimetry observations, which were done

for this level of altimetry products by the data provider (Mertz et al., 2017). The details in which tide gauge sea level records corrections were made in this study are described below.

3.2.1.2 Satellite altimetry data

The most appropriate data sets would be the coastal altimetry data, generated under several projects and provided at approximately 350 and 175 m along track distances (Cipollini et al., 2017). However, not all the satellite ground tracks hit the land near the studied tide gauge locations apart from the disadvantage of temporal sampling frequency. To overcome the limitation associated with the temporal sampling frequency of the along track altimetry data, daily gridded products were chosen over the simple along track product. The altimetry data were based on the gridded multi-mission AVISO (Archiving, Validation and Interpretation of Satellite Oceanographic Data; http://www.aviso.altimetry.fr/) altimetry observations from January 1993 to December, 2015. The data are currently distributed by the Copernicus Marine and Environment Monitoring Service (CMEMS; http://www.marine.copernicus.eu). The data were averaged to obtain monthly means, similar to the sampling frequency of the *in situ* time series.

Altimetry multi-mission (Jason-3, Sentinel-3A, HY-2A, Saral/AltiKa, Cryosat-2, Jason-2, Jason-1, T/P, ENVISAT, GFO, ERS1/2) data are available as 1/4°×1/4° Mercator projection grids (WGS 84 (EPSG 4326)). Each singular satellite mission is homogenised in regard to OSTM/Jason-2, the current reference mission. The sea level anomalies (SLA) are computed in relation to the twenty-year mean (1993-2012; Maheu et al., 2013). The data sets are produced in delayed-time based on the Geophysical Data Records (GDR). More details and description about the data sets are available from Mertz et al. (2017).

3.2.2. Methods of Analysis

Tide gauge records were divided into two data subsets, representing the satellite altimetry era (1993 and following years) and the period before (pre-1993). Two different gap filling processes

were investigated. Before filling the data gaps, the below corrections were applied to all data for the entire time series at each location.

3.2.2.1 Inverse barometer effect

Previous studies have demonstrated that atmospheric pressure fluctuations have measurable effects on oceanic motions (Wunsch and Stammer, 1997). Therefore, the *in situ* measurements were corrected for atmospheric loading through the well known Inverse Barometer (IB) effect (Doodson, 1924; Wunsch and Stammer, 1997). A simple IB correction is deemed sufficient, i.e. there is no need to apply a dynamic high-frequency atmospheric correction as the IB is a good approximation of the whole effect in open seas and probably in this area.

The reanalysis monthly sea surface pressure data from the National Centres for Environmental Prediction/National Centre for Atmospheric Research (NCEP/NCAR; Kalnay et al., 1996; http://www.ncep.noaa.gov/) were used for such correction. The data are gridded with 2.5 degree resolution in both latitude and longitude, in Pascal's (Pa), from the 1st of January, 1948 to the present. Thus, monthly sea surface pressure data sets were extracted at the nearest grid point to each tide gauge location. Then at any tide gauge site, the correction to IB was done using the following equation:

$$RSL_{IB} = RSL - IB \tag{3.1}$$

Where:

$RSL_{IB}$is the oceanic sea level change. RSL is the tide gauge relative sea level in metre. IB is the inverse barometer effect leading to oceanic sea level change. The IB was found through the equation:

$$IB = -\frac{D_P}{\rho_0 g} \tag{3.2}$$

In which:

$D_P$is the pressure fluctuations leading to IB effect in millibar. $\rho_0$is the reference density of sea water taken as 1025 kilogram per cubic metre and g is the local gravity in square metre per second. The pressure fluctuations are defined as the deviations from the mean over the time span of each tide gauge record.

3.2.2.2 Vertical land movement

The vertical land movement (VLM) can be directly assessed if the tide gauges are equipped with a global positioning system (GPS; Woppelmann et al., 2007). Since the studied region is not populated with such equipment and the existing ones do not provide long and reliable data sets, the assessment was done indirectly. The indirect correction to the VLM is done through the glacial isostatic adjustment (GIA), also known as the post glacial rebound. The GIA is the most modelled and known contributor to the VLM among others that include ground water and oil extraction, ground subsidence associated with sediment loading (e.g., in large river deltas) and, tectonic and volcanic deformation (Prandi et al., 2009). Hence, even when removing GIA from TGs the measured sea level is still relative and not directly comparable to satellite altimetry, although by approximation it can be done after removing any datum differences.

Monthly tide gauge SL records were corrected for GIA using the ICE-5G (VM2) model output (Peltier, 2004). The GIA data sets can be obtained from the PSMSL webpage already extracted for each tide gauge location. The VM2 designation refers to the radial variation of viscosity in the sub-lithosphere mantle (Peltier, 1998). Basically the GIA data sets, express the vertical velocity of the crust due to mass redistribution during a glacial cycle (Whitehouse, 2009; Tamisiea, 2011; Tamisiea and Mitrovica, 2011). Previous studies have shown that it is actually a

small fraction within the RSL, but not negligible when assessing sea level changes accurately (Tamisiea, 2011; Tamisiea and Mitrovica, 2011).

As a result, at each location, there is a need to calculate and subtract the magnitude of the monthly vertical land movement within tide gauge measurements provided by the PSMSL. In this study the following equation was used:

$$SSH = RSL_{IB} + VLM \tag{3.3}$$

In which:

SSH is the sea surface height. $RSL_{IB}$is the oceanic sea level change. VLM is the vertical land movement. For each time t, in month and with t_0 the origin of the time reference, the VLM was calculated using the equation:

$$VLM = GIA * (t - t_0) \tag{3.4}$$

3.2.2.3 Detrending and deseasoning the data

Prior to any comparison between the data sets, the time series were detrended and deseasoned to leave correlation due to the interannual signals. Concurrently, detrending and deseasoning the data helped to overcome the challenge of SL data referencing. With each tide gauge referenced to the local datum and the altimetry to the geoid, obtaining a common reference is always a challenge (Prandi et al., 2009). Previous studies have applied various methods to obtain a common reference such as computing the overlapping decadal mean sea level rates for each record (Holgate and Woodworth, 2004; Jevrejeva et al., 2006; Holgate, 2007), subtracting from each tide gauge record its mean value computed over the studied time span (Brundrit, 1995; Prandi et al., 2009).

3.3. Results and Discussion

3.3.1 During satellite altimetry era

In situ time series, adjusted to GIA and IB effects and then detrended with the seasonal cycle removed, were correlated to altimetry observations, also detrended with the seasonal cycle removed. Fig. 3.2 shows the correlation between TG measurements and regional altimetry observations. This helps identify areas within altimetry observations with strong correlations to sea level variability at each tide gauge location. Unless stated otherwise all correlations undertaken in this study were at 95 % confidence level..

The hypothesis is that: (i) strong correlations between tide gauge SL records and altimetry SL observations may be obtained along the coastline and (ii) the east and south coast may exhibit distinct correlation patterns, with the region around East London as the transition zone. With minor exceptions, the results seem to support these hypotheses (Fig. 3.2).

There is a strong correlation over the region in which Richards Bay and Durban tide gauges are located (Fig. 3.2A and B). This region corresponds to the so called Natal Bight (e.g. Lutjeharms et al., 2000; van Leeuwen et al., 2000; Lutjeharms, 2006), although the grid points with highest correlation coefficients propagate further downstream. East London and Port Elizabeth depict the lowest correlations values (Fig. 3.2C and D). On the other hand, the same tide gauge stations do not exhibit correlation patterns consistent to the above-mentioned hypothesis. Given the correlation patterns displayed in Fig. 3.2C and D, it is clear that the intermediate region of East London and Port Elizabeth make the transition between south and east coast. Knysna and Mossel Bay also share a similar correlation patterns, displaying a clear separation between south and south-east coast of South Africa (Fig. 3.2E and F). The Fig. 3.2 also illustrates that Simons Bay SL records are well correlated to south-west coast sea surface heights.

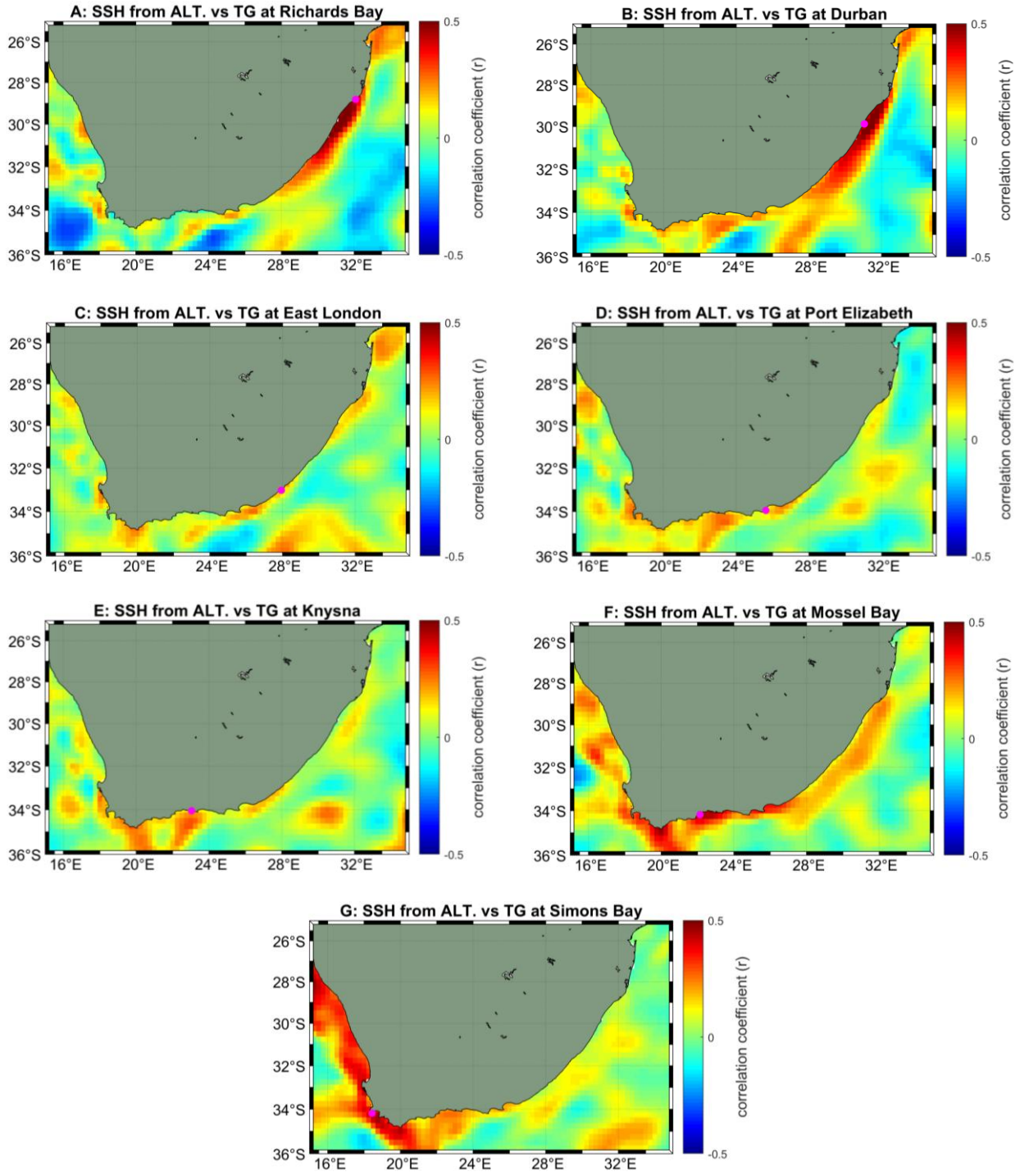

Fig. 3.2: Correlation between regional satellite altimetry observations and tide gauge records at: (A) Richards Bay, (B) Durban, (C) East London, (D) Port Elizabeth, (E) Knysna, (F) Mossel Bay and (G) Simons Bay, respectively. Magenta solid dote indicates the tide gauge location. The tide gauges are organised from east to south coast.

In all panels, there is a correlation separation zone, portrayed as a weak correlation area over the Agulhas Bank, between Mossel Bay and Simons Bay (see Fig 3.1 for more details on the bathymetry of the region). The separation area appears over the widest part of the bank. According to Lutjeharms (2006), at its widest the Agulhas Bank is 250 km wide, this area marking the division between the eastern and western Agulhas Bank. These two sub-regions of the bank have distinct characteristics. But sea level is probably influenced by the difference in the off-shelf currents on either side of the bank (e.g. Lutjeharms, 2006) that may explain the features noticed in Fig. 3.2. The eastern and western Agulhas Bank are dominated by warm and cold waters from of the intense southern Agulhas Current and sluggish Benguela Current, respectively (Lutjeharms, 2006). Additionally, the current starts to meander near Port Elizabeth and these meanders grow in amplitude downstream and there is a presence of a lee eddy directly to the east of the Agulhas Bank.

Having identified how the regional altimetry data sets correlate to each tide gauge sea level record, the area was reduced to a 1x1 degree rectangular box around each tide gauge location. Thus the comparisons between altimetry data sets and tide gauge sea level records were only made when the maximum distance between them is at most 100 km and the results are displayed in a rectangular box instead of a circular domain (Fig. 3.3). Using this method one still captures similar oceanic variability and reduces the error linked to the mean sea surface of a single altimetry point (Valladeau et al., 2012). The colour scales were not adjusted to the same range so that the grid point with highest correlation coefficients may easily identified. Strong correlation values are found one or two grid points from the tide gauge location. Weak correlations are observed between East London and Knysna. The reason for these correlation values was not further investigated as beyond the objectives of this study.

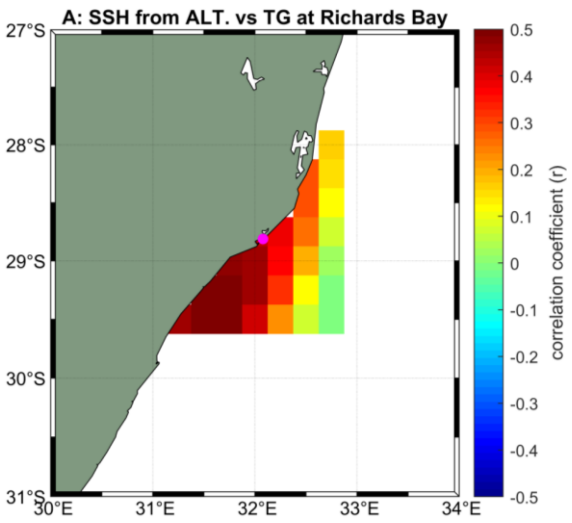
A: SSH from ALT. vs TG at Richards Bay
27°S
28°S
29°S
30°S
31°S
30°E
31°E
32°E
33°E
34°E
0.5
0.4
0.3
0.2
0.1
0
-0.1
-0.2
-0.3
-0.4
-0.5
correlation coefficient (r)

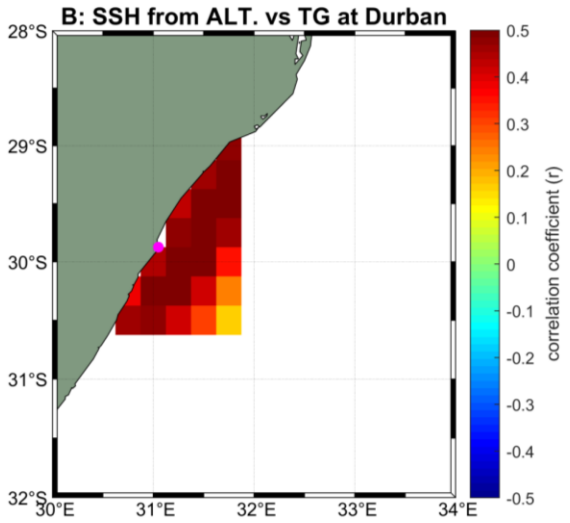
B: SSH from ALT. vs TG at Durban
28°S
29°S
30°S
31°S
32°S
30°E
31°E
32°E
33°E
34°E
0.5
0.4
0.3
0.2
0.1
0
-0.1
-0.2
-0.3
-0.4
-0.5
correlation coefficient (r)

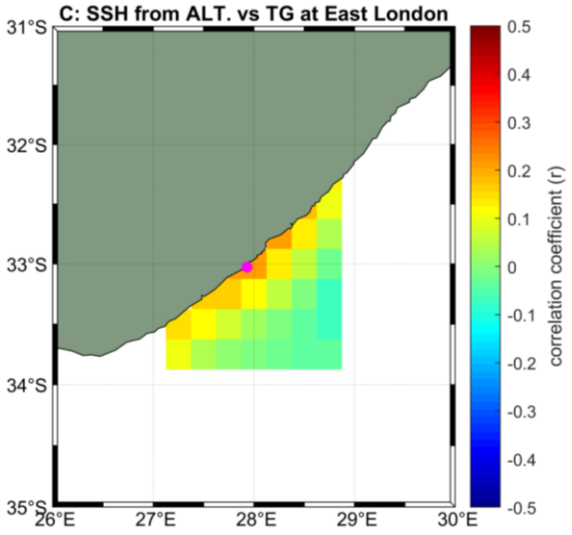
C: SSH from ALT. vs TG at East London
31°S
32°S
33°S
34°S
35°S
26°E
27°E
28°E
29°E
30°E
0.5
0.4
0.3
0.2
0.1
0
-0.1
-0.2
-0.3
-0.4
-0.5
correlation coefficient (r)

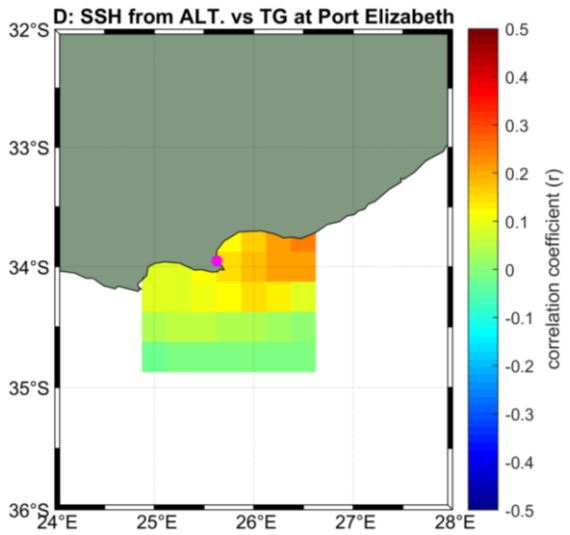
D: SSH from ALT. vs TG at Port Elizabeth
32°S
33°S
34°S
35°S
36°S
24°E
25°E
26°E
27°E
28°E
0.5
0.4
0.3
0.2
0.1
0
-0.1
-0.2
-0.3
-0.4
-0.5
correlation coefficient (r)

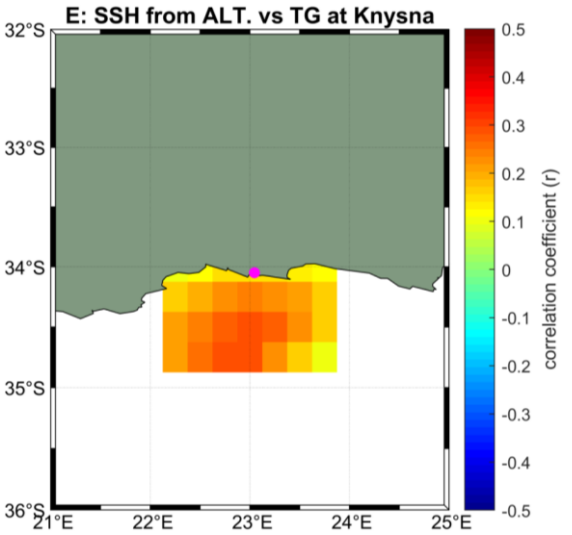
E: SSH from ALT. vs TG at Knysna
32°S
33°S
34°S
35°S
36°S
21°E
22°E
23°E
24°E
25°E
0.5
0.4
0.3
0.2
0.1
0
-0.1
-0.2
-0.3
-0.4
-0.5
correlation coefficient (r)

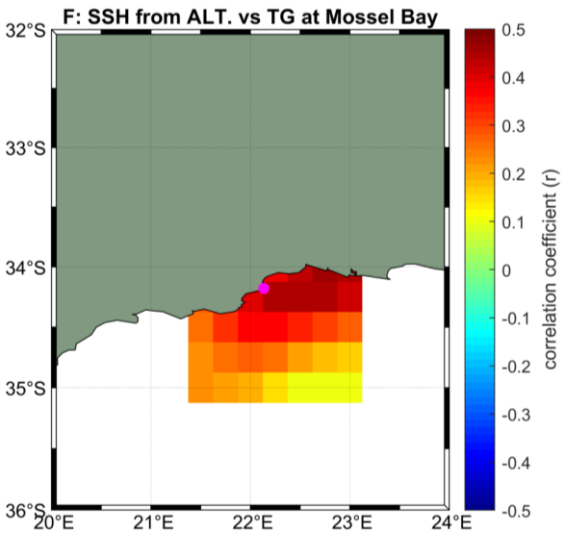
F: SSH from ALT. vs TG at Mossel Bay
32°S
33°S
34°S
35°S
36°S
20°E
21°E
22°E
23°E
24°E
0.5
0.4
0.3
0.2
0.1
0
-0.1
-0.2
-0.3
-0.4
-0.5
correlation coefficient (r)

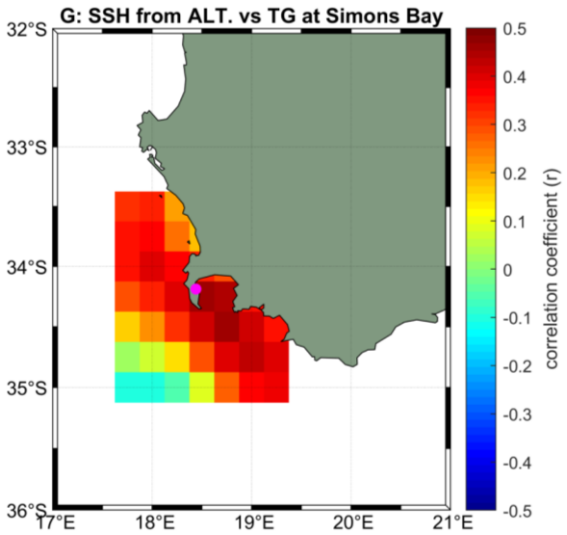

Fig. 3.3: Correlation between tide gauge records and satellite altimetry observations over one degree around the tide gauge locations, (A) Richards Bay, (B) Durban, (C) East London, (D) Port Elizabeth, (E) Knysna, (F) Mossel Bay and (G) Simons Bay, respectively. Magenta solid dote indicates the tide gauge location.

From each subset (each panel in Fig. 3.3), the data sets were extracted at grid points with maximum correlation to tide gauge sea level records. No correlation value threshold was defined. This choice takes into account the coastal dynamics over the region which is strongly influenced by the Agulhas Current. We are aware that the Agulhas Current signals may not well be captured by the satellite altimetry observations due to a number of reasons including the sampling frequency. Various authors have applied different correlation value thresholds according to the purpose of their studies (e.g. Mitchum, 1998; Becker et al., 2012; Meyssignac et al., 2012; Valladeau et al., 2012). In an exploratory analysis (not shown), it was found that the highest correlations are within the period of the Jason-2 satellite mission. Nevertheless, the order in which the correlations were the highest was not quantified given the scope of this study.

The data sets during this satellite mission are a blend of the largest number of satellite missions; this may explain the strongest correlation values found. Another explanation could be the improvements to the geophysical corrections and new re-tracking techniques (Cipollini et al., 2017) together with the new generation of radars (e.g. Vincent et al., 2006; Raney, 1998).

Table 3.1 shows the statistics of the comparisons between SL at grid point with the maximum correlation to the in situ SL records.

Table 3.1: The summary of the statistics for satellite altimetry era. r indicates the correlation coefficient. rmse indicates the root mean square error.

station	r	Altimetry std (cm)	TG std (cm)	rmse (cm)
Richards Bay	0.52	4.57	7.24	6.24
Durban	0.54	4.88	6.63	5.63
East London	0.21	3.87	9.57	9.48
Port Elizabeth	0.24	3.35	5.93	6.07
Knysna	0.30	2.70	9.32	8.88
Mossel Bay	0.45	2.88	3.77	3.55
Simons Bay	0.46	2.54	2.23	2.53

Fig. 3.4 depicts correlation between altimetry time series at grid points with maximum correlation to tide gauge time series and regional gridded altimetry data sets. The objective was to identify correlation areas in order to group tide gauges into regions. Fig. 3.4 also tests the second hypothesis in which the east and south coast may exhibit distinct correlation patterns, having the region around East London as the transition zone.

As can be seen, only Richards Bay and Durban (Fig. 3.4A and B) have a similar correlation pattern, consistent with Fig. 3.2. This may indicate that over the Natal Bight there are specific coastal dynamics processes (e.g. Lutjeharms et al., 2000; van Leeuwen et al., 2000; Lutjeharms, 2006) that influence both tide gauges. The correlation maps of East London and Port Elizabeth display a very narrow correlation area, hence limited to the coastline (Fig. 3.4C and D). This may be influenced by the very narrow continental shelf and the strong Agulhas Current (Lutjeharms, 2006), although around Port Elizabeth the shelf starts widening downstream. Previous studies have indicated Port Elizabeth as the region of the separation between the stable northern Agulhas Current and the unstable southern Agulhas Current (e.g. Lutjeharms, 2006; Paldor and Lutjeharms, 2009). At Knysna and Mossel Bay (Fig. 3.4E and F) the area of strongest correlation is slightly different. This may be surprising for such neighbouring places (see also Table 3.2). On

the other hand, the figure depicts two distinct correlation zones in the south coast, separated around Mossel Bay, in agreement with Fig. 3.2.

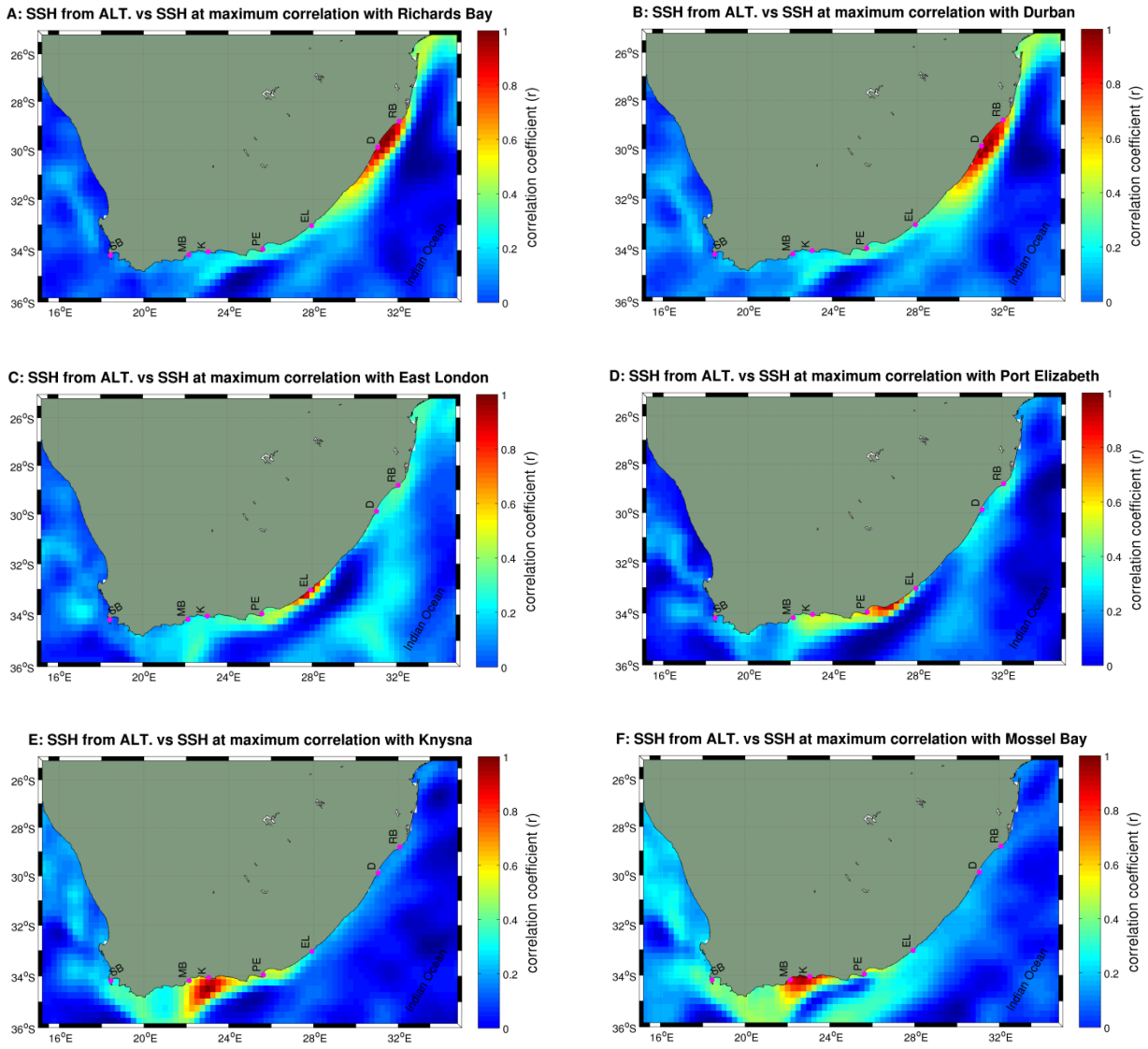

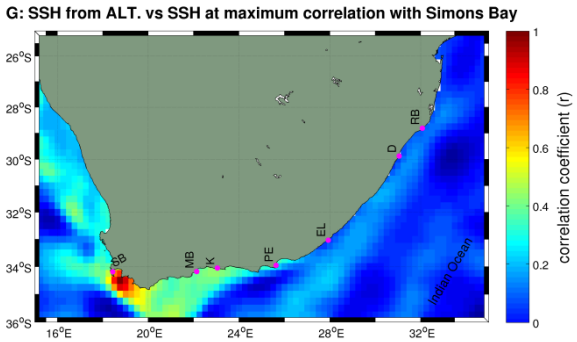

Fig. 3. 4: Correlation between SLA at grid points well correlated to the each tide gauge location and the regional satellite altimetry observations: (A) Richards Bay, (B) Durban, (C) East London, (D) Port Elizabeth, (E) Knysna, (F) Mossel Bay and (G) Simons Bay, respectively.

For a deeper understanding on the correlation between different sort of data sets representing the tide gauges sites, the analysis was conducted from another perspective. Fig. 3.5 illustrates such analysis in which the goal was to get insight into how sea level time series at different locations correlate with each other. It is noticeable that altimetry sea level data sets lead to different correlation values when compared to tide gauge records.

In general, although the time spans differ, the entire tide gauge sea level time series show similar correlation shapes to the same data source during the altimetry period. This may be attributed to the number of points used for each correlation analysis, in which they are deeply affected in the *in situ* time series by data gaps. The same reason may explain why the correlation line of the period prior to satellite altimetry is so distinct. To some extent, the red line is not consistent with Fig. 3.4. For instance, there is a good correlation between Mossel Bay and Simons Bay while two distinct zones are clear in Fig. 3.4. A further analysis points to the absence of a good correlation at lag-0 at the above-mentioned sites.

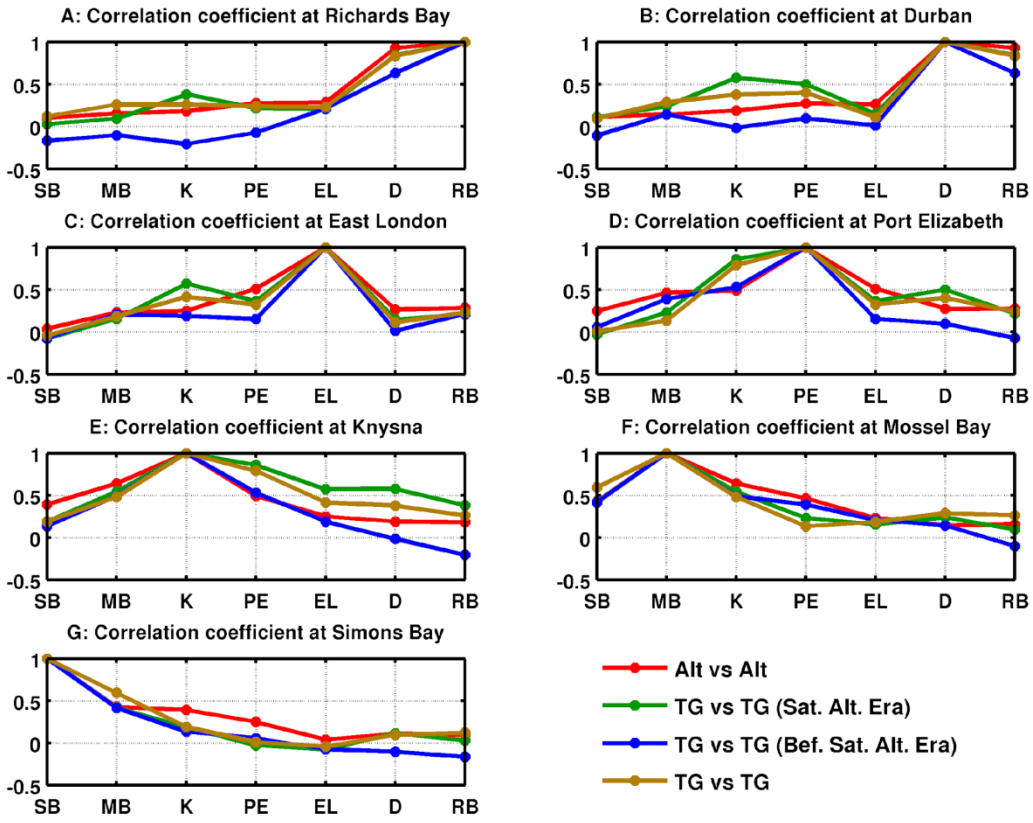

Fig. 3. 5: Summary of the correlations of different data sets and time spans. Red lines indicate the correlation between altimetry data sets from the grid point with the maximum correction to each tide gauge measurements. Green lines represent the correlation between tide gauge time series in the satellite altimetry era alone. Blue lines give the correlation between tide gauge time series prior to satellite altimetry alone. Brown lines illustrate the correlation of the entire tide gauge records at each site.

Fig. 3.6 depicts an overlay of the altimetry and tide gauge measurements for comparison. Fig. 3.6 depicts trends and jumps in both data sets, which enable the visualization of the possible differences prior to any gap filling process. In general, both sets of data show similar variability structure both in amplitude and high and low frequency variability.

At Richards Bay and Durban (Fig. 3.6A and B), *in situ* measurements show two batches of isolated high values that do not appear in the altimetry data sets. Also, at Richards Bay the altimetry depicts higher values than the tide gauge on two occasions. Still at Richards Bay, it is noticeable that around 2005 there was an event that forced the sea level to sink although it is more pronounced in the tide gauge records. From November to December 2002 there was a

remarkable event, mainly because it is consistently observed at Durban, East London, Port Elizabeth and Knysna (Fig. 3.6B, C, D and E). Unfortunately this event was not captured in the altimetry observations. Also, there are occasionally, higher and lower values in the tide gauge records that are not replicated in the altimetry at East London, Knysna and Mossel Bay (Fig. 3.6C, E and F). In contrast, at Simons Bay the tide gauge does not show some measurements as high as the altimetry (Fig. 3.6G).

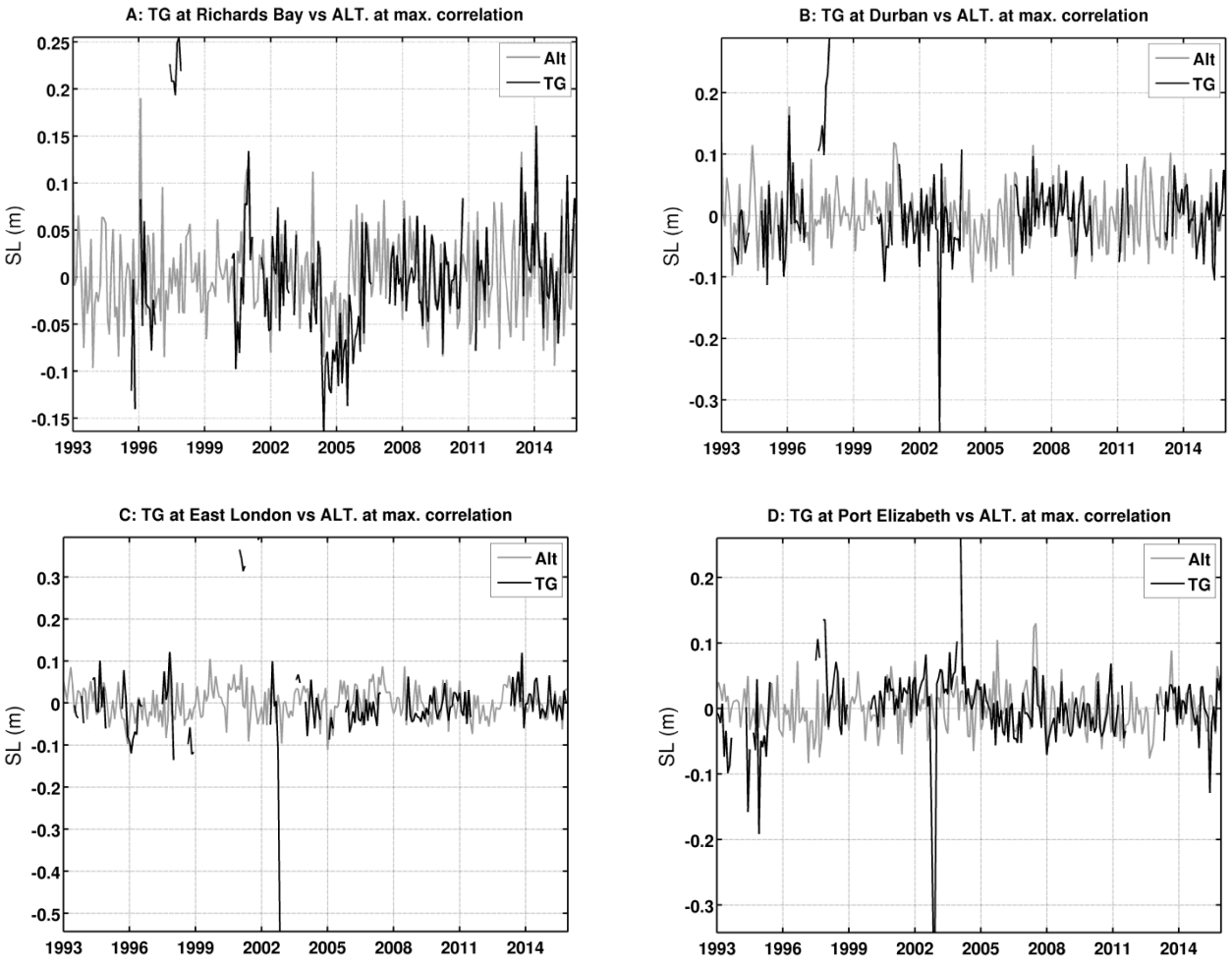

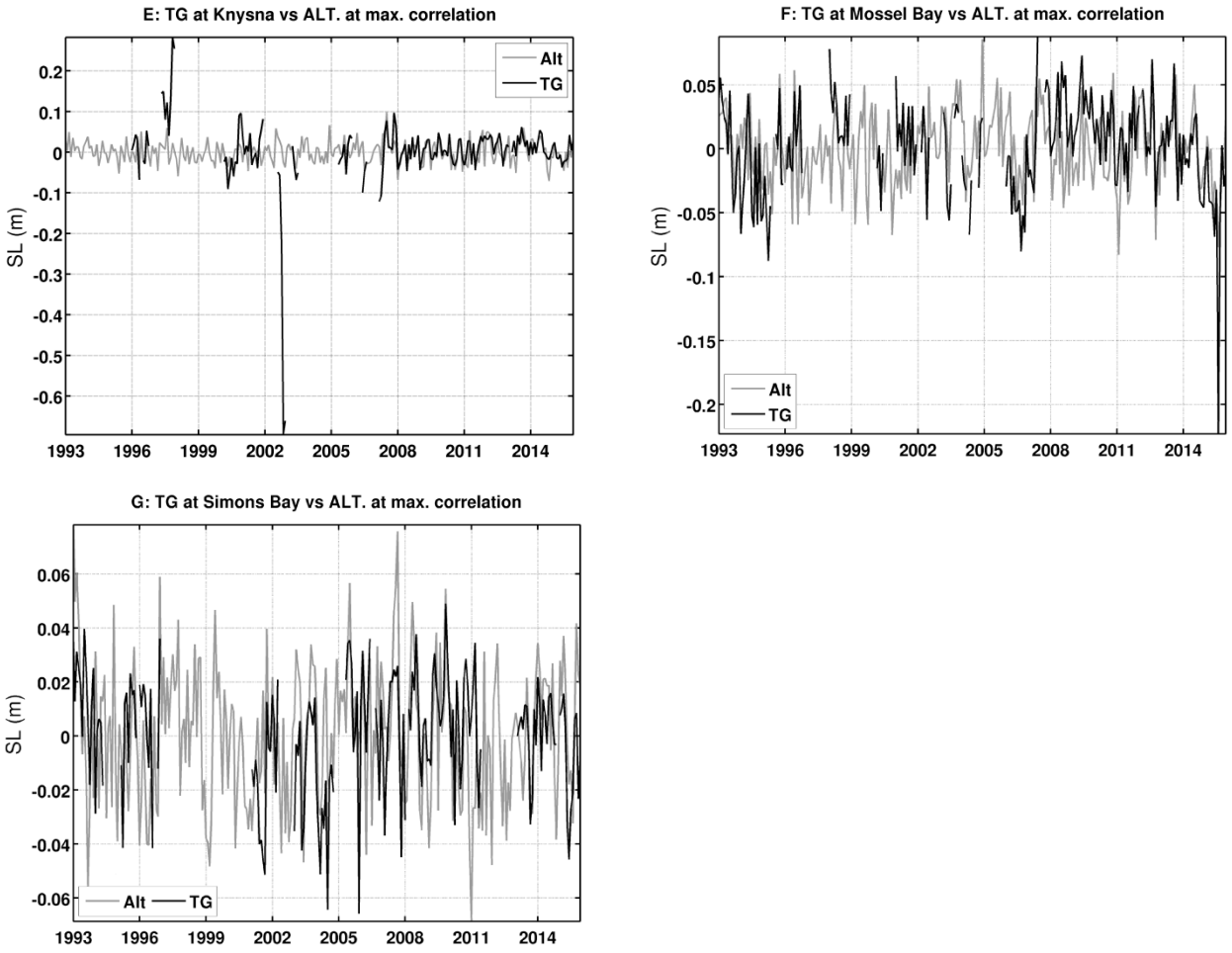

Fig. 3. 6: Comparison between satellite altimetry data at grid points with the strongest correlation and tide gauge records at (A) Richards Bay, (B) Durban, (C) East London, (D) Port Elizabeth, (E) Knysna, (F) Mossel Bay and (G) Simons Bay, respectively. Black lines represent the tide gauge time series and grey lines indicate the altimetry measurements from the grid points with maximum correlation.

It has been suggested by Garland and Mather (2007) and Mather et al. (2009) that sea level records from several tide gauges around southern Africa display some problems. According to them, mainly during the period 1998 to 2002, the recorded data sets were confused with the mean level, resulting in a datum shift. The error was inadvertently introduced in the derivation of the chart datum to land levelling datum conversion. As a consequence, for the period 1998 to 2002 artificially raising sea levels were noticeable. However, tide gauges records of the above mentioned period are largely not found from PSMSL archive. Garland and Mather (2007) corrected the shift in datum using monthly mean sea level records at Durban taking into

account that the mean sea level at Richards Bay, Durban and East London is approximately +0.2 m. None of these corrections have been made in the present study because any of these problems were not seen in the data.

All the descriptions so far have the ultimate goal of using the satellite altimetry data sets to fill the gaps in the *in situ* records. Tide gauge time series combined with altimetry data sets in the gaps to compose a new time series, are depicted in Fig. 3.7. The new time series are superimposed on the altimetry time series in each panel. As mentioned in the introduction, the decision concerning the removal of outliers will be made in Chapter 4, after assessing their impacts. However, it is worth mentioning that the decision will be mainly challenged by the events that have occurred in more than one site. At this stage it may seem prudent to remove all outliers, no matter how consistent the events.

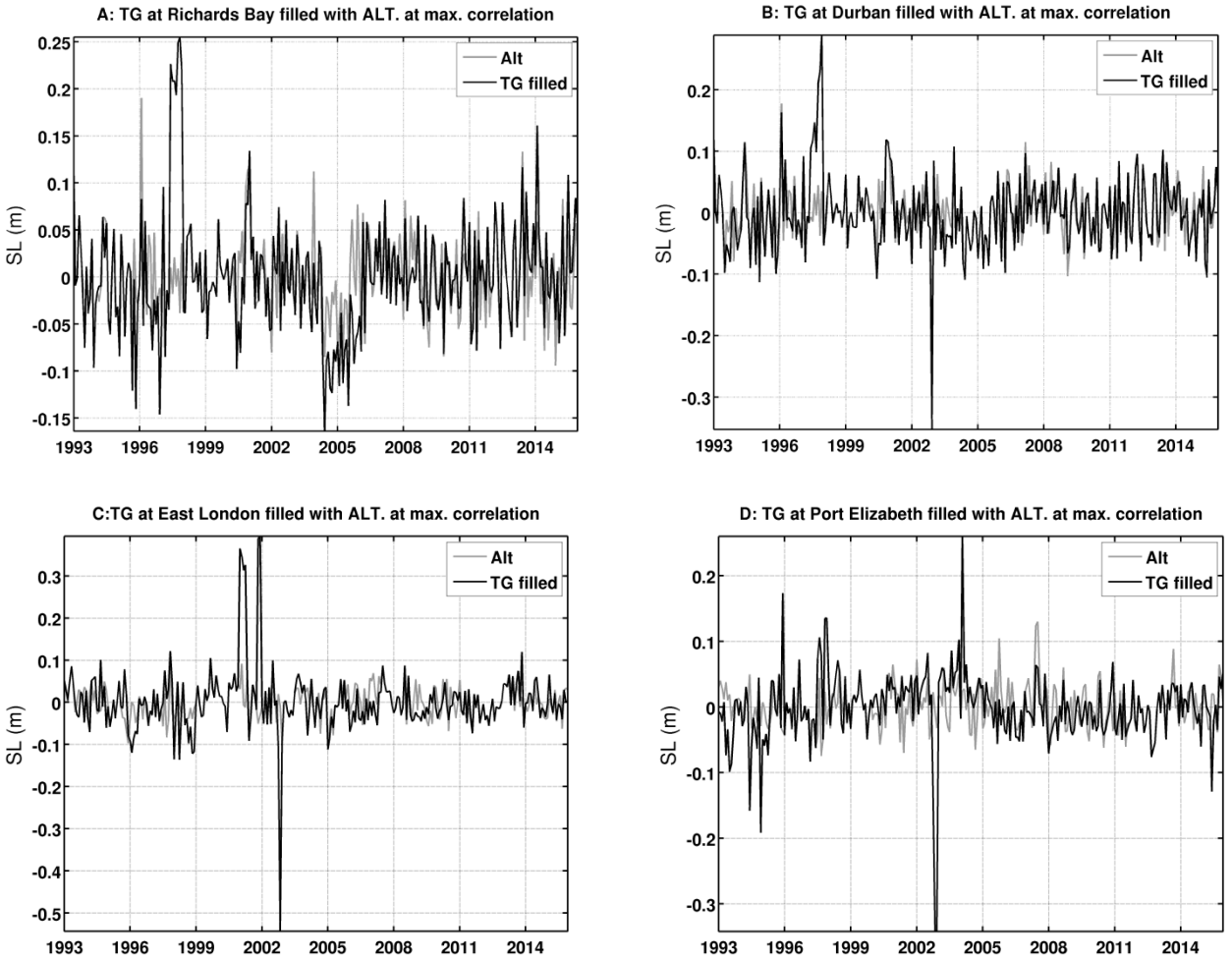

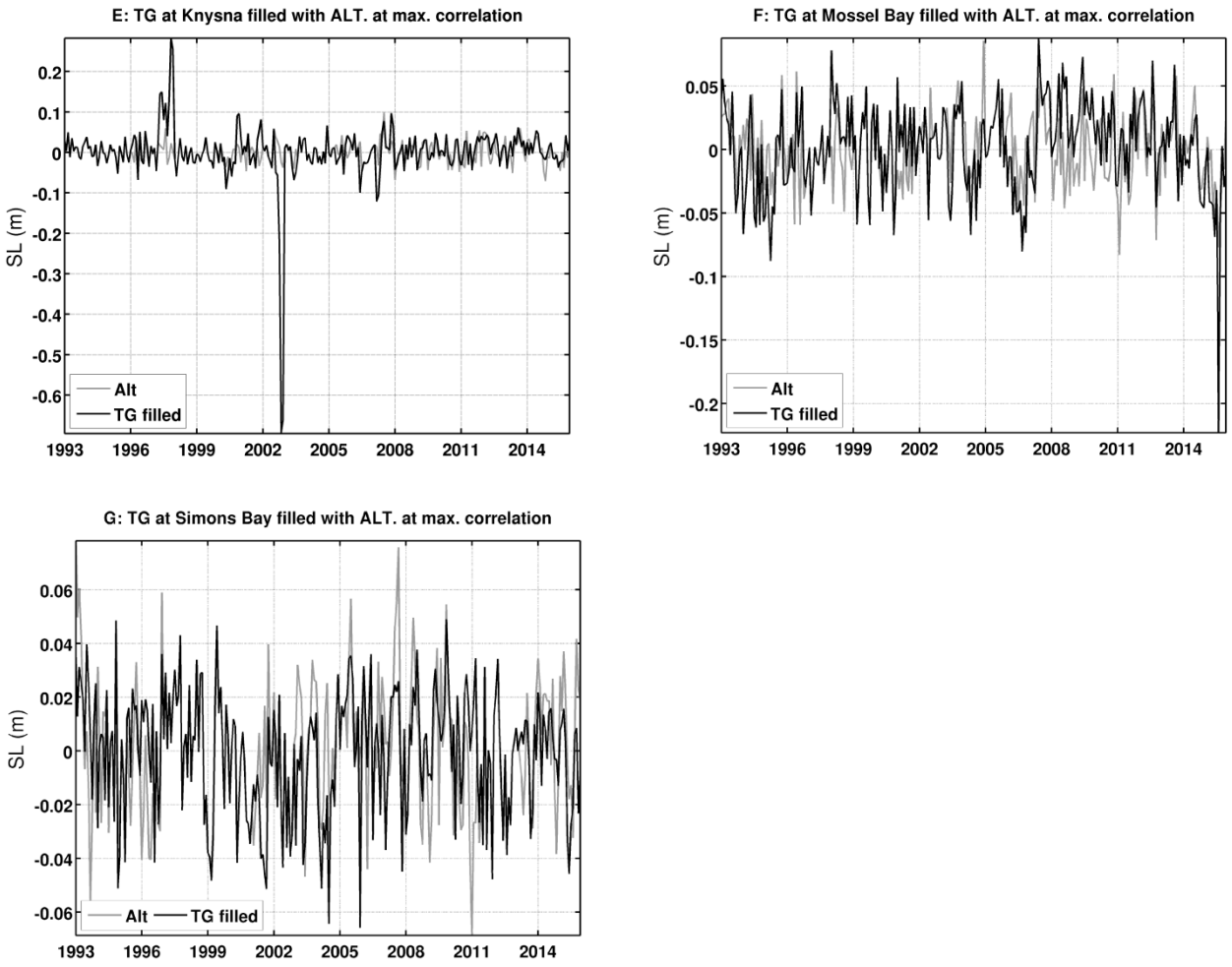

Fig. 3. 7: Tide gauge records at (A) Richards Bay, (B) Durban, (C) East London, (D) Port Elizabeth, (E) Knysna, (F) Mossel Bay and (G) Simons Bay, respectively, filled with satellite altimetry data. Black lines represent the tide gauge time series and grey lines indicate the altimetry measurements from the grid point with maximum correlation.

In this section, the satellite altimetry measurements were explored to fill the gaps in the tide gauge SL records. In the next section the discussion focus is on the period prior to satellite altimetry era. However, it can anticipated that the difference in data time span, the co-occurrence of data gaps, and the large distance between the tide gauge locations are limitations faced in this period.

3.3.2 Period prior to satellite altimetry

The corrections of the *in situ* time series were done prior to any separation of time periods. Thus the data discussed here are corrected to GIA and IB, and then detrended with the seasonal cycle removed. The insight into how sea level time series at each location correlate with each other prior to satellite altimetry can be seen in Fig. 3.5. In this figure, it should be noted that the line representing this period was remarkable compared to the others.

Table 3.2 shows the statistics over this period. The correlation values within the table are paired to give more insight. Based on the information within the table, data sets of one tide gauge location were used to fill another. This was done taking into consideration mainly the correlation value, the distance between them, and findings from the previous section. For instance, no matter how strong the correlation between Mossel Bay and Simons Bay, one cannot fill for the other because they are located in two different correlation zones (see Figs 3.2 and 3.4, for more details).

Table 3.2: The summary of the statistics for the period prior to satellite altimetry era. r indicates the correlation coefficient. rmse indicates the root mean square error.

Data1	Data2	Distance (km)	r	Data1 std (cm)	Data2 std (cm)	rmse (cm)
Richards Bay	Durban	155	0.63	4.83	4.54	4.03
Durban	East London	459	0.01	4.58	4.46	6.21
East London	Port Elizabeth	237	0.19	7.22	3.75	5.34
Port Elizabeth	Knysna	239	0.53	3.75	3.24	3.14
Knysna	Mossel Bay	85	0.49	4.77	3.63	4.05
Mossel Bay	Simons Bay	340	0.41	3.64	2.32	3.44

Fig. 3.8 shows the tide gauge stations that benefited from the adjacent station data sets to fill their gaps. Thus, tide gauge data sets at Richards Bay and Durban (Fig. 3.8A and B) were used to fill gap for each other. Data from East London and Port Elizabeth were used to fill gaps in both each others records (Fig. 3.8C and D). Lastly, data from Knysna and Mossel Bay filled for each other (Fig. 3.8E and F). It should be noted that the gaps at Simons Bay were not filled in this

period. The decision was made because the neighbouring station, Mossel Bay, is located on the other side of the Agulhas Bank, where regional altimetry has shown a clear difference in correlation patterns (Figs 3.2 and 3.4). In addition they are too far apart from each other (around 340 km, Table 3.2).

Richards Bay (Fig. 3.8, panel A) benefits a lot from the data sets of Durban. Thus Richards Bay may lose some of its intrinsic characteristics due to the presence of the oscillatory mode of variability of the sea level at Durban. Hence, Richards Bay needs to be carefully assessed in Chapter 4 in order to make a decision on whether or not it should be included in further studies. The percentage of gained points at other locations seems reasonable.

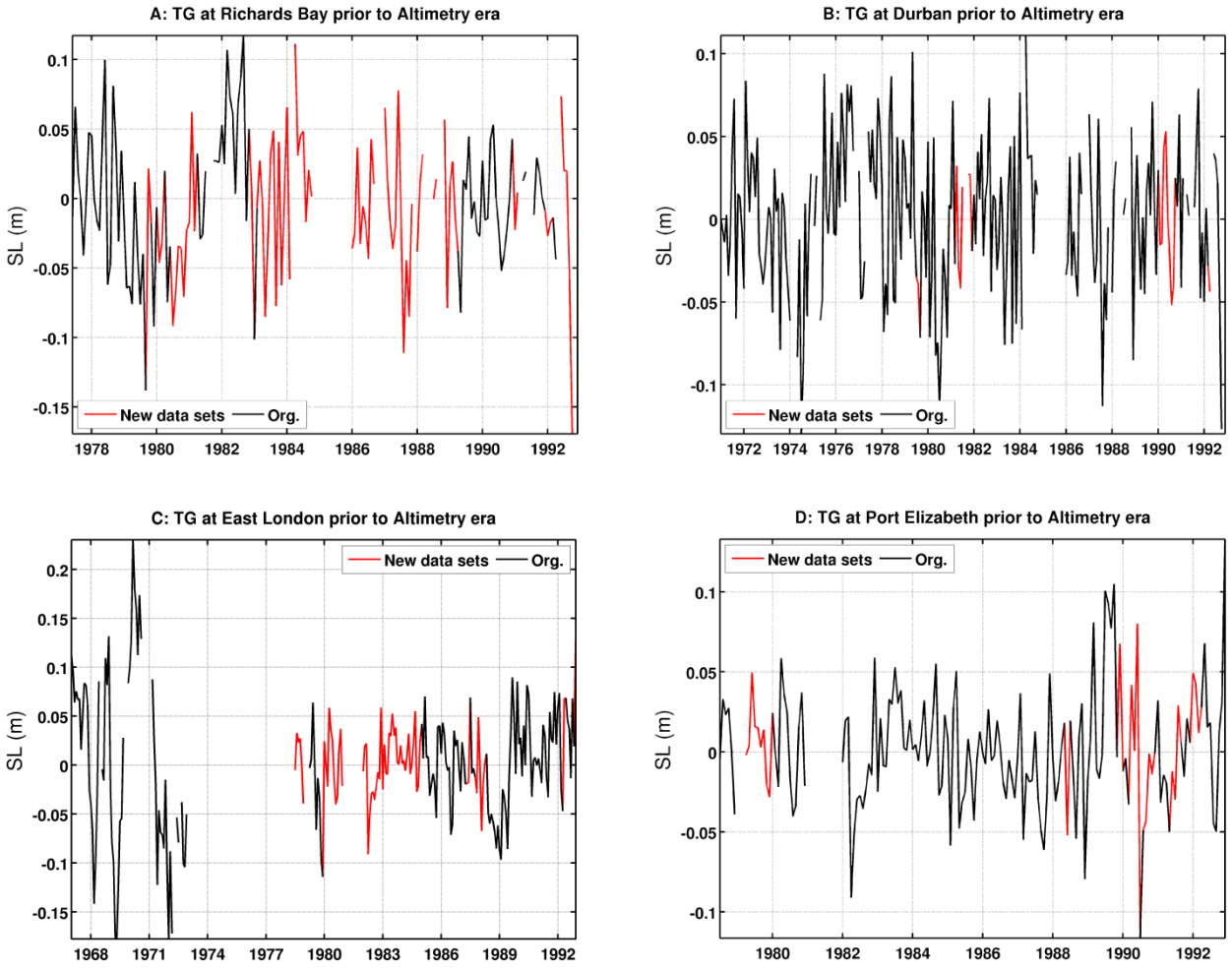

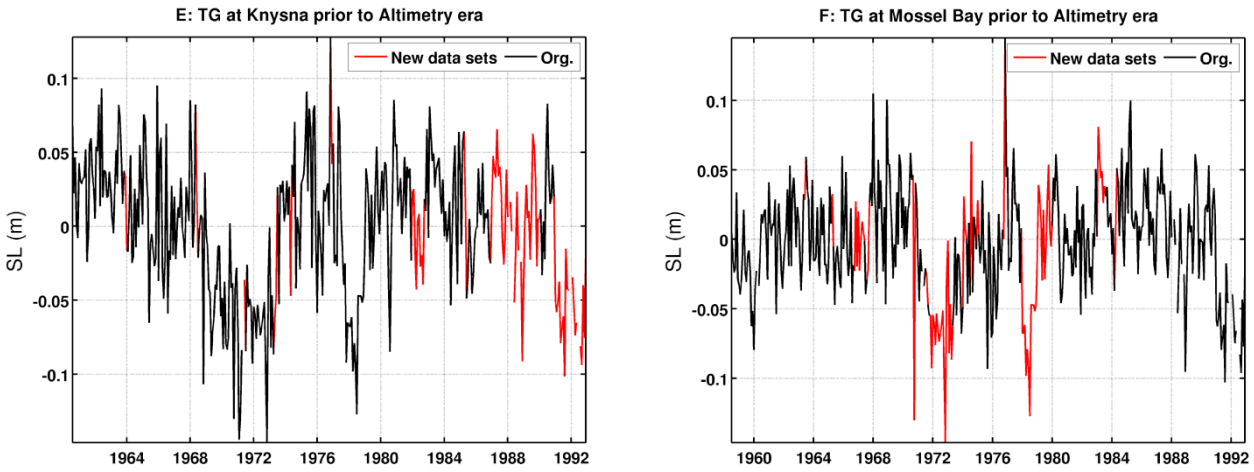

Fig. 3. 8: Tide gauge records at (A) Richards Bay, (B) Durban, (C) East London, (D) Port Elizabeth, (E) Knysna and (F) Mossel Bay, respectively filled by adjacent station records. Black lines indicate the original data sets and red lines show data gained from adjacent tide gauge records.

The next section discusses the details in which these time series were merged to build the new time series of a similar length to the original records.

3.3.3 The fuller sea level time series

At each tide gauge location the two subsets of filled data were concatenated to create one time series of a similar length to the original data. The process also included adding back the IB, GIA and the long-term trend components that were subtracted when detrending and removing the seasonal cycle from the data. These components belong to the data prior to any gap filling process. As mentioned above, it is intended to avoid false correlations and the challenge concerning referencing. Fig. 3.9 illustrates the final tide gauge time series after all gap filling steps.

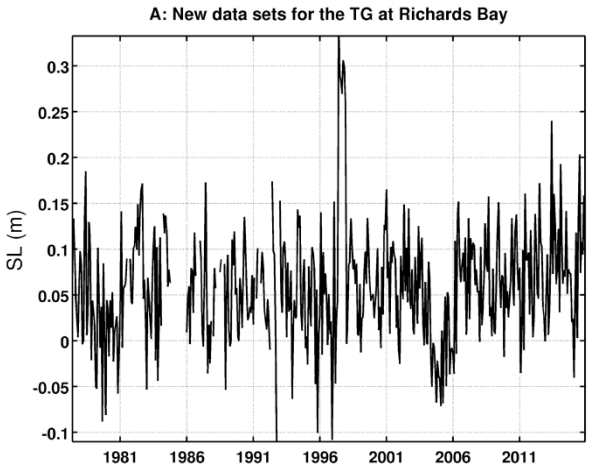
A: New data sets for the TG at Richards Bay
SL (m)
0.3
0.25
0.2
0.15
0.1
0.05
0
-0.05
-0.1
1981
1986
1991
1996
2001
2006
2011

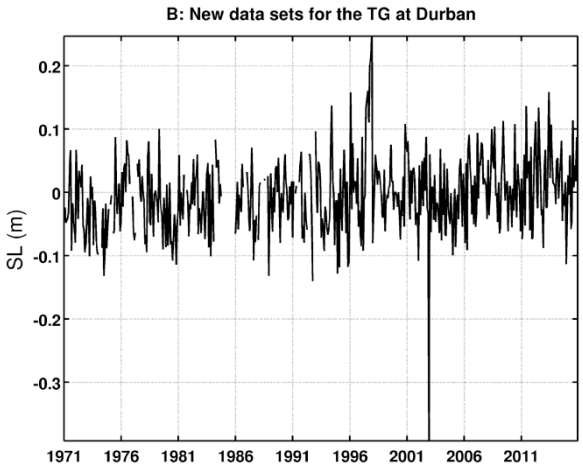
B: New data sets for the TG at Durban
SL (m)
0.2
0.1
0
-0.1
-0.2
-0.3
1971
1976
1981
1986
1991
1996
2001
2006
2011

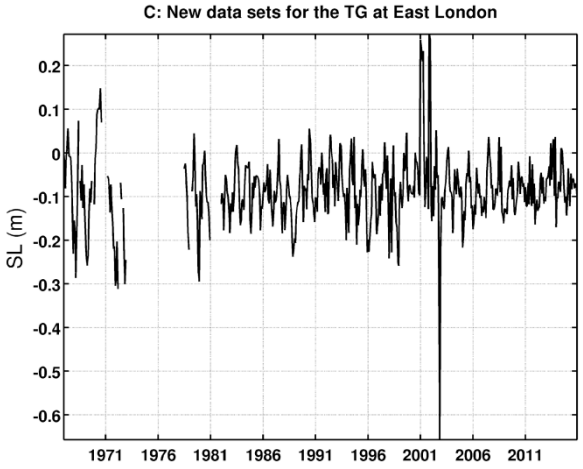
C: New data sets for the TG at East London
SL (m)
0.2
0.1
0
-0.1
-0.2
-0.3
-0.4
-0.5
-0.6
1971
1976
1981
1986
1991
1996
2001
2006
2011

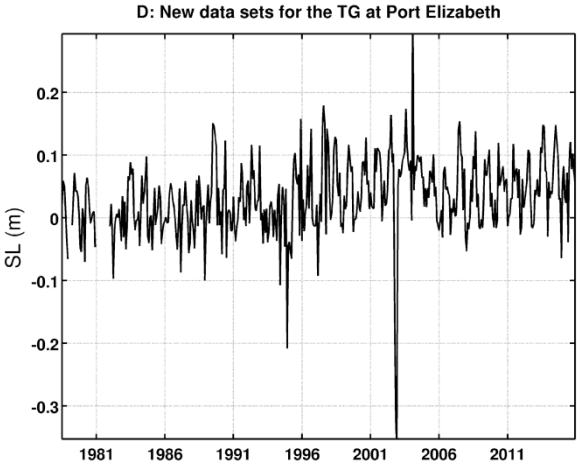
D: New data sets for the TG at Port Elizabeth
SL (m)
0.2
0.1
0
-0.1
-0.2
-0.3
1981
1986
1991
1996
2001
2006
2011

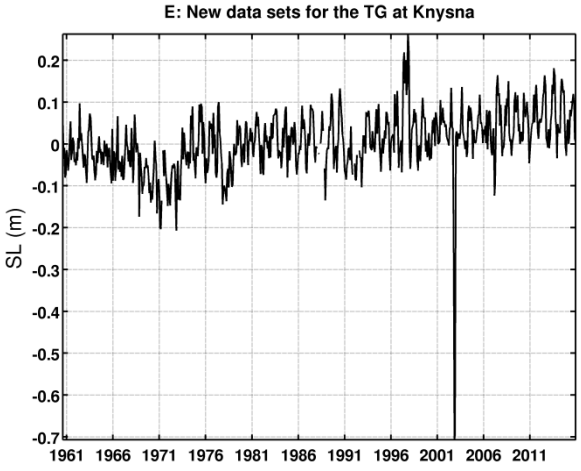
E: New data sets for the TG at Knysna
SL (m)
0.2
0.1
0
-0.1
-0.2
-0.3
-0.4
-0.5
-0.6
-0.7
1961
1966
1971
1976
1981
1986
1991
1996
2001
2006
2011

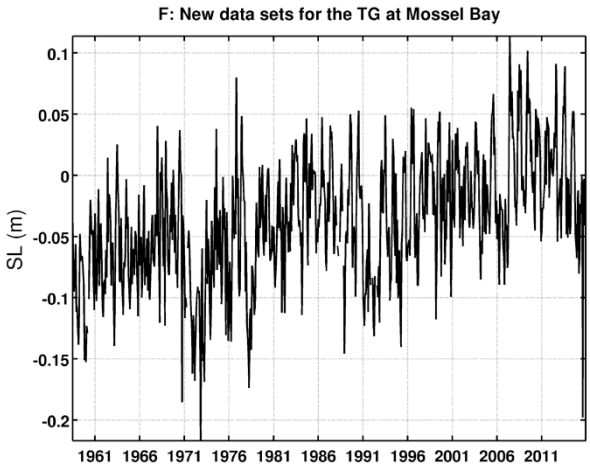
F: New data sets for the TG at Mossel Bay
SL (m)
0.1
0.05
0
-0.05
-0.1
-0.15
-0.2
1961
1966
1971
1976
1981
1986
1991
1996
2001
2006
2011

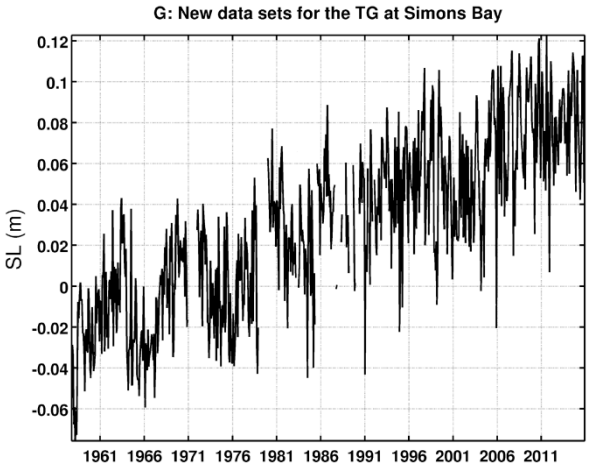

Fig. 3. 9: Tide gauge records at (A) Richards Bay, (B) Durban, (C) East London, (D) Port Elizabeth, (E) Knysna, (F) Mossel Bay and (G) Simons Bay, respectively after the gap filling process.

A lot of missing data have been extrapolated. The time series have no missing values from January, 1993 to December, 2015. Unfortunately, few data sets have been extrapolated prior to this period. The occurrence of data gaps at the same time has limited the achievement of this goal. Table 3.3 shows the details of the extrapolated data.

Table 3.3: The summary of the statistics of tide gauge records before and after gap filling process.

		Original data				gap-filled data		
station	ID	Count	Data coverage (%)	Starting date	Longest gap period (months)	Missing values (months)	Data coverage (%)	Longest gap period (months)
Richards Bay	RB	463	55	Jun-77	73	30	93.5	12
Durban	D	540	69	Jan-71	28	38	93.0	12
East London	EL	588	53	Jan-67	75	94	84.0	66
Port Elizabeth	PE	450	78	Jan-78	18	15	96.7	12
Knysna	K	665	71	Aug-60	60	8	98.8	2
Mossel Bay	MB	690	79	Jul-58	24	9	98.7	2
Simons Bay	SB	699	79	Oct-57	49	49	93.0	12

The cross-correlation analysis of the sea level at Richards Bay and Durban suggests that variability appears to be driven by the same forcing mechanisms (Figs 3.2 and 3.4), and because a significant portion of sea level data from Durban (70%) was used to fill the Richards Bay data gaps before satellite altimetry period (Fig. 3.8), it will be prudent to remove Richards Bay from

further analysis in Chapter 4. The results discussed in this study also highlight the need for further investigation using satellite altimetry along-track sea level anomaly observations and simulation model outputs. An attempt to utilise along-track data sets failed for reasons such as too few tracks passing near tide gauge locations, differences in lengths of satellite mission datasets, sampling resolution, etc. An attempt to use monthly averages of 10-day mean sea surface heights from the Hybrid Coordinate Ocean Model (HYCOM; Backeberg et al., 2014) also resulted in failure due to weak correlations with monthly mean tide gauge records, suggesting the need for more dedicated examination, beyond the scope of this study.

3.4. Summary and Conclusion

The viability of using satellite altimetry observations to fill the gaps in the monthly mean sea level records from the south and east coasts of South Africa was explored at seven individual tide gauges. The results suggest that it is worthwhile and the gaps were filled. The gridded Copernicus product used in this study appears to reproduce the required sea level variability well. Another expected outcome of this chapter concerns whether or not apparent outliers in the *in situ* measurements should be eliminated in the Chapter 4. Despite, the consistency of, for instance November - December 2002 event, the anomalously high/low values should regarded as outliers and removed from the monthly sea level data.

Taking into account the coastal dynamics over the region, it was decided to use the sea level data at grid points with the maximum correlation to the tide gauge without any correlation value threshold. This was achieved within a 1x1 degree rectangular box around each tide gauge studied. Although the correlations were not very strong, the results suggest that both the data sources conserve similar temporal structure at both high and low frequencies of sea level variability. These correlations results really advocate a specific coastal processing for the altimetry data in order to make the comparison more meaningful.

The study gives insight into the variability of sea level at a sub-regional scale. Different to daily sea level data, monthly data sets show that the east and south coast are not homogeneous. As

a result, the south coast can be separated into western and eastern Agulhas Bank sub-regions. The transition zone includes Port Elizabeth and East London. The east coast tide gauge stations are well correlated and are located within the Natal Bight. The results lead to a more cautious approach when conducting studies based on monthly mean sea level data over the southern Africa.

Prior to satellite altimetry, gaps were also filled with success. A limitation was the occurrence of missing values at the same time in adjacent tide gauges. This led to fewest data points recovered. Some studied sites are too far apart from each other, which also constrains the process of gap filling. The final datasets are fuller time series than the original datasets, permitting their study with more confidence and thus reducing the scepticism with regard to the conclusions drawn. However, despite the success in recovering a lot of data in this study, it is recommended that similar studies be conducted to combine satellite altimetry observations and simulation model output with the existing tide gauge records, to obtain more accurate results.

CHAPTER 4

Atmospheric and climatic drivers of tide gauge sea level variability along the east and south coast of South Africa

4.1. Introduction

Tide gauge (TG) data around southern Africa have been used to investigate sea level (SL) variability on only a few occasions in the past (Mather et al., 2009). This is because of the absence of good quality, long-term sea level records (Brundrit, 1984; 1995; Woodworth et al., 2007; Mather et al., 2009). Studies are needed in spite of this limitation in some regions to avoid the use of the global ocean mean estimate rates as reference for future projections at regional and local spatial scales (e.g. Mather et al., 2009).

Chapter 3 was dedicated to creating a fuller time series of tide gauge records. The results suggest that gaps in monthly TG sea level records can be successfully filled with satellite altimetry sea level observations. Prior to the satellite altimetry era, neighbouring pairs of tide gauge sites that correlated well with each other were identified and their records used to fill the gaps. Unfortunately, only a few data points could be filled in this way prior to the altimetry period because of co-occurring gaps in neighbouring TG sites. Additionally, large distances between tide stations resulted in poor cross-correlations, limiting the number of suitable neighbouring tide gauge sites that could be used to fill gaps.

Around southern Africa, various authors have already carried out investigations on timescales of sea level variability and their possible driving mechanisms, based mainly on tide gauge

records, daily and monthly means. Daily based sea level records have shown variability that ranges from 3 to 7 days or longer at some sites, but not longer than one month (e. g. Schumann, 1981, 1983; Brundrit et al., 1984; de Cuevas et al., 1986; Schumann and Brink, 1990). The variability is due to the passage of synoptic atmospheric disturbances, particularly the mesoscale atmospheric coastal lows (Reason and Jury, 1990) which propagate west to east along the South African coast (e. g. Schumann, 1981, 1983; Brundrit et al., 1984; de Cuevas et al., 1986; Schumann and Brink, 1990).

Using monthly means from the west coast of southern Africa, timescales of sea level variability ranging from months to years have been found (e.g. Brundrit, 1984; Brundrit et al., 1984; Brundrit et al., 1987). The timescales were grouped into three categories: (1) high-frequency (synoptic), (2) seasonal and (3) interannual contributions. The synoptic contributions were attributed to the effect of the coastal wind stress associated with mesoscale and synoptic weather systems. The seasonal contribution was associated with seasonally varying wind patterns. The interannual contribution was associated with the occurrence of the El Niño-Southern Oscillation (ENSO) phenomenon in the Pacific Ocean, via sea surface temperature (SST) modulation along the west coast of southern Africa. This SST modulation was actually found to start further north in the eastern equatorial Atlantic (Brundrit, 1984; Colberg et al., 2004). ENSO may also modulate the frequency and intensity of the various weather systems than can directly affect sea level (e.g. Singleton and Reason, 2007; Weldon and Reason, 2014). The synoptic and seasonal contributions were suggested to be responsible for over 55% and 25% of the monthly sea level variability, respectively (Brundrit, 1984). Han et al., (2010, 2014) provide some insight into how sea level has varied along the east coast of southern Africa, although their study aimed to describe the driving mechanisms of Indian Ocean SL variability at interannual and decadal timescales.

Specific studies on the drivers of the timescales of sea level variability along the east and south coast of South Africa were not found in the literature. Therefore, there is need to improve our understanding of local and regional SL variability, taking advantage of the improved monthly sea level data generated in Chapter 3. The objective of this study is to determine the timescales

of SL variability, identifying the corresponding drivers. The Empirical Mode Decomposition method (Huang et al., 1998; Huang and Wu, 2008), described in Chapter 2, was applied to assess different modes (timescales) of sea level variability. Where possible, the separated EMD modes have been compared with previous results in the literature due to the scarcity in local literature.

As with other statistical methods, EMD does not provide any information on the forces driving the changes. However, it gives a robust indication of the timescale of variability, which assist in identifying forcing mechanisms. Hence, in identifying timescales of variability that are consistent at multiple tide gauge locations, it is likely that their variability is governed by the same drivers (Ezer et al., 2013). Then to confirm and quantify the relationship of sea level variability with a specific driver, EMD is applied to a number of known drivers. If a relationship is found between sea level and one or more drivers, this suggests that there is a link to sea level variability and change (Ezer et al., 2013).

This Chapter is structured as follows: The data and methodologies applied in this study are described in Section 2, the Results and Discussion are presented in Section 3, and the Summary and Conclusion are given in Section 4.

4.2. Data and Methods

4.2.1. Data

To examine and advance the understanding of possible driving mechanisms of sea level variability, different data sets from several data sources were used. The details of each dataset used in this study are described below.

4.2.1.1 Sea Level Observations

The sea level data used here are the continuous tide gauge records generated and discussed in Chapter 3. Essentially, these data consist of all available monthly mean tide gauge records from the mid-1900s (depending on location) until December 2015, from seven sites along the east and south coasts of South Africa. The data sets were sourced from the Permanent Service for Mean Sea Level (PSMSL; Holgate et al., 2013; PSMSL, 2017; http://www.psmsl.org/). These raw data had gaps that needed to be eliminated or at least reduced so that the analysis could lead to reliable conclusions (Chapters 2 and 3). As a result, tide gauge measurements were combined with the gridded multi-mission Copernicus Marine and Environment Monitoring Service (CMEMS; http://www.marine.copernicus.eu) sea level satellite altimetry observations product, from January 1993 to December 2015. The process for combining the tide gauge data with satellite altimetry data is described in detail in Chapter 3, but essentially, using monthly data, the satellite altimetry grid point, within a 1x1 degree rectangular box, that correlated best with the tide gauge time series was identified and used to fill gaps during the satellite altimetry era. In the period prior to satellite altimetry, data from neighbouring sites that are well correlated are used to generate the continuous tide gauge record.

4.2.1.2 Large scale oceanographic and climate data

Several datasets were analysed to identify and evaluate the drivers of sea level variability and trends, including atmospheric and climate forcing. These are described below.

Sea Surface Pressure (SLP)

Monthly mean gridded reanalysis SLP from the National Centre for Environmental Prediction/National Centre for Atmospheric Research (NCEP/NCAR; Kalnay et al., 1996), downloaded from the webpage http://www.esrl.noaa.gov/psd/data/gridded/data.ncep.reanalysis.derived.html were used.

They consist of 2.5-degree global resolution in both latitude and longitude, in Pascals (Pa), from January 1948 to the present. The global data were used to study the large and regional scale relationships between SLP and regional sea level variability. In addition to this, the same monthly gridded SLP datasets were extracted at the nearest tide gauge location grid point to correct for the inverse barometer (IB) effect of the sea level records, described in Chapter 3.

Wind at 10 m

The monthly mean gridded reanalysis 10 m winds also from the NCEP/NCAR (Kalnay et al., 1996; http://www.esrl.noaa.gov/psd/data/gridded/data.ncep.reanalysis.derived.html) are used to investigate the large and regional scale relationships between wind and regional sea level variability. The gridded zonal and meridional components of the 10 m winds are available on a T62 Gaussian grid, and provided in metres per second (m/s), from January 1948 to the present. The gridded NCEP/NCAR Reanalysis 1 datasets were used due to the match with the tide gauge records time span.

Extended reconstructed sea surface temperature (ERSST)

Gridded monthly mean National Oceanic and Atmospheric Administration (NOAA) ERSST, version 4 (Huang et al., 2014), provided globally at 2 degree resolution in both latitude and longitude, in degree Celsius (°C), from January, 1854 to the present are used to investigate the large-scale relationships between SST and regional sea level variability. These data sets were downloaded from http://www.esrl.noaa.gov/psd/data/gridded/data.noaa.ersst.v4.html.

Dipole Mode Index (DMI)

Time series of monthly mean DMI (Saji et al., 1999), based on the NOAA ERSST, version 4 from January 1854 to present were downloaded from http://www.jamstec.go.jp/frcgc/research/d1/iod/e/iod/about_iod.html. The DMI is the main

index used for monitoring Indian Ocean Dipole (IOD) conditions. DMI is derived from the SST difference between the south-eastern equatorial Indian Ocean (90°E-110°E and 10°S-Equator) and the western equatorial Indian Ocean (50°E-70°E and 10°S-10°N). Positive and negative DMI values correspond to positive and negative IOD phenomenon, respectively (Saji et al., 1999). Previous studies (Saji et al., 1999; Ashok et al., 2001; Hendon, 2003; Behera et al., 2005; Manatsa et al., 2008; Manatsa et al., 2011) have indicated that the IOD has significant effects on the climate of the Indian Ocean rim countries, including the southern Africa region.

Multivariate ENSO Index (MEI)

In order to investigate the possible influence of ENSO events on sea level variability, time series of monthly means MEI (Wolter and Timlin, 1993; 1998), from December 1949 / January 1950 to the present, were downloaded from https://www.esrl.noaa.gov/psd/enso/mei/index.html. The MEI combines analysis of multiple meteorological and oceanographic components including SLP, zonal and meridional components of the surface wind, SST, surface air temperature and total cloudiness fraction of the sky over the tropical Pacific. These observations have been collected and published in the International Comprehensive Ocean-Atmosphere Data Set (ICOADS, Freeman et al., 2016) for many years. Therefore, MEI is considered to be the most complete index for ENSO monitoring and is derived twelve times per year for each sliding bi-monthly season, corresponding to January - February, February - March, and so on. ENSO has been shown to impact the climate in various part of the globe, including the region studied in this chapter (Lindesay, 1988; Reason et al, 2000).

Southern Annular Mode (SAM)

Time series of monthly mean SAM data, from January 1957 to present downloaded from https://legacy.bas.ac.uk/met/gjma/sam.html were utilised in this study. Also known as the Marshall Southern Annular Mode index (Marshall, 2003) or the Antarctic Oscillation, SAM is the index derived from the difference between the zonal pressure at the stations located at 40°S

and 65°S. The SAM index is used to monitor the north-south migration of the westerly wind belt over the Southern Ocean. Given that SAM is known to impact the strength and position of cold fronts, it influences the weather and climate of the Southern Hemisphere south of about 20°S, including southern Africa (Reason and Rouault, 2005; Gillett et al., 2006). Positive SAM events reflect a poleward contraction of the belt of strong westerly winds resulting in fewer low-pressure systems reaching southern Africa. In negative SAM events, the belt of strong westerly winds expands equatorward causing more cold fronts to reach southern Africa.

4.2.2. Methods

In order to achieve the objective of this study, several data processing and analysis methods were applied. The monthly sea level data show some anomalously high/low values that may be regarded as outliers. As a result, outliers were removed from the monthly sea level data using the 3 standard deviations threshold. Before analysis, the fuller sea level time series records (Chapter 3), were corrected for the inverse barometer effect.

This (inverse barometer) corrected fuller sea level time series still had data gaps. In Chapter 2 it was shown that the linear trend gap filling method gives the best results compared to two other methods tested: (i) linear interpolation and (ii) average value. Hence, the remaining missing values in these adjusted fuller SL time series records (hereafter sea level records or time series) were filled with the values of the linear trend.

The long-term linear trend and the seasonal cycle of each time series in this study were removed before analysis. EMD is used as a filter to separate the embedded timescales of either SL variability or drivers, as discussed in Chapter 2. Wavelet analysis (Torrence and Compo, 1998) is applied to identify the dominating frequency of the separated oscillatory modes/timescales. The separated timescales of both sea level variability and drivers are combined to form the sub-annual and interannual timescale (Chapter 2). The sub-annual timescale is the sum of the modes with a periodicity lower than approximately one and a half

years. The modes with a periodicity higher than approximately two years are summed to compute the interannual timescale.

Unless stated otherwise all correlations undertaken in this study were at 95 % confidence level. A two-sided t-test was undertaken to test the significance, at 95 % confidence level, of the corrections between the modes of the TG sea level and atmospheric surface fields at regional and large scale. Cross-correlations were carried out to examine the relationship between the modes of the sea level and potential drivers at interannual timescales. Hence, the statistical significance of the resultant correlation coefficients was tested based on Chelton (1983) at 5 % significance intervals. It was defined that positive and negative lag values should indicate that sea level is lagging and leading, respectively.

4.3. Results and Discussion

4.3.1. The timescales and driving mechanisms of the tide gauge sea level variability

Timescales of tide gauge sea level variability

Fig. 4.1 shows the oscillatory modes of sea level records at Durban when decomposed with the EMD method. It illustrates that the EMD decomposes the raw time series into nine (9) modes with different periodicity. The synthetic sea level data, which had monthly data spanning 45 years, discussed in Chapter 2 yielded a similar number of modes. Shorter time series yield fewer modes of variability (e.g. Fig. A1). This confirms that the number of the timescales is determined by the record length as suggested in previous studies (e.g. Ezer and Corlett, 2012; Ezer et al., 2013). The period for each mode, as identified by the wavelet analysis is indicated in the heading of each panel in Fig. 4.1.

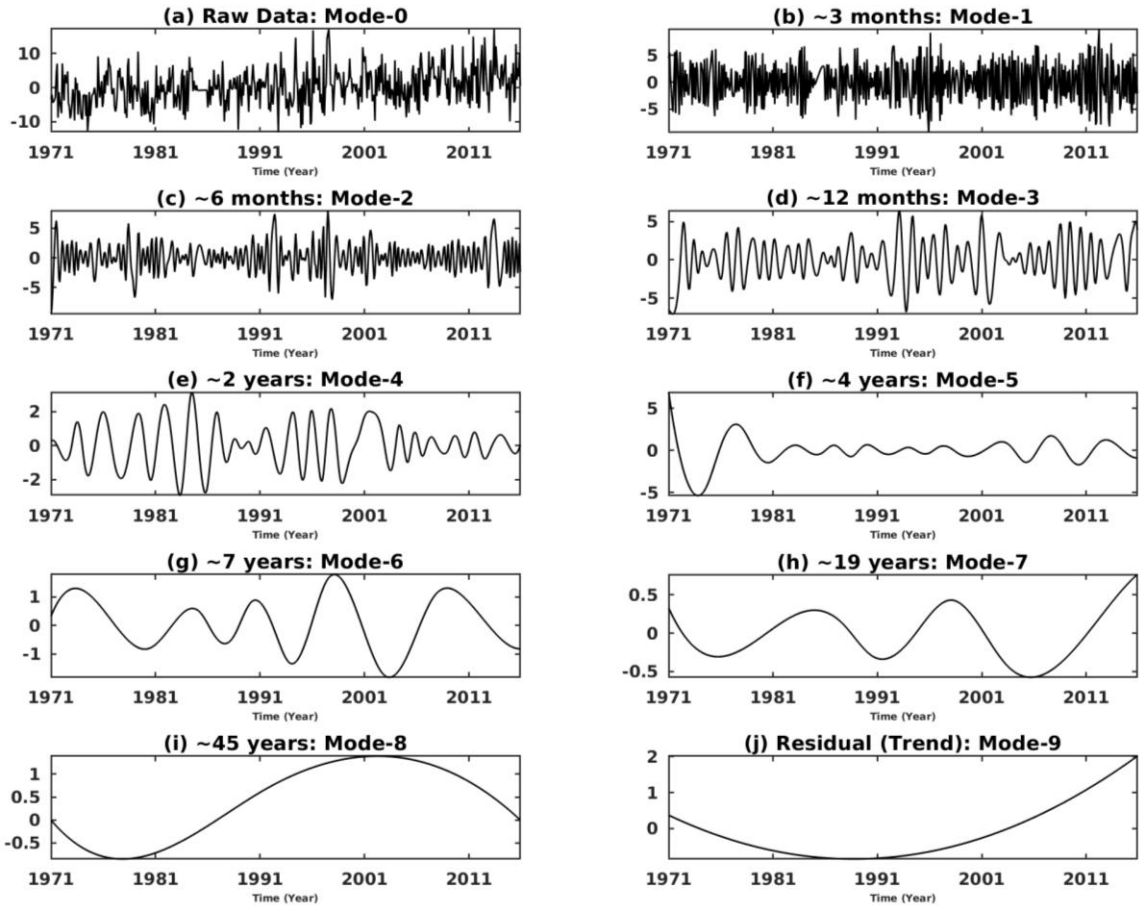

Fig. 4.1: Monthly sea level records at Durban (in cm) when decomposed with EMD. As a result, nine modes were found, mode 0 is the raw data, modes 1 - 8 are the oscillating modes, the last residual mode is the trend (mode-9).

Interestingly, the periodicity of each separated mode appears to match the periodicity of the synthetic data discussed in Chapter 2, which suggests that it depends on the sampling resolution and length of the time series. For each mode separated, in addition to the periodicity, changes are also evident in the amplitudes of the modes. The periodicity and amplitude of the modes may provide insight into which forcing mechanism might drive the variability and their contributions to the total sea level.

To our knowledge, there is no previous literature investigating the timescales of the sea level records at most of our studied sites. However, the temporal structure of the separated modes 1, 2 and 3 at Simons Bay (Fig. A6) agrees with the conclusions of the previous studies (Brundrit, 1995, Fig. 4). In an exploratory analysis Brundrit (1995) established the temporal structures

present in the monthly mean sea level from TGs along the coast of Namibia and South Africa and then examined the evidence of long-term trends. Analysing the longer term sea level variability at Simons Bay, Brundrit et al. (1984) noted an upward and downward trend from 1971 to 1979 and from 1980 to 1982, respectively. This finding is in agreement with an oscillation identified as mode 6 at Simons Bay (Fig. A6g). Along the south-western coast of Africa, Brundrit (1984) analysed monthly mean sea level records from 1969 to 1975 and found that the variations can be separated into (i) high-frequency, (ii) seasonal and (iii) interannual contributions. Separating variations in such relatively short length of the studied tide gauge records is quite remarkable, given also the difference in the technique applied, however, the results are consistent with the EMD separated modes.

Drivers of tide gauge sea level variability

It is difficult to ascertain which driver is embedded in the data when interpreting each mode. It is possible that each timescale (or even mode) may represent one physical driver. However, identifying a single driver for each separated timescale is challenging due to our limited knowledge of how sea level is linked to the various forcing mechanisms (e.g. Haigh et al., 2014). A key question to consider is whether it is possible to determine a physical meaning for each timescale or should the timescale isolated by EMD be determined according to the periodicity of known drivers.

Usually, the periodicities of drivers cover a range of timescales (Zebiak, 1993; Neelin et al., 1998; Saji et al., 1999, Marshall, 2003). As a consequence, a driver may have a measurable effect over a set of single modes of SL variability. Thus, it would be better to combine a number of modes with different periodicities in order to identify one physically meaningful range of frequencies to compare with known drivers. Therefore, at each tide gauge location, the separated oscillatory modes are grouped into sub-annual and interannual timescales of sea level variability (Fig. 4.2).

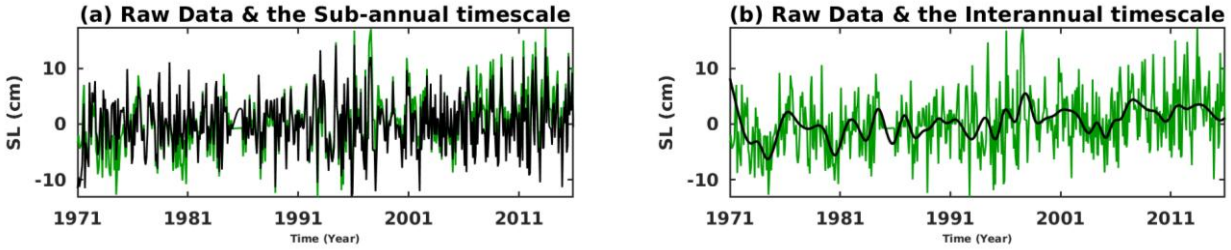

Fig. 4.2: An overlay of monthly tide gauge records at Durban (green line) and the ensemble mean of selected modes. (a) Black line (modes 1 to 3) represents the sub-annual modes. (b) Black line indicates the interannual modes (modes 4 to 9).

The motivation for combining modes of certain periodicities is described in Chapter 2. Modes 1-3 and modes 4-9 (see Fig. 4.1), comprise the sub-annual and interannual timescales of variability, respectively. For all tide gauge locations (see also Fig. B1, 2, 3, 4, 5 and 6), the root mean square (rms) of the sub-annual timescale can be as high as 6cm, with the exception of Simons Bay (Fig. B6b) which is smaller i.e. 2 cm. Additionally, the rms of the interannual timescale at all locations can be as high as 8 cm, with the exception of Durban (Fig. 4.2) which is smaller (2 cm).

In summary, for all TG locations, the EMD modes were grouped into two sets of timescales: (1) sub-annual and (2) interannual. These temporal scales of sea level variability are considered to be physically more meaningful, and hence easier to relate to known drivers of atmospheric conditions and climate variability. The next section is dedicated to identification of these drivers of variability.

4.3.2. Drivers of tide gauge sea level variability at sub-annual timescale

At this timescale only the atmospheric forcing was considered. This is due to the fact that previous studies have indicated that the mesoscale and synoptic weather disturbances are the driving mechanisms of the southern Africa coastal sea level variability at this timescale, based

on daily mean (Schumann, 1981, 1983; Brundrit et al., 1984; de Cuevas et al., 1986; Schumann and Brink, 1990) and monthly mean (Brundrit, 1984; Brundrit et al.; 1984) tide gauge records, respectively. Therefore, the time series at each studied TG site were correlated with the time series at each grid point of the regional atmospheric data and the statistical significance of the resultant correlation was estimated through a two-sided t-test.

Fig. 4.3 illustrates the correlation between SL variability and regional gridded SLP at sub-annual timescales. The highest correlation (largest in absolute value and negative) is found offshore. It means that when sea level is high at a tide gauge location and its surrounding area, SLP is low offshore. Surface low-pressure systems e.g., cut-off lows, mid-latitude cyclones, mesoscale coastal lows, are associated with a clockwise (cyclonic) wind circulation in the Southern Hemisphere and over the study region (e.g. Taljaard, 1972; van Loon, 1972; Preston-Whyte and Tyson, 1988; Tyson and Preston-Whyte, 2000). It is also evident that the offshore correlation values are higher on the south coast, between East London and Simons Bay, implying a stronger connection with surface low-pressure systems. Since sea level records were corrected to IB effect and the linear trend as well as seasonal cycle removed in both datasets, the effect of static pressure is removed. Consequently, the correlation with coastal sea level variability illustrated here may be explained in term of its interaction with wind variations.

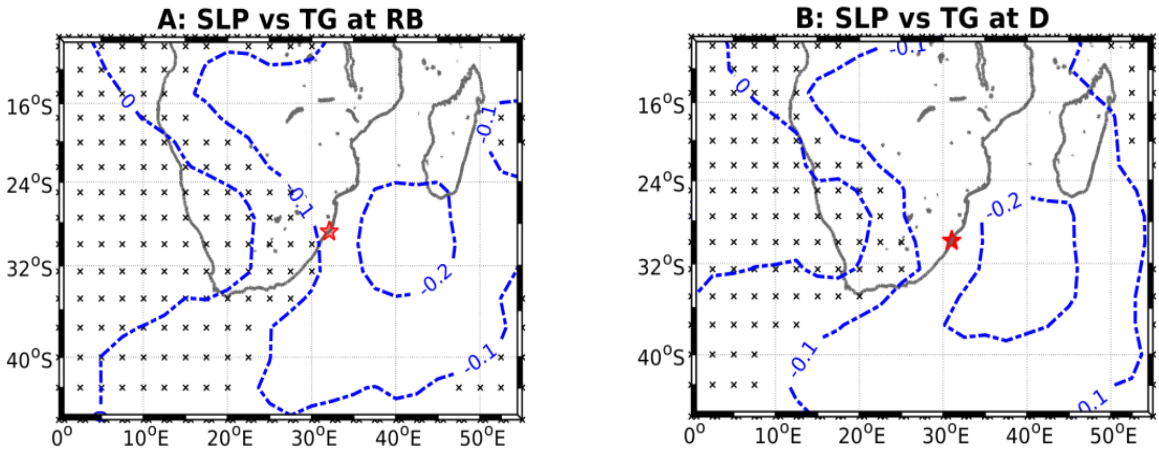

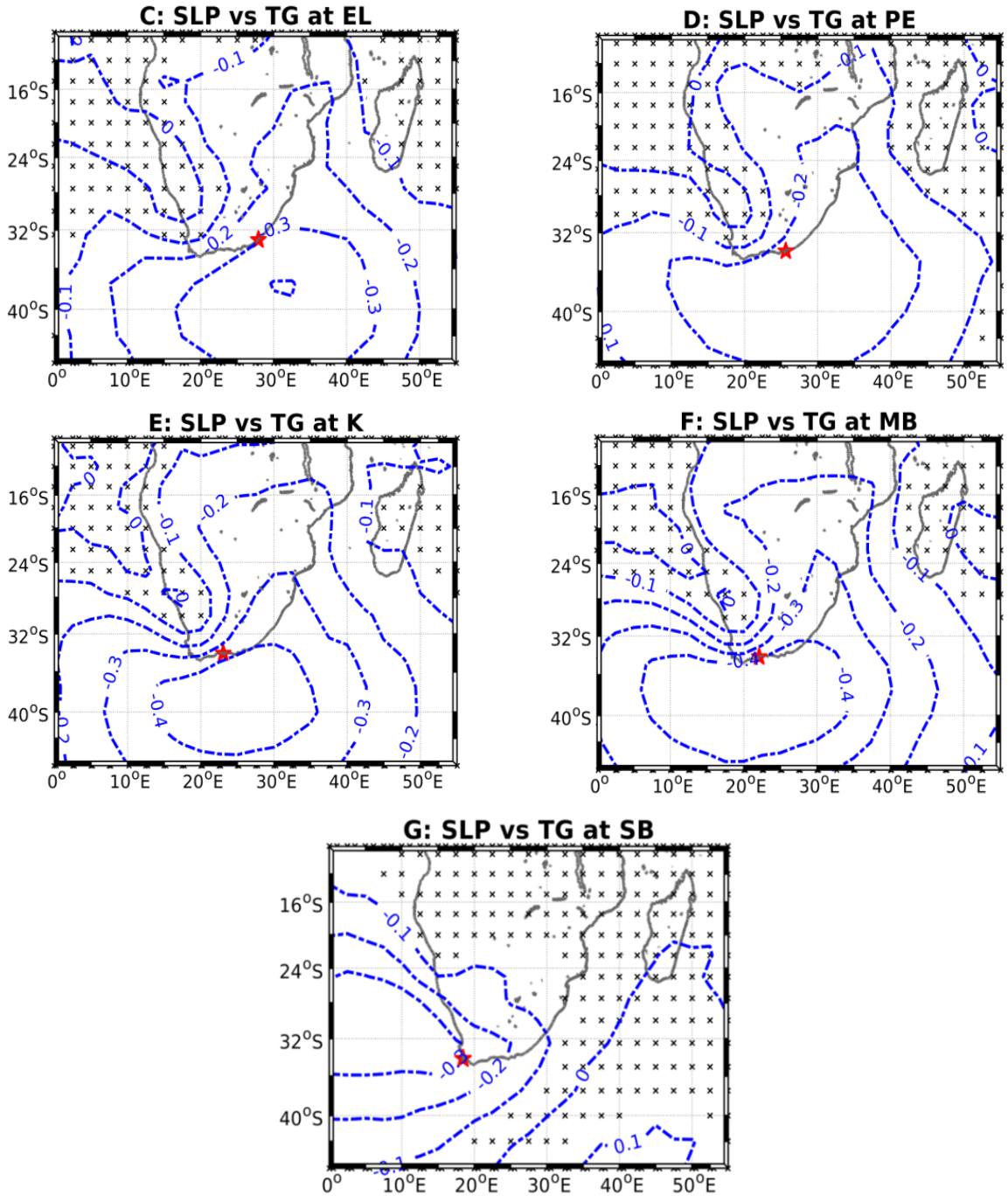

Fig. 4.3: Correlation, at the sub-annual timescale, between regional gridded monthly mean SLP and monthly mean SL records at (A) Richards Bay, (B) Durban, (C) East London, (D) Port Elizabeth, (E) Knysna, (F) Mossel Bay and (G) Simons Bay, respectively. Red stars indicate the tide gauge location. Black crosses indicate area statistically non-significant at 95 % confidence level, estimated using a two-sided t-test.

In order to understand the effect of the wind on coastal sea level variability, u- and v-components of wind were examined separately. Fig. 4.4 shows the correlation between regional 10 m zonal winds and SL variability. In fact, the wind correlation appears to be strong near the coast, which is consistent with Fig. 4.3. Overall, positive zonal winds (westerly winds) are associated with high sea level at all tide sites under consideration. As a result, when sea level is high at the tide gauge and vicinity, the zonal wind is also high along the coast. This positive correlation indicates that the zonal component of the winds is associated with westerlies at this timescale. However, zonal winds seem to not have a significant association with sea level variability at Simons Bay (Fig. 4.4G). The complex coastal topography near Simons Bay (Cape Peninsula, False Bay, etc) or the effect of the onshore winds to the north (where the correlation is highest) seems to mask the relationship with the zonal wind at this station. With the exception of Simons Bay, the results also confirm that the impact of the zonal wind on coastal sea level variability is high on the south coast.

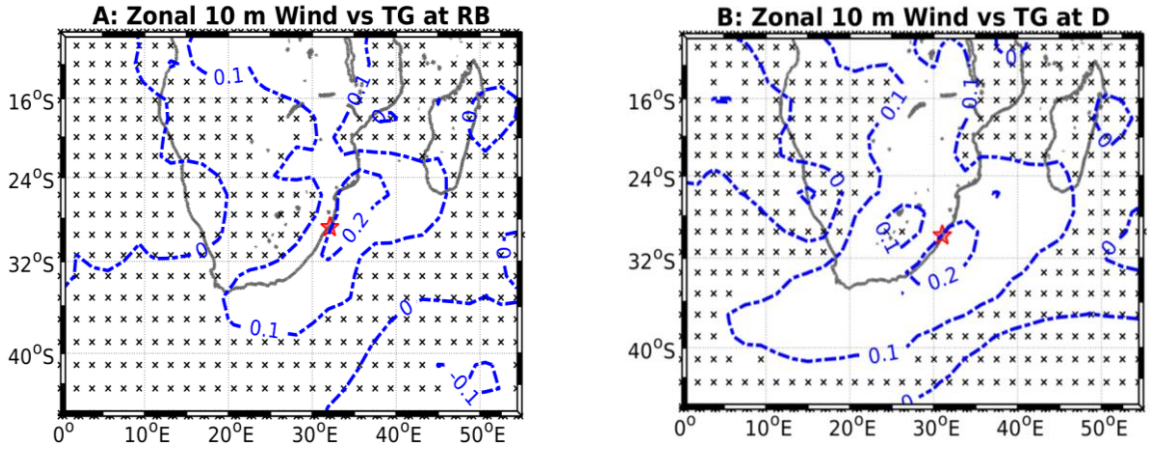

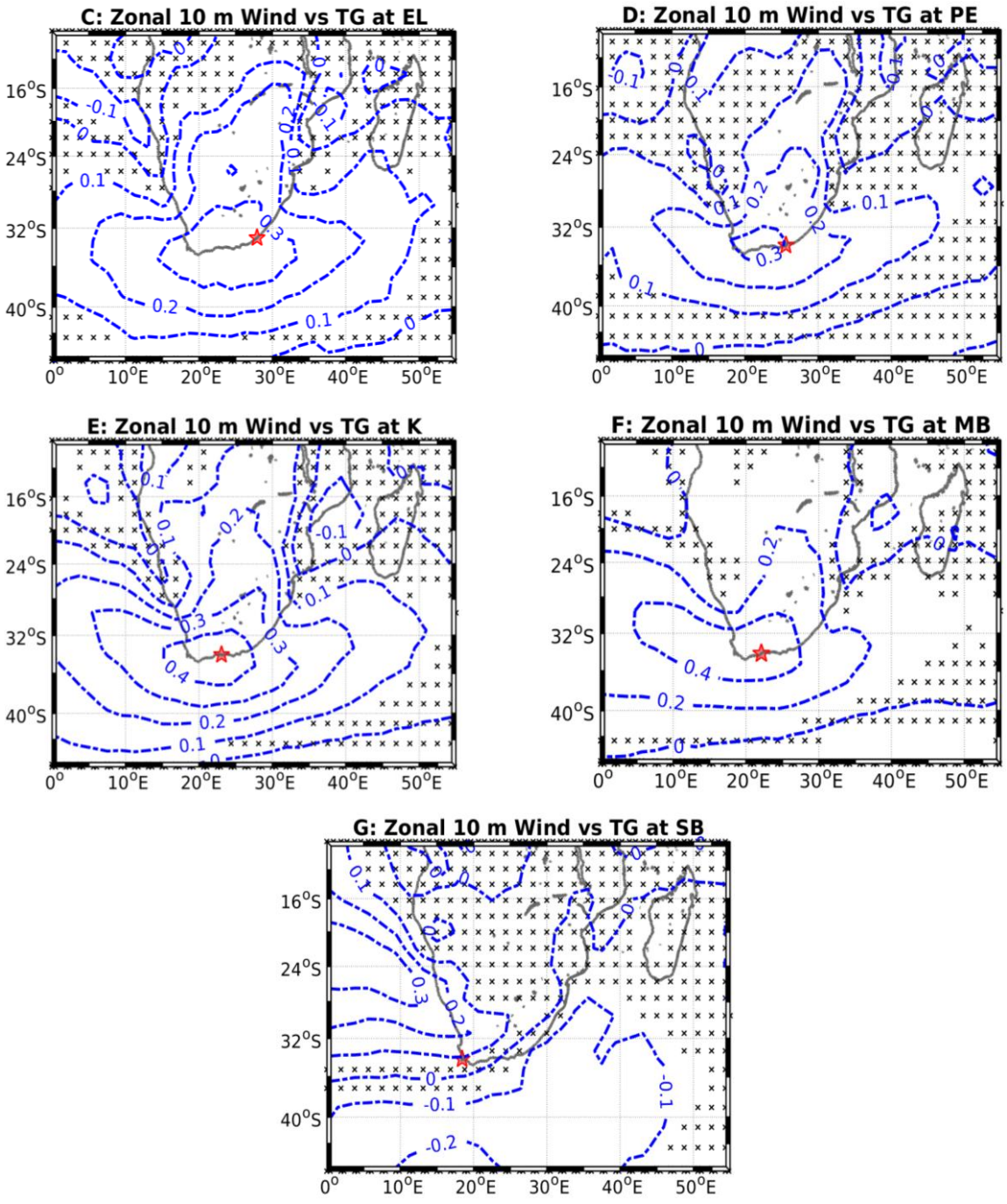

Fig. 4.4: Correlation, at the sub-annual timescale, between regional gridded monthly mean zonal wind at 10 m above the mean sea surface and monthly mean SL records at (A) Richards Bay, (B) Durban, (C) East London, (D) Port Elizabeth, (E) Knysna, (F) Mossel Bay and (G) Simons Bay, respectively. Red stars indicate the tide gauge location. Black crosses indicate area statistically non-significant at 95 % confidence level, estimated using a two-sided t-test.

Fig. 4.5 displays the correlation between regional 10 m meridional wind and sea level variability at sub-annual timescale. Positive meridional winds (southerly winds) are associated with high sea level at Richards Bay and Durban tide gauge locations (Fig. 4.5A and B). However, at Knysna, Mossel Bay and Simons Bay it is the negative meridional component of the wind (northerly winds) that is associated with high coastal sea levels (Fig. 4.5E, F and G). Neither positive nor negative meridional winds seem to have a significant association with sea level at East London and Port Elizabeth (Fig. 4.5C and D). The sea level at Knysna and Mossel Bay (Fig. 4.5E and F, and less strongly Port Elizabeth and Simons Bay (Fig. 4.5D and G)) seems to have a good correlation with the meridional wind to the west of the station. It is noticeable that Richards Bay and Durban, East London and Port Elizabeth, and Knysna and Mossel Bay exhibit a similar correlation pattern, which also portrait the sub-regions found and mentioned in Chapter 3 (Fig. 3.3). The results also indicate that zonal winds are a major influencing factor for SL variability, due to higher correlations when compared to the meridional wind component. Thus, the results suggest the westerlies as the main wind driving mechanism of sea level variability at timescale, especially on the south coast.

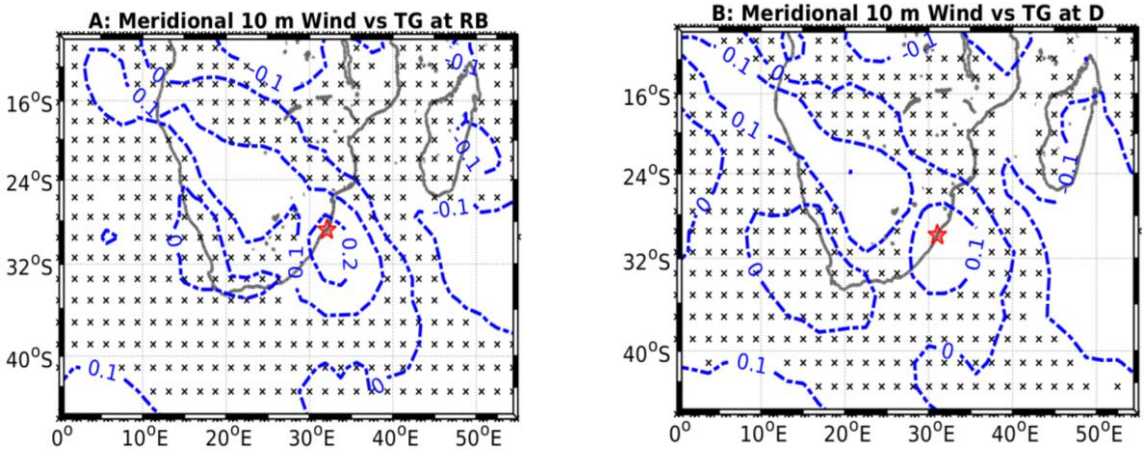

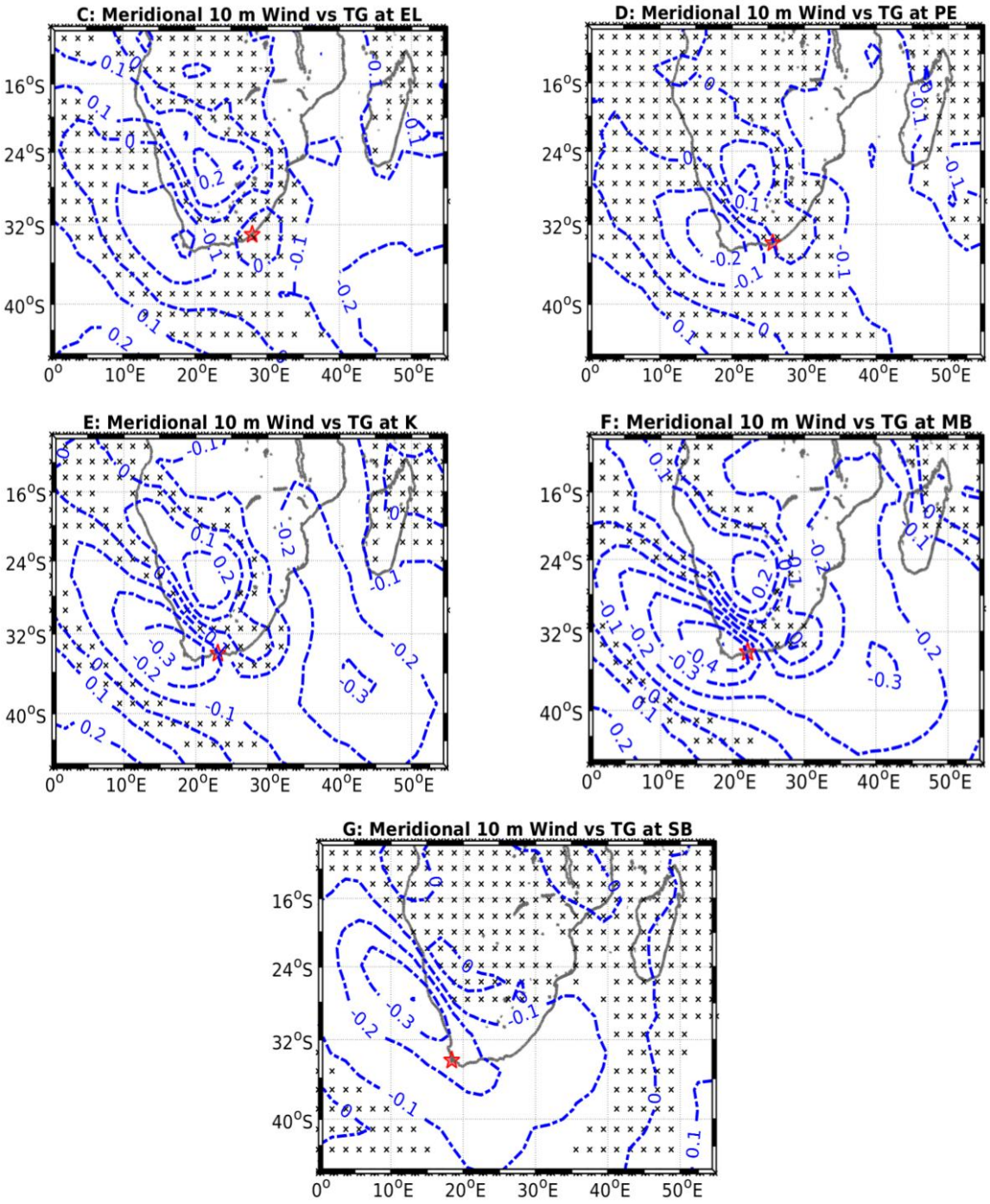

Fig. 4.5: Correlation, at sub-annual timescale, between regional gridded monthly mean meridional wind at 10 m above the mean sea surface and monthly mean SL records at (A) Richards Bay, (B) Durban, (C) East London, (D) Port Elizabeth, (E) Knysna, (F) Mossel Bay and (G) Simons Bay, respectively. Red stars indicate the tide gauge location. Black crosses indicate area statistically non-significant at 95 % confidence level, estimated using a two-sided t-test.

It should be noted however that given the correlations values in Figs. 4.3, 4 and 5, winds may not explain 100% of the variability at the sub-annual timescale. Nevertheless, the analyses contribute significantly to an improved understanding of the effect of atmospheric forcing at this timescale. How coastal sea level along the east and south coasts of South Africa respond to the mesoscale and synoptic weather systems is discussed in the next section.

4.3.2.1 The response of coastal sea level to strong anomalies in the atmospheric forcing

To further understand how the mesoscale and synoptic weather systems are associated with coastal sea level along the east and south coasts of South Africa in the annual cycle, composite average differences between high and low (using one and a half standard deviation threshold) sea level events were calculated and mapped (Fig. 4.6). Composite analysis hence focuses on the stronger signals and may give a clearer picture than the regular correlations, which include the often noisy weak anomalies. The colour scale on the right panels of Fig. 4.6 show the SLP differences during high and low SL events, while the vectors indicate the corresponding change in the direction and magnitude of the winds at 10 m.

Overall, there is a consistent positive SLP difference centred over southern Africa sub-continent. Surface high-pressure systems are associated with a counter-clockwise (anti-cyclonic) wind circulation in the Southern Hemisphere and over the study region (e. g. Taljaard, 1972; van Loon, 1972; Preston-Whyte and Tyson, 1988; Tyson and Preston-Whyte, 2000). The negative SLP difference over the Southern Ocean is notable, producing a north-south pressure gradient. The composite winds are consistent with the pressure pattern. As can be seen, as one move from a station to the next, there is a consistent eastward displacement of the core of the positive SLP difference, resulting in a west-east pressure gradient is followed by the change in wind strength and direction.

The features displayed in Fig. 4.6 are consistent with the correlations between regional SLP and 10 m winds, and tide gauge SL variability discussed above, and hence point to the mechanism in which wind variations are associated with coastal sea level at sub-annual timescale. The association between wind variations and coastal SL variability can be explained through Ekman transport dynamics (Pugh, 1987). Thus, wind variations (mainly longshore winds) induce an onshore water mass transport towards the tide gauge location, i.e. to the left of the wind direction in the Southern Hemisphere (Pugh, 1987).

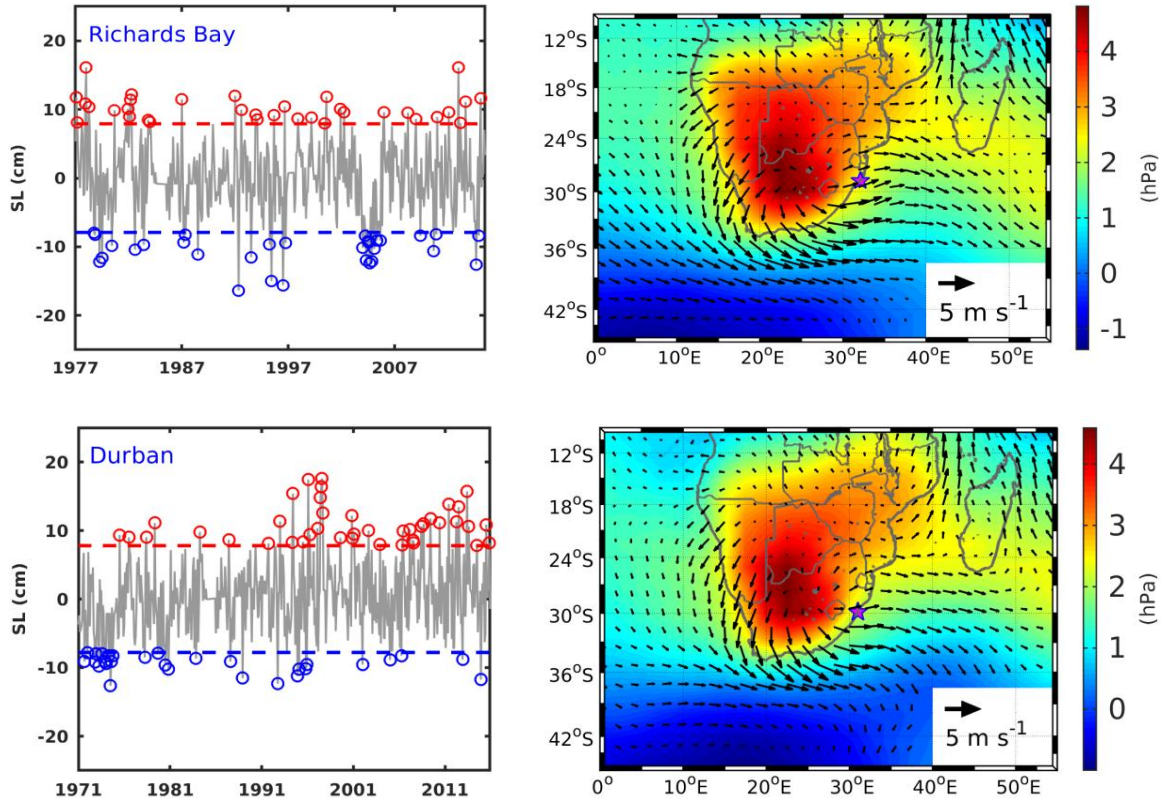

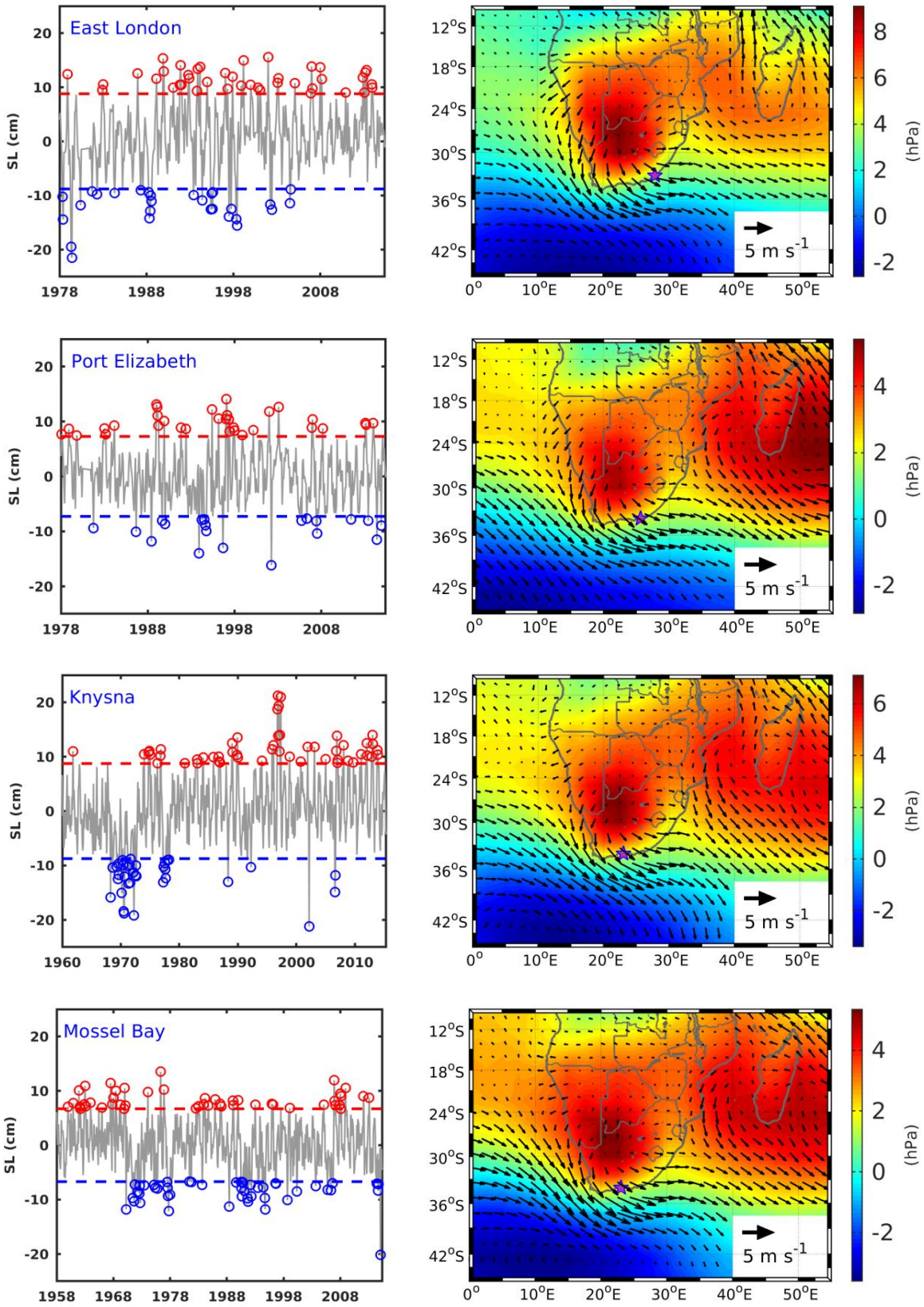
East London
Port Elizabeth
Knysna
Mossel Bay
SL (cm)
(hPa)
5 m s-1
12°S
18°S
24°S
30°S
36°S
42°S
0°
10°E
20°E
30°E
40°E
50°E

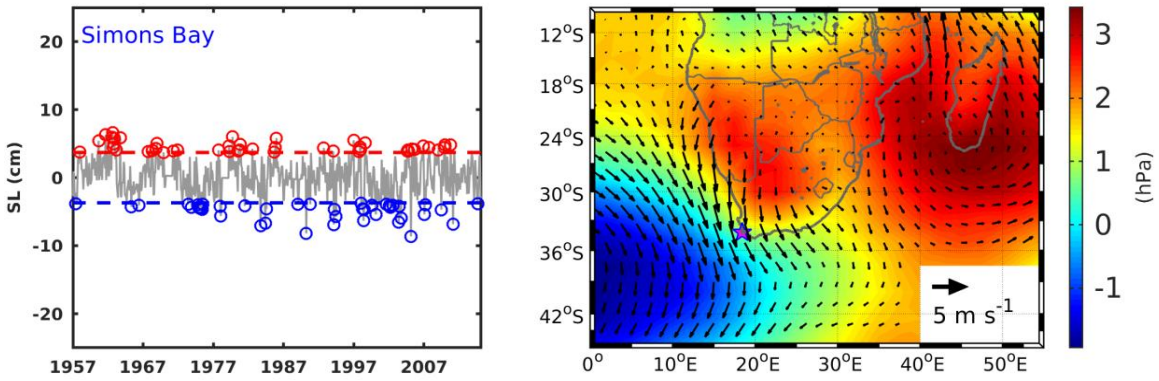

Fig. 4.6: (Left) Monthly mean sea level, with high events (>1.5 standard deviations, red circles) and low events (<1.5 standard deviations, blue circles) at different tide stations. (Right) Composite mean of the differences of the SLP (colour) and 10-m winds (vectors) corresponding to high and low events in the sea level. Magenta stars indicate the tide gauge location.

In our region, the physical mechanism by which SLP gradient anomalies and the corresponding wind variations influence monthly mean coastal SL variability, although mentioned in previous studies, has neither been shown nor explained to our knowledge, for a number of reasons, including the limitations of data. In fact, it is even emphasised that given, for instance, the poor data quality, conclusions were based solely on visual correlations and the consistency of the results with the studies conducted out elsewhere around the globe (Brundrit, 1984; Brundrit et al., 1984; Brundrit et al., 1987).

In summary, the results presented here indicate that SLP gradient anomalies cause enhanced alongshore winds leading to an increased or decreased coastal SL through Ekman transport dynamics, at the sub-annual timescale (Fig. 4.6), suggesting that sea level responds to the mesoscale and synoptic weather systems in the annual cycle, in agreement with previous literature (Brundrit, 1984; Brundrit et al., 1984; 1987). It turns out, however, that the response of coastal sea level variability to longshore wind variations associated with mesoscale and synoptic weather systems is commonly used to describe the propagation characteristics of coastal trapped waves along the coast of southern Africa on timescales of days (de Cuevas et al., 1986; Schumann and Brink, 1990). Hence, when analysing Fig. 4.6 from south to east coasts i.e. from Simons Bay to Richards Bay, one can notice that if a coastal trapped wave is generated

in the west coast it would travel clockwise to the east, in agreement with Chelton and Davis (1982). According to Chelton and Davis (1982), the lagged response to the disturbances along the eastern boundary regions can also be detected in monthly mean TG records.

Brundrit (1984) suggested that the mesoscale and synoptic atmospheric disturbances are responsible for 5 cm of the variability in the monthly mean sea level data. These weather systems propagate from the west to south coast around southern Africa. The periodicity and amplitude of the sum of the sub-annual modes appear to confirm this. On the south coast, the amplitude of sub-annual timescale variability is around 5 cm, consistent with the results of Brundrit (1984), along the west coast. In contrast to the south coast, the east coast, from Port Elizabeth equatorwards, shows sub-annual amplitudes greater than 5 cm (Fig. 4.2 and Appendix B). The causes of this increase in amplitude were not further investigated, given the scope of this study.

Synoptic atmospheric disturbance patterns contribution is 30 to 50 cm amplitude in the daily mean sea level data around the southern African coast, allowing the study of propagation characteristics of coastally trapped waves (de Cuevas et al., 1986; Schumann and Brink, 1990). Furthermore, the influence of the mesoscale and synoptic atmospheric disturbances as the drivers of sea level variability tend to be less important at longer timescales (e.g. Richter et al., 2012), but are not negligible (e.g. Sturges and Douglas, 2011; Calafat et al., 2013; Dangendorf et al., 2014).

4.3.3. Drivers of tide gauge sea level variability at interannual timescales

Brundrit (1984) indicated that interannual sea level variability along the west coast of southern Africa has an association with identical phenomenon to ENSO, operating in the eastern equatorial Atlantic and extending its influence southward along the west coast of southern Africa, through coastal SST modulation. Positive and negative phases of ENSO and IOD have also been shown to be associated with the interannual SLA variability via wind stress and volume

transport variations in the southern South China Sea (Soumya et al., 2015). The mechanism by which modes of climate variability are related to coastal SL variability is yet not fully understood (Woodworth et al., 2009; Ezer et al., 2016). The consensus so far is that the climate indices do not influence coastal SL directly, instead they modulate the oceanic circulation patterns as well as the frequency and intensity of the various regional weather systems that can directly affect coastal sea levels (Chen et al., 2014; Dangendorf et al., 2014; Park and Sweet, 2015; Chafik et al., 2017).

Linear correlations were used to examine whether there is a possible connection between the modes of climate variability (IOD, ENSO and SAM) and coastal sea level variability along the south and east coasts of South Africa. The time series examined are the separated EMD oscillatory modes, grouped as the interannual timescale; the statistical significance of the resulting correlation coefficients was tested based on Chelton (1983). Moreover, the correlations were carried out at multiple time lags to see whether or not there is a lagged response of the coastal SL variability to the examined modes of climate variability and the parameters used to generate the those climate indices. To our knowledge, previous studies investigating such connections over the studied region are not found in the literature.

Fig. 4.7 shows the correlation between the dipole mode index and tide gauge sea level data, at the interannual timescale. The results suggest varying degrees of influence of the DMI over the studied region. However, only at Durban and Port Elizabeth the correlation coefficients are statistically significant. The highest correlation values of approximately 0.38 and 0.23 are noted at Durban and Richards Bay, respectively. At both tide gauge sites, the coherence in the variability of SL and DMI is also noticeable. This suggests that DMI has an influence on sea level variability on the east coast. The correlation between DMI and sea level variability at Port Elizabeth is also remarkable, with a correlation of –0.5 at 6 months lag. There are, on occasion, strongly positive or negative IOD events that co-occur with anomalously high/low sea level events. Despite there not being a consistently strong relationship between sea level and the IOD as shown by the correlation with DMI, the 1997 positive IOD event, regarded as one of the

strongest (e.g. Soumya et al., 2015) appears to have led to positive sea level anomalies at all sites.

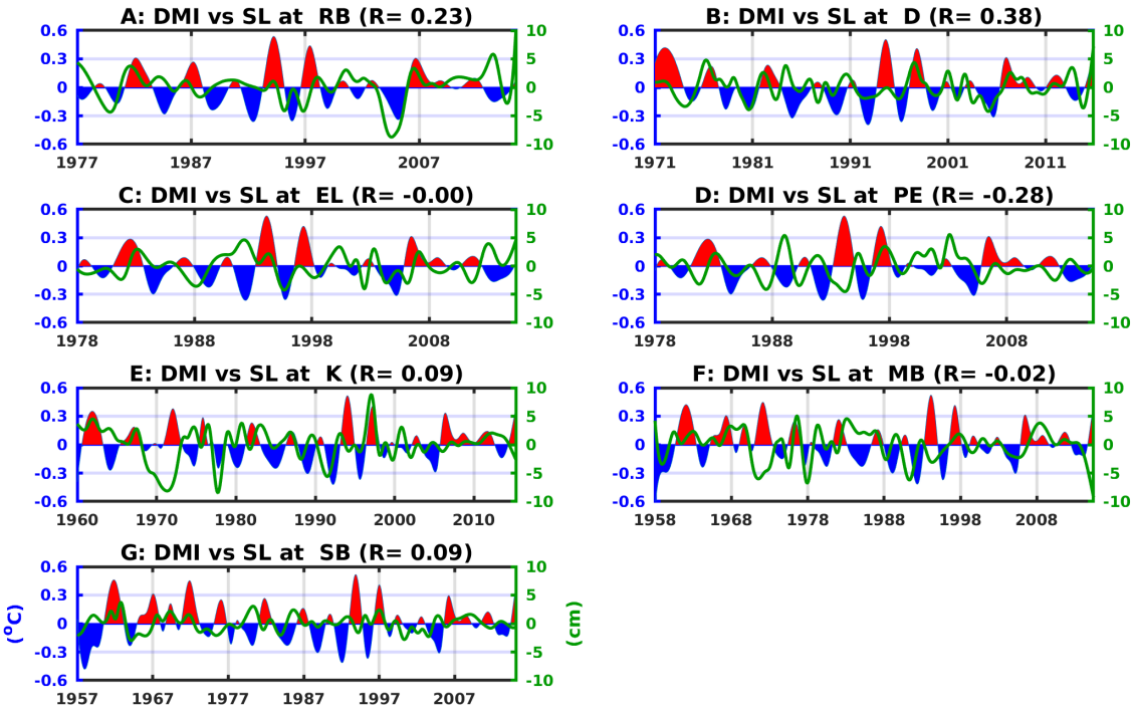

Fig. 4.7: Time series of interannual Dipole Mode Index (DMI) and SL records at (A) Richards Bay, (B) Durban, (C) East London, (D) Port Elizabeth, (E) Knysna, (F) Mossel Bay and (G) Simons Bay. Correlation coefficients are found in the panel titles.

Monthly time series of the Subtropical Indian Ocean Dipole index were also correlated to SL variability at the interannual timescale. The SIOD results are similar to the IOD ones, discussed above.

To further investigate the impact of climate indices, a correlation between a multivariate ENSO index and sea level variability was examined (Fig. 4.8). It is challenging to draw conclusions about consistent relationships due to the inconsistent correlations and the lack of statistical significance even down to 90% confidence level. While the correlations between MEI and sea level at the various sites are very weak, the highest correlation was found at Durban, approximately 0.18 at 6 months lag. Nevertheless, analysing individual strong ENSO events (not

shown) it is obvious that strong El Niño events tend to lead to high sea level at all sites. Similarly, strong La Niña events tend to lead to low sea level events. The mechanism through which ENSO is transmitted to high/low sea level remains unclear. However, Brundrit et al., 1987, correlated the high sea level in the eastern South Atlantic to the strong 1982-1983 El Niño events. This finding is in agreement with the current results (Fig. 4.8G).

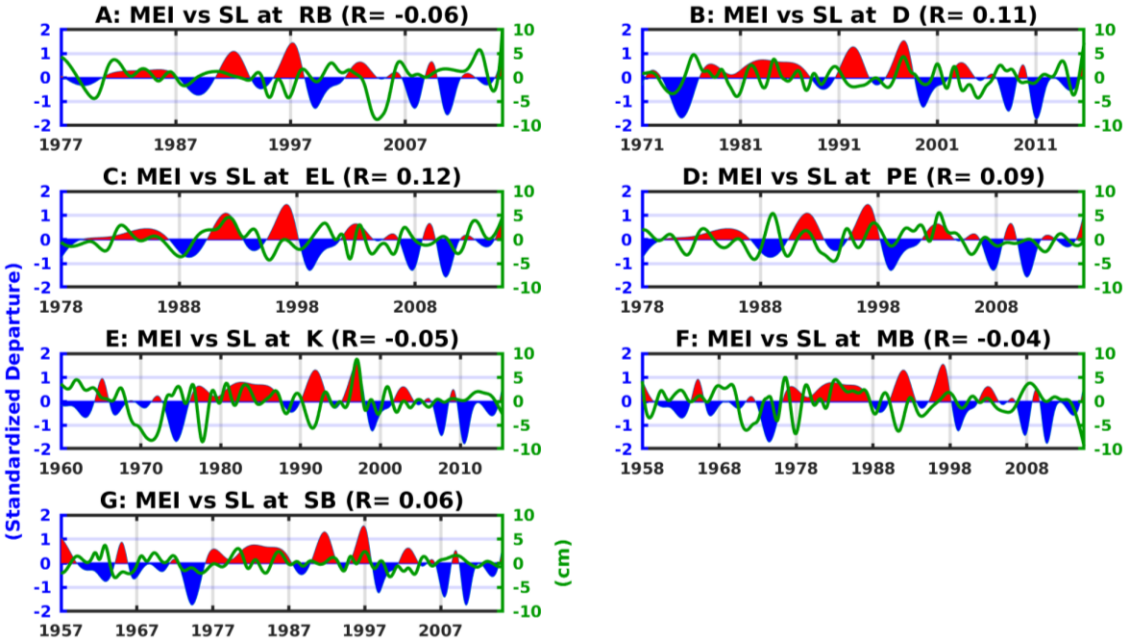

Fig. 4.8: Time series of interannual Multivariate ENSO Index (MEI) and SL records at (A) Richards Bay, (B) Durban, (C) East London, (D) Port Elizabeth, (E) Knysna, (F) Mossel Bay and (G) Simons Bay. Correlation coefficients are found in the panel titles.

There are several ENSO indices, derived from different parameters including SLP and SST, although the choice was to use MEI due to its completeness, as described in the data section. To support this choice, other ENSO indices were also examined and the results were comparable to the ones discussed above.

A correlation between SAM and sea level variability was also carried out (Fig. 4.9). The results suggest that SAM has a measurable influence on coastal sea level in the region. The highest correlation value was found at Simon's Bay (approximately 0.3 at 3-month lag). High sea levels

at Simon's Bay appear to be most likely to be observed up to 3 months prior to a positive SAM event. The mechanism by which it operates was not further investigated. However, positive SAM events reflect a poleward contraction of the belt of strong westerly winds resulting in fewer low-pressure systems reaching southern Africa, as mentioned above. Overall, negative SAM events lead to high SL at Richards Bay, Durban, East London and Port Elizabeth and, positive SAM events lead to high SL at Knysna, Mossel Bay and Simons Bay.

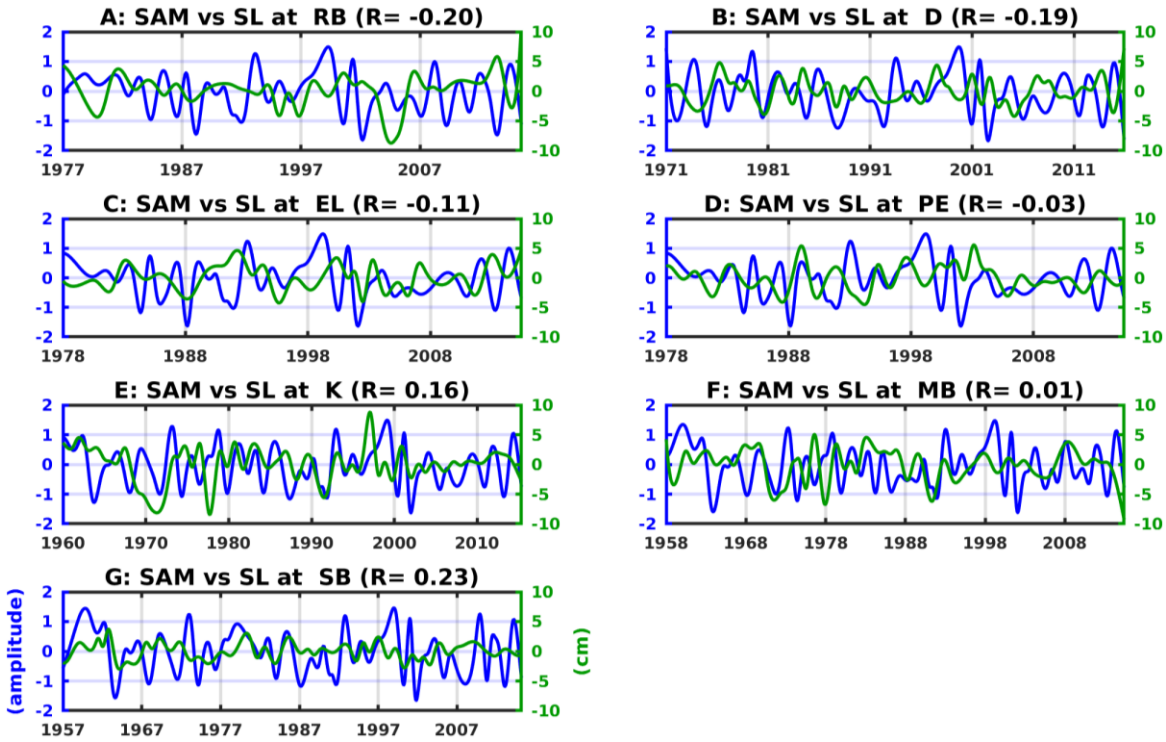

Fig. 4.9: Time series of interannual Southern Annular Mode (SAM; Marshall, 2003) and SL records at (A) Richards Bay, (B) Durban, (C) East London, (D) Port Elizabeth, (E) Knysna, (F) Mossel Bay and (G) Simons Bay. Correlation coefficients are found in the panel titles.

The influence of the climate indices on sea level variability at the interannual timescale has been examined. Results suggest that at this timescale, tide gauge SL variability is only weakly influenced by ENSO, IOD, and SAM.

4.3.3.1 The combined influence of the modes of climate variability

To further understand how the three modes of climate variability (ENSO, IOD and SAM) under consideration are associated with the coastal SL along the east and south coasts of South Africa at the interannual timescale, composite average differences between positive and negative (using 0.75 standard deviation threshold) MEI, DMI and SAM index events were calculated and the results are displayed in Fig. 4.10. The colour scale shows the magnitude of the sea level differences during positive and negative events of ENSO, IOD and SAM, respectively. With the exception of East London, the resulting SL differences during ENSO events are essentially zero. However, positive IOD events appear to force high coastal sea levels compared to negative IOD events. It appears that negative SAM events have the tendency to induce higher coastal sea levels than positive SAM events. Fig. 4.10 hardly gives an indication of a pattern in the modulated SL differences that would help identify any sub-regional impacts. It turns out however, that East London displays a unique pattern, in agreement with the results discussed above.

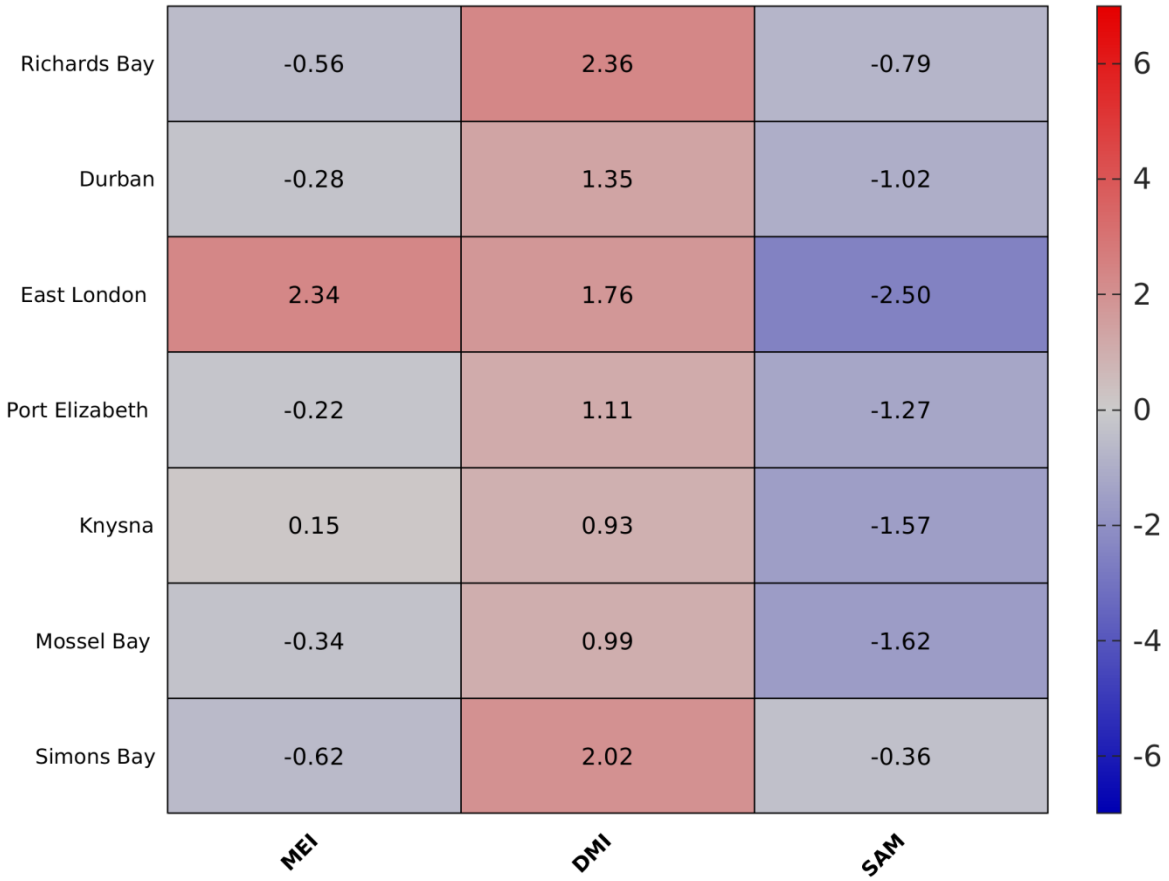

Fig. 4.10: Sea level composite mean difference (cm) based on MEI (ENSO), DMI (IOD) and SAM indices at all studied tide gauges. The tide gauges are labelled with their names (y-axis), from east to south. Colour indicates the magnitude of SL differences during positive and negative indices.

Assuming that for instance, a particular positive or negative ENSO event may occur during months in which positive or negative IOD or SAM events are observed, the impact of the paired interaction between the three modes of climate variability and coastal SL was further investigated. Fig. 4.11 shows the results of SL differences during the interaction of MEI-DMI, MEI-SAM and DMI-SAM, respectively.

With minus exceptions, the combinations +MEI/+DMI and +DMI/-SAM appear to modulate consistent positive SL differences, implying that high coastal sea levels are observed during months of El Niño/positive IOD and positive IOD/negative SAM events, respectively. On the contrary, low coastal sea levels appear to be more likely to be observed during months of El

Niño/negative IOD and El Niño/positive SAM events, respectively +MEI/-DMI and +MEI/+SAM combinations, with the exception of East London. A remarkably high SL difference is noticeable at Simons Bay during the combination +MEI/-DMI. There is a good chance for high monthly sea levels to be recorded at Richards Bay and Durban, and low monthly sea levels at other tide gauge sites during months of the combination positive IOD/positive SAM (+DMI/+SAM). Positive sea level differences are observed in the combination +MEI/-SAM, with the exception of Mossel Bay and Simons Bay, implying that high monthly SL levels are recorded during months of El Niño/negative SAM events. It is noteworthy that East London has a particular association with all the combinations. Hence, all the combinations appear to induce high SL differences at East London, with the exception of the combination +DMI/+SAM.

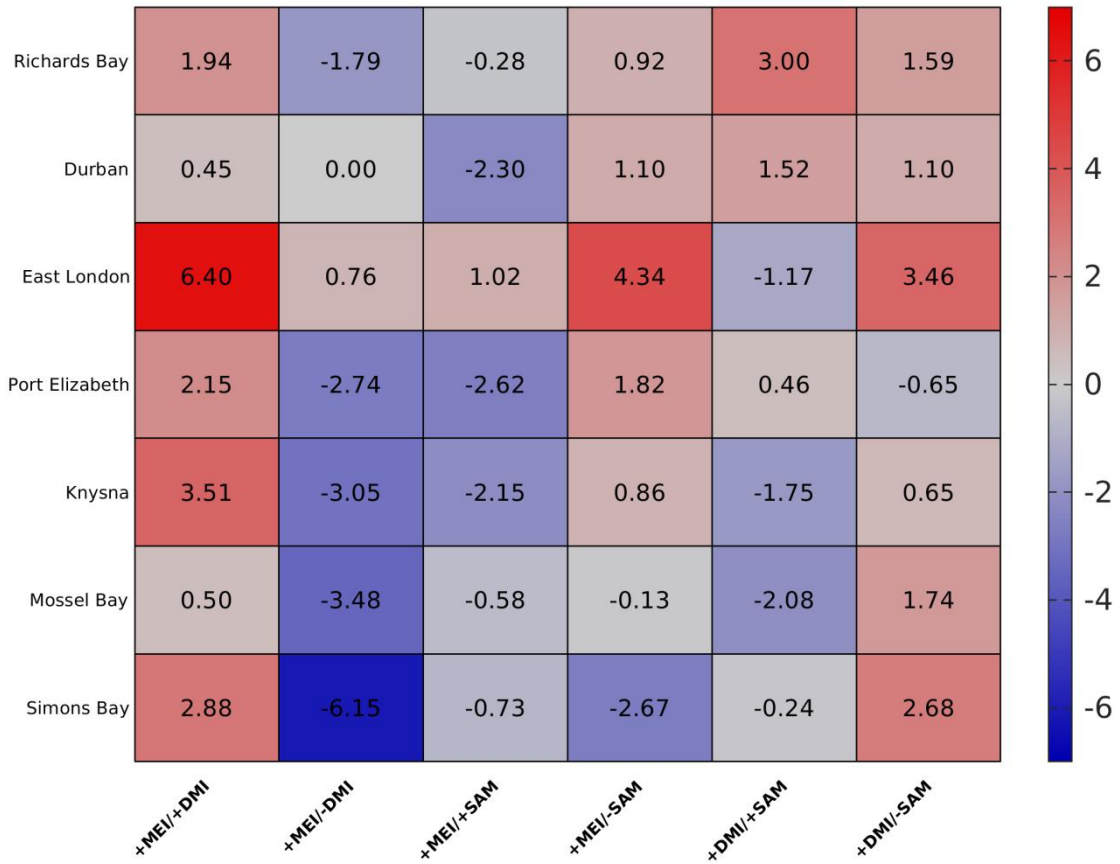

Fig. 4.11: Sea level composite average differences (cm) at all studied tide gauges, based on MEI/DMI, MEI/SAM and DMI/SAM climate indices combinations. The tide gauges are labelled with their names (y-axis), from east to south. Colour indicates the magnitude of SL differences during the climate indices combinations.

Furthermore, anomalously high sea level months (using one and a half standard deviation above mean threshold) were identified (see Fig. 4.6) and these events were plotted in the space of two climate indices (Appendix C). This allowed describing how each tide gauge is most influenced by a specific combination of the modes of climate variability (MEI/DMI, MEI/SAM and DMI/SAM). High and low sea level events were in the above associated with the mesoscale and synoptic weather systems to explain the atmospheric forcing in the sub-annual non-seasonal variability. Here, the assumption is that those mesoscale and synoptic weather systems may have been modulated by the interaction of the climate indices and then affect coastal sea levels which would be consistent with other studies in the literature (Chen et al., 2014; Dangendorf et al., 2014; Park and Sweet, 2015; Chafik et al., 2017).

Overall, all the studied tide gauge sites (not shown) indicate that the interaction +MEI/+DMI is likely to induce anomalously high coastal sea level, consistent with the results of sea level composite average differences discussed above (Fig. 4.11). Moreover, one cannot draw a sound conclusion regarding the pair of interaction that affects coastal sea level the most when examining the combinations of MEI and SAM indices during high sea level months at the studied TG stations. Additionally, most of the studied tide gauge sites are dominated by the interaction +DMI/+SAM (not shown), which indicates that there is high chance to be recorded high sea levels during months of positive IOD/positive SAM events, not consistent with the results of sea level composite average differences.

To summarise, different combinations of the climatic modes of variability (MEI/DMI, MEI/SAM and DMI/SAM) were examined to further understand the impact of their interaction on local and regional coastal sea level. The results suggest a varying degree of influences, with East London displaying a unique connection as well as being the separation point for east and south effects.

4.3.3.2 The influence of large scale atmospheric surface fields

As mentioned above, previous studies have also associated tide gauge SL variability with ENSO through large-scale sea surface temperature patterns (e.g. Brundrit, 1984; Brundrit et al., 1984; Brundrit et al., 1987) and large-scale wind patterns (e.g. Han et al., 2010; Han et al., 2014). Thus, the parameters (SST, SLP, zonal and meridional winds) used to generate the examined climate indices were further investigated separately. Note that SSTs compose the oceanic component of the indices while SLP and winds are the atmospheric component hence, they are often combined to monitor the ocean – atmosphere interactions dynamics that drive the large scale interannual climate variability (Trenberth, 1997; Neelin et al., 1998; Saji et al., 1999; Trenberth and Stepaniak, 2001).

The objective herein is to clarify some of the inconsistencies in the results above, and hence advance the understanding of the influence of climate modes of variability on local and regional sea level. Hence, examining the temporal and spatial behaviour of the underlying parameters may give an indication of what should be expected when analysing the impact of the climate indices. Moreover, this investigation may give more insight into where to focus when studying the relationship between climate drivers and coastal sea level variability as a suggestion for a new approach. Additionally, it is of interest to investigate the mechanism in which climate indices influence coastal SL. Therefore, the interannual time series at each tide site were correlated with the data sets at each grid point of the global surface fields and the statistical significance of the resulting correlation was estimated through a two-sided t-test. Fig. 4.12 displays the correlation between tide gauge sea level variability and gridded global ERSST, at the interannual timescale. The correlation for most of the areas from which the climate indices are derived, including IOD and ENSO, are not statistically significant at the 95% confidence level. This to some extent explains why the indices evaluated above did not yield a strong relationship with sea level.

A closer look to the maps of Fig. 4.12A, B and D reveal that Richards Bay, Durban and Port Elizabeth tide gauge SL records correlate with the SSTs over some of the tropical and

subtropical Indian Ocean boxes, which explains the coefficients found in Fig. 4.7A, B and D. Additionally, a clear high correlation is also noticeable between sea level at Simon's Bay and the SSTs over the western tropical Indian Ocean box (Fig. 4.12G), without displaying any correlation dipole (i.e. both the south-eastern equatorial Indian Ocean and the western equatorial Indian Ocean boxes display a positive correlation), hence highlighting the need for a further investigation of processes.

In the tropical Pacific region, SST anomalies are commonly used for monitoring ENSO conditions and hence to derive the indices (e.g. Trenberth, 1997; Neelin et al., 1998; Trenberth and Stepaniak, 2001). For instance, SST anomaly index from Niño 3.4 region is the most used in science amongst all other indices including MEI because it goes up to part of the Niño 3 and Niño 4 region, including further into the Southern Hemisphere (Trenberth and Hoar, 1996). However, with the exception of East London (Fig. 4.12C), none of the studied sites have a strong correlation with SSTs over Niño 3.4 region. Significant correlations between SSTs over Niño 1+2 and tide gauge records at Durban, East London and Simons Bay are also noticeable. It is noteworthy that SSTs at surrounding areas of the tide gauge appear to be important at all tide gauge sites, in agreement with Dangendorf et al. (2014) who suggest that in a simplified way, local SL variability can be viewed as the sum of atmospheric forcing and steric changes (due to temperature and salinity variations).

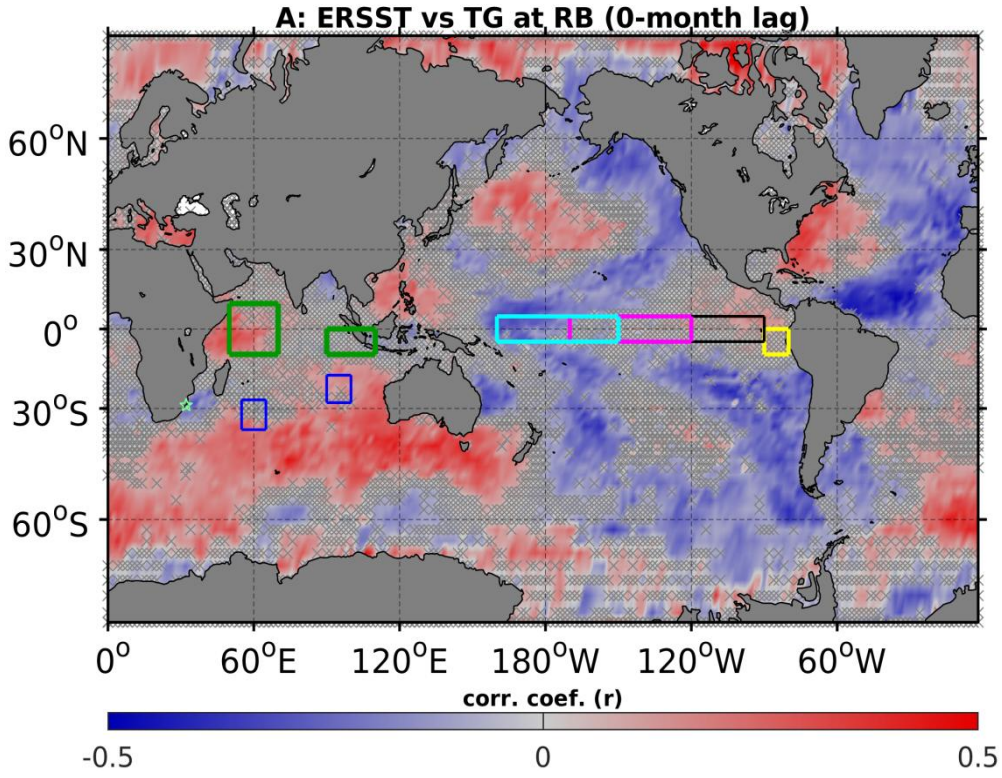
A: ERSST vs TG at RB (0-month lag)
60°N
30°N
0°
30°S
60°S
0°
60°E
120°E
180°W
120°W
60°W
corr. coef. (r)
-0.5
0
0.5

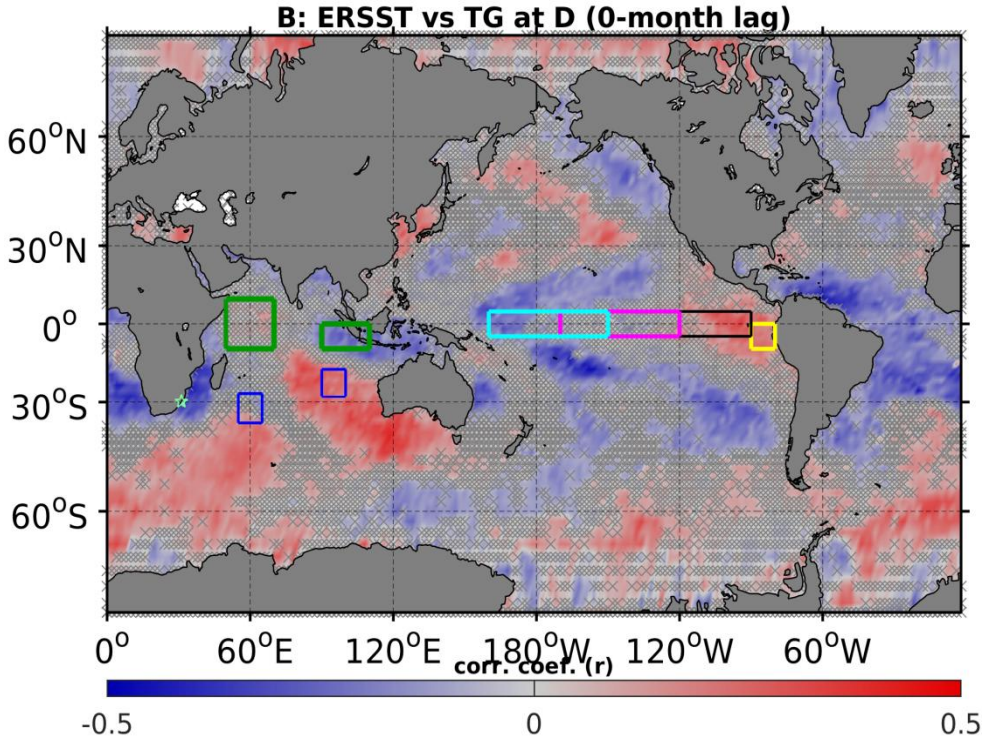
B: ERSST vs TG at D (0-month lag)
60°N
30°N
0°
30°S
60°S
0°
60°E
120°E
180°W
120°W
60°W
corr. coef. (r)
-0.5
0
0.5

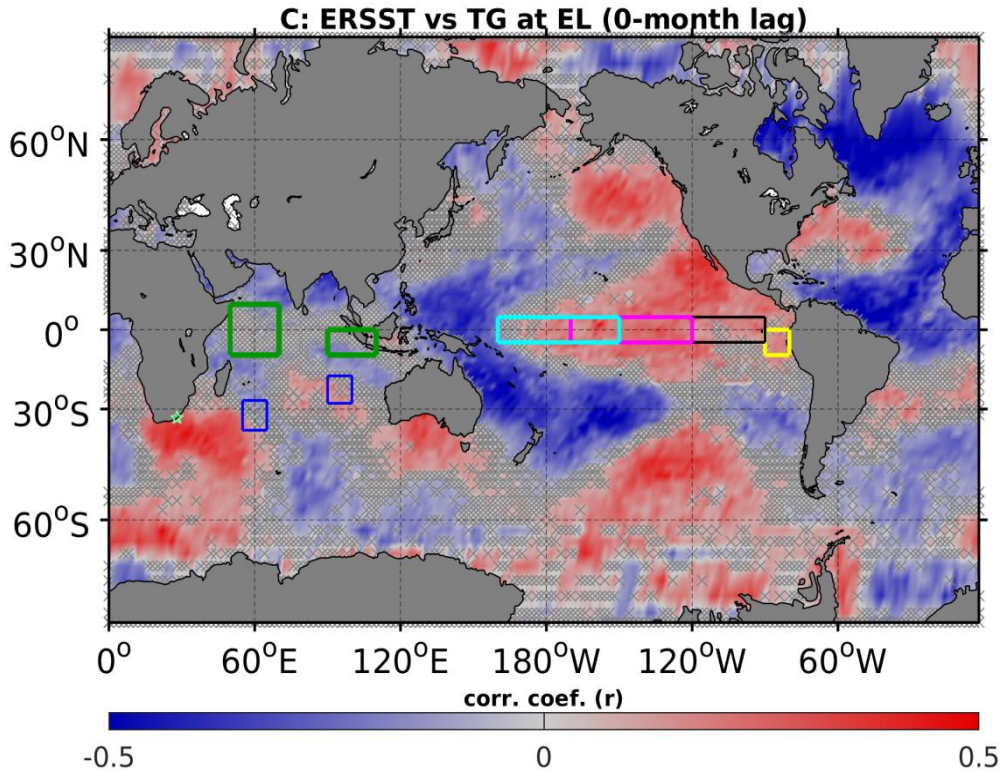
C: ERSST vs TG at EL (0-month lag)
60°N
30°N
0°
30°S
60°S
0°
60°E
120°E
180°W
120°W
60°W
corr. coef. (r)
-0.5
0
0.5

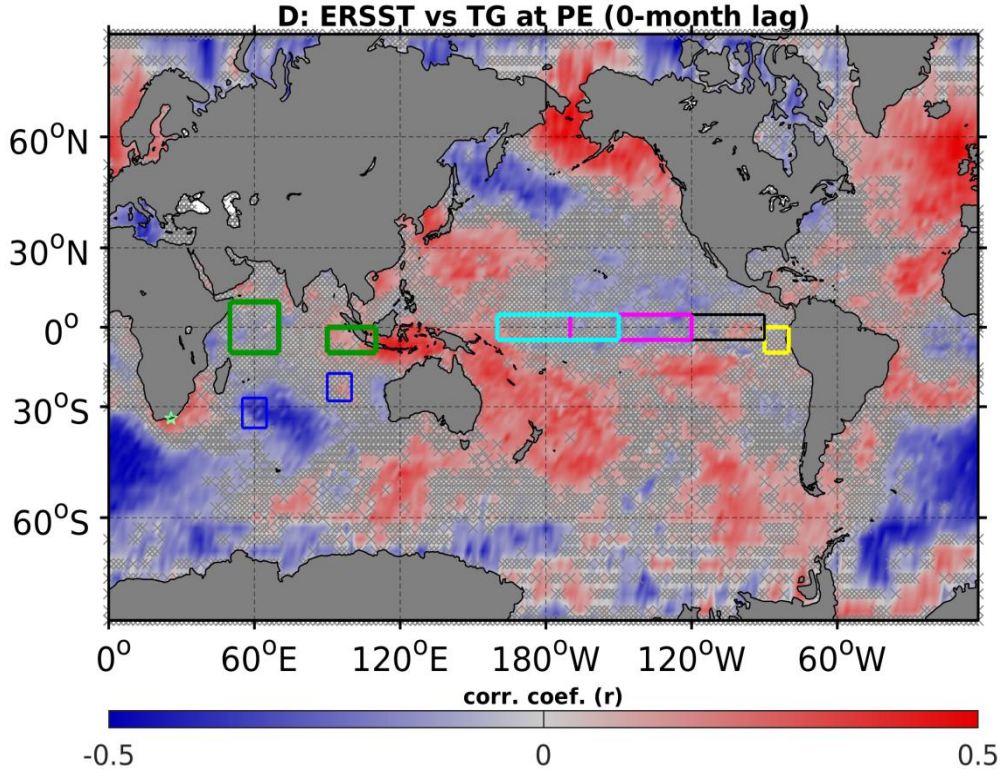
D: ERSST vs TG at PE (0-month lag)
60°N
30°N
0°
30°S
60°S
0°
60°E
120°E
180°W
120°W
60°W
corr. coef. (r)
-0.5
0
0.5

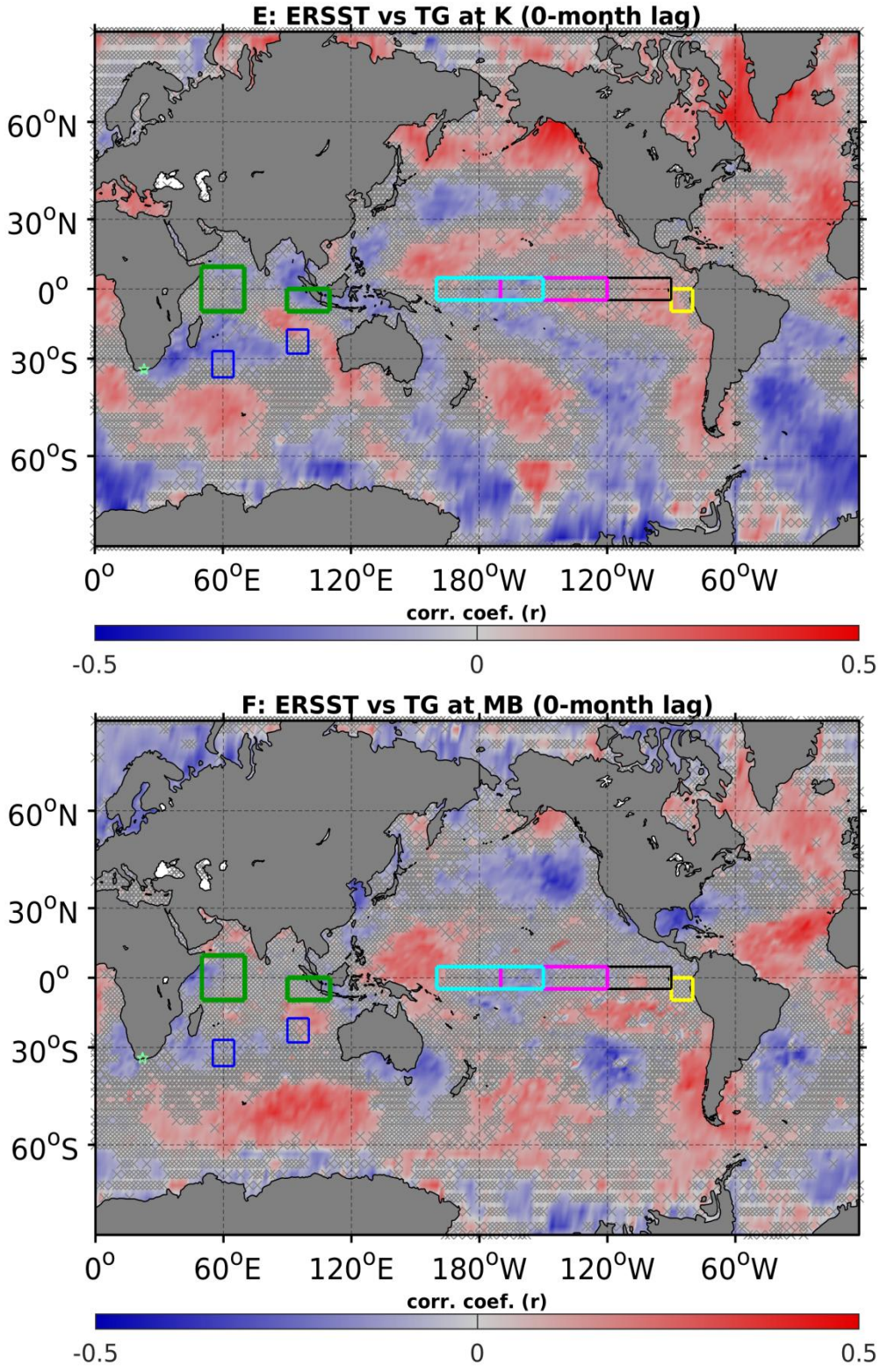
E: ERSST vs TG at K (0-month lag)
60°N
30°N
0°
30°S
60°S
0°
60°E
120°E
180°W
120°W
60°W
corr. coef. (r)
-0.5
0
0.5
F: ERSST vs TG at MB (0-month lag)
60°N
30°N
0°
30°S
60°S
0°
60°E
120°E
180°W
120°W
60°W
corr. coef. (r)
-0.5
0
0.5

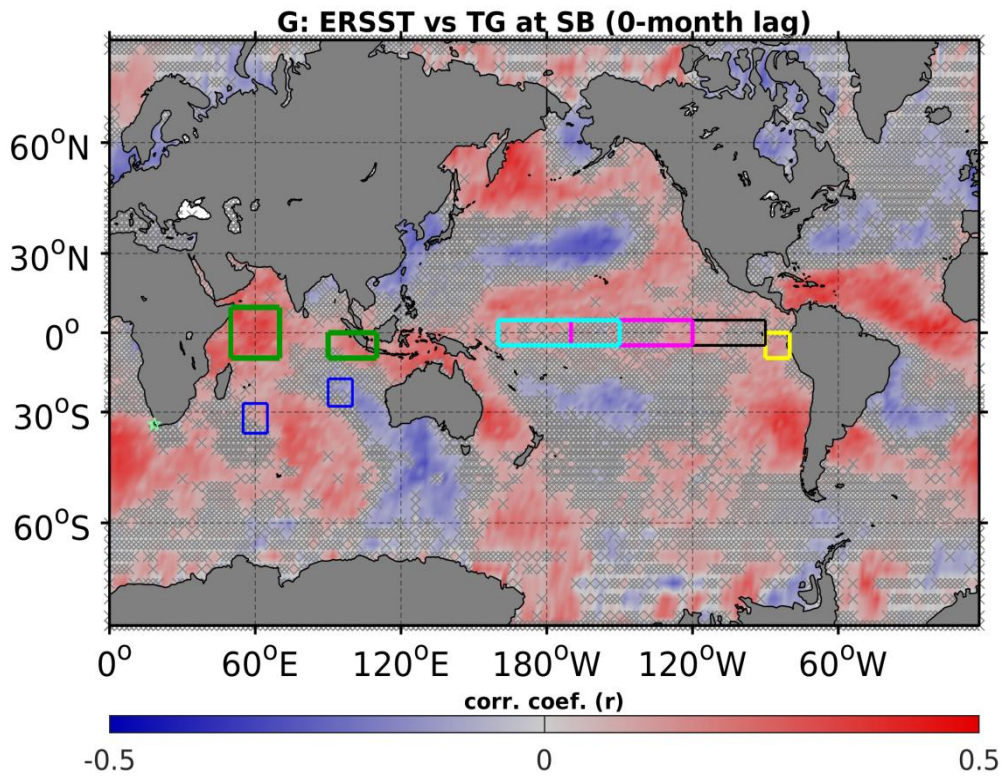

Fig. 4.12: Correlation, at interannual timescale, between global gridded monthly mean extended reconstructed SST and monthly mean SL records at (A) Richards Bay, (B) Durban, (C) East London, (D) Port Elizabeth, (E) Knysna, (F) Mossel Bay and (G) Simons Bay, respectively. Green stars indicate the tide gauge location. Grey crosses indicate area statistically non-significant at 95% significance level, estimated using a two-sided t test. Different coloured boxes indicate the regions based on which most of the climate indices are derived. The green boxes indicate the western (left) and eastern (right) tropical Indian region. The blue boxes represent the western (left) and eastern (right) subtropical Indian Ocean region. The yellow, black, magenta and cyan boxes indicate Niño 1+2, 3, 3.4 and 4 regions, respectively.

Global gridded sea level pressure was correlated to tide gauge records at the interannual timescale, Fig 4.13. The SLP is normally used for monitoring the conditions of the Southern Oscillation and so quantify the Southern Oscillation Index (SOI). The SOI is defined as the difference between anomalous barometric pressures over Darwin (12°S; 130°E) and Tahiti (17°S; 149°W). Consequently, considering the correlation of the maps in Fig. 4.13, one should expect a weak correlation if one uses SOI to correlate to SL variability in South Africa. With the exception of East London (Fig. 4.13C), none of the studied sites have shown a strong correlation with SLP over large part of the tropical Pacific. Overall, Fig. 4.13 emphasises the importance of

the regional and local SLP in coastal SL variability, at the interannual timescale, consistent with the findings of Sturges and Douglas (2011). Although their study focused on decadal variability, here we found that even at the interannual timescale, coastal SL can be associated with SLP.

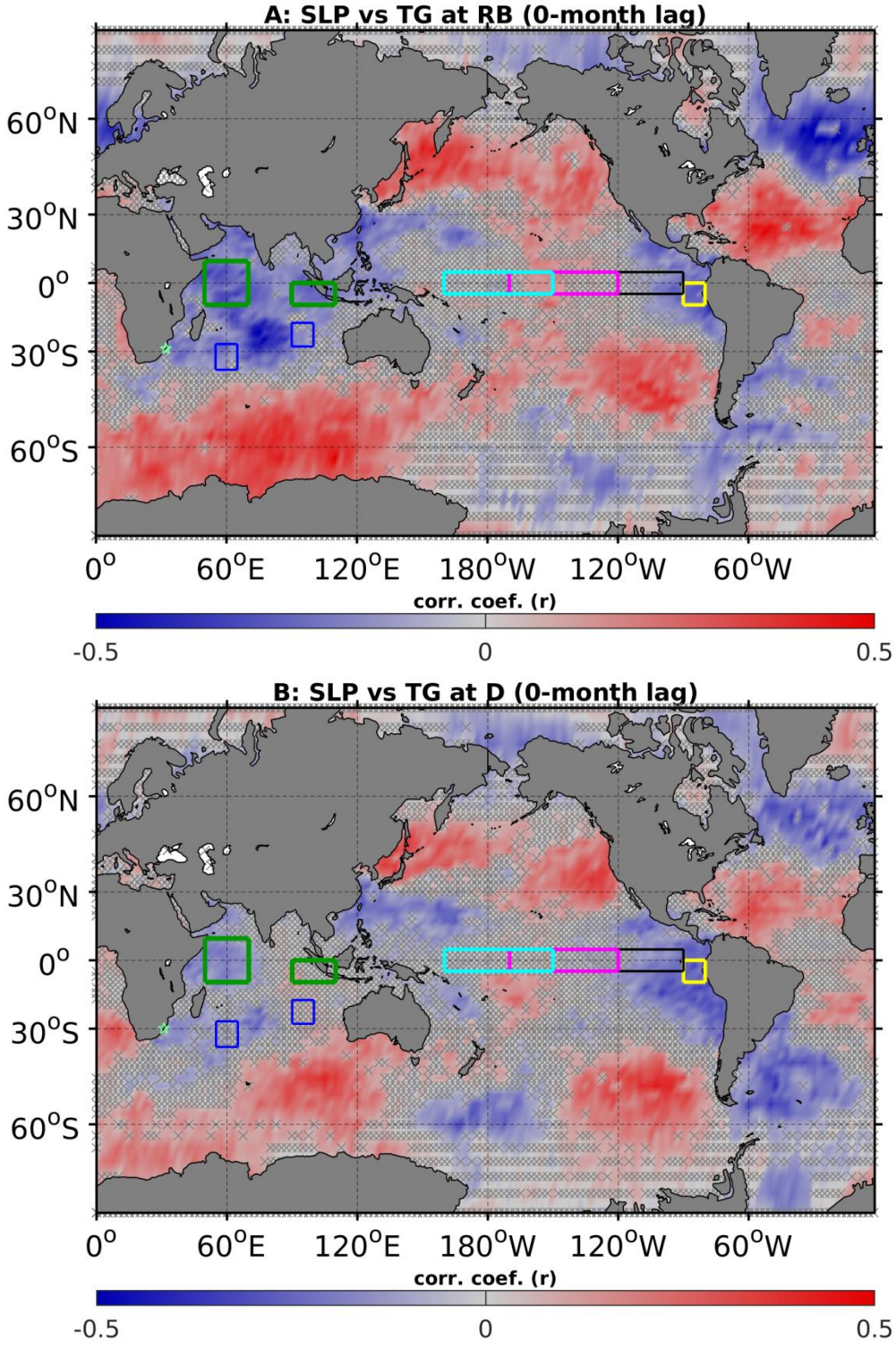

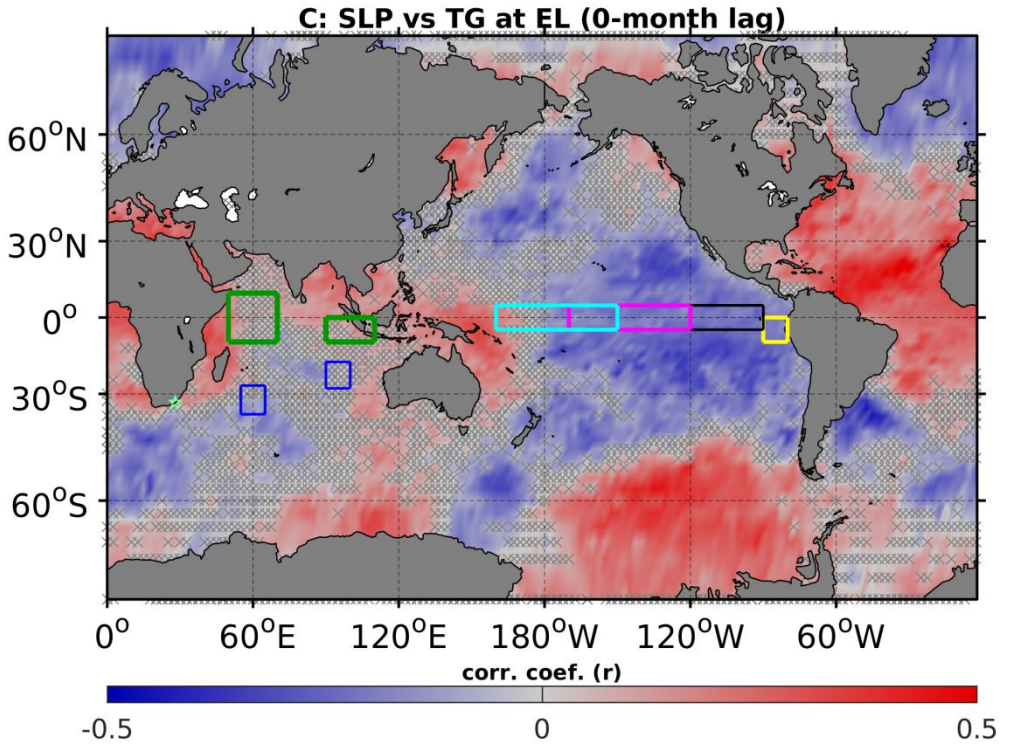
C: SLP vs TG at EL (0-month lag)
60°N
30°N
0°
30°S
60°S
0°
60°E
120°E
180°W
120°W
60°W
corr. coef. (r)
-0.5
0
0.5

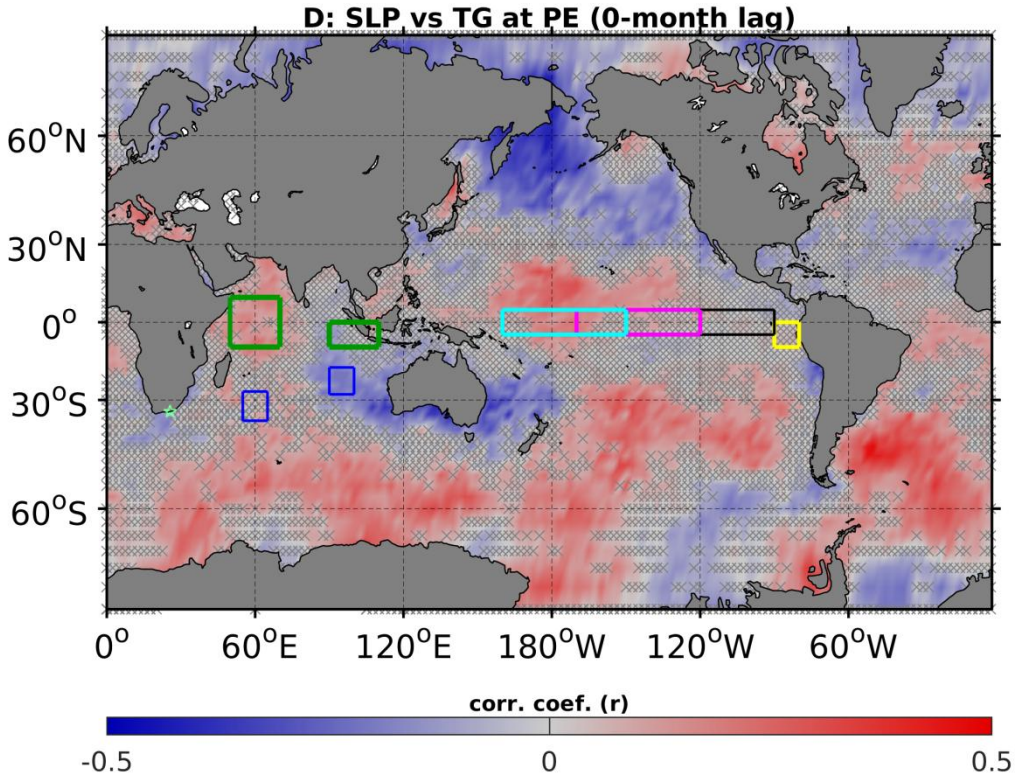
D: SLP vs TG at PE (0-month lag)
60°N
30°N
0°
30°S
60°S
0°
60°E
120°E
180°W
120°W
60°W
corr. coef. (r)
-0.5
0
0.5

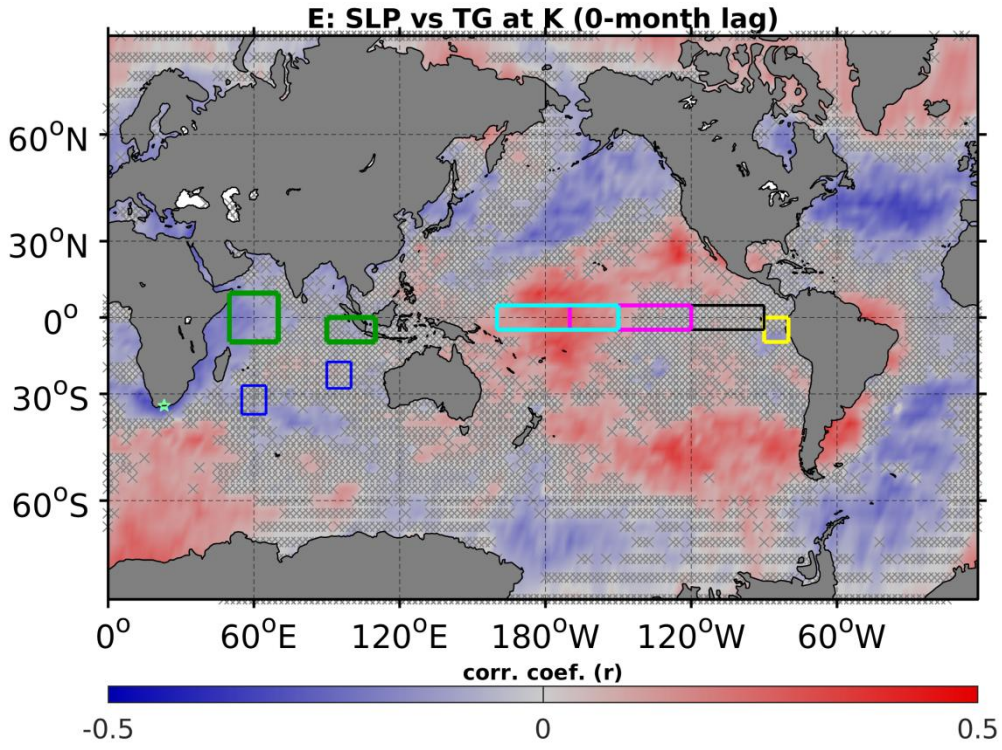
E: SLP vs TG at K (0-month lag)
60°N
30°N
0°
30°S
60°S
0°
60°E
120°E
180°W
120°W
60°W
corr. coef. (r)
-0.5
0
0.5

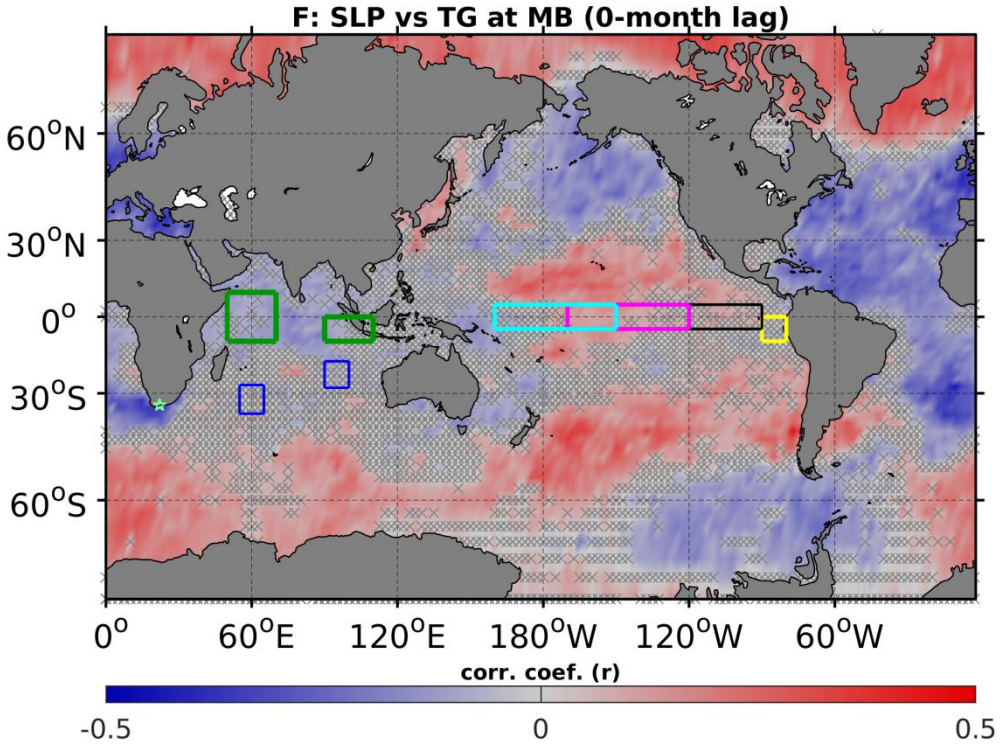
F: SLP vs TG at MB (0-month lag)
60°N
30°N
0°
30°S
60°S
0°
60°E
120°E
180°W
120°W
60°W
corr. coef. (r)
-0.5
0
0.5

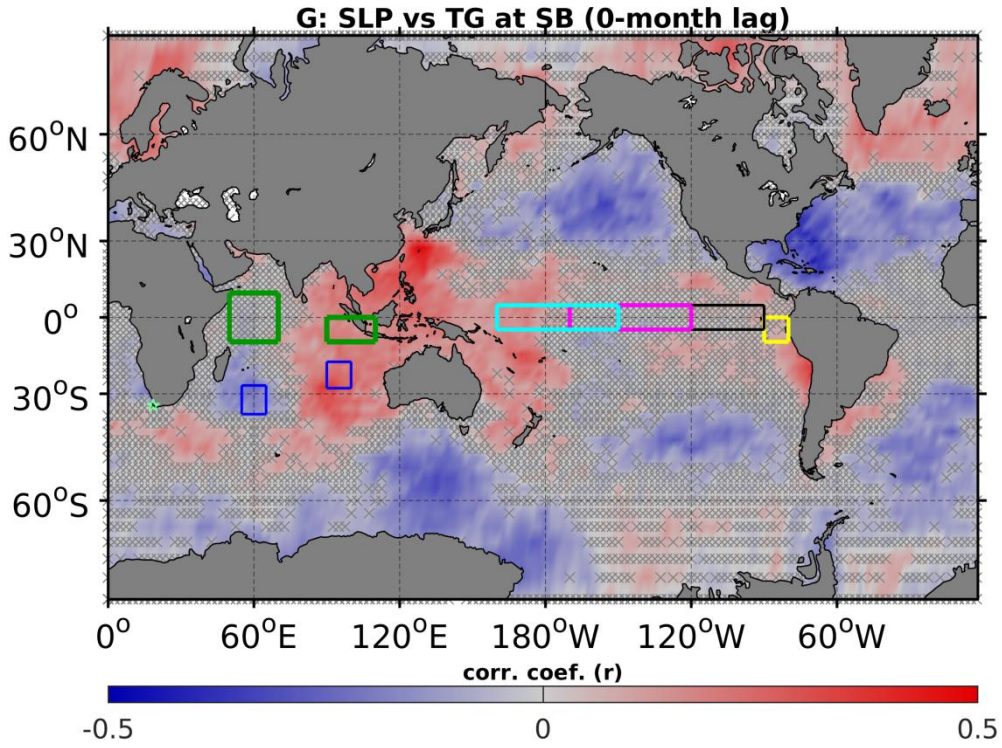

Fig. 4.13: Correlation, at the interannual timescale, between global gridded monthly mean SLP and monthly mean SL records (A) Richards Bay, (B) Durban, (C) East London, (D) Port Elizabeth, (E) Knysna, (F) Mossel Bay and (G) Simons Bay, respectively. Green stars indicate the tide gauge location. Grey crosses indicate area statistically non-significant at 95% confidence level, estimated using a two-sided t-test. Different coloured boxes indicate the regions based on which most of the climate indices are derived. The green boxes indicate the western (left) and eastern (right) tropical Indian region. The blue boxes represent the western (left) and eastern (right) subtropical Indian Ocean region. The yellow, black, magenta and cyan boxes indicate Niño 1+2, 3, 3.4 and 4 regions, respectively.

SLP maps of the results with lags up to 12 month were produced and the shift in significant areas was noted. However, the overall outcomes did not change much with any of these lags. It is worth noting that at a 12-month lag, the results are comparable with sub-annual timescales (Fig. 4.3); this requires further analysis.

The global zonal component of 10 m winds was also correlated to sea level variability at the interannual timescale (Fig. 4.14). Overall, the correlations patterns of the maps in Fig. 4.14 are consistent with Fig. 4.13. However, regional and local zonal winds seem to have a significant

association with sea level variability at East London, Knysna and Simons Bay (Fig. 4.14C and E). Sea level at Richards Bay, Durban, Port Elizabeth, Mossel Bay and Simons Bay appear to have a significant association with zonal winds over Niño 3 region (Fig. 4.14A, B, D, F and G). Sea level at East London, on the other hand, appears to have a significant association with zonal winds over Niño 3.4 and Niño 4 region (Fig. 4.14C). The physical meaning of such association requires further investigation.

The shift in the significant areas was noticed when sea level variability at each tide gauge site was lagged to 10 m zonal winds up to 12 months to produce the resulting correlation maps. However, like the global SLP the overall outcome did not change that much and at a 12-month lag the results were comparable with the sub-annual timescale (Fig.4.4). The latter was not examined further given the objective of this study.

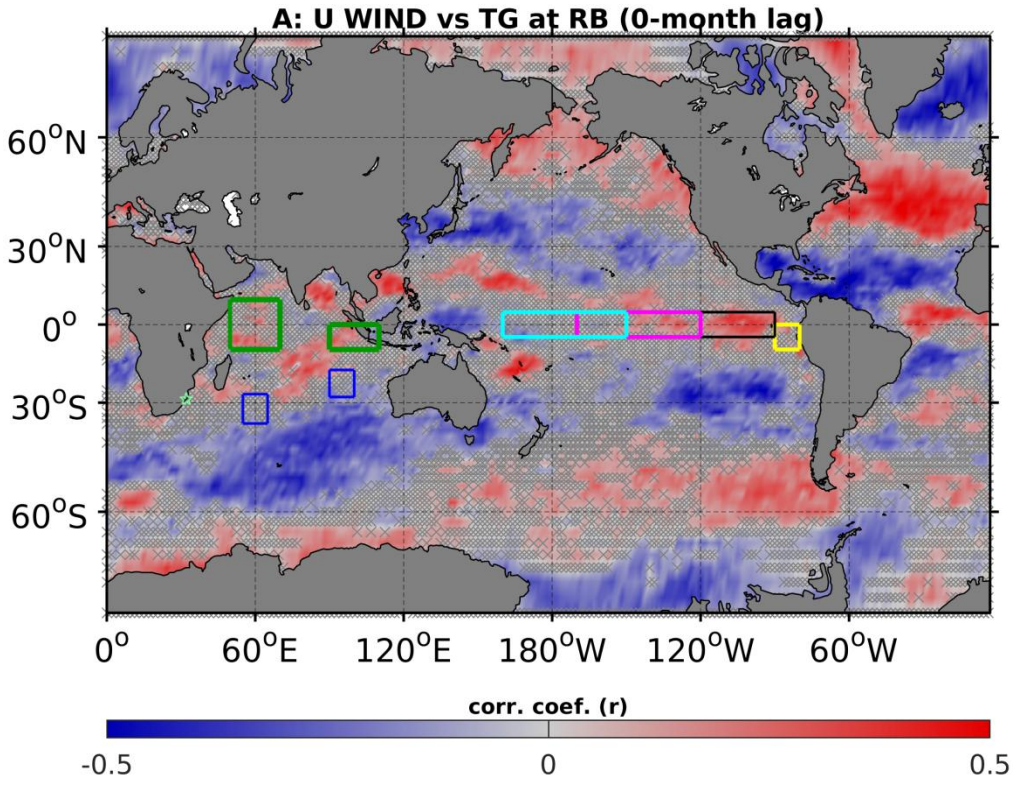
A: U WIND vs TG at RB (0-month lag)
60°N
30°N
0°
30°S
60°S
0°
60°E
120°E
180°W
120°W
60°W
corr. coef. (r)
-0.5
0
0.5

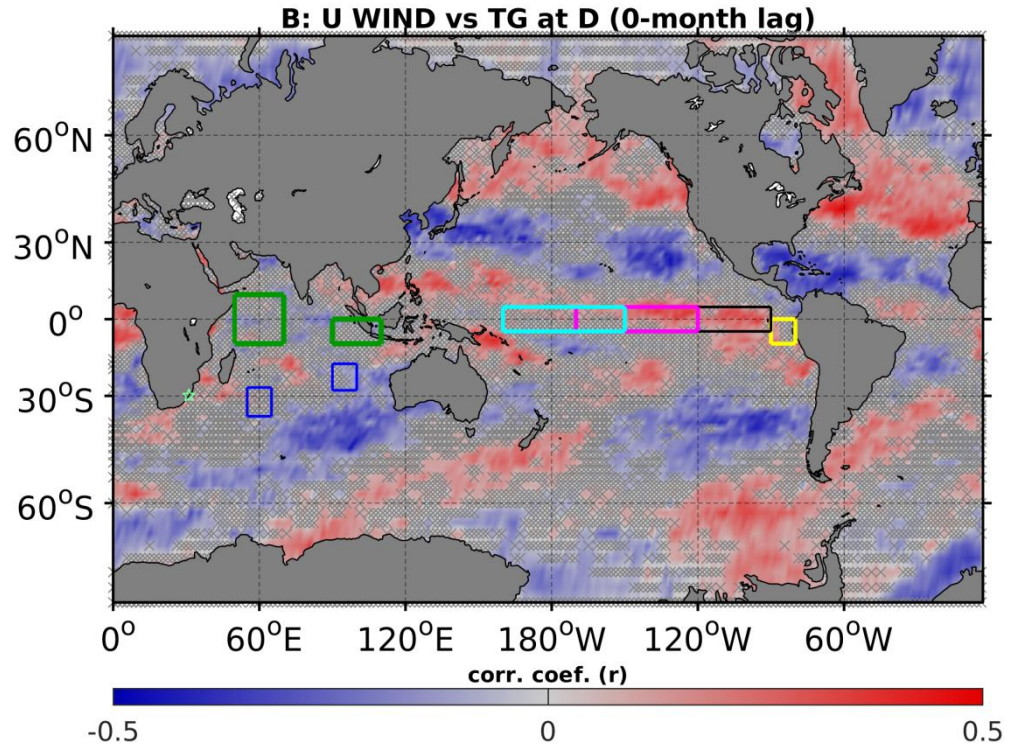
B: U WIND vs TG at D (0-month lag)
60°N
30°N
0°
30°S
60°S
0°
60°E
120°E
180°W
120°W
60°W
corr. coef. (r)
-0.5
0
0.5

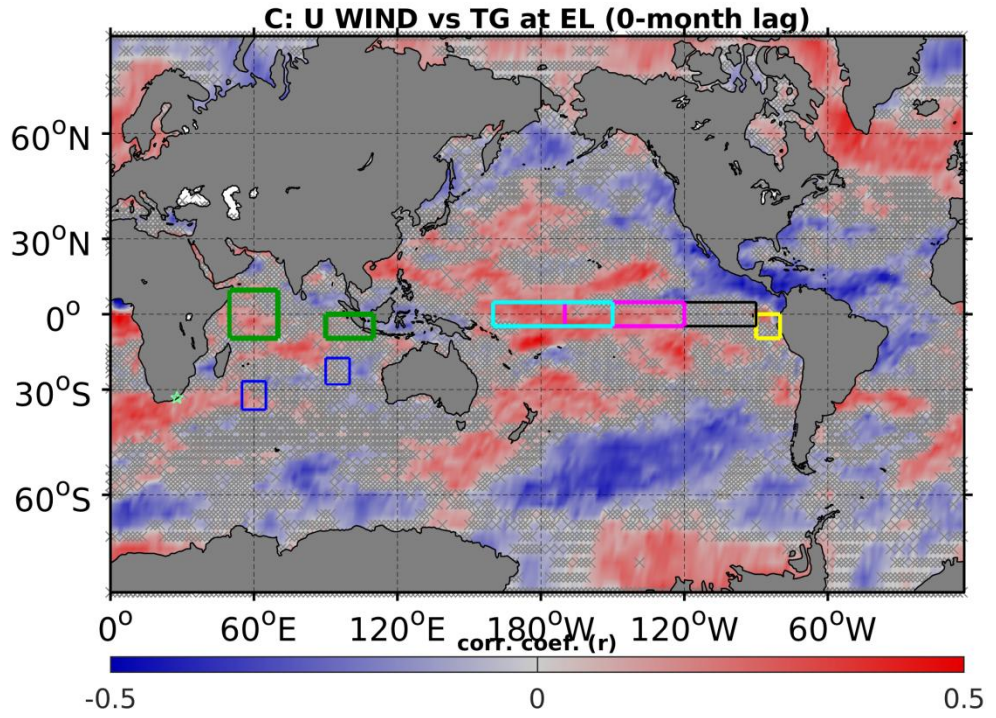
C: U WIND vs TG at EL (0-month lag)
60°N
30°N
0°
30°S
60°S
0°
60°E
120°E
180°W
120°W
60°W
corr. coef. (r)
-0.5
0
0.5

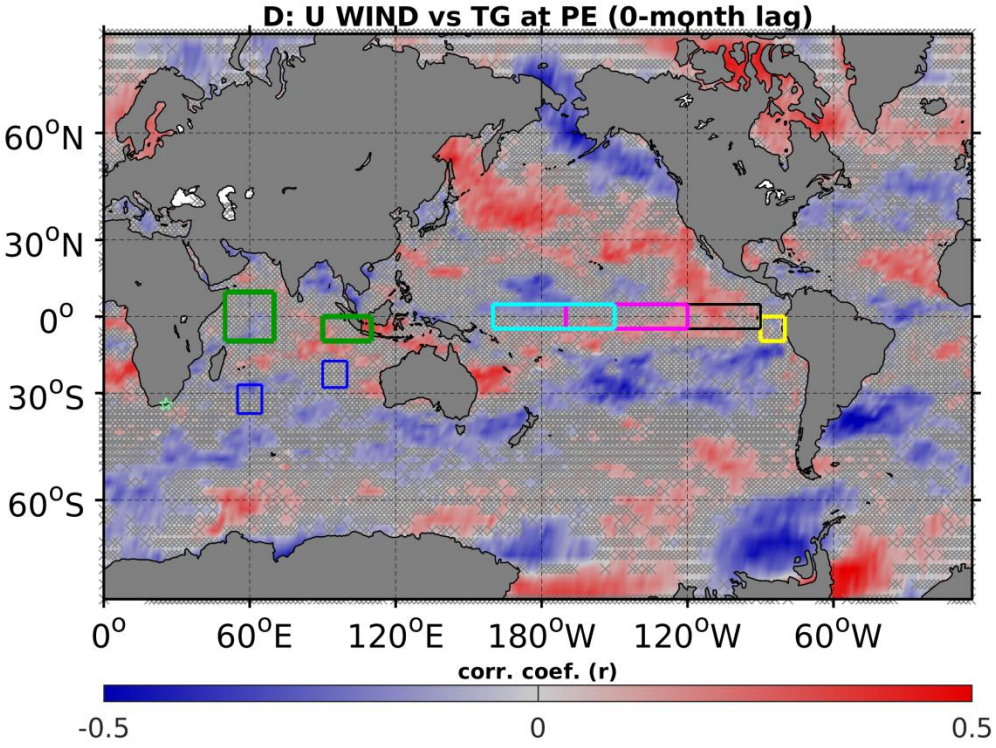
D: U WIND vs TG at PE (0-month lag)
60°N
30°N
0°
30°S
60°S
0°
60°E
120°E
180°W
120°W
60°W
corr. coef. (r)
-0.5
0
0.5

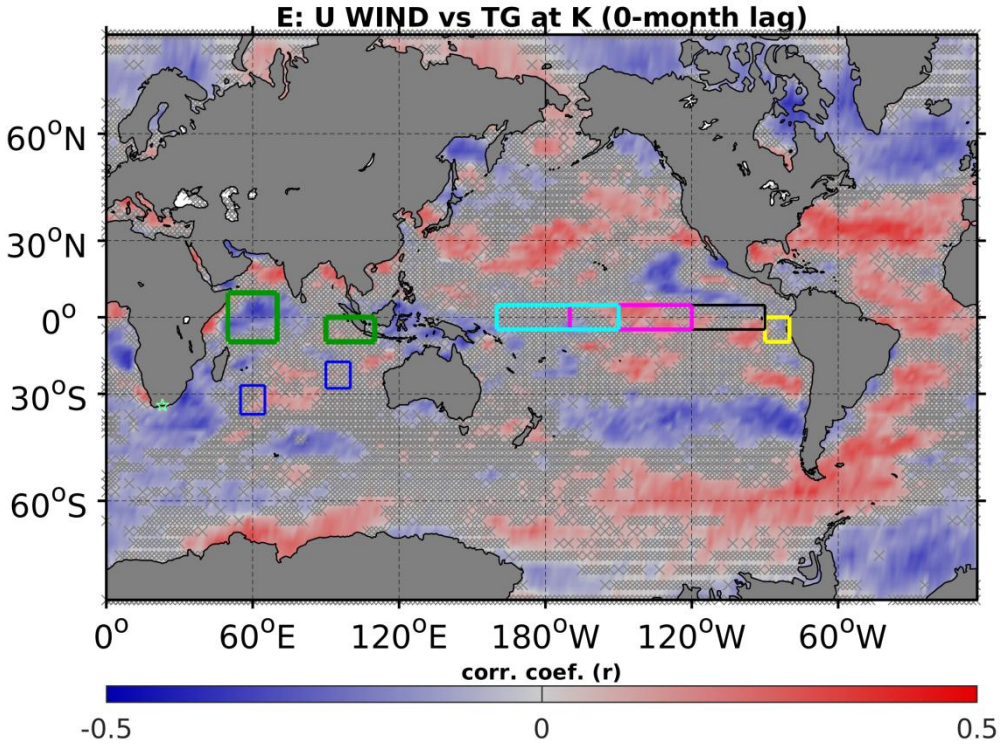
E: U WIND vs TG at K (0-month lag)
60°N
30°N
0°
30°S
60°S
0°
60°E
120°E
180°W
120°W
60°W
corr. coef. (r)
-0.5
0
0.5

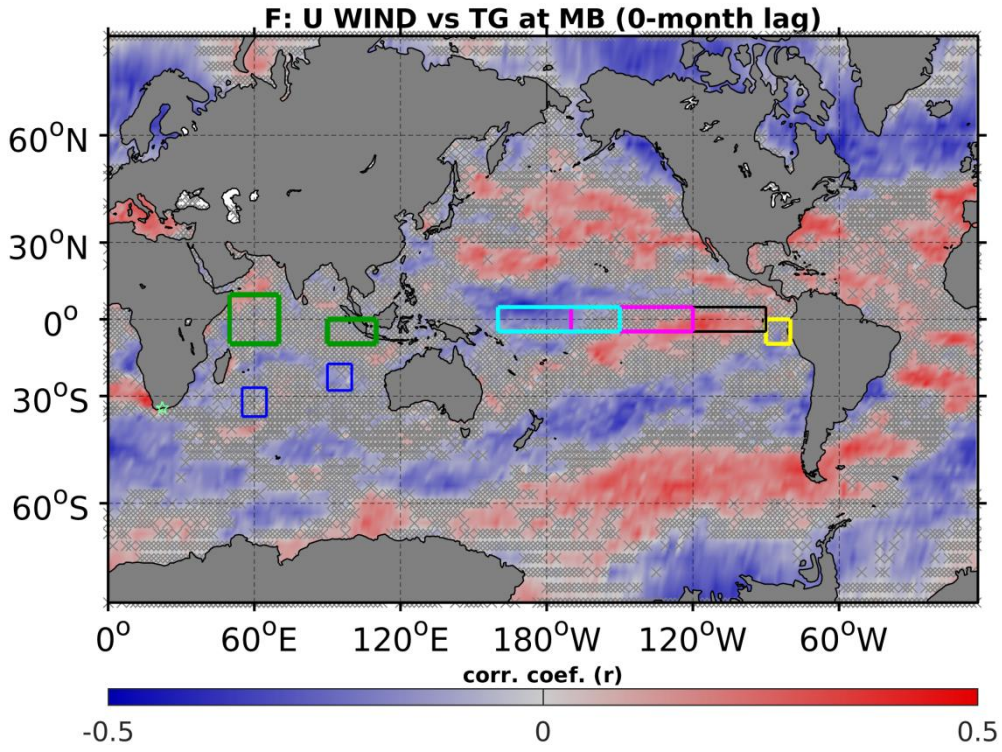
F: U WIND vs TG at MB (0-month lag)
60°N
30°N
0°
30°S
60°S
0°
60°E
120°E
180°W
120°W
60°W
corr. coef. (r)
-0.5
0
0.5

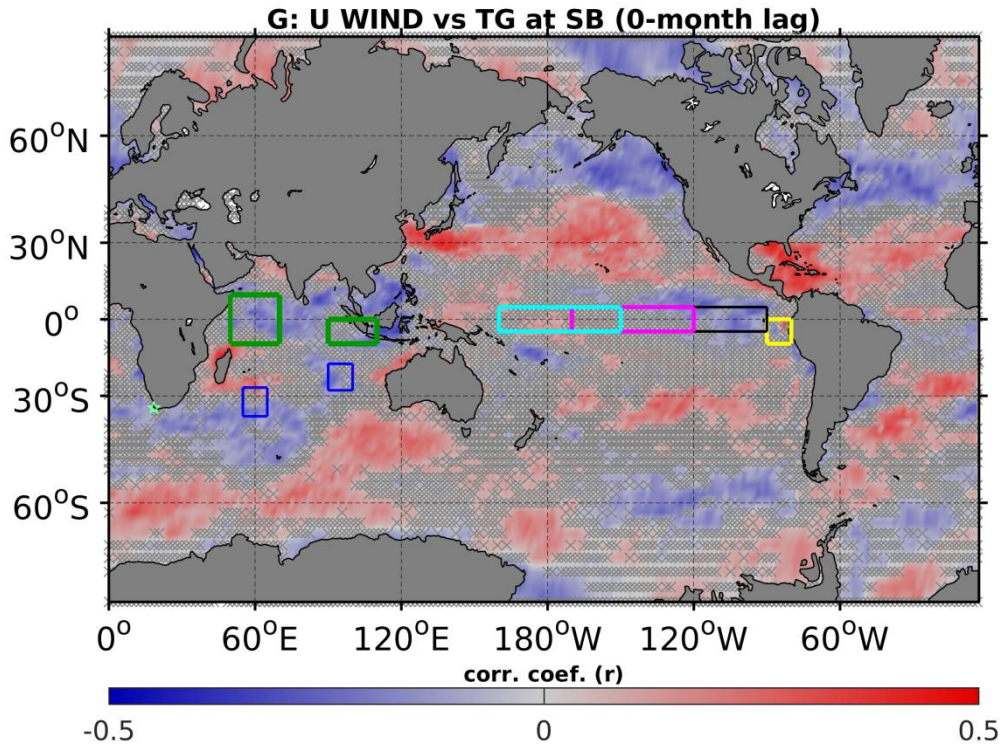

Fig. 4.14: Correlation, at the interannual timescale, between global gridded monthly mean zonal wind at 10 m above the mean sea level and monthly mean SL records (A) Richards Bay, (B) Durban, (C) East London, (D) Port Elizabeth, (E) Knysna, (F) Mossel Bay and (G) Simons Bay, respectively. Green stars indicate the tide gauge location. Grey crosses indicate area statistically non-significant at 95% confidence level, estimated using a two-sided t-test. Different coloured boxes indicate the regions based on which most of the climate indices are derived. The green boxes indicate the western (left) and eastern (right) tropical Indian region. The blue boxes represent the western (left) and eastern (right) subtropical Indian Ocean region. The yellow, black, magenta and cyan boxes indicate Niño 1+2, 3, 3.4 and 4 regions, respectively.

The global meridional component of 10 m winds were also correlated to sea level variability at interannual timescales (Fig. 4.15). In general, the maps in Fig. 4.15 indicate that the meridional component of winds has less association with the regions from which the modes of climate variability are generated. The local and regional meridional component of winds seems, however to account significantly for the coastal SL variability. Theoretically, it makes sense given that, for instance, the cell linked to ENSO has a pronounced zonal component (Neelin et al., 1998). El Niño and La Niña events are due to a weakening or strengthening of the surface westward winds.

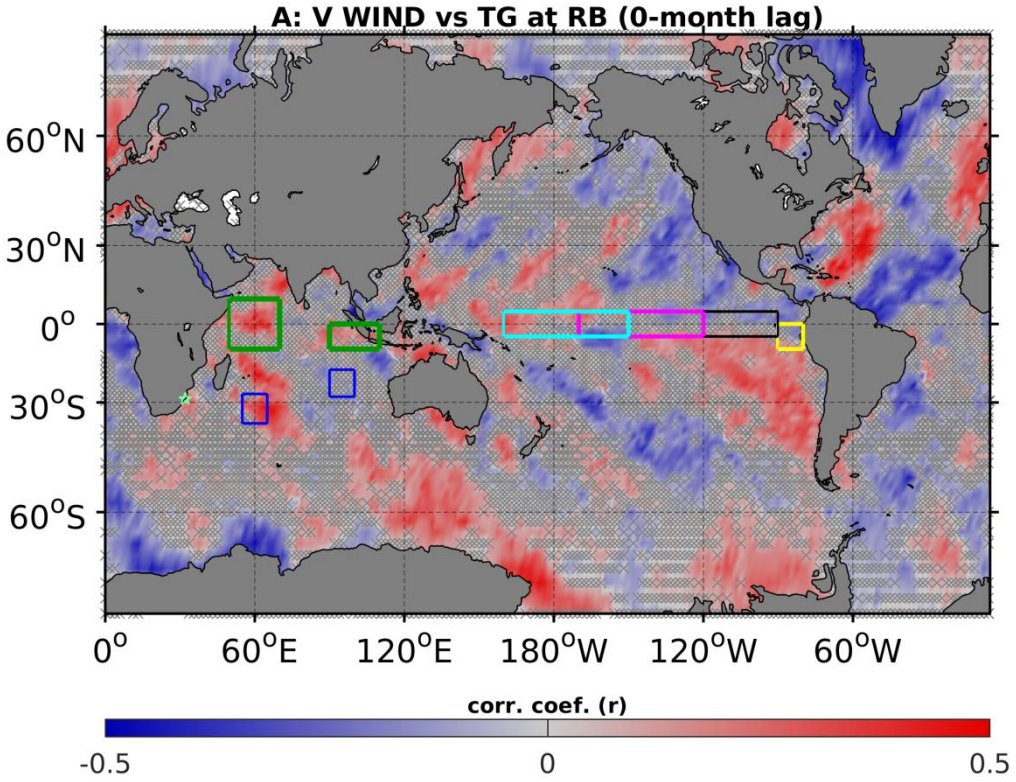
A: V WIND vs TG at RB (0-month lag)
60°N
30°N
0°
30°S
60°S
0°
60°E
120°E
180°W
120°W
60°W
corr. coef. (r)
-0.5
0
0.5

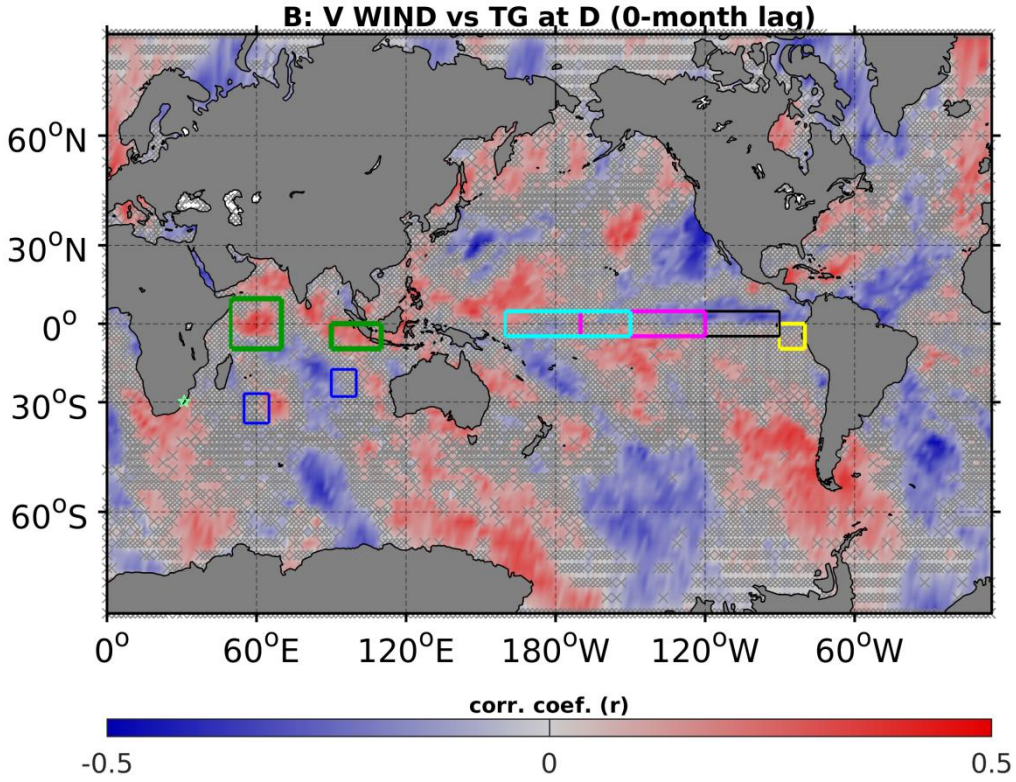
B: V WIND vs TG at D (0-month lag)
60°N
30°N
0°
30°S
60°S
0°
60°E
120°E
180°W
120°W
60°W
corr. coef. (r)
-0.5
0
0.5

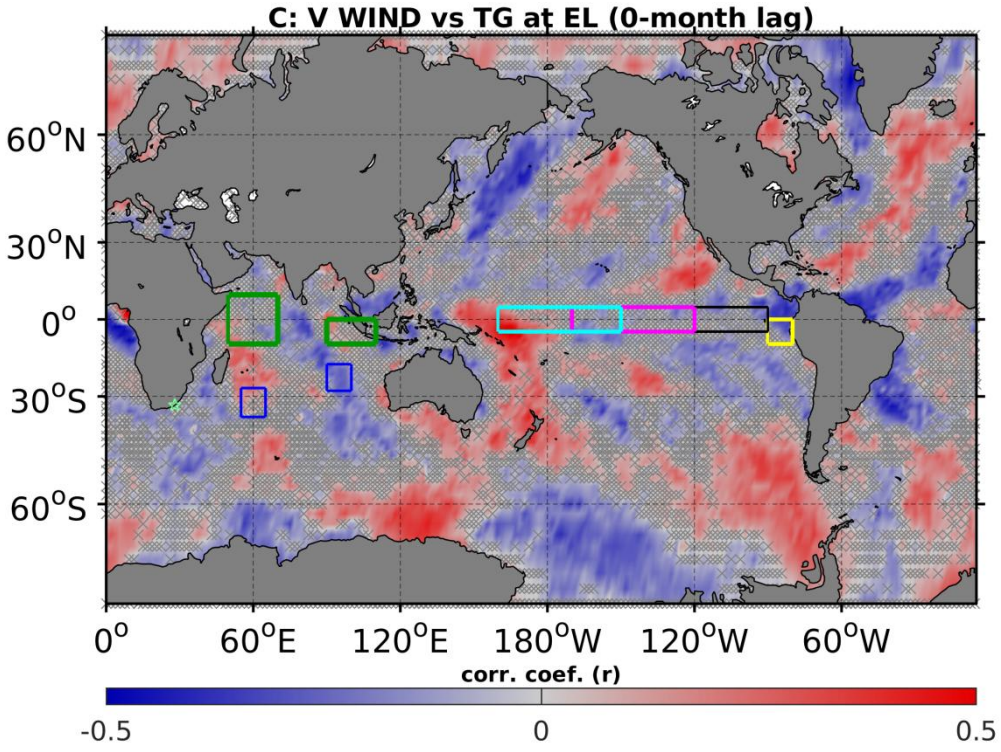
C: V WIND vs TG at EL (0-month lag)
60°N
30°N
0°
30°S
60°S
0°
60°E
120°E
180°W
120°W
60°W
corr. coef. (r)
-0.5
0
0.5

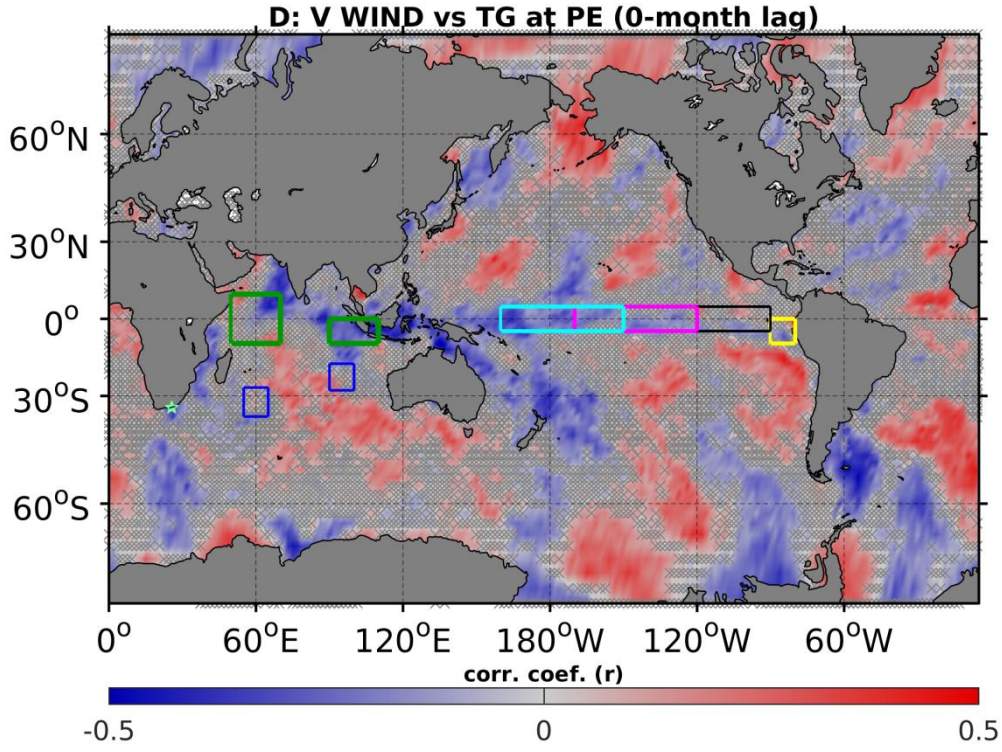
D: V WIND vs TG at PE (0-month lag)
60°N
30°N
0°
30°S
60°S
0°
60°E
120°E
180°W
120°W
60°W
corr. coef. (r)
-0.5
0
0.5

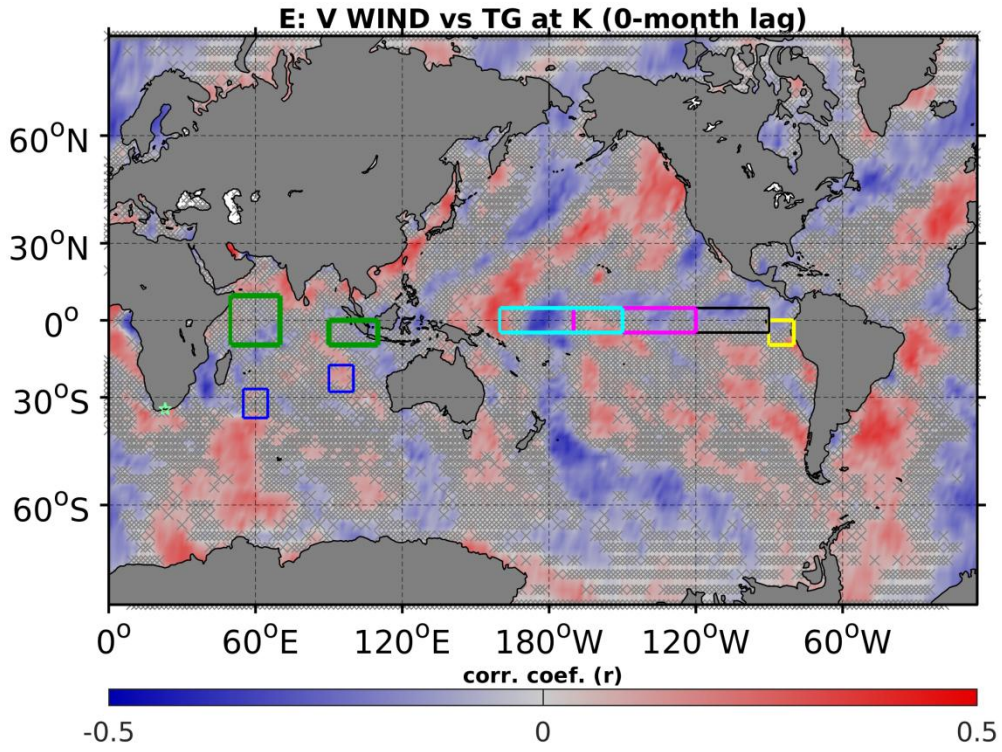
E: V WIND vs TG at K (0-month lag)
60°N
30°N
0°
30°S
60°S
0°
60°E
120°E
180°W
120°W
60°W
corr. coef. (r)
-0.5
0
0.5

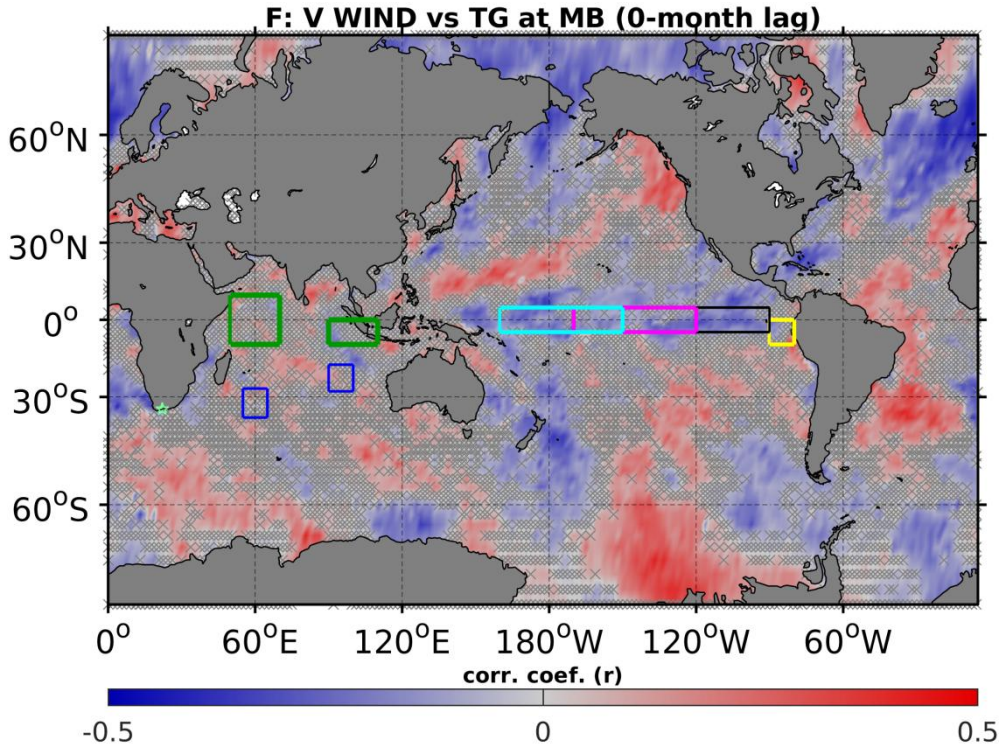
F: V WIND vs TG at MB (0-month lag)
60°N
30°N
0°
30°S
60°S
0°
60°E
120°E
180°W
120°W
60°W
corr. coef. (r)
-0.5
0
0.5

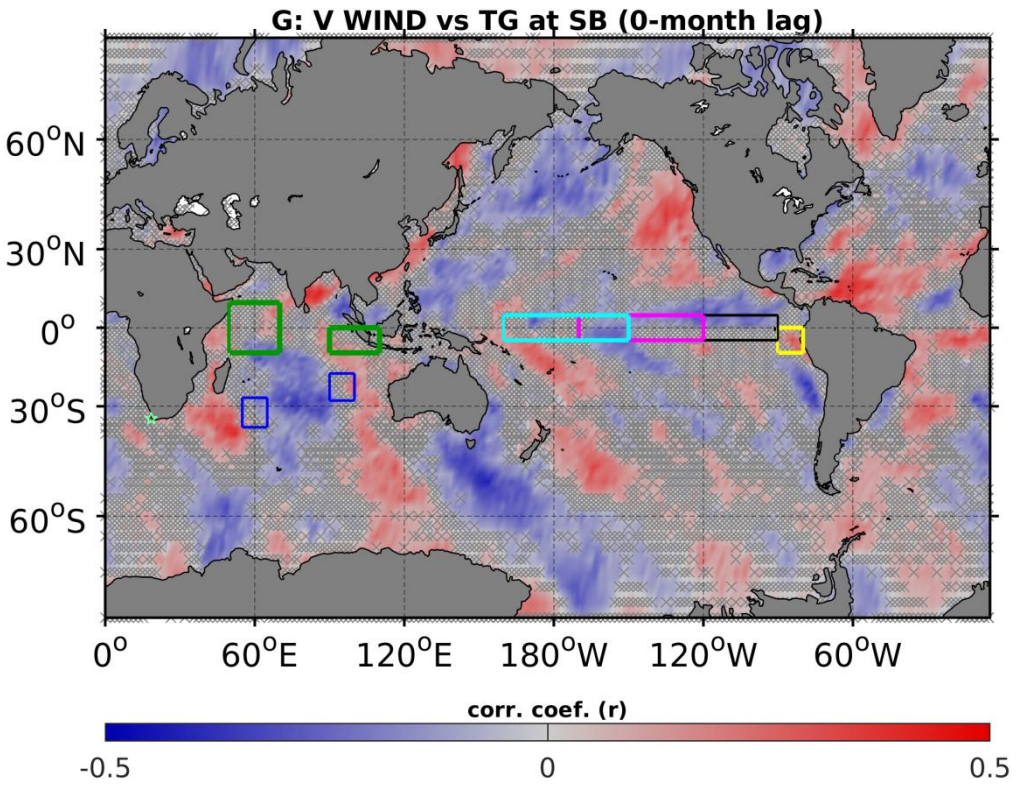

Fig. 4.15: Correlation, at the interannual timescale, between global gridded monthly mean meridional wind at 10 m above the mean sea level and monthly mean SL records at (A) Richards Bay, (B) Durban, (C) East London, (D) Port Elizabeth, (E) Knysna, (F) Mossel Bay and (G) Simons Bay, respectively. Green stars indicate the tide gauge location. Grey crosses indicate area statistically non-significant at 95% confidence level, estimated using a two-sided t-test. Different coloured boxes indicate the regions based on which most of the climate indices are derived. The green boxes indicate the western (left) and eastern (right) tropical Indian region. The blue boxes represent the western (left) and eastern (right) subtropical Indian Ocean region. The yellow, black, magenta and cyan boxes indicate Niño 1+2, 3, 3.4 and 4 regions, respectively.

To summarise, the underlying parameters of the climatic modes of variability were correlated to local and regional coastal sea level. It is important to note that the areas selected for the various indices are areas where SST, SLP, and winds are not well correlated with coastal sea level. Nevertheless, this does indicate that regions other than those from which the climate indices are derived, do influence SL variability in South Africa at the interannual timescale.

In fact, at the interannual timescale, measurable correlations between tide gauge SL variability, and local and regional ERSST, SLP and 10 m zonal wind were found in agreement with the

literature of the other regions (Chen et al., 2014; Dangendorf et al., 2014; Park and Sweet, 2015; Chafik et al., 2017). Additionally, sea level at East London has consistently shown a significant association with the variations over Niño 3.4, Niño 4 regions and vast regions of the Pacific Ocean, which due to its location may indicate that it captures the signals via the Agulhas Current. However, this statement needs to be substantiated by further investigation.

4.4. Summary and Conclusion

Monthly mean sea level records, at seven individual tide gauge locations, from the south and east coast of South Africa were used to study the timescales of variability, their relationships to atmospheric forcing and modes of climate variability. These SL records are fuller sea level data (Chapter 3), which allowed the application of the Empirical Mode Decomposition method in order to separate the various oscillating modes. It was shown (Chapter 2) that the EMD method is an efficient and relatively simple method to obtain the time scales of variability within any sea level record. The temporal structure of the separated modes at Simons Bay is in agreement with the conclusions of the previous studies based on different methods (Brundrit, 1984; Brundrit et al., 1984; Brundrit, 1995).

It was found to be challenging to identify which driver is embedded in the data when interpreting each mode, as found in similar studies in other regions (e.g. Haigh et al., 2014). Thus, the oscillatory modes identified by the EMD were summed to obtain a physically more meaningful timescale. Namely, the sub-annual timescale, which was the ensemble of the modes with a periodicity lower than approximately 18 months. The modes with a periodicity longer than approximately two years were summed to compute the interannual timescale. Using these two time series, the driving processes of tide gauge SL records were investigated at sub-annual and interannual timescales, by comparing and correlating these to atmospheric forcing and known climate indices as well as their input data. It was supported by the fact that, along the south-western coast of Africa, Brundrit (1984) analysed monthly mean sea level records from 1969 to 1975 and found that the variations can be separated into (i) high-frequency, (ii) seasonal and (iii) interannual contributions.

At the sub-annual time scale, sea level responds to regional zonal and meridional winds associated with mesoscale and synoptic weather disturbances in the annual cycle. These results were in agreement with previous studies (Brundrit, 1984; Brundrit et al., 1984; Brundrit et al., 1987). It is hypothesised that through Ekman transport dynamics, SLP and longshore winds increase and decrease the coastal SL at this timescale.

At the interannual timescale, the results suggest a connection between coastal SL variability and climate indices, although it is not consistent across the set of tide stations nor particularly strong. Strong positive ENSO events tend to increase coastal SL while strong negative ENSO events tend to decrease, however the relationship is not consistent. Overall, strong IOD events tend to have a similar influence as the strong ENSO events. The results also suggest that, in general, negative SAM events lead to high coastal SL events. It was noticed that particular ENSO and IOD strong events were in phase with SL variability suggesting the need of further analysis to understand to what extent ENSO and IOD modulate coastal sea level.

To further understand how the three modes of climate variability (ENSO, IOD and SAM) under consideration are associated with the coastal SL at interannual timescale, composite average differences between positive and negative (using 0.75 standard deviation threshold) MEI, DMI and SAM events were calculated. The results are in agreement with the linear correlations by suggesting that in general, high monthly coastal sea levels are more likely during El Niño, positive IOD and negative SAM events, respectively. La Niña events appear to induce low monthly coastal sea levels in approximately similar magnitude to El Niño.

The impact of the paired interaction between the three modes of climate variability and coastal SL in months with higher sea level than 1.5 standard deviations above mean sea level was further investigated. The results suggest that the influence of modes of climate variability on local and regional coastal SL can be quantified through their binary interactions despite further investigation is necessary to substantiate statement. Thus, in most of the locations the likelihood of anomalously high coastal sea levels during months of El Niño/positive IOD and positive IOD/positive SAM events, is fairly high. The combinations of MEI and SAM indices in months of anomalously high sea level months at the TG stations under consideration prevented

us to draw a sound conclusion concerning the dominate interaction, suggesting a need of further analysis.

Furthermore, the main parameters used to derive the climate indices suggested that the areas selected for the various indices are areas where SST, SLP, and winds are not well correlated with coastal sea level. Instead, the results indicate that variability in regions other than those from which the climate indices are derived influence SL variability in South Africa at interannual timescales. In fact, significant correlation between tide gauge SL variability and local and regional SST, SLP and 10 m zonal wind was found, suggesting that the modes of climate variability do not influence coastal SL directly. They however seem to modulate the local and regional ocean and atmosphere conditions that control coastal SL variability, as indicated in the literature of other regions (Chen et al., 2014; Dangendorf et al., 2014; Park and Sweet, 2015; Chafik et al., 2017).

Given the results of this study, further investigations are necessary to understand the regional atmospheric circulation patterns associated with each binary interaction. This would help explain wind and pressure variation characteristics associated with specific combinations of the modes of climate variability and their effects on coastal sea level. Additionally, results suggest the need to study the possible influence of the Agulhas Current on coastal sea level. It has been noted throughout this study that sea level variability at East London has a particular connection with climate indices and this may be due to its location and Agulhas Current dynamics.

CHAPTER 5

The relationship between coastal sea level variability and the Agulhas Current

5.1 Introduction

In Chapter 4, the timescales of sea level (SL) variability were calculated and their driving mechanisms investigated. However, identifying a single driver for each separate timescale is challenging due to our limited knowledge of how sea level is linked to the various forcing mechanisms. Therefore, the timescales of SL variability extracted using the Empirical Mode Decomposition analysis, were grouped into sub-annual and interannual timescales, and then their relationships to possible driving mechanisms were investigated.

The sub-annual timescale indicates how sea level responds to the mesoscale and synoptic weather systems in the annual cycle, including seasonal and annual large-scale wind and atmospheric pressure pattern changes. The interannual timescale, in those cases where a significant correlation is found, indicates an association with the modes of climate variability including El Niño-Southern Oscillation (ENSO), Indian Ocean Dipole (IOD) and Southern Annular Mode (SAM) through large-scale sea surface temperature patterns and large-scale pressure and wind patterns.

Nevertheless, studies have indicated that tide gauge records are also associated with the ocean dynamics (e.g. Levermann et al., 2005; Sweet et al., 2009; Ezer and Corlett, 2012; Sallenger et al., 2012; Calafat and Chambers, 2013; Ezer et al., 2013; Ezer, 2015; Park and Sweet, 2015). However, as yet it is a challenge in sea level research to separate ocean dynamics (internal

climate variability) from the external forcing (anthropogenic and/or natural; e.g. Calafat and Chambers, 2013). This challenge arises due to the fact that internal ocean climate variability is also connected to large scale modes of climate variability, although it is not clear yet to what extent this may be true (e.g. Calafat and Chambers, 2013; Park and Sweet, 2015).

In this chapter we investigate the Agulhas Current (AC) dynamics in order to relate ocean dynamics to coastal sea level. The Agulhas Current is a very narrow western boundary current which flows from approximately 27°S to 34°S along the east and south coasts of South Africa (e.g. Gordon, 1985; Bryden et al., 2005; Lutjeharms, 2006). The AC flow is strongly influenced and directed by the bottom topography (Lutjeharms and van Ballegooyen, 1984; Siedler et al., 2001). The Current follows the continental slope from Maputo in Mozambique, to the tip of the Agulhas Bank (Cape Agulhas, near 35°S, 20°E). At this point, the momentum of the current overcomes the vorticity balance holding the current to the topography and the current leaves the shelf. A large part then re-circulates back to the south into the Indian Ocean, while a small but important part enters the Atlantic Ocean.

The AC is part of the greater Agulhas system which is believed to play an important role in the global climate (Beal et al., 2011). It is a wind driven western boundary current implying that its transport has an annual cycle, with the maximum throughout the austral summer and the minimum in the austral winter, based on 18 years of along-track satellite altimetry observations (Krug and Tournadre, 2012), 3 years of *in situ* measurements (Beal et al., 2015), and 22 years of proxy time series (Beal and Elipot, 2016).

It has been suggested that the Agulhas Current is the largest western boundary current in the world ocean, with an estimated net transport of approximately 100 Sverdrups (Sv) (e.g. Siedler et al., 2001; Lutjeharms, 2006; Beal et al., 2015) at its southern end; comparable western boundary currents transport less, ranging from the Brazil Current (16.2 Sv) to the Kuroshio (42 Sv). The results of Stramma and Lutjeharms (1997) suggest that its sources are mainly the East Madagascar Current (25 Sv), the Mozambique Current (5Sv) and a reticulated part of the Agulhas Current itself (35 Sv).

Different data and methods have been applied to determine the core position of the AC. The core of the northern Agulhas Current has been found meandering less than 15 km to either side in the analysis of the temperature sections across the region between 28°S 30' and 34°S (Gründlingh, 1983). Rouault and Penven (2011) suggest that the landward edge of the current is less than 50 km away from the shore except at Port Elizabeth where its mean position was approximately 50 km off the coast. Their aim was to study the fluctuations in the path of the northern Agulhas Current using hourly SST imagery from 1 June 2004 and 19 October 2010, supported by merged altimetry maps of absolute geostrophic current velocities.

On the other hand, Krug and Tournadre (2012) claim that from the along-track altimetry datasets, the mean position of the Agulhas Current core is 113 km off the coast (near Port Elizabeth), with the inshore and offshore edges at 81 km and 145 km from the shore, respectively. These results are strongly correlated to the one from the 1/3° gridded altimetry datasets with r=0.7 at the 95% confidence level. The average core position using the high frequency sea surface temperature (SST) imagery was 124 km from the coast, with the inshore and offshore edges at 85 km and 165 km from the coast, respectively. Additionally, the latter findings were correlated to the results using the merged-altimetry maps of absolute geostrophic currents with r=0.73 with 95% confidence. The study was carried out in order to investigate the variability of the path, width and velocity of the Agulhas current, along TOPEX/Poseidon (T/P) and Jason-1/2/3 (J1/2/3) track#20 from 1992 to 2011.

However, Krug et al. (2014) suggest that the Agulhas Current core was centred approximately 100 and 200 km off the coast along TOPEX/Poseidon and Jason-1/2/3 track#20 and #198 (near Port Elizabeth and Mossel Bay), respectively. The study was based on absolute geostrophic velocities, derived from gridded absolute dynamic topography (ADT) maps, along TOPEX/Poseidon and Jason-1/2/3 track altimetry observations, between 1993 and 2012, and *in situ* measurements of current speeds and directions from 5 April 2009 to 17 April 2010, at locations close to the ground track#198 transect.

Additionally, *in situ* measurements reveal that, along T/P and J1/2/3 ground track#96 transect (near East London), the current core mean position is approximately 50 km off the coast

shifting to about 150 km during a meander event (Beal et al., 2015; Elipot and Beal, 2015). The data were collected under the Agulhas Current Time-Series Experiment (ACT) array from April 2010 to February 2013.

While a detailed investigation has been done on the various estimations of the position of the AC and its core, it should be stressed that the position does not affect the coastal sea level per se. It is rather the intensity of the surface current that is related (via geostrophy) to the sea level (e.g. Ezer et al., 2013; Ezer, 2015). It is therefore realistic to think that variability in the Agulhas Current transport will be reflected by variability in the coastal SL, at least at scales compatible with geostrophic or quasi-geostrophic balance.

Given the above, the hypothesis is that the Agulhas Current dynamics may have significant influences on coastal sea level. This hypothesis is substantiated by the fact that in Chapter 4, sea level variability at East London has shown a particular connection with climate indices, suggesting that it may capture these signals via the Agulhas Current. To our knowledge, there is no previous literature investigating this hypothesis. However, similar studies in other regions have indicated significant correlations between western boundary currents, for instance the Gulf Stream and coastal sea level variability (e.g. Blaha, 1984; Ezer, 2001, 2013, 2015; Sweet et al., 2009; Ezer et al., 2013; Park and Sweet, 2015).

Thus, the objective of this study is to assess how the AC transport and offshore position influences the coastal SL. This was achieved by calculating the AC path and core position relative to the coast by using an ADT gradient approach (e.g. Ezer et al., 2013) described below. To validate this approach, the AC path has been compared with previous results in the literature. Thereafter the possible connection between the AC core location and volume transport was investigated. Finally, we investigated how variation in the transport and position of the Agulhas Current induces coastal sea level variability.

5.2 Data and Methods

5.2.1. Data

To examine and hence understand the possible influence of the Agulhas Current on coastal SL, different datasets from several data sources were analysed. The details of each dataset utilised in this study are described below.

5.2.1.1 Tide gauge sea level time series

The sea level data are the continuous tide gauge records generated and discussed in Chapter 3. These data consist of all available monthly mean tide gauge records from the mid-1900s (depending on location) until December 2015, from seven sites along the east and south coast of South Africa. The data sets were sourced from the Permanent Service for Mean Sea Level (PSMSL; Holgate et al., 2013; PSMSL, 2017; http://www.psmsl.org/). These raw data had gaps that needed to be reduced or eliminated so that the analysis could have reliable conclusions (Chapters 2 and 3). As a result, tide gauge measurements were combined with the gridded multi-mission Copernicus Marine and Environment Monitoring Service (CMEMS; http://www.marine.copernicus.eu) SL satellite altimetry observations product, from January 1993 to December 2015. The process of combining the tide gauge data with satellite altimetry data is described in detail in Chapter 3. Briefly, the grid points that best correlate with the tide gauges, within a 1x1 degree rectangular box were identified and used to fill gaps in the monthly tide gauge records during the satellite altimetry era (after appropriate corrections, for instance IBE and GIA and removal of the seasonal cycle and long term linear trend). In the period prior to the satellite altimetry era, data from neighbouring sites that are well correlated were used to generate the continuous tide gauge record.

5.2.1.2 Satellite altimetry data

The altimetry products were produced by Ssalto/Duacs and distributed by Aviso (Archiving, Validation and Interpretation of Satellite Oceanographic data), with support from Cnes (http://www.aviso.altimetry.fr/duacs/). The data are provided in delayed time for the global ocean in terms of 10-days along-track absolute dynamic topography and daily maps of ADT heights and currents (MADT H and UV). The ADT data set is the sea surface height above the geoid and so allows to best study current's path. The along-track ADT data from six tracks measured by T/P and J1/2/3, Fig. 1, from October 1992 to December 2015 are used.

Gridded MADT H and UV maps are derived from available multi-satellite altimetry data (Jason-3, Sentinel-3A, HY-2A, Saral/AltiKa, Cryosat-2, Jason-2, Jason-1, T/P, ENVISAT, GFO, ERS1/2 and even Geosat) and provided on a 1/4° Cartesian grid, from January 1993 to December 2015. Both along-track and gridded maps are computed with respect to a twenty-year mean (1993-2012; Maheu et al., 2013). Satellite altimetry data were then averaged in monthly means for consistency with the sea level data. More details and description about the data sets are available from Pujol et al. (2016).

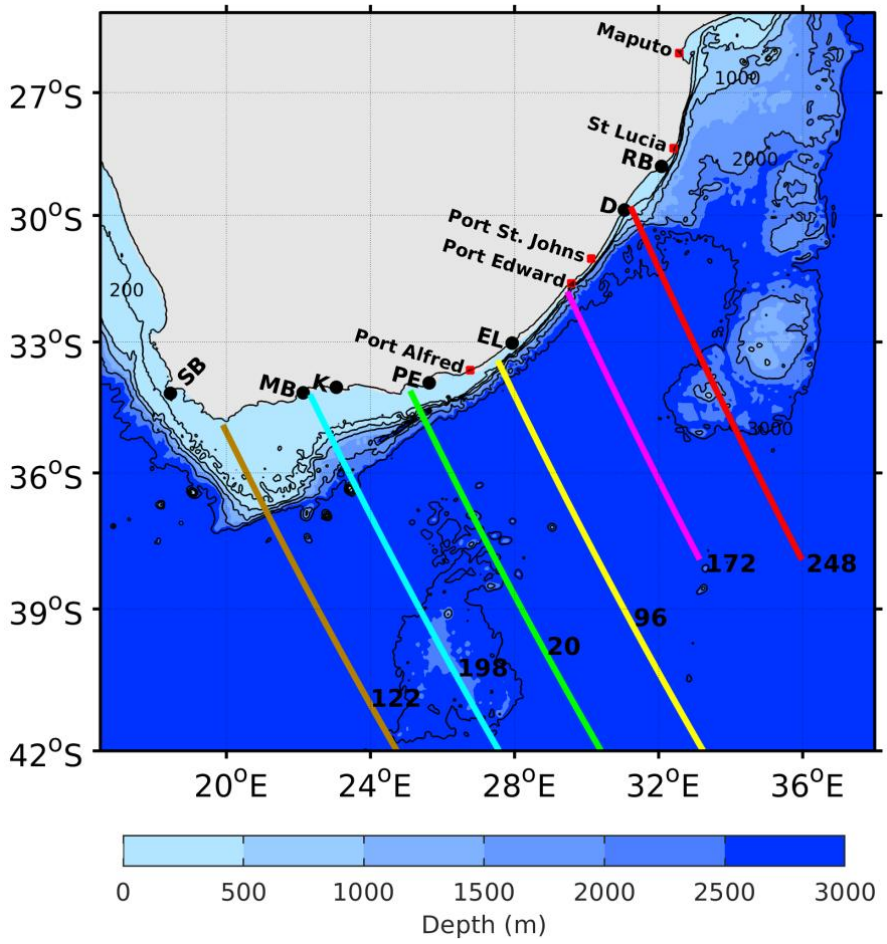

Fig. 5.1: Ground track locations under consideration (tracks are labelled with their number) and bathymetry of southern Africa. Solid black dotes are the tide gauge locations. The tracks refer to T/P and Jason J1/2/3 ground tracks (ascending passes). Note that “RB”, “D”, “EL”, “PE”, “K”, “MB” and “SB” means Richards Bay, Durban, East London, Port Elizabeth, Knysna, Mossel Bay and Simons Bay, respectively.

Monthly mean along-track ADT observations were utilised to identify the AC path and hence its core positions, as described below. Additionally, due to eddies and meandering events, monthly mean gridded MADT H and UV maps were used to ensure that the along-track area in consideration for identifying the AC path, does not sometimes include the return current. This process takes into account the dynamics over the region studied and allows overcoming the possible limitations of the approach when locating the maximum gradient of the AC current.

5.2.1.3 The Agulhas Current transport data

The Agulhas Current transport data were used to investigate whether the variation in the current volume transport may lead to measurable effects on its onshore side. The AC transport time series are based on *in situ* observations from April 2010 to February 2013 under the ACT framework (Beal et al., 2015; Elipot and Beal, 2015) that were then combined with the coinciding along-track satellite altimetry measurements to reconstruct 22-year proxy data. The AC box transport (Tbox) is the flow measured in a fixed area of the ACT array. The AC jet transport (Tjet) takes into account the offshore displacements of the current. The proxy data were built based on the strong relationship between the *in situ* current transport and sea surface height and slope along the ACT array at 34°S. More details and descriptions of the data sets are available from Leber and Beal (2014), Beal et al. (2015), Elipot and Beal (2015) and Beal and Elipot (2016).

5.2.2 Methods

In order to achieve the objective of this study, several data processing and analysis methods were applied. As described in Chapter 4, outliers were removed from the monthly sea level data using the 3 standard deviations threshold. The EMD analysis (Huang et al., 1998; Huang and Wu, 2008), described in Chapter 2 was applied as a filter to separate the embedded timescales within the studied time series. Wavelet analysis (Torrence and Compo, 1998) was applied to identify the global frequency of the separated timescales. The separated timescales were also combined to compose the sub-annual and interannual timescale as described in Chapter 2. The sub-annual timescale is the sum of the modes with periodicities shorter than approximately 18 months. The modes with periodicities longer than approximately two years were summed to compute the interannual timescale. Unless stated otherwise all correlations shown in this study are above the 95% confidence level, and calculated after the removal of the linear long-term trend and seasonal cycle. The statistical significance of the resultant correlation coefficients was tested based on Chelton (1983) at 5% significance intervals. Cross-

correlations were carried out to examine the possible existence of a lagged relationship between the studied time series.

To better identify the typical AC path across the tracks, maps of monthly gridded absolute dynamic topography overlaid by monthly gridded absolute geostrophic velocity and tracks transects were produced (Fig. 5.2). The maps produced were combined to create an animation allowing a better visual examination of the typical AC path. Therefore, we have limited the detection of the AC core position to a small region (200 - 500km from the coastline) due to the Agulhas Retroflection Current (ARC).

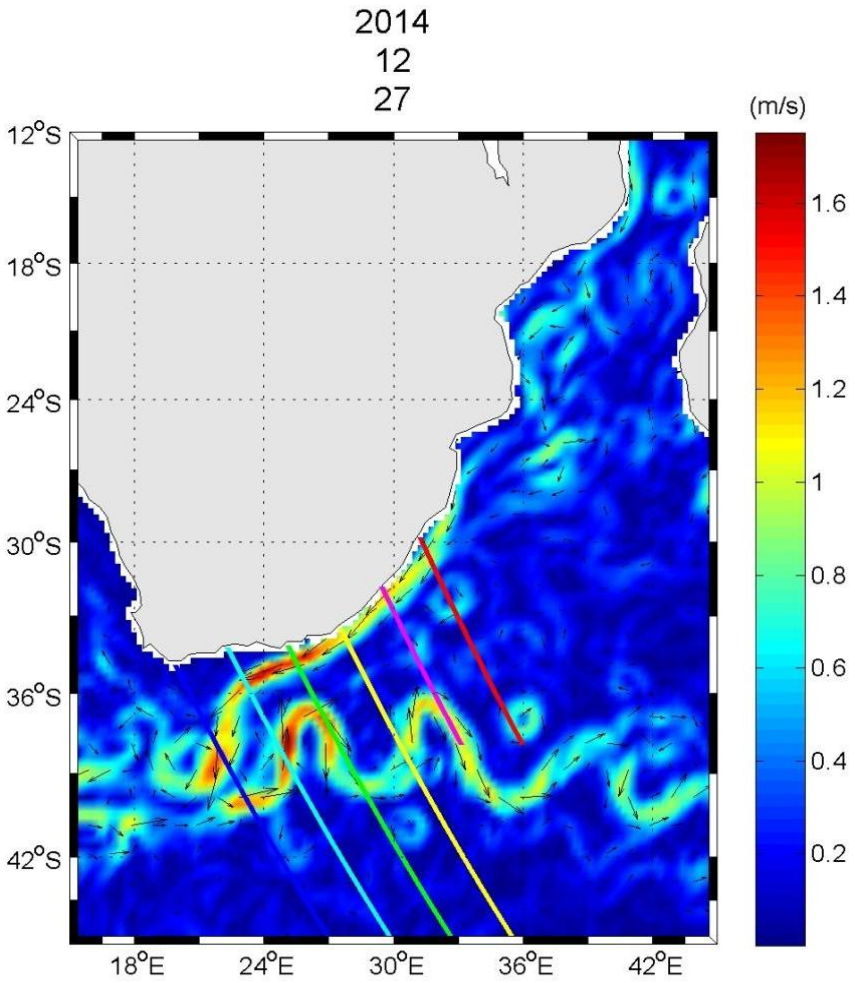

Fig. 5.2: A map of an overlay of monthly gridded ADT, monthly gridded absolute geostrophic velocity and tracks transects (colourful oblique solid lines) based on which the AC typical path was assessed. Arrows indicate the current direction.

The coast to AC gradient approach (Ezer et al., 2013) was applied to locate the AC path and hence, its core positions. The approach is based on the geostrophic equations as follow:

$$U_g = -\frac{g}{f}\frac{\partial h}{\partial y} \text{ and } V_g = \frac{g}{f}\frac{\partial h}{\partial x} \quad (5.1)$$

Where Ug and Vg are the zonal and meridional geostrophic velocity components, h is the absolute dynamic topography, f is the Coriolis parameter, g is the gravity acceleration and x and y are the distances in length and latitude.

The geostrophic relationship underpins the gradient approach for determination of the AC path and hence the core position, Fig. 5.3. The coast to AC gradient approach was validated by comparing the results with the ones available in the literature (e.g. Rouault and Penven, 2011; Krug and Tournadre, 2012; Krug et al., 2014; Beal et al., 2015).

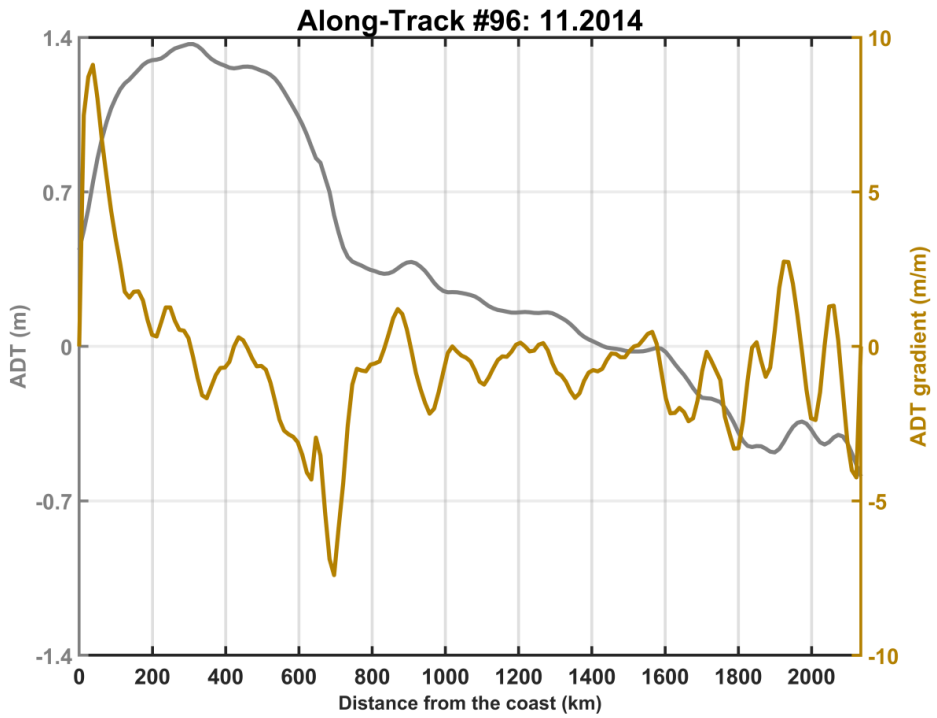

Fig. 5.3: An overlay of along-track ADT (gray solid line) and its gradient (brown solid line). The maximum gradient represents the core location. The ADT refers to one pass of Jason-2, track#96. The AC gradient was derived based on the coast to AC gradient approach (e.g. Ezer et al., 2013).

By extracting the location of the maximum gradient for successive time steps in the along-track data, a time series of Agulhas Current core locations was created for each satellite path studied and the AC core location time series was then correlated to the AC transport time series.

Note that different data records often are a result of using different techniques and/or instruments which may lead to discrepancies in the conclusions drawn (Ezer, 2015). A closer examination of both Tjet and Tbox datasets was performed in which the EMD analysis was performed on both 10-day and monthly-mean Tjet and Tbox data sets to see whether the separated mode's shapes were similar in the two definitions of AC transport. Special attention was paid to the last mode, which is commonly considered as the trend (e.g. Ezer et al., 2013). After performing the EMD analysis, the results suggested that Tjet is more suitable to undertake the analyses given the similarity in the shape of both 10-day and monthly EMD trends.

Furthermore, calculations were carried out to trace whether the transport measured at the ACT array is in any way related to the one measured at the selected tide sites and if so how long it would take, given the mean surface velocity of 1.8 m/s (Beal et al., 2015). The results indicated that from East London to the ACT array and, from the ACT array to Port Elizabeth, the measured current may have taken 9 and 29 hours, respectively. Moreover, from tide sites located in the northern AC region and, to the tide sites located in the southern AC region, the measured current may have taken 3 and 6 days, respectively.

5.3. Results and Discussion

5.3.1. The Agulhas Current core location

Fig. 5.4 shows Hovmöller plots of the Agulhas Current along-track gradient at each ground track studied. The discontinuities (the interruptions within the red colour) in the current path are noticeable on all track transects. These discontinuities are more visible in ground track #248. In addition, the narrowest current width is portrayed at the same track transect. Track #248

transect is geographically located in the Natal Bight which various studies have indicated to be the origin of the Agulhas meander events (e.g. de Ruijter et al., 1999; Beal and Bryden, 1999; Bryden et al., 2005). In fact, previous studies have indicated the occurrence of meander events (Bryden et al., 2005; Rouault and Penven, 2011) and coastal trapped waves (Schumann and Brink, 1990) as responsible for these discontinuities in the Agulhas core (red colour) in Fig. 5.4.

For all tracks, Fig. 5.4 highlights a very stable current, especially along its inshore edge. The figure also depicts a weaker nearshore counter-current over the continental shelf (light blue), with the exception of track #172 and #96. The geographical location of both ground tracks corresponds to regions where the continental shelf is narrow. The counter-current is considered to be the Slope Current, indicated by the contribution to the increased coastal sea level (e.g. Csanady and Hamilton, 1988; Ezer et al., 2013). As shown by Ezer et al. (2013) the Slope Current dynamics is dictated by offshore displacement of the core of western boundary currents. The findings portrayed in Fig. 5.4 are consistent with previous studies related to the AC path (e.g. Rouault and Penven, 2011; Krug and Tournadre, 2012; Beal et al., 2015).

As stated above, the location of the maximum gradient is considered as the AC core position. Overall, the figure depicts a steady current core position, especially with respect to the coast. It may indicate a strong connection with the continental shelf as pointed out in previous studies (e.g. Gründlingh, 1983; Lutjeharms and van Ballegooyen, 1984; de Ruijter et al., 1999; Siedler et al., 2001; Bryden et al., 2005). Clearly, the current core changes its position over time, being observed further offshore frequently. These offshore shifts of the core location have been shown to be due to meander events (e.g. Rouault and Penven, 2011; Krug et al., 2014; Beal et al., 2015). In general, the coast to AC gradient approach despite its simplicity, seems to be suitable to be used to determine the core position due to the consistency with the previous findings (e.g. Rouault and Penven, 2011; Krug and Tournadre, 2012; Krug et al., 2014; Beal et al., 2015).

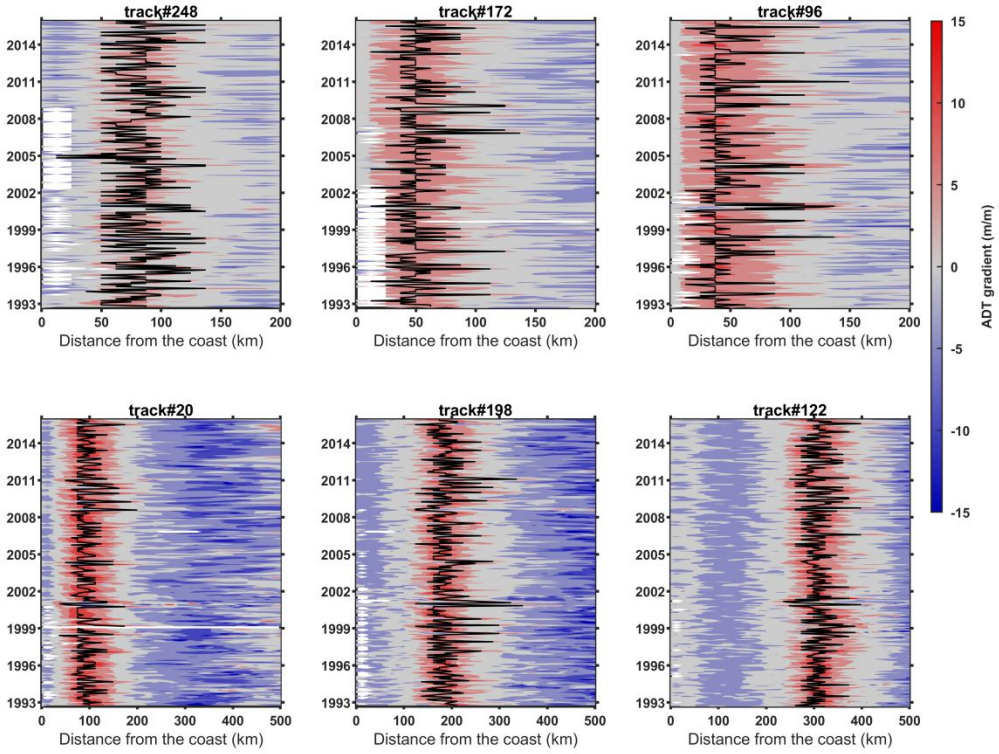

Fig. 5.4: Agulhas along-track ADT gradient showing the AC current path (in red) along each track from the coast. The AC core location is shown black. White patches show missing values. The slope Current is depicted in blue inshore of the AC path in some transects. Note that the panels are arranged from north to south and hence, tracks #248, #172, #96, #20, #198 and #122 are near Durban, Port Edward, East London, Port Elizabeth, Mossel Bay and Simons Bay, respectively.

To give an overview of how dependent the AC current is to topographic steering by the continental shelf, monthly geographical core positions over the time span studied are shown in Fig. 5.5. As can be seen, the current core position is generally along the 1000 m isobath. The current flows close to the coast where a steep continental slope is observed, as also suggested in previous studies (e.g. Lutjeharms and van Ballegooyen, 1984; de Ruijter et al., 1999). The stability of the core position is indicated by the superposition of the geographical locations over time. The results also suggest that the variability in the Agulhas Current transport may have a clear and measurable influence on the East London and Port Elizabeth tide gauge sites given

their proximity to the geographical location of the ACT array and due to the particularly narrow shelf in those two sites.

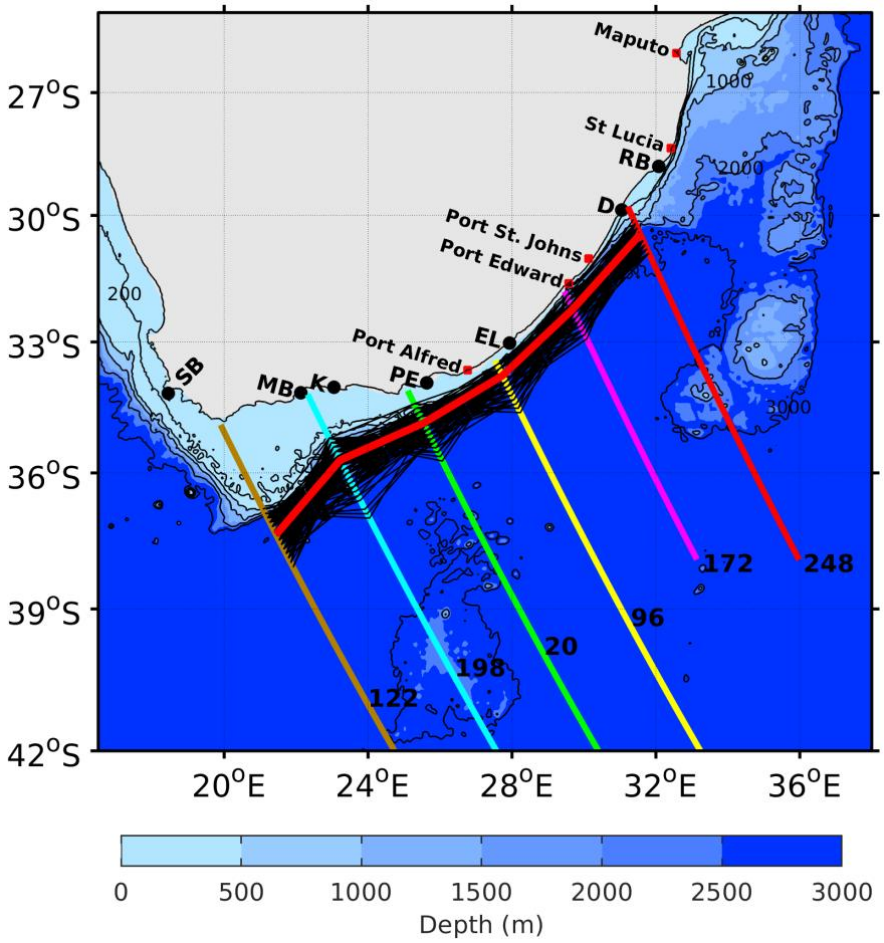

Fig. 5.5: Thin black lines indicate monthly locations of the AC core. The solid red line represents the climatology i.e. the mean location. Coloured oblique lines indicate the geographical locations of ground tracks. The 200 m isobath (black) marks the approximate position of the shelf break. Another important display is 1000 m isobath to indicate the variation in the continental slope. Note that “RB”, “D”, “EL”, “PE”, “K”, “MB”, and “SB” indicates Richards Bay, Durban, East London, Port Elizabeth, Knysna, Mossel Bay and Simons Bay, respectively.

The Agulhas Current core positions were determined by deriving the geographical position of the maximum gradient on monthly data based on the coast to AC gradient approach. The connections between the core position of the Agulhas Current and transport are discussed in the next section.

5.3.2 Correlation between Agulhas Current strength and core position

For this study we focus on track #96, essentially along the ACT array at 34°S (Beal et al., 2015), for comparison with existing results in the literature. This investigation provides an indication of which of the time series, transport or core position is the most suitable for studying the influence of the AC on the local coastal sea level. A correlation coefficient of 0.41 is found between monthly AC jet transport and AC core position at lag zero, Fig. 5.6. The resultant correlation coefficient implies that a steady current is observed on almost half of the occasions when the core position shifted further offshore. In fact, *in situ* measurements have indicated a narrower, stronger current to be the typical flow along the continental slope (Beal et al., 2015). In other words, in its offshore movement the AC is usually broader, deeper and slower. As a result, larger mass transport is expected to be directly proportional to offshore displacements, and the large deviations from the mean transport in Fig. 5.6 confirms this statement. A correlation coefficient of 0.27 (not shown) at zero lag was found between monthly AC box transport and core position, indicating the limitation of the transport data to account for the offshore shifts of the current.

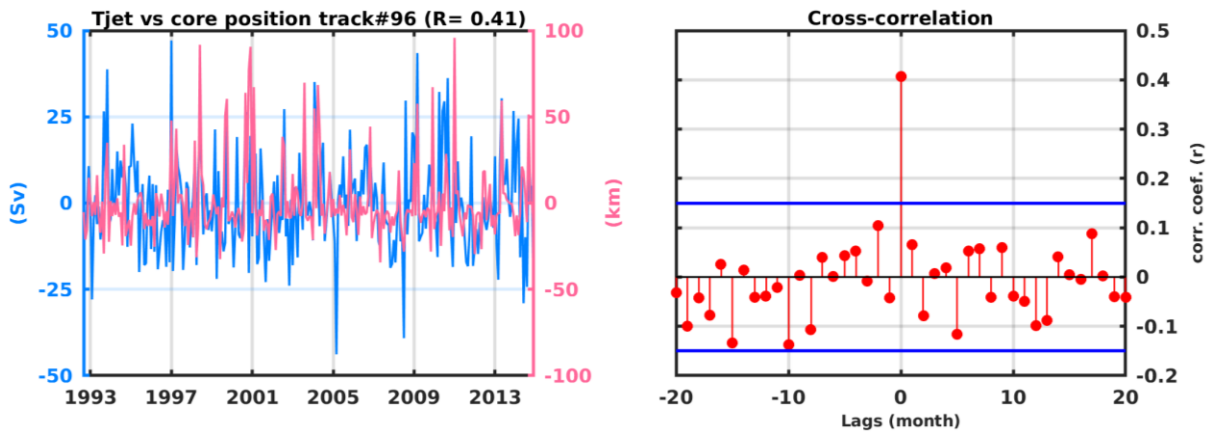

Fig. 5.6: Correlation between monthly anomalies of Tjet and core location across T/P – J1/2/3 ground track #96. Cross-correlation analysis indicates no lag between either time series correlation. In the left panel, the jet transport in Sverdrups is given in blue and the core position in kilometres is given in light red. In the right panel, the horizontal blue lines indicate the 95% confidence bounds.

Furthermore, the relation between the AC transport and the core position at each timescale embedded within the monthly time series was investigated. In general, all timescales depicted a correlation between the AC jet transport and the core position although not all are statistically significant at high confidence intervals, Fig. 5.7. Fig. 5.7 does not show the oscillatory modes of variability that are correlated below the 90% confidence level. Modes 1 and 2 indicate timescales of approximately 3 and 6 month periods, respectively. Modes 4 and 5 indicate timescales of approximately 2 and 4 year periods, respectively. Finding significant correlations only at these frequencies seems reasonable given the data time span studied, approximately 22 years. The strong correlation at mode 4 (R=0.45; Fig. 5.7c) is notable, indicating a good connection prior to 2005. In fact, it is interesting how the time series are synchronised over the period 1993 - 2005. The reason for this was not investigated further given the scope of this study. Fig. 5.7d also depicts strong correlation indicating a direct connection, although with 90% confidence. Overall, the separated oscillatory modes portray a stronger correlation between the AC transport and the core position, indicating that a similar correlation may be found at the sub-annual timescale. The longer term modes (not shown) indicate a shift to an inverse correlation between the time series studied.

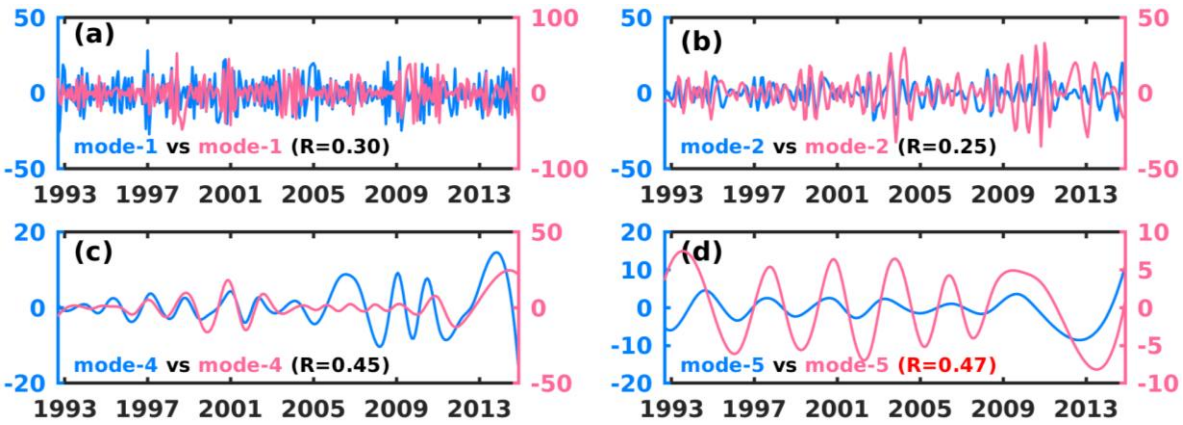

Fig. 5.7: Correlation between monthly anomalies of transport (Tjet) and core location of the AC, at different timescales, separated by EMD analysis. For a better comparison, the long-term linear trend and the seasonal cycle were removed from the original time series. All correlation coefficients depicted were found at lag zero. In all panels, the jet transport in Sverdrups is shown blue and the core position in kilometres from the coast in light red. Correlations statistically significant at 90% confidence level are in red.

To further investigate the correlation between the AC transport and core position, the modes of variability were combined to produce the sub-annual and interannual timescales in the same manner as described for the TG data in Chapter 2. Fig. 5.8 illustrates the correlation between the AC transport and AC core position at the sub-annual timescale. As can be seen, no significant changes are observed with regard to the correlation coefficient found in monthly raw time series (Fig. 5.6). This indicates that, in the annual cycle the Current is stable enough so that no significant changes can be detected relating to its transport and core position, a finding also suggested in previous studies (e.g. Krug and Tournadre, 2012; Beal et al., 2015).

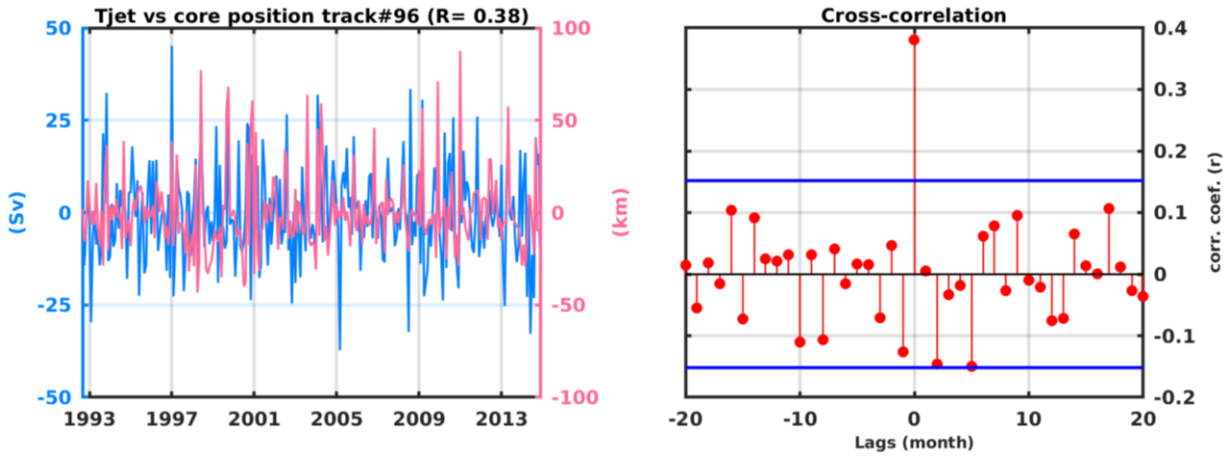

Fig. 5.8: Correlation, at the sub-annual timescale, between monthly anomalies of Tjet and core location. Each time series represents the ensemble mean of selected modes. In the left panel, the jet transport in Sverdrups is blue and the core position in kilometres from the coast is in red. In the right panel, the horizontal blue lines indicate the 95% confidence bounds.

However, a correlation coefficient of R=0.35 at zero lag was found at the interannual timescale, (Fig. 5.9). The maximum correlation coefficient of approximately 0.4 (statistically significant at 90% confidence level) is notable when the current transport lags by two months (Fig. 5.9). The lagged correlation between both time series was also displayed at the longer term oscillatory modes although not quantified. Between 1997 and 2001, the figure indicates a strong tendency towards offshore core position displacements, in contrast with the tendency over the last 10 years. In other words, the current seems to have been mostly oscillating around its mean position over the recent period, in agreement with Backeberg et al. (2012) and Beal and Elipot (2016). A negative mean kinetic energy (MKE) trend and a positive eddy kinetic energy (EKE) trend have been found in the southern Agulhas Current (Backeberg et al., 2012) and along the ACT array at 34°S (Beal and Elipot, 2016), suggestion that the Current is getting weaker and more variable. The AC transport on the other hand, shows large deviations from its mean flow implying a broader, deeper and slower current flow also suggested by Beal and Elipot (2016) and based on the same data.

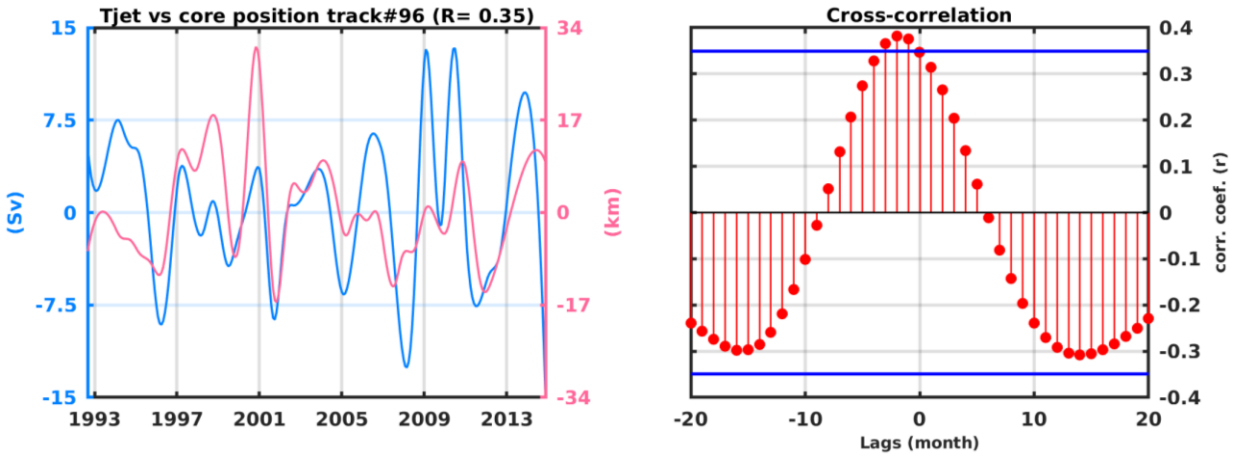

Fig. 5.9: Correlation, at the inter-annual timescale, between monthly anomalies of Tjet and core location. In the left panel, the jet transport in Sverdrups is given in blue and the core position in kilometres from the coast is in red. In the right panel, the horizontal blue lines indicate the 90% confidence bounds.

Significant correlations were found between the AC transport and its core position. However, the results do not indicate which of these two time series is best suited to quantify the possible effects of the Agulhas Current on coastal sea level. However, the definition of AC jet transport seems to be more realistic since it takes into account the offshore displacements of the boundary current and hence improves the correlation with the core position based on the coast to AC gradient approach.

5.3.3. Correlation between the Agulhas Current transport and coastal sea level

To investigate the influence of the Agulhas Current on coastal sea level, two tide gauge sites were selected, at East London and Port Elizabeth, due to their proximity to ACT array's geographical location and the shelf is at its narrowest in these two locations, as suggested above. Fig. 5.10 shows the correlation between monthly means of AC jet transport and the East London tide gauge records. A correlation coefficient of R=0.13 (statistically significant at 90% confidence level) is found when the transport leads sea level by one month. Despite this weak correlation, the result suggests a link given that in this region of the Agulhas meanders, eddies

and coastal trapped waves are frequent (de Cuevas et al., 1986; Schumann and Brink, 1990; Rouault and Penven, 2011; Krug et al., 2014; Beal et al., 2015), the location of the tide gauge and the presence of a narrow and steep shelf may result in unclear onshore influence of the current. East London tide gauge is located in a harbour enclosed in the Buffalo estuary.

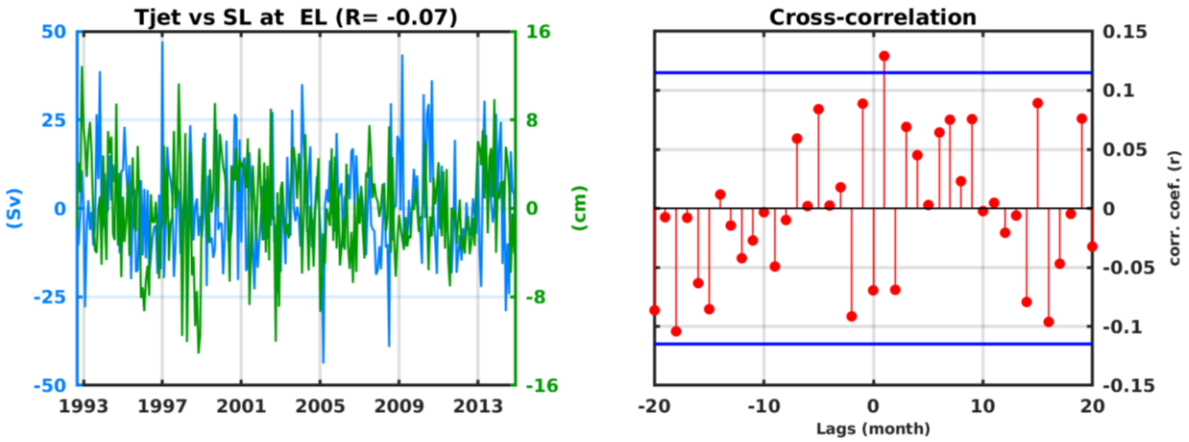

Fig. 5.10: Correlation between monthly anomalies of Tjet and SL at East London. In the left panel, the jet transport in Sverdrups is given in blue and the tide gauge record in centimetres is given in green. In the right panel, the horizontal blue lines indicate the 95% confidence bounds.

The high frequency modes separated through the EMD analysis indicate a correlation between monthly means of AC jet transport and East London tide gauge records, Fig. 5.11. The figure only displays the statistically significant correlations. In general, larger volume transport indicates low sea level at East London. The high correlation at mode 3 is noticeable at a period of approximately one year (Fig. 5.11b). As stated above, larger volume transport tends to occur simultaneously with the offshore core shifts (Fig. 5.7) at these modes. Thus the tide site may be affected by the direct influence of current transport dynamics due to a narrow shelf and steep slope (Fig. 5.5). The results appear to be in line with the findings displayed in Fig. 5.4 where the offshore core displacements are accompanied by offshore expansion of the negative ADT gradient on the shoreward side of the current.

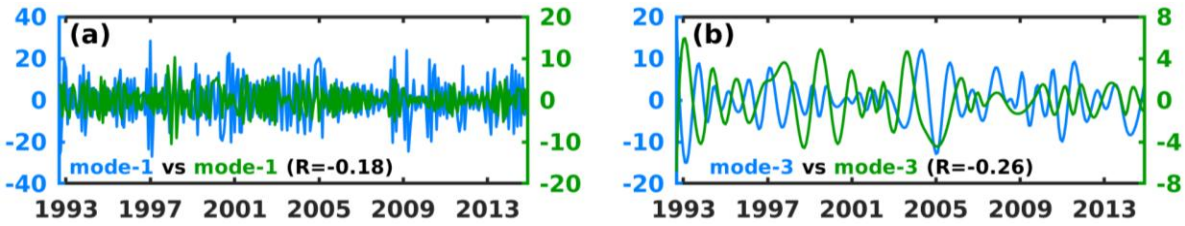

Fig. 5.11: Correlation between monthly anomalies of Tjet and sea level at EL, at different timescales. The long-term linear trend and seasonal cycle have been removed in both time series. All correlation coefficients depicted were found at lag zero and are significant at 95% confidence. In all panels, the jet transport in Sverdrups is in blue and the tide gauge record in centimetres is shown in green.

Fig. 5.12 suggests no correlation at the monthly timescale between the jet transport and the sea level records at Port Elizabeth, even at 90% confidence level. The tide site belongs to the region of widening of the continental shelf, which may result in unclear influence of the current at this timescale. But it is also possible that the altimetry data do not capture the appropriate dynamics. Indeed, the application of dedicated coastal altimetry techniques should be recommended here as it would improve the quality of the altimeter records in the last few tens of km from the coast. It should be noted that the transport data do not exhibit the exact aspect of the offshore region of the tide site, which is more likely to have different dynamics of offshore shifts of the core current. However, these data are expected to yield significant correlations at embedded oscillatory modes given the proximity between the measurement source and the tide location, as mentioned above.

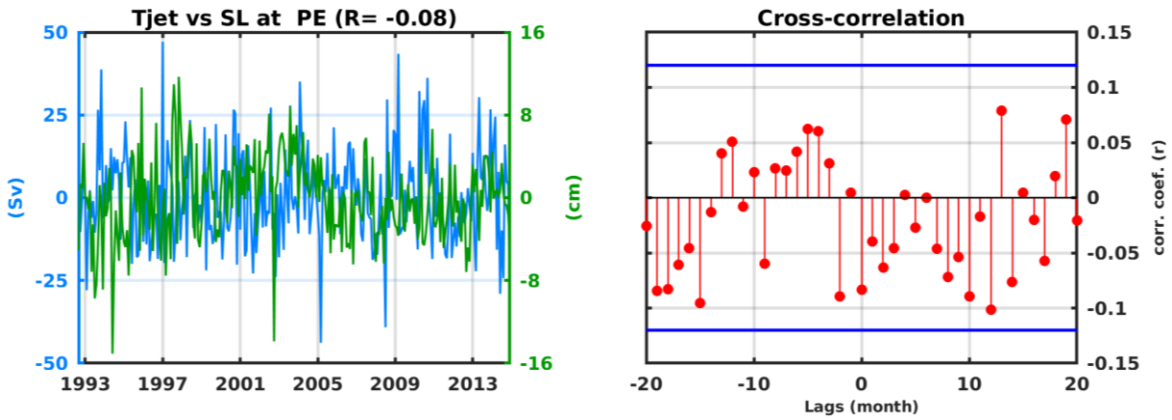

Fig. 5.12: Correlation between monthly anomalies of Tjet and SL at Port Elizabeth (PE). The long-term linear trend and seasonal cycle have been removed in both time series. In the left panel, the jet transport in Sverdrups is in blue and the tide gauge record in centimetres is shown in green. In the right panel, the horizontal blue lines indicate the 95% confidence bounds.

When decomposed through EMD analysis the time series depicts a significant correlation in some modes (Fig. 5.13). Modes 3 and 4 have particularly strong correlations, showing an inverse and direct proportionality, respectively. Similarly to East London, high frequency modes indicate that larger volume transport may indicate low sea level at Port Elizabeth. The only exception is mode 4 (Fig. 5.13c), approximately 2 year period, in which climatic modes may be forcing a direct proportionality (synchronisation), noticeable in the years known for strong El Niño events in the literature. As a result, large volume transport forces high sea levels at this mode's periodicity.

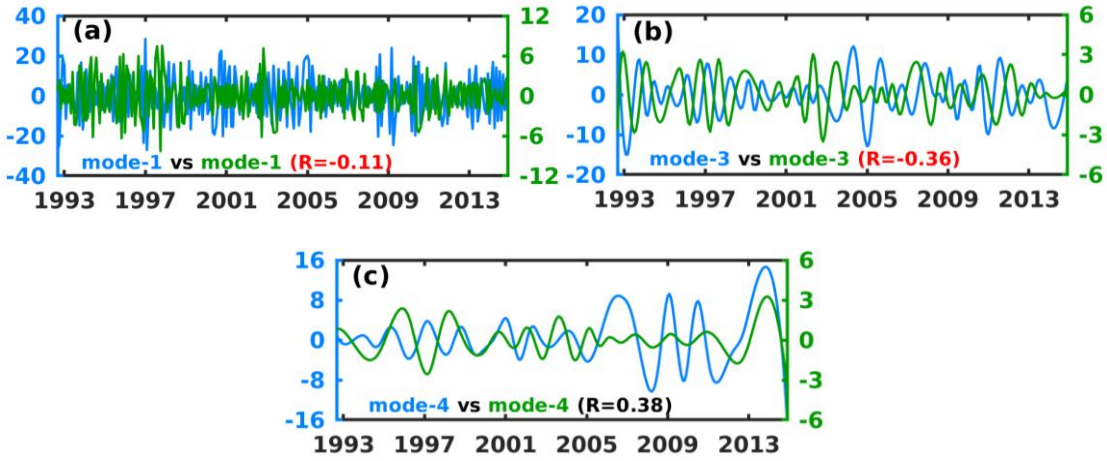

Fig. 5.13: Correlation between monthly anomalies of Tjet and SL at PE, at different timescales. The long-term linear trend and seasonal cycle have been removed in both time series. All correlation coefficients depicted were found at lag zero. In all panels, the jet transport in Sverdrups is in blue and the tide gauge record in centimetres is shown in green. Correlations statistically significant at 90% confidence are shown in red.

The results suggest that variations in AC volume transport are indeed influencing the coastal SL at both study sites, especially at the high frequency modes. At the longer term modes, although there is a similar indication, the short length of the time series appears to be preventing a solid conclusion. Both tide gauge sites are located near regions dominated by mesoscale eddy activities, as also indicated by Beal and Elipot (2016); this explains the broadening of the current instead of its strengthening during the satellite altimetry era. This may also explain the weaker correlations in such a narrow continental shelf region, where the current flows close to the coast. The correlation between the Agulhas Current core position and sea level at East London and Port Elizabeth yielded R= 0.16 and 0.05 (not shown) significant at 95% confidence, respectively. No statistically significant correlations were found in the separated modes (not shown). Given the limitation of the core location time series in showing a significant influence of the AC on coastal sea level, the ADT at the core position time series were used to replace the core position time series. Therefore, to further study the possible influence of the AC on coastal SL the study was conducted in terms of the variation of the ADT at core position, and the results are discussed in the next section.

5.3.4. Correlation between the ADT at the Agulhas Current core position and coastal sea level

The ADT at the AC core locations were used to assess the effect of the current on its shoreward side. Fig. 5.14 illustrates the correlation between monthly ADT and sea level records at East London. A correlation R=0.24 is found at zero lag, which suggests that the hypothesis is correct. Of particular interest are the correlations at 10 and 12 month lags which may be due to the annual cycle of the current, when it changes from stronger to weaker climatological currents or vice-versa.

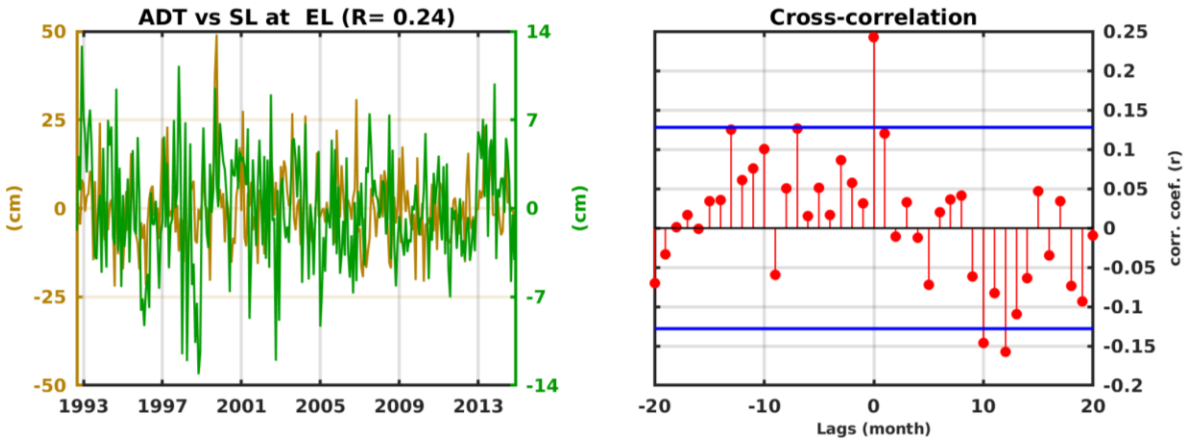

Fig. 5.14: Correlation between monthly anomalies of ADT at the core location and SL at East London. The long-term linear trend and seasonal cycle have been removed from both time series. Left panel, brown and green colours indicate the ADT and SL, respectively, in centimetres. Right panel, the horizontal blue lines indicate the 95% confidence bounds.

Fig. 5.15 displays the correlation of the separated timescales. These particularly high correlations range from approximately 3 months (mode 1) to 4 years (mode 5) periods. Overall, the shorter and longer term modes indicate that high ADT may influence high sea level at the East London tide site. Here it is clearer that ADT at the core position is a better proxy than core location time series for assessing the influence of the Current on coastal sea level. The phase match of the time series between 1997 and 2001 is also noticeable (Fig. 5.15b), which may

indicate the action of an external driving mechanism. The big data gap in East London original SL time series, between 1997 and 2001, and then filled with altimetry data may be influencing this synchronisation, implying essentially that we are correlating of the same data. However, if this is the case a similar phase match should be expected where other big data gaps have occurred. In summary, the AC contribution is responsible for over 62 % of the monthly SL variability at this tide gauge site.

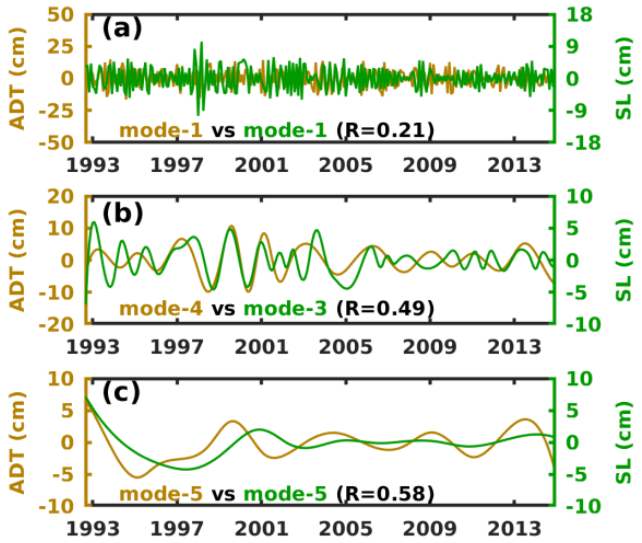

Fig. 5.15: Correlation between monthly anomalies of ADT at the core position and SL at East London, at different timescales. The long-term linear trend and seasonal cycle have been removed in both time series. All correlation coefficients depicted were found at lag zero. In all panels, brown and green colours indicate the ADT and SL in centimetres, respectively.

In contrast to East London, no clear pattern is found at Port Elizabeth, possibly due to the source region in which the ADT time series was generated (i.e. the ADT time series is from the larger distance from track #96), a wider continental shelf and further distance from the AC (Fig. 5.16). Nevertheless, both time series depict a similar low frequency variability pattern through a visual analysis. At both positive and negative 7-month lags significant correlations are displayed, possibly as a result of the annual cycle of the current. Using the ADT along-track #20 (not shown) a significant correlation coefficient of R= -0.15 is found when the ADT at the core

position lags by one month; this may suggest that due to a wide continental shelf the AC contribution to the monthly SL variability at this tide site can be explained through a Slope Counter Current (Csanady and Hamilton, 1988; Ezer et al., 2013). This Slope Current may be the result of coastal trapped wave propagation (e.g. de Cuevas et al., 1986; Schumann and Brink, 1990) and the southward passage of offshore meander events (e.g. Krug and Tournadre, 2012).

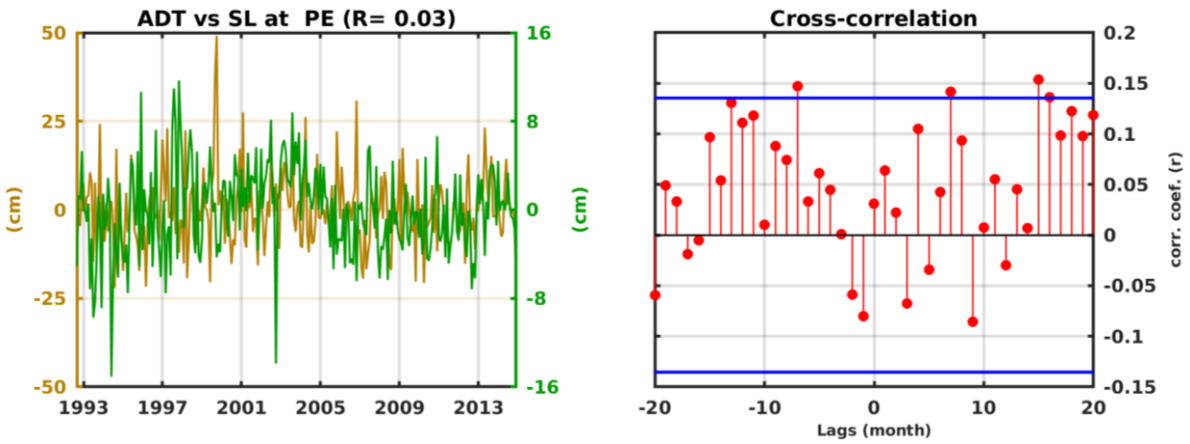

Fig. 5.16: Correlation between monthly anomalies of ADT at the core location and SL at Port Elizabeth. The long-term linear trend and seasonal cycle have been removed in both time series. Left panel, brown and green colours indicate the ADT and SL in centimetres, respectively. Right panel, the horizontal blue lines indicate the 95% confidence bounds.

Although the ADT time series do not represent the boundary current dynamics off the coast of Port Elizabeth, the low frequency modes displayed significant correlations. However, the results are not helpful for drawing a sound conclusion regarding the influence of the current on coastal sea level. The indication is that high ADT at the core position may influence low sea level at Port Elizabeth at longer term frequencies. This is in contrast to significant correlations found at high frequency modes based on along-track #20 ADT.

Higher ADTs are directly proportional to higher coastal sea levels, which is the inverse of the relation between the transport and SL time series. Fig. 5.17 illustrates an example where the recorded SL at East London in September, 2013 was approximately 12 cm higher than in September, 2014. As can be seen, in 2013 the AC flow was stronger and close to the continental

shelf, resulting in higher ADT at the core location. On the other land, weaker flow further offshore was observed in 2014, resulting in lower ADT at the core position. The limitation of satellite altimetry data is noticeable in displaying more details in coastal areas where there are missing values about 30 km from the coast towards the open ocean. Again, a good case for application of coastal altimetry data to get more insight into the feature of the last few tens of km from the coast.

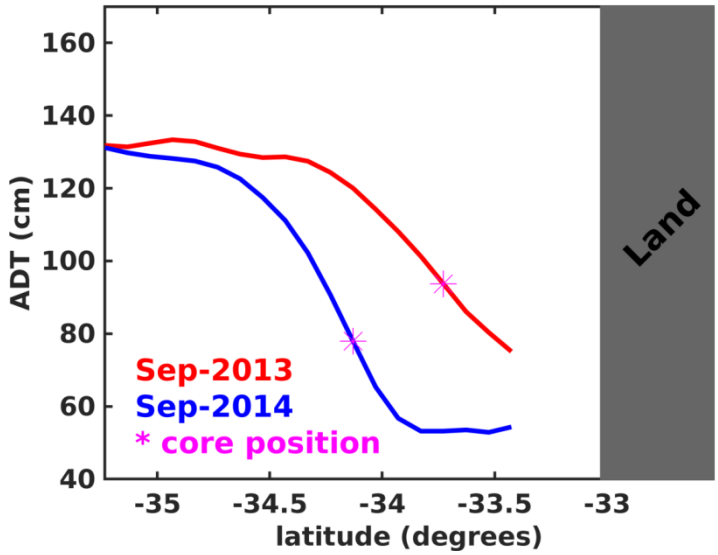

Fig. 5.17: Display of the physical mechanism in which the AC drivers coastal SL at East London. Red and blue solid lines indicate the along-track #96 ADT when the Current was near the coast and further offshore, respectively. For reference, the grey box indicates the geographical location of the land and the tide gauge.

The results suggest that the use of the ADT at the AC core location may be the best way for assessing the influence of the current on its shoreward side. At East London, the separated modes revealed details missing in the correlation between the transport and sea level data. There remain discrepancies and open questions concerning the impact of the AC at Port Elizabeth, explained by the limited and inconsistent results discussed. Particular attention was given to the last mode, considered as the trend; the results are compared with the linear trends and discussed in the following section.

5.3.5. The time series trends

To get more insight into the connection between the AC and coastal sea level, linear and EMD trends of the studied time series are displayed in Fig. 5.18. The EMD trend shapes of the AC jet transport are noticeable, as are core position and SL at Port Elizabeth when compared with linear regression trends. The results are consistent with the exception of Fig. 5.18e which may indicate the limited influence of the AC at Port Elizabeth. Over the last 10 years AC transport has been reducing (Fig. 5.18a). This is confirmed by the reduction in the offshore displacements over the same time span (Fig. 5.18b). On the other hand, the ADT at the AC core position displays a slight increase over the same period (Fig. 5.18c). Overall, one cannot notice significant changes in the linear trend shapes. The latter is consistent with the finding by Elipot and Beal (2016) who reported a similar non-significant decreasing trend in both box and jet transport. In contrast, a strengthening trend and poleward shift is suggested by Yang et al. (2016), based on observational data and climate model simulations.

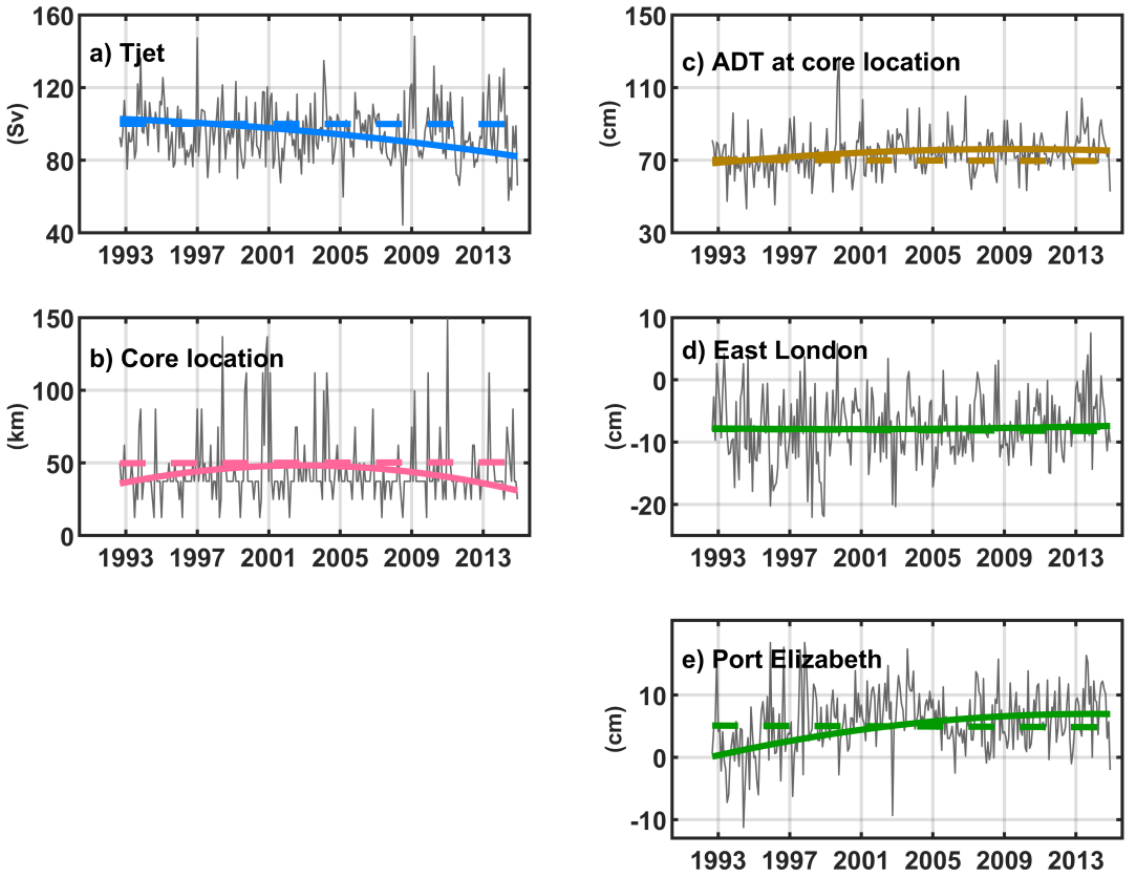

Fig. 5.18: Linear (dashed lines) and EMD (solid lines) trends of the studied monthly time series. (a) AC jet transport. (b) AC core position. (c) ADT at the core position. (d) Sea level at East London. (e) Sea level at Port Elizabeth. The linear trends were derived after the removal of the seasonal cycles. The EMD trends were separated from the raw monthly time series due to its ability to filter out the appropriate seasonal cycle modes including those representing the effects of mesoscale and synoptic weather disturbance and climatic forcing.

The results suggest that the Agulhas Current has a measurable influence on coastal sea level. The degree to which it influences the coast varies according to the region due to the width of the continental shelf. The results highlight the need for more and consistent data, especially *in situ* measurements, for solving the possible discrepancies with previous studies. We also highlight the need for better observations of cross-shelf dynamics and processes (e.g. Krug et al., 2017). Furthermore, the selected tide gauge sites for assessing the impact of the AC on coastal SL seem enough for drawing valid conclusions, given that the selection was based on other results rather than empirical assumptions.

5.4. Summary and Conclusion

Two tide gauge sites (East London and Port Elizabeth) out of seven previously selected, were used to assess how the Agulhas Current transport and offshore position influences the coastal sea level. This pair of tide stations is adjacent to the geographical positions of the ACT array, where previous studies regarding the AC path and core position have been conducted. Thus, the conclusions cannot be extended to the whole east and south coast of South Africa but, are only valid for the area around the two tide sites. This study was motivated by the open questions that remained in Chapter 4 when identifying the timescales and driving mechanisms of sea level variability, and the fact that studies have indicated the existence of significant correlations between western boundary currents, for instance the Gulf Stream and coastal SL variability (e.g. Blaha, 1984; Ezer, 2001, 2013, 2015; Sweet et al., 2009; Ezer et al., 2013; Park and Sweet, 2015).

It was found that the coast to AC gradient approach, although simple, is suitable for determining the Current path and core position due to its agreement with the previous findings. A good correlation was also found between the AC jet transport and its core position, consistent with previous studies over the globe (e.g. Ezer, 2001; Ezer et al., 2013). A closer comparison with the literature reveals some similarity in the Tjet definition and derivation of the core position as the reason for this good correlation. The AC jet transport is the maximum flow captured each time the current exceeded half of its mean position within 300 km offshore, along the ACT array (Leber and Beal, 2014; Beal et al., 2015).

The results suggest that variations in AC transport are indeed influencing the coastal SL in both studied sites, especially at the high frequency modes. At the longer term modes, although giving a similar indication, the short length of the time series appears to be preventing sound conclusions. An attempt to use the Simple Ocean Data Assimilation (SODA; Giese and Ray, 2011) mass transport data set was not successful due to a weaker correlation with the transport data used in this study. The Agulhas Current core position time series exhibited more limitations for studying the influence of the AC on coastal sea level.

Thus, the ADT at the AC core locations were used to assess the effect of the current on its shoreward side, assuming that at this position higher and lower ADTs correspond to stronger and weaker currents, respectively; this hypothesis was supported by observations. It was also shown that the AC contribution is responsible for over 62 % of the monthly SL variability at East London.

However, the results suggested that impact of AC on the coastal SL vary with varying continental shelf width, eddies and meandering events, as well as coastal processes. A slight upward EMD trend was observed in both SL and ADT at the core location time series, in response to a downward trend in jet transport and core position EMD observed over the last ten years. More and consistent data are needed for a better understanding of Agulhas Current variations and their implications for regional coastal sea level variability. These sustained observations should come from new *in situ* arrays, ocean gliders and an extension of the tide gauge network, ideally at Port St. Johns, Port Edward and Port Alfred (see Fig. 5.5). Additionally, should come from the application of model simulations outputs and dedicated coastal altimetry techniques, and finally from a merge of *in situ*, model simulations and satellite altimetry data, particularly to obtain longer time series.

CHAPTER 6

Conclusions and recommendations

The drivers of coastal sea level variability along the east and south coast of South Africa have been investigated. It has been achieved through a set of research questions posed in Chapter 1 according to the objectives as also formulated in Chapter 1. The extent to which the objectives have been reached is discussed in this concluding chapter. This chapter also proposes recommendations to improve this research work and the sea level science in the region as a whole.

6.1 Summary

1. **What are the timescales of sea level variability measured by the tide gauges?**

This question is discussed in Chapters 2, 3, and 4.

This question is of crucial importance in southern African sea level context, especially as a starting point to accurately advance our understanding of how sea level has varied in time, based on tide gauge observations. The historical tide gauge sea level records in southern Africa have many gaps of differing length, making it difficult to use analyses that require a continuous record. Additionally, there is lack of a consensus on the most suitable method to be applied (e.g. Bart et al., 2012) to separate the sea level timescales therefore, the process is one of the great challenges in sea level research (e.g. Emery and Aubrey, 1991; Gornitz, 1995; Bart et al., 2012).

Given the above, monthly mean synthetic altimetry sea level records, representing seven individual tide gauges, from the south and east coast of South Africa have been used to

obtain the embedded timescales of variability. These timescales have been separated through the Empirical Mode Decomposition (EMD) method. As a result, variability of varying frequencies has been identified. The number of timescales found depends on the time series sampling resolution and length. Taking advantage of the fact that EMD has the limitation of not being able to handle the data gaps, the sensitivity of the method when dealing with data gaps is tested on artificially created gaps to quantify their effects in terms of how they distort the expected results. The missing values have been filled by linear interpolation, average value and linear trend value methods. It has been shown that although the similarity in the global frequency of the separated modes from data with and without gaps, whichever gap filling method is applied, the separated EMD timescales will display a distorted temporal structure of the continuous time series.

Then the viability of using satellite altimetry observations to fill the gaps in the monthly mean sea level records from the south and east coasts of South Africa has been explored at the same seven individual tide gauges and gaps have been filled successfully. Thus, using monthly data, the satellite altimetry grid point, within a 1x1 degree rectangular box, that correlated best with the tide gauge time series has been identified and used to fill gaps during the satellite altimetry era. In the period prior to satellite altimetry, data from neighbouring sites that are well correlated have been used to generate the continuous tide gauge record.

These fuller tide gauge time series have yielded 8 (Richards Bay, East London and Port Elizabeth) to 9 (Durban, Knysna, Mossel Bay and Simons Bay) modes of variability depending of the record time span. The global periodicity of the separated timescales ranges from approximately 3 months to 45 years cycles. Additionally, the separated modes have displayed varying amplitudes that may provide insight into which forcing mechanisms might drive the variability and its contribution to the total sea level.

2. What are the driving mechanisms of the determined variability?

This question is discussed in Chapters 4 and 5.

Given that the periodicities of the drivers cover a range of timescales (Zebiak, 1993; Neelin et al., 1998; Saji et al., 1999, Marshall, 2003) it is challenging to determine what driver is embedded in the sea level time series when interpreting each mode. It is possible that each timescale may contain a physical driver. However, identifying a single driver for each separated timescale is challenging due to our limited knowledge of how sea level is linked to the various forcing mechanisms (e.g. Haigh et al., 2014). A key question to consider is whether it is possible to determine a physical meaning for each timescale or should the timescale isolated by the EMD be determined according to periodicity of known drivers. Thus, the oscillatory modes identified through the EMD have been summed to obtain a physically more meaningful timescale. Namely, the sub-annual timescale, which is the ensemble of the modes with a periodicity lower than approximately 18 months. The modes with a periodicity longer than approximately two years are summed to compute the interannual timescale. Using these two time series, the driving processes of tide gauge sea level records have been investigated at sub-annual and interannual timescales, by comparing and correlating these to atmospheric forcing and known climate indices.

a) Are regional and global drivers responsible for part of the observed changes in sea level records?

This question is discussed in Chapter 4.

At the sub-annual time scale, sea level responds to regional winds associated with mesoscale and synoptic weather disturbances in the annual cycle. These results were in agreement with previous studies (Brundrit, 1984; Brundrit et al., 1984; Brundrit et al., 1987). The hypothesis is that through Ekman transport dynamics SLP and longshore winds increase or decrease the coastal sea level at this timescale. Composite analyses support this hypothesis.

At the interannual timescale, the results have suggested a connection between coastal sea level variability and climate indices, although it is not consistent across the various TGs or strong. Strong positive ENSO events tend to increase coastal sea level while

strong negative ENSO events tend to decrease. Overall, strong IOD events tend to have a similar influence as the strong ENSO events. The results have also suggested that, in general negative SAM events lead to high coastal sea level events. It has been noticed that particular ENSO and IOD strong events were in phase with sea level variability suggesting the need of further analysis to understand to what extent ENSO and IOD modulate coastal sea level.

To further understand how the three modes of climate variability (ENSO, IOD and SAM) under consideration are associated with the coastal sea level at interannual timescale, composite average differences between positive and negative (using 0.75 standard deviation threshold) MEI, DMI and SAM events have been calculated. The results were in agreement with the linear correlations by suggesting that in general, high monthly coastal sea levels are more likely during El Niño, positive IOD and negative SAM events, respectively. La Niña events appear to induce low monthly coastal sea levels in approximately similar magnitude to El Niño.

The impact of the paired interaction between the three modes of climate variability and coastal SL in months with higher sea level than 1.5 standard deviations above mean sea level has been further investigated. The results suggest that the influence of modes of climate variability on local and regional coastal SL can be quantified through their binary interactions despite further investigation is necessary to substantiate statement. Thus, in most of the locations the likelihood of anomalously high coastal sea levels during months of El Niño/positive IOD and positive IOD/positive SAM events, is fairly high. The results of the combinations of MEI and SAM indices in months of anomalously high sea level months at the TG stations under consideration have prevented us to draw a sound conclusion concerning the dominating interaction, suggesting a need of further analysis.

Furthermore, the main parameters used to derive the climate indices have suggested that the areas selected for the various indices are areas where SST, SLP, and winds are not well correlated with South African coastal sea level. Nevertheless, the results have indicated that regions other than those from which the climate indices are derived

influence sea level variability in South Africa at interannual timescales. In fact, measurable correlation between tide gauge sea level variability and local and regional SST, SLP and 10 m zonal wind has been found, suggesting that the modes of climate variability do not influence coastal sea level directly, they however seem to modulate the local and regional ocean and atmosphere conditions that control coastal sea level variability, as indicated in the literature of other regions (Chen et al., 2014; Dangendorf et al., 2014; Park and Sweet, 2015; Chafik et al., 2017).

b) Is the coastal sea level related to the offshore position and transport of Agulhas Current?

This question is discussed in Chapter 5.

The results have suggested that variations in Agulhas Current (AC) transport are indeed influencing the coastal sea level in both East London and Port Elizabeth sites, especially at the high frequency modes. At the longer term modes, although giving a similar indication, the short length of the time series appears to be preventing sound conclusions. The absolute dynamic topography (ADT) at the AC core locations have been used to assess the effect of the current on its shoreward side. The results have suggested that the AC contribution is responsible for over 62 % of the monthly sea level variability at East London.

Additionally, the influence of AC on the coastal sea level has been found to vary according to the continental shelf width, eddies and meandering events, as well as coastal processes. A slight upward EMD trend has been observed in both sea level and ADT at the core location time series, in response to a downward trend in AC jet transport and core position EMD observed over the last ten years.

The two tide gauge sites (East London and Port Elizabeth) selected to assess the effect of the Agulhas Current on coastal sea level along the east and south of South Africa have been suggested by the results throughout Chapter 5. Moreover, this pair of tide stations is adjacent to the geographical positions of the Agulhas Current Time-Series Experiment

array, where previous studies regarding the AC path and core position have been conducted.

6.2 Conclusion

This PhD thesis documents the first study to investigate the drivers of sea level variability measured by the tide gauges along the east and south of southern Africa. The coastal sea level variability was found to be influenced by atmospheric and climatic drivers as well as by variations in the Agulhas Current across a range of different timescales. The atmospheric drivers, i.e. local and regional winds were found influencing the sub-annual sea level variability. Overall, there is a consistent positive SLP difference centred over southern Africa sub-continent, producing a counter-clockwise (anti-cyclonic) wind circulation and thus causing longshore winds on the east and south coast. The association between wind variations and coastal sea level variability can be explained through Ekman transport dynamics (Pugh, 1987). Thus, wind variations (mainly longshore winds) induce an onshore water mass transport towards the tide gauge location, i.e. to the left of the wind direction in the Southern Hemisphere (Pugh, 1987). The modes of climate variability (ENSO, IOD and SAM) were investigated as the forcing factors of the interannual sea level variability. The sea level variability in southern Africa region is not strongly correlated to modes of climate variability, unlike other Indian Ocean rim areas (e.g. White et al., 2014; Soumya et al., 2015). Moreover, this work highlighted the challenge to infer the impact of the climate indices on coastal sea level in the southern Africa region. The Agulhas Current variations were found responsible for over 62% of the monthly sea level variability at East London indicating its dominance on timescales ranging from a few months to decades. How much of this percentage of 62% is due to the use of altimetry data to fill the several gaps in the EL tide gauge records require a further investigation. Moreover, the results were not sufficiently consistent to suggest a firm conclusion at Port Elizabeth. Furthermore, this study pointed out to the need of additional effort for acquiring ocean dynamics data especially along the shelf. Additionally, the results rather suggest that more complex numerical models and better data are required to fully

understand the processes in this region. Nevertheless, the results suggest that changes in local atmospheric circulation patterns modulated either regionally or remotely as well as in ocean dynamics should be taken into account when assessing the regional coastal planning, management, engineering and sea level rise projections.

6.3 Recommendations for Future Work

- In chapter 2, the results have suggested that, despite minor exceptions, filling the gaps with the linear trend value is the best way to obtain mode shapes similar to the ones from the data without gaps. The method is far better when the modes are combined. However, filling sea level data gaps with more sophisticated techniques including machine learning methods is a way to be explored.

- Despite the success in extrapolating a lot of data sets in Chapter 3, it is recommended to conduct similar studies intending to combine satellite altimetry along-track observations and/or model simulations outputs in the exiting tide gauge records, for obtaining more accurate results. However, given that not all altimetry tracks cross near tide gauge locations appropriate validations are required. A close collaboration with the research institutions or groups working on retracking the data should be explored. For instance, the C-Rise project provides improved, reprocessed coastal altimetry data in the region, carried out by the ALES algorithm (Passaro et al., 2014). Additionally, the south and east Africa region is also benefited from altimetry products of X-TRACK post-processing algorithm (Birol et al., 2017). A prior validation of the model simulations outputs is also necessary given that generally these are not designed specifically for sea level studies and their coarse resolution may misrepresent important features of coastal sea level.

- Individual events such as the November - December 2002 outlier event, have not been analysed in detail yet, given that they represent probably the one of the most interesting feature in the records. To what extent these are really outliers in term of

measurement errors or a result of oceanographic (or meteorological) conditions, needs to be investigated.

- Regardless of the success in showing the physical mechanism by which SLP gradient anomalies and the corresponding wind variations influence monthly mean coastal SL variability, it would be interesting to dig deeper into the various timescales (within the sub-annual timescale) and restrict the range of periods at which the correlation with pressure and/or wind remain significant.

- Great insights into interannual sea level variability were discussed in Chapter 4. However, the deficiencies and open questions still remain given the objective of this study rather than providing an exhaustive study of the subject. Thus, it is suggested using the zonal and meridional components of wind stress rather than 10 m winds to detect possible discrepancies with the results discussed here. Winds stress data that were used initially had to be rejected due to their failure to represent important features in Southern Hemisphere.

- Investigations are necessary in order to understand the extent to which coastal sea level is connected to the local and regional ocean, and atmosphere conditions modulated by climate forcings as suggested by the results in Chapter 4. Additionally, further investigations are necessary to understand the regional atmospheric circulation patterns associated with each binary interaction of the modes of climate variability. It will allow explaining the characteristics wind and pressure variations associated with a specific combination of the modes of climate variability and how significant are the effects on coastal sea level.

- The analyses discussed in Chapter 5 should be extended to tide gauges other than East London and Port Elizabeth. It seems worth conducting a similar analysis on track #172 using a virtual station off Port Edward (see Fig. 5.1). Studies based on better observations of cross-shelf dynamics and processes (e.g. Krug et al., 2017) may be helpful in such dynamic shelf regions. Further analyses based on model simulations

representing the great Agulhas Current should also be explored to overcome the limitation imposed by data availability.

- Modelling studies separating local and remote influences might be very important in future studies given the poor data quality, which makes any observational study hard to judge.

Bibliography

Ablain, M., J. F. Legeais, P. Prandi, M. Marcos, L. Fenoglio-Marc, H. B. Dieng, J. Benveniste and A. Cazenave (2016): Satellite Altimetry-Based Sea Level at Global and Regional Scales. *Surv. Geophys.*, **38**, 7 – 31. DOI: 10.1007/s10712-016-9389-8.

Alberti, T., F. Lepreti, A. Vecchio, E. Bevacqua, V. Capparelli and V. Carbone (2014): Natural periodicities and Northern Hemisphere – Southern Hemisphere connection of fast temperature changes during the last glacial period: EPICA and NGRIP revisited. *Clim. Past*, **10**, 1751–1762. doi:10.5194/cp-10-1751-2014.

Alexander, M. A. (2010): Extratropical air-sea interaction, sea surface temperature variability, and the Pacific decadal oscillation. *Amer. Geophys. Union*, **189**, 123–148. doi:10.1029 /2008GM000794.

Anthoff D., R.J. Nicholls, R.S.J. Tol and A.T. Vafeidis (2006): Global and regional exposure to large rises in sea-level: a sensitivity analysis. *Tyndall Centre for climate change Research*, Working paper 96

Ashok, K., Z. Guan and T. Yamagata (2001): Impact of the Indian Ocean dipole on the relationship between the Indian monsoon rainfall and ENSO. *Geophys. Res. Lett.*,**28**, 4499 – 4502. https://doi.org/10.1029/2001GL013294.

Backeberg, B. C., F. Counillon, J. A. Johannessen and M.–I. Pujol (2014): Assimilating Along-track SLA data using the EnOI in an Eddy Resolving Model of the Agulhas System. *Ocean Dynamics*, **64**, 1121 – 1136.

Backeberg, B. C., P. Penven and M. Rouault (2012): Impact of intensified Indian Ocean winds on mesoscale variability in the Agulhas system. *Nat. Clim. Change*, **2**, 608 – 612. doi:10.1038/nclimate1587.

Bart, F., M. van Koningsveld and M. J. F. Stive (2012): Trends in Sea-Level Trend Analysis. *J. Coastal Res.*, **28**, 311 – 315. DOI: 10.2112/JCOASTRES-11A-00024.1.

Beal, L. M., and H. L. Bryden (1999): The velocity and vorticity structure of the Agulhas Current at 32°S. *J. Geophys. Res.*, **104**, 5151 – 5176. doi:10.1029/1998JC900056.

Beal, L. M., and S. Elipot (2016): Broadening not strengthening of the Agulhas Current since the early 1990s. *Nature*, **540**, 570 – 573. doi:10.1038/nature19853

Beal, L. M., S. Elipot, A. Houk, and G. M. Leber (2015): Capturing the Transport Variability of a Western Boundary Jet: Results from the Agulhas Current Time-Series Experiment (ACT). *J. Phys. Oceanogr.*, **45**, 1302 – 1324. DOI: 10.1175/JPO-D-14-0119.1

Beal, L. M., W. P. M. de Ruijter, A. Biastoch, R. Zahn, and SCOR/WCRP/IAPSO Working Group 136 (2011): On the Role of the Agulhas system in Ocean Circulation and Climate. *Nature*, **472**, 429 – 436.

Becker, M., B. Meyssignac, C. Letetrel, W. Llovel, A. Cazenave and T. Delcroix (2012): Sea level variations at tropical Pacific islands since 1950. *Glob. Planet. Chang.*,**80-81**, 85 – 98. https://doi.org/10.1016/j.gloplacha.2011.09.004

Becker, M., M. Karpytchev, M. Davy and K. Doekes (2009): Impact of a shift in mean on the sea level rise: application to the tide gauges in the Southern Netherlands. *Cont. Shelf Res.*, **29**, 741 – 749.

Behera, S. K., J. Luo, S. Masson, P. Delecluse, S. Gualdi, A. Navarra and T. Yamagata (2005): Paramount Impact of the Indian Ocean Dipole on the East African Short Rains: A CGCM Study. *J. Clim.*, **18**, 4514 – 4530. https://doi.org/10.1175/JCLI3541.1.

Birol, F. and F. Niño (2015): Ku– and Ka-band Altimeter Data in the Northwestern Mediterranean Sea: Impact on the Observation of the Coastal Ocean Variability. *Marine Geodesy*, **38**:sup1, 313 - 327. DOI: 10.1080/01490419.2015.1034814.

Birol, F., N. Fuller, F. Lyard, M. Cancet, F. Niño, C. Delebecque, S. Fleury, F. Toublanc, A. Melet, M. Saraceno, F. Léger (2017): Coastal Applications from Nadir Altimetry: Example of the X-TRACK Regional Products. *Adv. Space Res.*, **59** (4), 936 – 953. doi:10.1016/j.asr.2016.11.005

Blaha, J. P. (1984): Fluctuations of Monthly Sea Level as Related to the Intensity of the Gulf Stream from Key West to Norfolk. *J. Geophys. Res.*, **89**, 8033 – 8042.

Boon, J. D., J. M. Brubaker and D. R. Forrest (2010): Chesapeake Bay land subsidence and sea level change, *in App. Mar. Sci. and Ocean Eng., Report No. 425*, Virginia Inst. of Mar. Sci., Gloucester Point, VA.

Brundrit, G. B. (1984): Monthly mean sea level variability along the west coast of southern Africa. *S. Afr. J. Mar. Sci*, **2**, 195 – 203.

Brundrit, G. B. (1995): Trends of Southern African Sea Level: Statistical Analysis and Interpretation. *S. Afr. J. Mar. Sci*, **16**, 9 – 17.

Brundrit, G. B., B. A. de Cuevas and A. M. Shipley (1984): Significant Sea-level Variations along the West Coast of Southern Africa 1979 – 83. *S. Afr. J. Sci.*, **80**, 80 – 82.

Brundrit, G. B., B. A. de Cuevas and A. M. Shipley (1987): Long-term sea-level variability in the eastern South Atlantic and a comparison with that in the eastern Pacific. *S. Afr. J. Mar. Sci*, **5**, 73 – 78. doi: 10.2989/025776187784522531.

Bryden, H. L., L. M. Beal, and L. M. Duncan (2005): Structure and Transport of the Agulhas Current and Its Temporal Variability. *J. Oceanogr.*, **61**, 479 – 492. doi:10.1007/ s10872-005-0057-8.

Butterworth, S. (1930): On the Theory of Filter Amplifiers. *InWireless Engineer*(also called *Experimental Wireless and the Wireless Engineer*), **7**, 536 – 541.

Calafat, F. M. and D. P. Chambers (2013): Quantifying Recent Acceleration in Sea Level Unrelated to Internal Climate Variability. *Geophys. Res. Lett.*, **40**, 3661 – 3666. Doi:10.1002/grl.50731.

Calafat, F. M., D. P. Chambers and M. N. Tsimplis (2013): Inter-annual to decadal sea-level variability in the coastal zones of the Norwegian and Siberian Seas: The role of atmospheric forcing. *J. Geophys. Res. Oceans*, **118**, 1287 – 1301. doi:10.1002/jgrc.20106.

Cazenave, A., K. Dominh, L. Soudarin, F. Ponchaut and C. Le Provost (1999): Sea level changes from TOPEX/ POSEIDON altimetry and tide gauges, and vertical crustal motions from DORIS, *Geophys. Res. Lett.*, **26**, 2077 – 2080.

Cazenave et al (2018): Global sea-level budget 1993–present, *Earth Syst. Sci. Data*, **10**, 1551 – 1590, https://doi.org/10.5194/essd-10-1551-2018.

Chafik, L., J. E. Ø. Nilsen and S. Dangendorf (2017): Impact of North Atlantic Teleconnection Patterns on Northern European Sea Level. *J. Mar. Sci. Eng.*, **5**, 1 – 23. doi:10.3390/jmse5030043

Chambers, D. P. (2015): Evaluation of empirical mode decomposition for quantifying multi-decadal variations and acceleration in sea level records. *Nonlin. Processes Geophys.*, **22**, 157 – 166. doi:10.5194/npg-22-157-2015

Chambers, D. P.; M. A. Merrifield and R. S. Nerem (2012): Is there a 60-year oscillation in global mean sea level? *Geophys. Res. Lett.*, **39** (L18607). doi:10.1029/2012GL052885.

Chambers, D. P., A. Cazenave, N. Champollion, H. Dieng, W. Llovel, R. Forsberg, K. von Schuckmann and Y. Wada (2016): Evaluation of the Global Mean Sea Level Budget between 1993 and 2014. *Surveys in Geophysics*, 1 – 19, doi:10.1007/s10712-016-9381-3.

Chelton, D. B. (1983): Effects of Sampling Errors in Statistical Estimation. *Deep Sea Res.*, **30**, 1083 – 1103. Doi:10.1016/0198-0149(83)90062-6.

Chelton, D. B. and R. E. Davis (1982): Monthly mean sea-level variability along the west coast of North America. *J. phys. Oceanogr.*, **12**, 757-784.

Cheng, Y., H. Plag, B. D. Hamlington, Q. Xu and Y. He (2015): Regional sea level variability in the Bohai Sea, Yellow Sea, and East China Sea. *Cont. Shelf Res.*, **111**, 95 – 107.

Church, J. A. and N. J. White (2011): Sea-level rise from the late 19th to the early 21st century. *Surv. Geophys.*, **32**, 585 – 602.

Church, J. A., N. J. White and J. M. Arblaster (2005): Significant decadal-scale impact of volcanic eruptions on sea level and ocean heat content. *Nature*, **438**, 74 – 77.

Church, J. A., N. J. White, C. M. Domingues, D. P. Monselesan andE. R. Miles (2013b): Chapter 27 - Sea-Level and Ocean Heat-Content Change. *International Geophysics*, **103**, 697 - 725. http://dx.doi.org/10.1016/B978-0-12-391851-2.00027-1.

Church, J. A., P. L. Woodworth, T. Aarup, and W. S. Wilson, (eds.) 2010: Understanding Sea-Level Rise and Variability. Wiley-Blackwell, Hoboken, NJ, USA, 428 pp. DOI:10.1002/9781444323276.

Church, J. A., P. U. Clark, A. Cazenave, J. M. Gregory, S. Jevrejeva, A. Levermann, M. A. Merrifield, G. A. Milne, R. S. Nerem, P. D. Nunn, A. J. Payne, W. T. Pfeffer, D. Stammer and A. S. Unnikrishnan (2013a): Sea Level Change. In: Climate Change 2013: The Physical Science Basis. Contribution of Working Group I to the Fifth Assessment Report of the Intergovernmental Panel on Climate Change [Stocker, T.F., D. Qin, G.-K. Plattner, M. Tignor, S.K. Allen, J. Boschung, A. Nauels, Y. Xia, V. Bex and P.M. Midgley (eds.)]. Cambridge University Press, Cambridge, United Kingdom and New York, NY, USA.

Cipollini, P. F. M. Calafat, S. Jevrejeva, A. Melet and P. Prandi (2017): Monitoring Sea Level in the Coastal Zone with Satellite Altimetry and Tide Gauges. *Surv. Geophys.*, **38**, 33 – 57. DOI: 10.1007/s10712-016-9392-0.

Cipollini, P., J. Benveniste, J.Bouffard, W. Emery, C. Gommenginger, D. Griffin, J. Høyer, A. Kurapov, Kr. Madsen, F. Mercier, L. Miller, A. Pascual, M. Ravichandran, F. Shillington, H. Snaith, P. Ted Strub, D. Vandemark, S. Vignudelli, J. Wilkin, P. Woodworth, J. Zavala-Garay (2010): The role of altimetry in coastal observing systems. *Proceedings of OceanObs Conference* 9:181 – 191.

Clark, P. U., J. A. Church, J. M. Gregory and A. J. Payne (2015): Recent Progress in Understanding and Projecting Regional and Global Mean Sea Level Change. *Curr. Clim. Change Rep.*, **1**, 224 – 246.

Colberg, F., C. J. C. Reason and K. Rodgers (2004): South Atlantic response to ENSO induced climate variability in an OGCM. *J. Geophys. Res.*, **109**, C12015, doi 10.1029/2004JC002301.

Csanady, G. T., and P. Hamilton (1988): Circulation of Slopewater. *Cont. Shelf Res.*, **8**, 565 – 624.

Dangendorf, S., F. M. Calafat, A. Arns, T. Wahl, I. D. Haigh, and J. Jensen (2014): Mean sea level variability in the North Sea: Processes and implications. *J. Geophys. Res. Oceans*, **119**, 6820 – 6841. doi:10.1002/2014JC009901.

Dangendorf, S., M. Marcos, G. Wöppelmann, C. P. Conrad, T. Frederikse and R. Riva (2017): Reassessment of 20th century global mean sea level rise. *Proceedings of the National Academy of Sciences*. doi:10.1073/pnas.1616007114.

DeConto, R. M. and D. Pollard (2016): Contribution of Antarctica to past and future sea-level rise. *Nature*, **531**, 591 – 597. doi:10.1038/nature17145.

de Cuevas, B. A., G. B. Brundrit and A. M. Shipley (1986): Low-frequency sea-level fluctuations along the coasts of Namibia and South Africa. *Geophys. J. R. asrr. Soc.*, **87**, 33 – 42.

de Ruijter, W. P. M., J. R. E. Lutjeharms, and P. J. van Leeuwen (1999): Generation and Evolution of Natal Pulses: Solitary Meanders in the Agulhas Current. *J. Phys. Oceanogr.*, **29**, 3043 – 3055.

Doodson, A. T. (1924): Meteorological Perturbations of Sea-Level and Tides. *Geophys. J. Int.*, **1**, 124 – 147. doi:10.1111/j.1365-246X.1924.tb05363.x

Douglas, B. C. (1992): Global Sea Level Acceleration. *J. Geophys. Res*., **97**, 12699 – 12706. Doi:10.1029/92JC01133.

Emery, K. O. and D. G. Aubrey (1991): Sea Levels, Land Levels, and Tide Gauges. *Springer-Verlag*, New York, 237 pp. doi: 10.1007/978-1-4613-9101-2.

Emery, W. J. and R. E. Thomson (2004): Data Analysis Methods in Physical Oceanography. *ELSEIVIER*, 2nd and rev. edn..

Elipot, S., and L. M. Beal (2015): Characteristics, Energetics, and Origins of Agulhas Current Meanders and Their Limited Influence on Ring Shedding. *J. Phys. Oceanogr.*, **45**, 2294 – 2314. DOI: 10.1175/JPO-D-14-0254.1.

Ezer, T. (2001): Can Long-term Variability in the Gulf Stream Transport be Inferred from Sea Level? *Geophys. Res. Lett.*, **28**, 1031 – 1034. doi:10.1029/2000GL011640.

Ezer, T., (2013): Sea Level Rise, Spatially Uneven and Temporally Unsteady: Why the U.S. East Coast, the Global Tide Gauge Record, and the Global Altimeter Data Show Different Trends. *Geophys. Res. Lett.*, **40**, 5439 – 5444. doi:10.1002/2013GL057952.

Ezer, T. (2015): Detecting Changes in the Transport of the Gulf Stream and the Atlantic Overturning Circulation from Coastal Sea Level Data: The Extreme Decline in 2009 – 2010 and Estimated Variations for 1935 – 2012. *Global and Planetary Change*, **129**, 23 – 36.

Ezer, T. and W. B. Corlett (2012): Is sea level rise accelerating in the Chesapeake Bay? A demonstration of a novel new approach for analyzing sea level data. *Geophys. Res. Lett.*, **39**, L19605, doi:10.1029/2012GL053435.

Ezer, T., I. D. Haigh and P. L. Woodworth (2016): Nonlinear Sea-Level Trends and Long-Term Variability on Western European Coasts. *J. Coast. Res.*, **32**, 744 – 755. Coconut Creek (Florida), ISSN 0749-0208.

Ezer, T., L. P. Atkinson, W. B. Corlett and J. L. Blanco (2013): Gulf Stream's induced sea level rise and variability along the U.S. mid-Atlantic coast. *J. Geophys. Res.-Oceans*, **118**, 685–697, doi:10.1002/jgrc.20091.

Fasullo, J. T., Boening, C., Landerer, F. W. and R. S. Nerem (2013): Australia's unique influence on global sea level in 2010–2011. *Geophys. Res. Lett.*, **40**, 4368–4373, https://doi.org/10.1002/grl.50834.

Feng, Y., X. Chen and N. E. Huang (2011): On the Sea Level Rising Rate Since 1993. WCRP Open Science Conference, C38 – Th19B, Denver.

Freeman, E., S. D. Woodruff, S. J. Worley, S. J. Lubker, E. C. Kent, W. E. Angel, D. I. Berry, P. Brohan, R. Eastman, L. Gates, W. Gloeden, Z. Ji, J. Lawrimore, N. A. Rayner, G. Rosenhagen, and S. R. Smith (2016): ICOADS Release 3.0: a major update to the historical marine climate record. *Int. J. Climatol.*, **37**, 2211 – 2232. DOI: 10.1002/joc.4775

Fu, L. L. and *P. -Y. Le* Traon (2006): Satellite altimetry and ocean dynamics. *C. R. Geoscience, **338**,* 1063-1076. https://doi.org/10.1016/j.crte.2006.05.015.

Fujii, Y. and K. Nakane (1997): Reevaluation of anomalous vertical crustal movement associated with the 1964 Niigata, Japan, earthquake. *Pure and Applied Geophysics*, **149**, 115 – 127.

Garland, G. and A. A. Mather (2007): Recent sea level change at Durban and implications for management. *Proceedings of the 8th international conference MEDCOAST 07,* Alexandria, Egypt, pp 1309 – 1319.

Giese, B. S., and S. Ray (2011): El Niño Variability in Simple Ocean Data Assimilation (SODA), 1871–2008, *J. Geophys. Res.*, **116**, C02024, doi:10.1029/2010JC006695.

Gillett, N. P., T. D. Kell, and P. D. Jones (2006): Regional climate impacts of the Southern Annular Mode. *Geophys. Res. Lett.*, **33**, L23704, doi:10.1029/2006GL027721.

Goodbred, S. L. and S. A. Kuehl (2000): The significance of large sediment supply, active tectonism and eustasy on margin sequence development: Late Quaternary stratigraphy and evolution of the Ganges-Brahmaputra delta. *Sedimentary Geology*, **133**, 227 – 248.

Gordon, A. L. (1985): Indian-Atlantic Transfer of Thermocline Water at the Agulhas Retroflection. *Science*, **227**, 1030 - 1033.

Gornitz, V. (1995): Monitoring sea level changes. *Climatic Change*, **31**, 515 - 544, doi:10.1007/BF01095160.

Gregory, J. M., N. J. White, J. A. Church, M. F. P. Bierkens, J. E. Box, M. R. Van den Broeke, J. G. Cogley, X. Fettweis, E. Hanna, P. Huybrechts, et al. (2013): Twentieth-century global mean sea level rise: is the whole greater than the sum of the parts? *J. Clim.*, **26**, 4476 – 4499. doi:10.1175/JCLID-12-00319.1.

Gründlingh, M. L. (1983): On the Course of the Agulhas Current. *S. Afr. Geogr. J.*, **65**, 49 – 57.

Haigh, I. D., T. Wahl, E. J. Rohling, R. M. Price, C. B. Pattiaratchi, F. M. Calafat and S. Dangendorf (2014): Timescales for Detecting a Significant Acceleration in Sea Level Rise. *Nat. Commun.*, **5**, 3635. doi:10.1038/ncomms4635.

Han, W., G. A. Meehl, B. Rajagopalan, J. T. Fasullo, A. Hu, J. Lin, W. G. Large, J. Wang, X. Quan, L. L. Trenary, A. Wallcraft, T. Shinoda and S. Yeager (2010): Patterns of Indian Ocean sea level change in a warming climate. *Nat. Geosci.*, **3**, 546 – 550. doi:10.1038/NGEO901

Han, W, J. Vialard, M. J. McPhaden, T. Lee, Y. Masumoto, M. Feng and W. P. M. de Ruijter (2014): Indian Ocean Decadal Variability: A Review. *Bull. Am. Meteorol. Soc.*, **95**, 1679 – 1703. doi:10.1175/BAMS-D-13-00028.1.

Hay, C. C., E. Morrow, R. E. Kopp and J. X. Mitrovica (2015): Probabilistic reanalysis of twentieth-century sea-level rise. *Nature*, **517**, 481 – 484. doi:10.1038/nature14093.

Hendon, H. H. (2003): Indonesian rainfall variability: Impacts of ENSO and local air-sea interaction. *Am. Meteorol. Soc.*, **16**, 1775 – 1790. https://doi.org/10.1175/1520-0442(2003)016<1775:IRVIOE>2.0.CO;2

Holgate, S. J. (2007): On the decadal rates of sea level change during the twentieth century. *Geophys. Res. Lett.*, **34**, L01602, doi:10.1029/2006GL028492.

Holgate, S. J., A. Matthews, P. L. Woodworth, L. J. Rickards, M. E. Tamisiea, E. Bradshaw, P. R. Foden, K. M. Gordon, S. Jevrejeva and J. Pugh (2013): New data systems and products at the permanent service for mean sea level. *J. Coast. Res.*, **29**, 493 – 504. doi:10.2112/JCOASTRES-D-12-00175.1.

Holgate, S. J and P. L. Woodworth, (2004): Evidence for enhanced coastal sea level rise during the 1990s.*Geophys. Res. Lett.* , **31**, L07305, doi:10.1029/2004GL019626.

Huang, B., V. F. Banzon, E. Freeman, J. Lawrimore, W. Liu, T. C. Peterson, T.M. Smith, P. W. Thorne, S. D. Woodruff, and H. -M. Zhang (2014): Extended Reconstructed Sea Surface Temperature version 4 (ERSST.v4): Part I. Upgrades and intercomparisons. *J. Clim.*, **28**, 911 – 930. doi:10.1175/JCLI-D-14-00006.1.

Huang, N. E. and Z. Wu (2008): A review on Hilbert-Huang transform: the method and its applications on geophysical studies. *Rev. Geophys.*, **46.** doi:10.1029/2007RG000228.

Huang, N. E., M. Wu, W. Qu, S. R. Long and S. S. P. Shen (2003): Applications of Hilbert – Huang transform to non-stationary financial time series analysis. *Appl. Stochastic Models Bus. Ind.,* **19***, 245 – 268.* DOI: 10.1002/asmb.501.

Huang, N. E., Z. Shen and S. R. Long (1999): A new view of nonlinear water waves: The Hilbert spectrum. *Annu. Rev. Fluid Mech.*, **31**, 417 – 457. doi:10.1146/annurev.fluid.31.1.417.

Huang, N. E, Z. Shen, S. R. Long, M. C. Wu, H. H. Shih, Q. Zheng, N. Yen, C. C. Tung and H. H. Liu (1998): The empirical mode decomposition and the Hilbert spectrum for nonlinear and non-stationary time series analysis. *Proc. R. Soc. London*, **454**, 903 – 995. doi:10.1098/rspa.1998.0193.

INGC (2009): Main Report: INGC Climate Change Report: Study on the impact of climate change on disaster risk in Mozambqiue. (K. Asante, R. Brito, G. Brundrit, P. Epstein, A. Fernandes, M. R. Marques, A. Mavume, M. Metzger, A. Patt, A. Queface, R. Sanchez del Valle, M. Tadross, R. Brito (eds.)). : INGC, Mozambique.

IOC (1985): Manual on Sea Level Measurement and Interpretation: Volume I - Basic Procedures. Intergovernmental Oceanographic Commission, Manuals and Guides, **14**, 1 – 78.

Jevrejeva, S., A. Grinsted, J. C. Moore and S. Holgate (2006): Nonlinear trends and multiyear cycles in sea level records. *J. Geophys. Res.*, **111**, C09012, doi:10.1029/2005JC003229.

Jevrejeva, S., J. C. Moore, A. Grinsted, A. P. Matthews, G. and Spada (2014): Trends and acceleration in global and regional sea levels since 1807. *Global and Planetary Change*, **113**, 11 – 22. doi:10.1016/j.gloplacha.2013.12.004.

Jevrejeva, S., L. P. Jackson, R. E. M. Riva, A. Grinsted and J. C. Moore (2016): Coastal sea level rise with warming above 2°C. *Proceedings of the National Academy of Sciences*, **113**, 13342 – 13347. doi:10.1073/pnas.1605312113.

Kalnay, E., M. Kanamitsu, R. Kistler, W. Collins, D. Deaven, L. Gandin, M. Iredell, S. Saha, G. White, J. Woollen, Y. Zhu (1996): The NCEP/NCAR 40-Year Reanalysis Project. *Bull.Am. Meteorol. Soc.*, **77**, 437 – 471.

Kenigson, J. S. and W. Han (2014): Detecting and understanding the accelerated sea-level rise along the east coast of US during recent decades. *J. Geophys. Res.*, **119**, 8749 – 8766. doi:10.1002/2014JC010305.

Komar, P.D., J.C. Allan and P. Ruggiero (2011): Sea level variations along the U.S. Pacific Northwest coast: tectonic and climate controls. *J. Coast. Res.*, **27**, 808 – 823.

Kopp, R. E., C. C. Hay, C. M. Little, J. X. Mitrovica (2015): Geographic variability of sea-level change. *Curr. Clim. Change Rep.*, **1**, 192 – 204. doi:10.1007/s40641-015-0015-5.

Kopp, R. E., R. M. Horton, C. M. Little, J. X. Mitrovica, M. Oppenheimer, D. J. Rasmussen, B. H. Strauss and C. Tebaldi, (2014): Probabilistic 21st and 22nd century sea-level projections at a global network of tide-gauge sites. *Earth's Future*, **2**, 383 – 406. doi:10.1002/2014EF000239.

Krug, M., and J. Tournadre (2012): Satellite Observations of an Annual Cycle in the Agulhas Current. *Geophys. Res. Lett.*, **39**, L15607. doi:10.1029/2012GL052335

Krug, M., J. Tournadre, and F. Dufois (2014): Interactions between the Agulhas Current and the Eastern Margin of the Agulhas Bank. *Cont. Shelf Res.*, **81**, 67 – 79. doi:10.1016/j.csr.2014.02.020.

Krug, M., S. Swart and J. Gula (2017): Submesoscale Cyclones in the Agulhas Current. *Geophys. Res. Lett.*, **44**, 346 – 354.

Le Bars, D., S. Drijfhout and H. de Vries (2017): A high-end sea level rise probabilistic projection including rapid Antarctic ice sheet mass loss. *Environmental Research Letters*, **12**, 044 013, doi:10.1088/1748-9326/aa6512.

Leber, G. M., and L. M. Beal (2014): Evidence that Agulhas Current Transport is Maintained during a Meander. *J. Geophys. Res. Oceans*, **119**, 3806 – 3817. doi:10.1002/2014JC009802.

Levermann, A., A. Griesel, M. Hofmann, M. Montoya, and S. Rahmstorf (2005): Dynamic Sea Level Changes Following Changes in the Thermohaline Circulation, *Clim. Dyn.*, **24**, 347 – 354. DOI 10.1007/s00382-004-0505-y.

Lindesay, J. A. (1988): South African rainfall, the Southern Oscillation and a Southern Hemisphere semi-annual cycle. *Int. J. Climatol.*, **8**, 17 – 30. https://doi.org/10.1002/joc.3370080103.

Liu, Z. (2012): Dynamics of interdecadal climate variability: A historical perspective. *J. Climate*, **25**, 1963–1995. doi:10.1175/2011JCLI3980.1

Lutjeharms, J. (2006): The Agulhas Current. *Springer-Verlag, Berlin Heidelberg*, NewYork

Lutjeharms, J., and R. C. van Ballegooyen (1984): Topographic Control in the Agulhas Current System. *Deep Sea Res.*, **31**, 1321 – 1337. https://doi.org/10.1016/0198-0149(84)90004-9.

Lutjeharms, J. R. E., H. R. Valentine, and R.C. van Ballegooyen (2000): The hydrography and water masses of the Natal Bight, South Africa. *Cont. Shelf Res.*, **20**, 1907 – 1939.

Maheu, C., M. -I. Pujol and Y. Faugère (2013): Change of the SSALTO/Duacs reference period. Aviso+ Newsletter#9http://www.aviso.altimetry.fr/fileadmin/documents/newsstand/Newsletter/aviso_users_news09.pdf. Access 30 October 2018

Manatsa, D., C. H. Matarira and G. Mukwada (2011): Relative Impacts of ENSO and Indian Ocean Dipole/Zonal Mode on the east SADC Rainfall. *Int. J. Climatol*., **31**, 558 – 577. DOI:10.1002/joc.2086.

Manatsa, D., W. Chingombe and C. H. Matarira (2008): The Impact of the Positive Indian Ocean Dipole on Zimbabwe Droughts. *Int. J. Climatol*., **28**, 2011 – 2029. DOI:10.1002/joc.1695.

Mavume, A., L. Rydberg, M. Rouault, and J. Lutjeharms (2009): Climatology and Landfall of Tropical Cyclones in the South- West Indian Ocean. *Western Indian Ocean J. Mar. Sci.*, *8*(1), 19 – 39. http://doi.org/10.4314/wiojms.v8i1.56672.

Mather, A. A., G.G. Garland and D.D. Stretch (2009): Southern African Sea Levels: corrections, influences and trend. *S. Afr. J. Mar. Sci.*, **31**, 145 – 156.

Marshall G. J. (2003): Trends in the Southern Annular Mode from observations and reanalyses. *J. Clim.*, **16**, 4134 – 4143.

Meehl, G. A., J. M. Arblaster and W. G. Strand (1998): Global scale decadal climate variability. *Geophys. Res. Lett.*, **25**, 3983–3986. doi:10.1029/1998GL900088.

Mertz, F., V. Rosmorduc, C. Maheu and Y. Faugère (2017): Product User Manual for Sea Level SLA products. http://apdrc.soest.hawaii.edu/doc/CMEMS-SL-PUM-008-032-051.pdf. Access 13 July 2017

Meyssignac, B, M. Becker, W. Llovel and A. Cazenave (2012): An Assessment of Two-Dimensional Past Sea Level Reconstructions Over 1950–2009 Based on Tide-Gauge Data and Different Input Sea Level Grids. *Surv. Geophys.*, **33**, 945 – 972. DOI: 10.1007/s10712-011-9171-x.

Miller, L. and B. C. Douglas (2007): Gyre-scale atmospheric pressure variations and their relation to 19th and 20th century sea level rise. *Geophys. Res. Lett.*, **34**, L16602.

Milne, G. A., W. R. Gehrels, C. W. Hughes and M. E. Tamisiea (2009): Identifying the causes of sea-level change. *Nature Geosci.*, **2**, 471 – 478. doi: 10.1038/ngeo544.

Mitchum, G. T. (1998): Monitoring the stability of satellite altimeters with tide gauges. *J. Atmos. Oceanic Tech.,* **15**, 721 – 730.

Neelin, J. D., D. S. Battisti, A. C. Hirst, F. Jin, Y. Wakata, T. Yamagata and S. E. Zebiak (1998): ENSO Theory, *J. Geophys. Res.*, **103**, 14261 – 14290.

Nerem, R. S. and G. T. Mitchell (2002): Estimates of vertical crustal motion derived from differences of TOPEX/POSEIDON and tide gauge sea level measurements. *Geophys. Res. Lett.*, **29**, 1934. doi:10.1029/2002GL015037.

Paldor, N. and J. R. E. Lutjeharms (2009): Why is the stability of the Agulhas Current geographically bimodal?.*Geophys. Res. Lett.*, **36**, L14604, doi:10.1029/2009GL038445.

Park, J. and W. Sweet (2015): Accelerated Sea Level Rise and Florida Current Transport. *Ocean Sci.*, **11**, 607 – 615. doi:10.5194/os-11-607-2015.

Passaro, M., P. Cipollini, S. Vignudelli, G. D. Quartly and H. M. Snaith (2014): ALES: A multi-mission adaptive subwaveformretracker for coastal and open ocean altimetry. *Rem. Sens. Env.*, **145**, 173 – 189. doi:10.1016/j.rse.2014.02.008.

Peltier, W. R. (1998): Postglacial Variations in the Level of the Sea: Implications for Climate Dynamics and Solid-Earth Geophysics. *Rev. Geophys.*, **36**, 603 – 689.

Peltier, W. R. *(2004): Global Glacial Isostasy and the Surface of the Ice-Age Earth: The ICE-5G (VM2) Model and GRACE. Ann. Rev. Earth and Planet. Sci.,* ***32****, 111 - 149.*doi: 10.1146/annurev.earth.32.082503.144359.

Percival D. B. and A. T. Walden (1993): Spectral Analysis for Physical Applications - Multitaper and Conventional Univariate Techniques. *Cambridge University Press*, 612 pp.

Prandi, P., A. Cazenave and M. Becker (2009): Is coastal mean sea level rising faster than the global mean? A comparison between tide gauges and satellite altimetry over 1993–2007. *Geophys. Res. Lett.*, **36**, L05602, doi:10.1029/2008GL036564.

Preston-Whyte, R. A. and P. D. Tyson (1988): The Atmosphere and Weather of Southern Africa. *Oxford University Press – South Africa*, 374 pp.

PSMSL (2017): Permanent Service for Mean Sea Level: "Tide Gauge Data", Retrieved 12 Jun 2017 from http://www.psmsl.org/data/obtaining/.

Pugh, D. T. (1987): Tides, Surges and Mean Sea-Level. *John Wiley & Sons*, 472 pp.

Pujol, M.I., Y. Faugère, G. Taburet, S. Dupuy, C. Pelloquin, M. Ablain, and N. Picot (2016): DUACS DT2014: The new Multi-mission Altimeter Data set Reprocessed over 20 years. *Ocean Sci.*, **12**, 1067 – 1090.

Rakodi, C. and D. Treloar (1997): Urban development and coastal zone management. An international review. *Third World Planning Review*, **19**, 401–424.

Raney, R. K. (1998): The delay/Doppler radar altimeter. *IEEE Transactions on Geoscience and Remote Sensing*, **36** (5), 1578 – 1588. doi: 10.1109/36.71886Ray, R. D. and B. C. Douglas (2011): Experiments in reconstructing twentieth-century sea levels, *Progress in Oceanography*, **91**, 496 – 515. doi:10.1016/j.pocean.2011.07.021.

Reason, C. J. C. and M. R. Jury (1990): On the generation and propagation of the Southern African coastal low. *Quart. J. Roy. Met. Soc.*, **116**, 1133 – 1151.

Reason, C. J. C. and M. Rouault (2005): Links between the Antarctic Oscillation and winter rainfall over western South Africa. *J. Geophys. Res.*, **32**, L07705, doi:10.1029/2005GL022419.

Reason, C. J. C., R. J. Allan, J. A. Lindesay and T. J. Ansell (2000): ENSO and Climatic Signals across the Indian Ocean basin in the Global Context: Part I, Interannual Composite Patterns. *Int. J. Climatol.*, **20**, 1285 – 1327.

Richter, K., J. E. Ø. Nilsen, and H. Drange (2012): Contributions to sea level variability along the Norwegian coast for 1960–2010. *J. Geophys. Res.*, **117**, C05038, doi:10.1029/2011JC007826.

Roblou, L., F. Lyard, M. Le Henaff and C. Maraldi (2007): X-track, a new processing tool for altimetry in coastal oceans. *Proc. 'Envisat Symposium 2007', Montreux, Switzerland*

Rodolfo, K. S. and F. P. Siringan (2006): Global sea-level rise is recognised, but flooding from anthropogenic land subsidence is ignored around northern Manila Bay, Philippines. *Disasters*, **30**, 118 – 139.

Rouault, M. J., and P. Penven (2011): New Perspectives on Natal Pulses from Satellite Observations, *J. Geophys. Res.*, **116**, C07013, doi:10.1029/2010JC006866.

Saji, N., B. N. Goswami, P. Vinayachandran and T. Yamagata (1999): A Dipole Mode in the Tropical Indian Ocean. *Nature*, **401**, 360 – 363.

Sallenger, A. H., K. S. Doran, and P. Howd (2012): Hotspot of Accelerated Sea-level Rise on the Atlantic Coast of North America. *Nat. Clim. Change*, **24**, doi:10.1038/NCILMATE1597.

Schumann, E. H. (1981): Low Frequency Fluctuations Off the Natal Coast. *J. Geophys. Res.*, **86**, 6499 – 6508.

Schumann, E. H. (1983): Long-period Coastal Trapped Waves off the south-east coast of southern Africa. *Contin. Shelf Res.*, **2**, 97 – 107.

Schumann, E. H. and K. H. Brink (1990): Coastal-Trapped Waves off the Coast of South Africa: Generation, Propagation and Current Structures. *J. Phys. Oceanogr.*, **20**, 1206 – 1218.

Scott, D. B. and F. S. Medioli (1978): Vertical zonations of marsh foraminifera as accurate indicators of former sea levels. *Nature,* **272**, 528 – 531, http://dx.doi. org/10.1038/272528a0.

Scott, D. B. and F. S. Medioli (1980): Quantitative studies of marsh foraminifera distributions in Nova Scotia: Implications for sea level studies. *Cushman Foundation for Foraminiferal Research Special Publication*, **17**, 58 pp.

Siedler, G., J. Church and J. Gould (2001): Ocean Circulation and Climate. *Academic Press.*

Singleton, A. T. and C. J. C. Reason (2007): Variability in the characteristics of cut-off low pressure systems over subtropical southern Africa. *Int. J. Climatol.*, **27**, 295 – 310.

Soumya, M., P. Vethamony and P. Tkalich (2015): Inter-annual Sea Level Variability in the southern South China Sea. *Glob. Planet. Chang.*,**133**, 17 – 26.

Stammer, D. and A. Cazenave (eds) (2017). *Satellite Altimetry over Oceans and Land Surfaces*. 1st ed. Boca Raton. CRC Press. 670pp. https://doi.org/10.1201/9781315151779.

Stammer, D., A. Cazenave, R. M. Ponte, M. E. Tamisiea (2013): Causes for contemporary regional sea level changes. *Annu. Rev. Mar. Sci.*, **5**, 21 – 46. doi:10.1146/annurev-marine-121211-172406.

Strachan, K. L., J. M. Finch, T. Hill and R. L. Barnett (2014): A late Holocene sea-level curve for the east coast of South Africa. *S. Afr. J. Sci.,* **110**, 1 – 9. http://dx.doi.org/10.1590/sajs.2014/20130198.

Stramma, L., and J. Lutjeharms (1997): The flow Field of the Subtropical Gyre in the South Indian Ocean into the Southeast Atlantic Ocean: A Case Study. *J. Geophys. Res.*, **99**, 14053 – 14070.

Strassburg, M. W., B. D. Hamlington, R. R. Leben, P. Manurung, J. Lumban Gaol, B. Nababan, S. Vignudelli and K.-Y. Kim (2015): Sea level trends in Southeast Asian seas. *Clim. Past*, **11**, 743–750. doi:10.5194/cp-11-743-2015.Sturges, W. and B. C. Douglas (2011): Wind Effects on Estimates of Sea Level Rise. *J. Geophys. Res.*, **116**, C06008, doi.org/10.1029/2010JC006492.

Sweet, W., C. Zervas, and S. Gill (2009): Elevated East Coast Sea Level Anomaly: June - July 2009. *NOAA Tech. Rep. No. NOS CO-OPS 051*, NOAA National Ocean Service, Silver Spring, MD, 40 pp.

Taljaard, J. J. (1972): Synoptic Meteorology of the Southern Hemisphere. In: Newton C. W. (eds) Meteorology of the Southern Hemisphere. Meteorological Monographs, vol 13. American Meteorological Society, Boston, MA. doi.org/10.1007/978-1-935704-33-1_8

Tamisiea, M. E. (2011): Ongoing glacial isostatic contributions to observations of sea level change. *Geophys. J. Int.*, **186**, 1036–1044. doi: 10.1111/j.1365-246X.2011.05116.x.

Tamisiea, M. E. and J. X. Mitrovica (2011): The moving boundaries of sea level change: Understanding the origins of geographic variability. *Oceanography,* **24**, 24 – 39, doi:10.5670/oceanog.2011.25.

Taylor, K. E. (2001): Summarizing Multiple Aspects of Model Performance in a Single Diagram. *J. Geophys. Res.*, **106**, 7183 – 7192.

Thomson, R. E. and W. J. Emery (2014): *Data Analysis Methods in Physical Oceanography,* 3rd ed. Elsevier, 716 pp

Torrence, C. and G. P. Compo (1998): A Practical Guide to Wavelet Analysis. *Bull. Am. Meteorol. Soc.*, **79**, 61 – 78.

Trenberth, K. E. (1997): The Definition of El Niño. *Bull.Am. Meteorol. Soc.*, **78**, 2771 – 2778.

Trenberth, K. E. and D. P. Stepaniak (2001): Indices of El Niño Evolution. *J. Clim.*, **14**, 1697 – 1701.

Trenberth, K. E. and T. J. Hoar (1996): The 1990--1995 El Niño-Southern Oscillation Event: Longest on record. *Geophys. Res. Lett.*, **23**, 57 – 60.

Tyson, P. D. and R. A. Preston-Whyte (2000): The Weather and Climate of Southern Africa. *Oxford University Press – Incorporated*, 396 pp.

Valladeau. G., J. F. Legeais, M. Ablain, S. Guinehut and N. Picot (2012): Comparing Altimetry with Tide Gauges and Argo Profiling Floats for Data Quality Assessment and Mean Sea Level Studies. *Marine Geodesy*, **35**, 42 – 60. DOI:10.1080/01490419.2012.718226.

vanLeeuwen, P. J., W. P. M. de Ruijter and J. R. E. Lutjeharms (2000): Natal pulses and the formation of Agulhas rings. *J. Geophys. Res.*, **105**, 6425 – 6436.

van Loon, H. (1972): Wind in the Southern Hemisphere. In: Newton C. W. (eds) Meteorology of the Southern Hemisphere. Meteorological Monographs, vol 13. American Meteorological Society, Boston, MA.

Vignudelli, S., A. G. Kostianoy, P. Cipollini and J. Benveniste (eds.) (2011): *Coastal Altimetry*. Berlin, Springer, 566pp. Doi.10.1007/978-3-642-12796-0.

Vincent, P., N. Steunou, E. Caubet, L. Phalippou, L. Rey, E. Thouvenot and J. Verron (2006): AltiKa: a Ka-band Altimetry Payload and System for Operational Altimetry during the GMES Period. *Sensors,* **6***,* 208 – 234.

Visser, H., S. Dangendorf and A. C. Petersen (2015): A Review of Trend Models Applied to Sea Level Data with Reference to the Acceleration-deceleration Debate. *J. Geophys. Res.*, **120**, 3873 – 3895. Doi:10.1002/2015JC010716.

Watson, C. S., N. J. White, J. A. Church, M. A. King, R. J. Burgette and B. Legresy (2015): Unabated Global Mean Sea-Level Rise over the Satellite Altimeter Era. *Nat. Clim. Change*, **5**, 565 – 568. https://doi.org/10.1038/nclimate2635, 2015.

Weldon, D. and C. J. C. Reason (2014): Variability of rainfall characteristics over the south coast region of South Africa. *Theor. Appl. Climatol.*, **115**, 177 – 185. DOI 10.1007/s00704-013-0882-4.

White, N. J., Haigh I. D., J. A. Church, T. Koen, C. S. Watson, T. R. Pritchard, P. J. Watson, R. J. Burgette, K. L. McInnes, Z.-J. You, X. Zhang and P. Tregoning (2014): Australian sea levels – Trends, regional variability and influencing factors. *Earth-Science Reviews*, **136**, 155 – 174. doi.org/10.1016/j.earscirev.2014.05.011.

Whitehouse, P. (2009): Glacial isostatic adjustment and sea-level change. State of the art report. Technical Report TR-09-11. Durham University.100 pp.

Wolter, K., and M.S. Timlin (1993): Monitoring ENSO in COADS with a seasonally adjusted principal component index.*Proc. of the 17th Climate Diagnostics Workshop*, Norman, OK, NOAA/NMC/CAC, NSSL, Oklahoma Clim. Survey, CIMMS and the School of Meteor., Univ. of Oklahoma, 52 - 57.

Wolter, K., and M. S. Timlin (1998): Measuring the strength of ENSO events - how does 1997/98 rank? *Weather,* **53,** 315 - 324.

Woodworth, P. L. (1990): A Search for Accelerations in Records of European Mean Sea Level. *Int. J. Climatol.*, **10**, 129 – 143. Doi:10.1002/joc.3370100203

Woodworth, P.L., A. Aman and T. Aarup (2007): Sea level monitoring in Africa. *Afr. J. Mar. Sci*, **29**, 321 – 330. DOI: 10.2989/AJMS.2007.29.3.2.332.

Woodworth, P. L., N. J. White, S. Jevrejeva, S. J. Holgate, J. A. Church and W. R. Gehrels (2009): Evidence for the Accelerations of Sea Level on Multi-decade and Century Timescales. *Int. J. Climatol*., **29**, 777 – 789. doi:10.1002/joc.1771.

Woppelmann, G., B. Martin Miguez, M. N. Bouin and Z. Altamimi (2007): Geocentric sea level trend estimates from GPS analyses at relevant tide gauges worldwide. *Glob. Planet. Chang.*, **57**, 396 – 406.

Wu, Z. and N. E. Huang (2009): Ensemble empirical mode decomposition: A noise-assisted data analysis method. *Advances in Adaptive Data Analysis*, **1**, 1 – 41.

Wunsch, C. and D. Stammer (1997): Atmospheric loading and the oceanic "inverted barometer" effect. *Rev. Geophys.*, **35**, 79 – 107.

Yang, H., G. Lohmann, W. Wei, M. Dima, M. Ionita, and J. Liu (2016): Intensification and Poleward Shift of Subtropical Western Boundary Currents in a Warming Climate. *J. Geophys. Res. Oceans,* **121,** 4928 – 4945. doi: 10.1002/2015JC011513

Zhang, X. and J. A. Church (2012): Sea level trends, interannual and decadal variability in the Pacific Ocean. *Geophys. Res. Lett.*, **39**, L21701.

Zebiak, S. E. (1993): Air-Sea Interaction in the Equatorial Atlantic Region. *J. Clim.*, **6**, 1567 – 1586.

Zervas, C. (2009): Sea Level Variations of the United States 1854–2006. *NOAA Technical Report NOS CO-OPS 053*, 75 pp.

Appendices

A. Monthly sea level records at sites along the south and east coast of South Africa when decomposed with the EMD analysis.

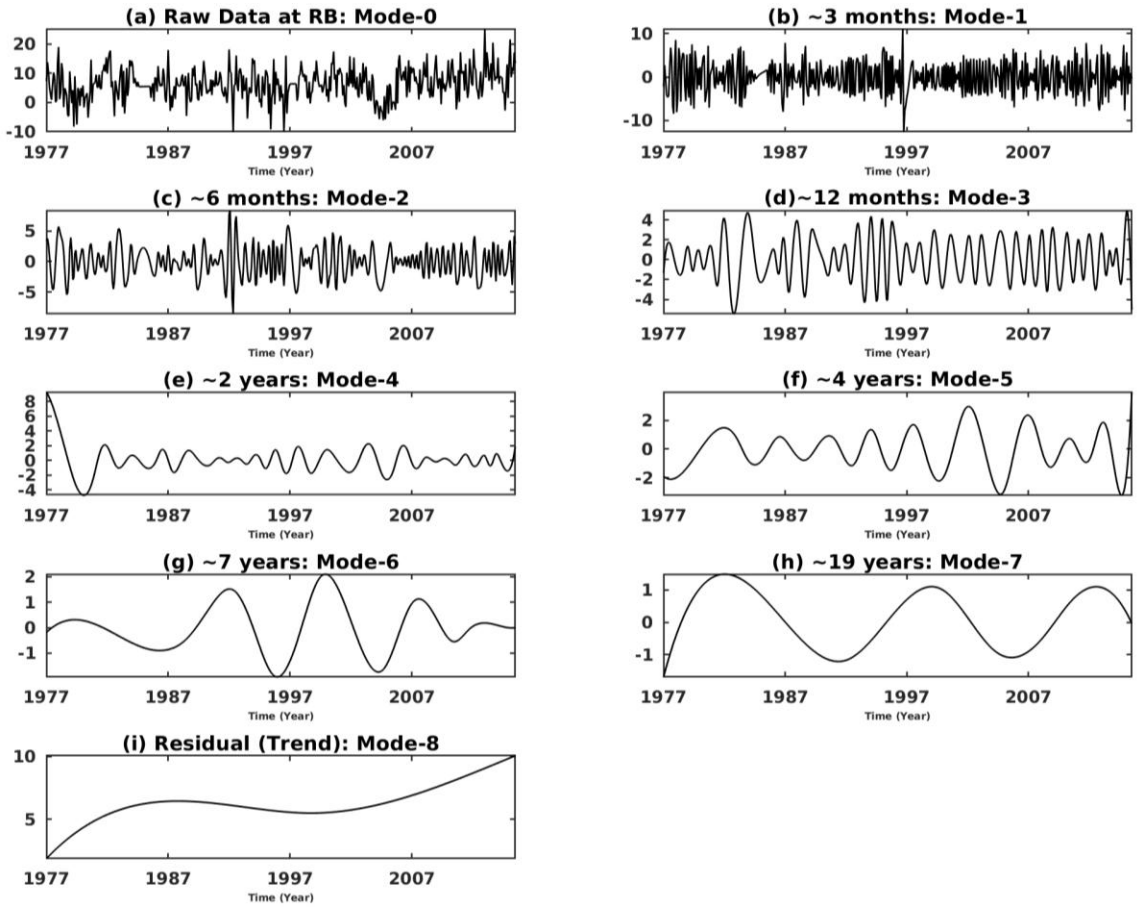

A.1: Monthly sea level record at Richards Bay (in cm) decomposed into its constituent modes using the EMD. Mode 0 is the raw data, modes 1 - 7 are the oscillating modes, and the remaining residual mode is the trend (mode-8).

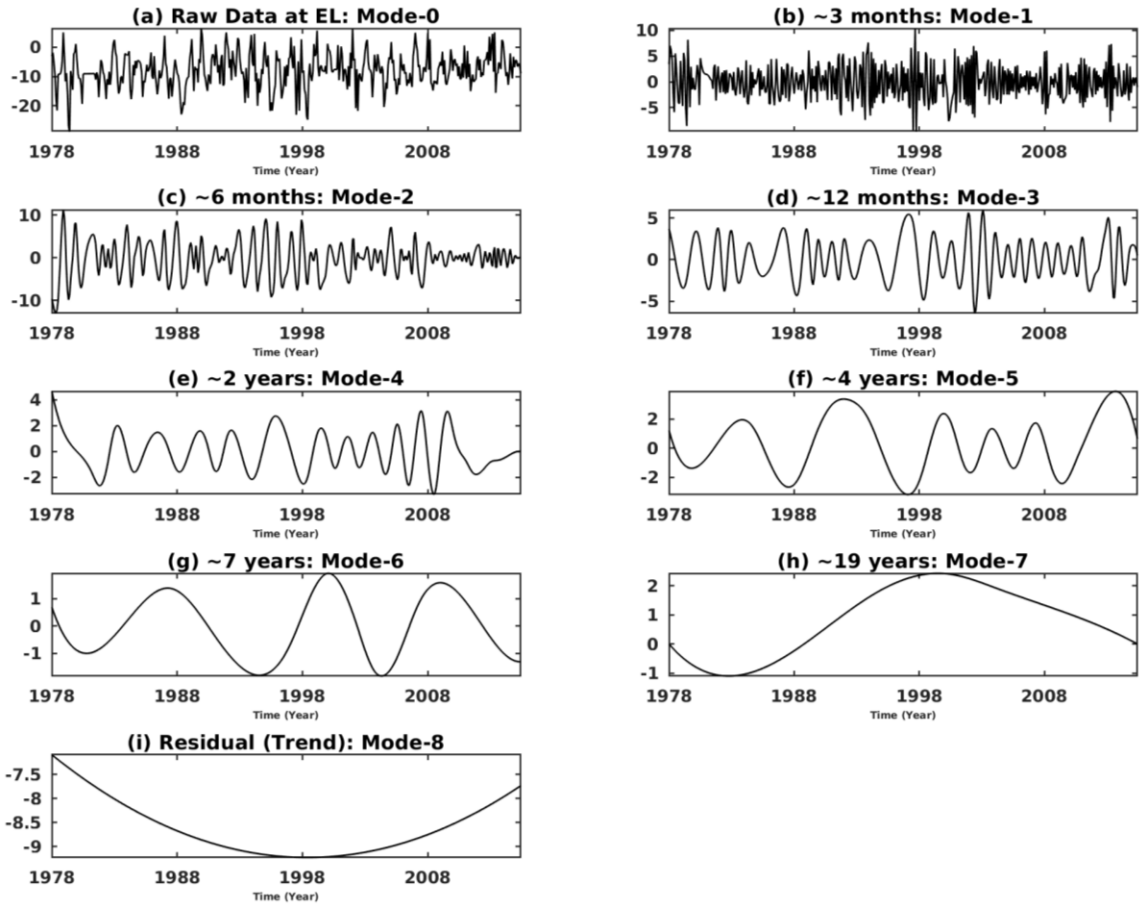

A.2: Monthly sea level record at East London (in cm) decomposed into its constituent modes using the EMD. Mode 0 is the raw data, modes 1 - 7 are the oscillating modes, and the remaining residual mode is the trend (mode-8).

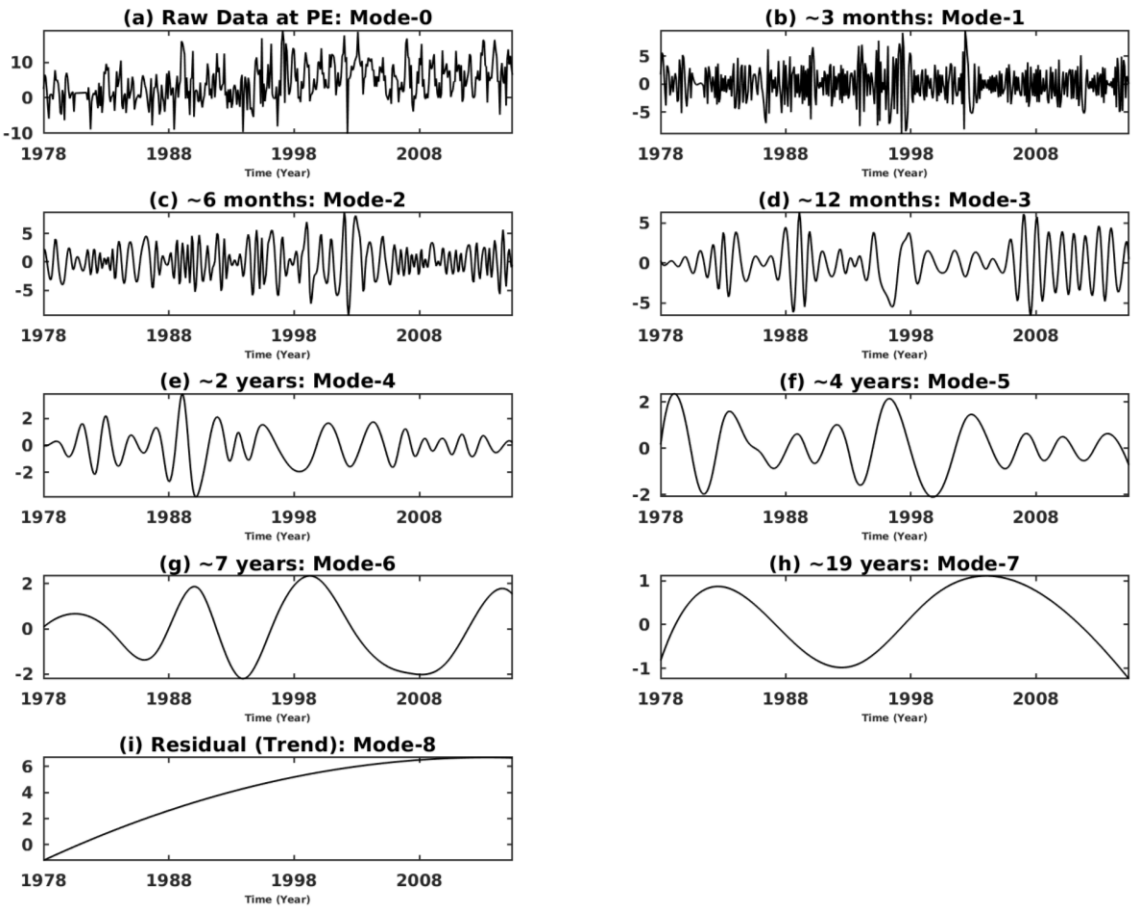

A.3: Monthly sea level record at Port Elizabeth (in cm) decomposed into its constituent modes using the EMD. Mode 0 is the raw data, modes 1 - 7 are the oscillating modes, and the remaining residual mode is the trend (mode-8).

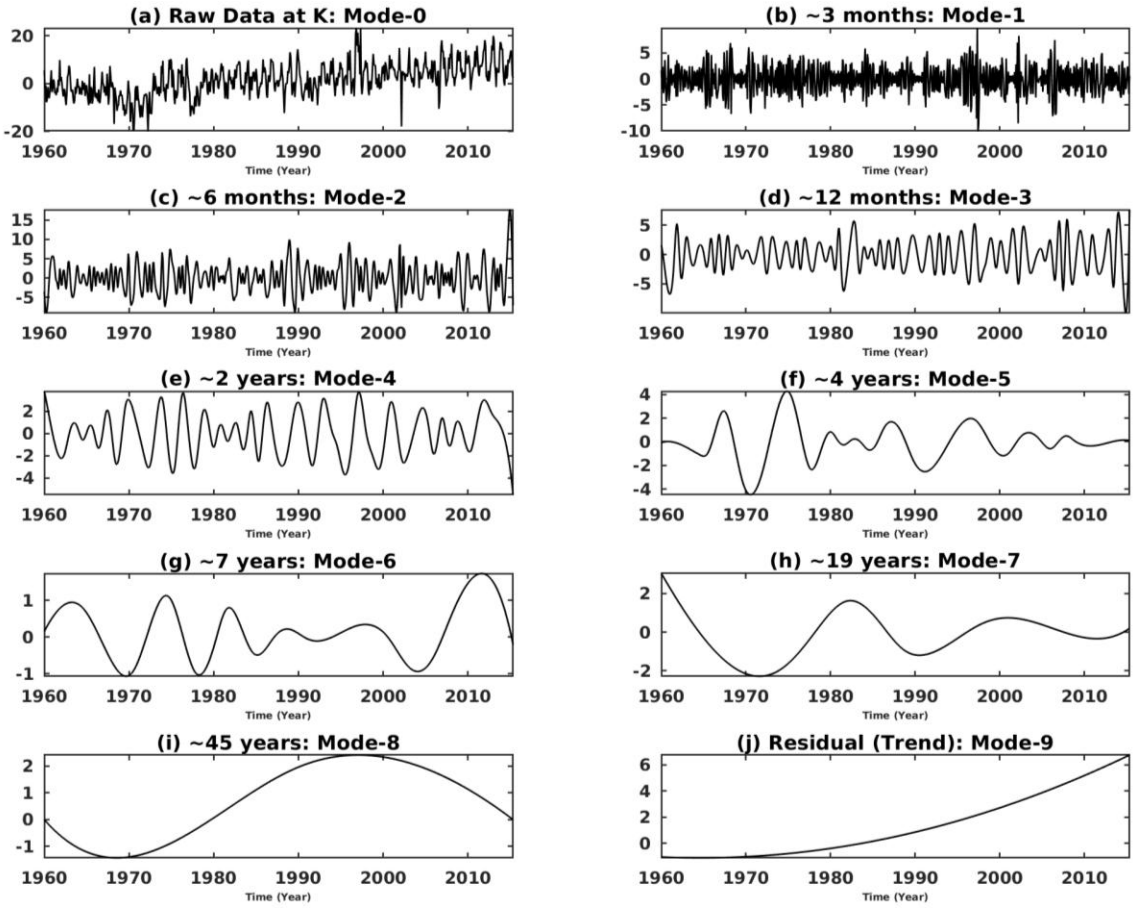

A.4: Monthly sea level record at Knysna (in cm) decomposed into its constituent modes using the EMD. Mode 0 is the raw data, modes 1 - 8 are the oscillating modes, and the remaining residual mode is the trend (mode-9).

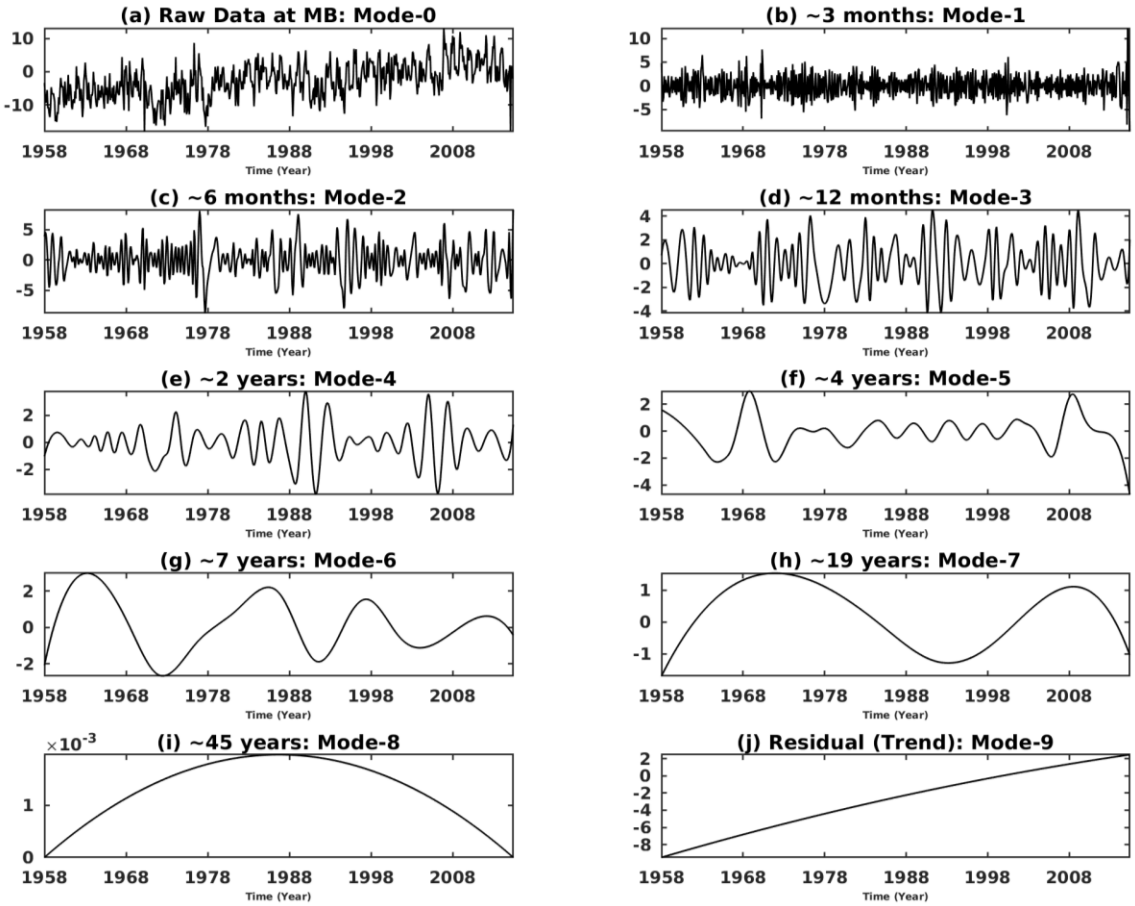

A.5: Monthly sea level record at Mossel Bay (in cm) decomposed into its constituent modes using the EMD. Mode 0 is the raw data, modes 1 - 8 are the oscillating modes, and the remaining residual mode is the trend (mode-9).

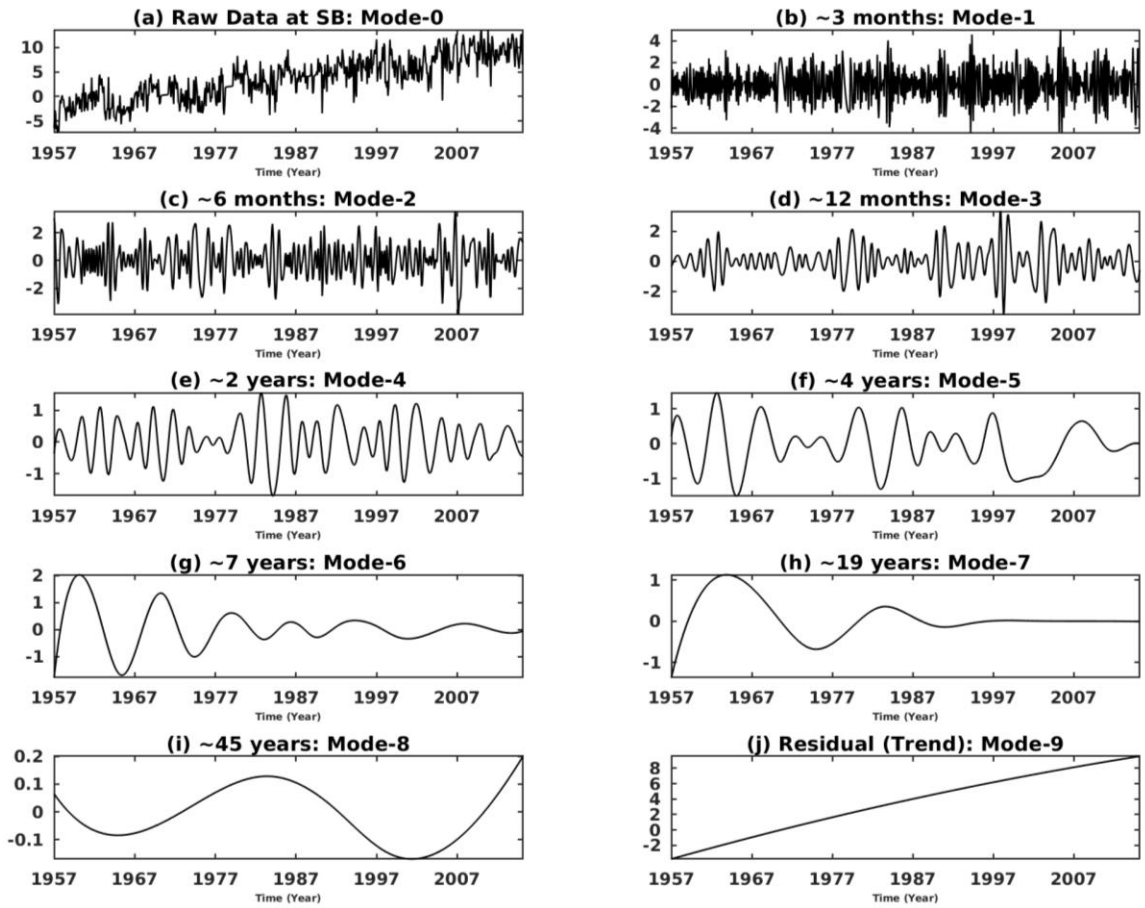

A.6: Monthly sea level record at Simons Bay (in cm) decomposed into its constituent modes using the EMD. Mode 0 is the raw data, modes 1 - 8 are the oscillating modes, and the remaining residual mode is the trend (mode-9).

B. Sub-annual and interannual timescales at each tide station.

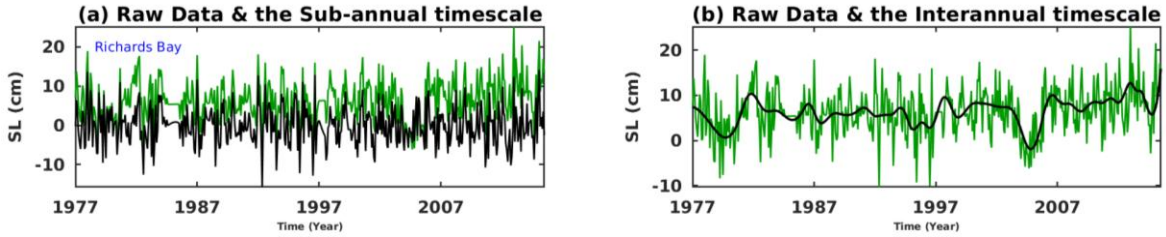

B.1: An overlay of monthly tide gauge records at Richards Bay (green line) and the ensemble mean of the separated modes. (Left) Black line (modes 1 to 3) represents the sub-annual timescale. (Right) Black line indicates the interannual timescale (modes 4 to 8).

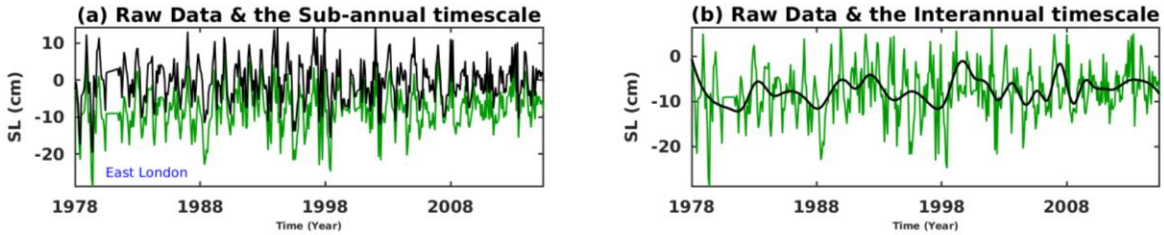

B.2: An overlay of monthly tide gauge records at East London (green line) and the ensemble mean of the separated modes. (Left) Black line (modes 1 to 3) represents the sub-annual timescale. (Right) Black line indicates the interannual timescale (modes 4 to 8).

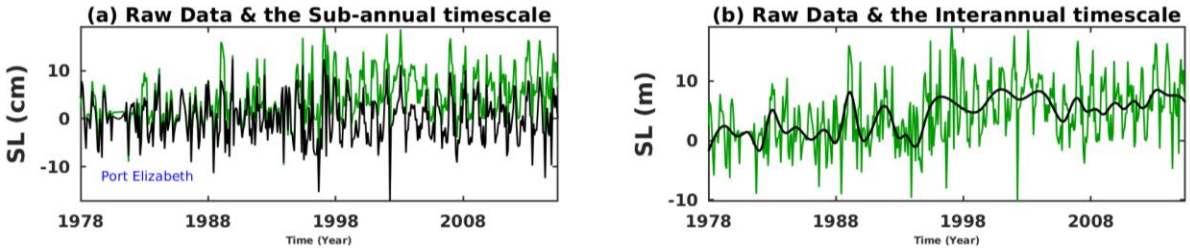

B.3: An overlay of monthly tide gauge records at Port Elizabeth (green line) and the ensemble mean of the separated modes. (Left) Black line (modes 1 to 3) represents the sub-annual timescale. (Right) Black line indicates the interannual timescale (modes 4 to 8).

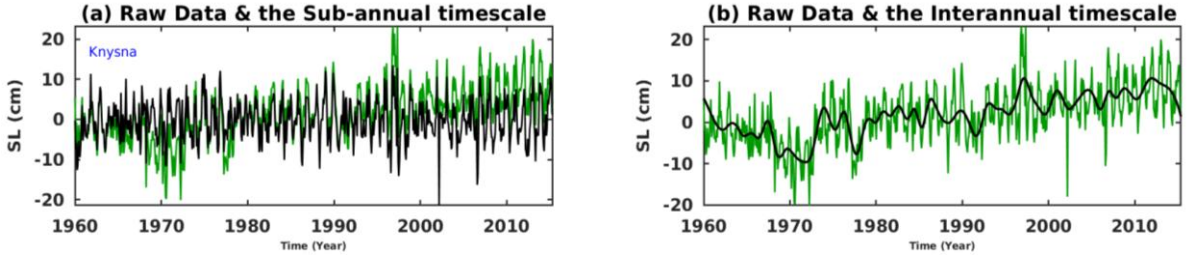

B.4: An overlay of monthly tide gauge records at Knysna (green line) and the ensemble mean of the separated modes. (Left) Black line (modes 1 to 3) represents the sub-annual timescale. (Right) Black line indicates the interannual timescale (modes 4 to 9).

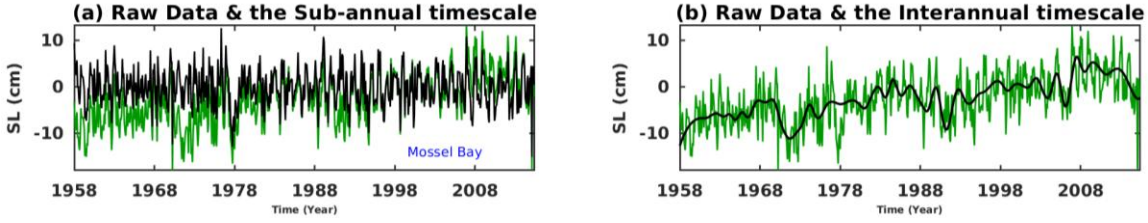

B.5: An overlay of monthly tide gauge records at MosselBay (green line) and the ensemble mean of the separated modes. (Left) Black line (modes 1 to 3) represents the sub-annual timescale. (Right) Black line indicates the interannual timescale (modes 4 to 9).

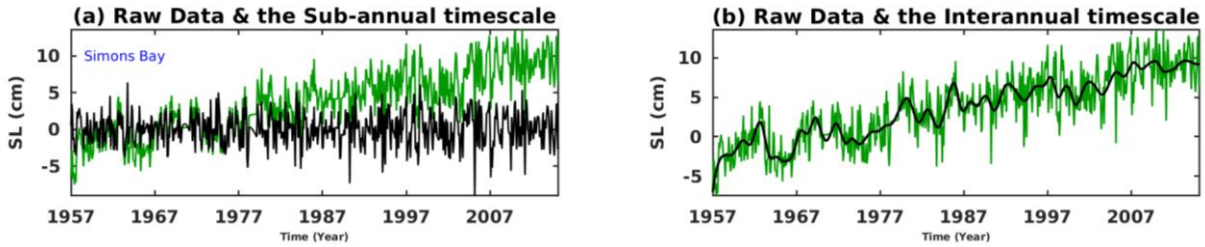

B.6: An overlay of monthly tide gauge records at Simons Bay (green line) and the ensemble mean of the separated modes. (Left) Black line (modes 1 to 3) represents the sub-annual timescale. (Right) Black line indicates the interannual timescale (modes 4 to 9).

C. Anomalously high sea level months during the combination of the modes of climate variability

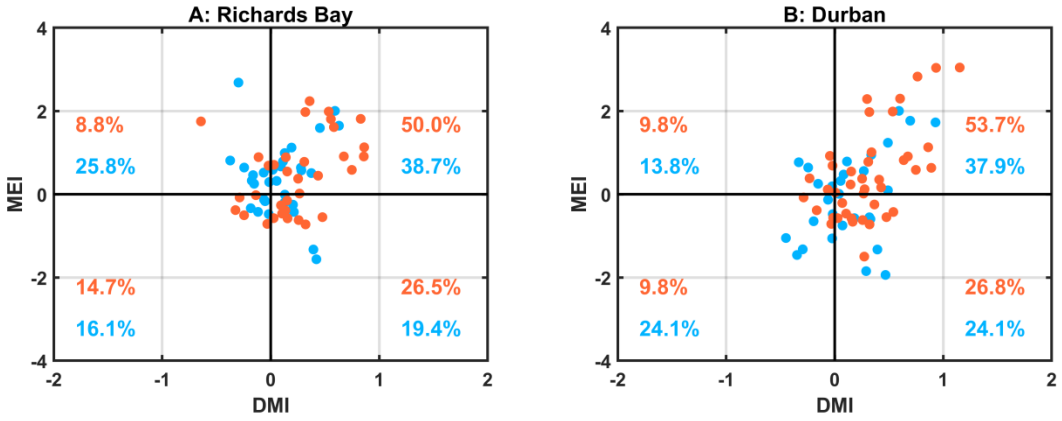

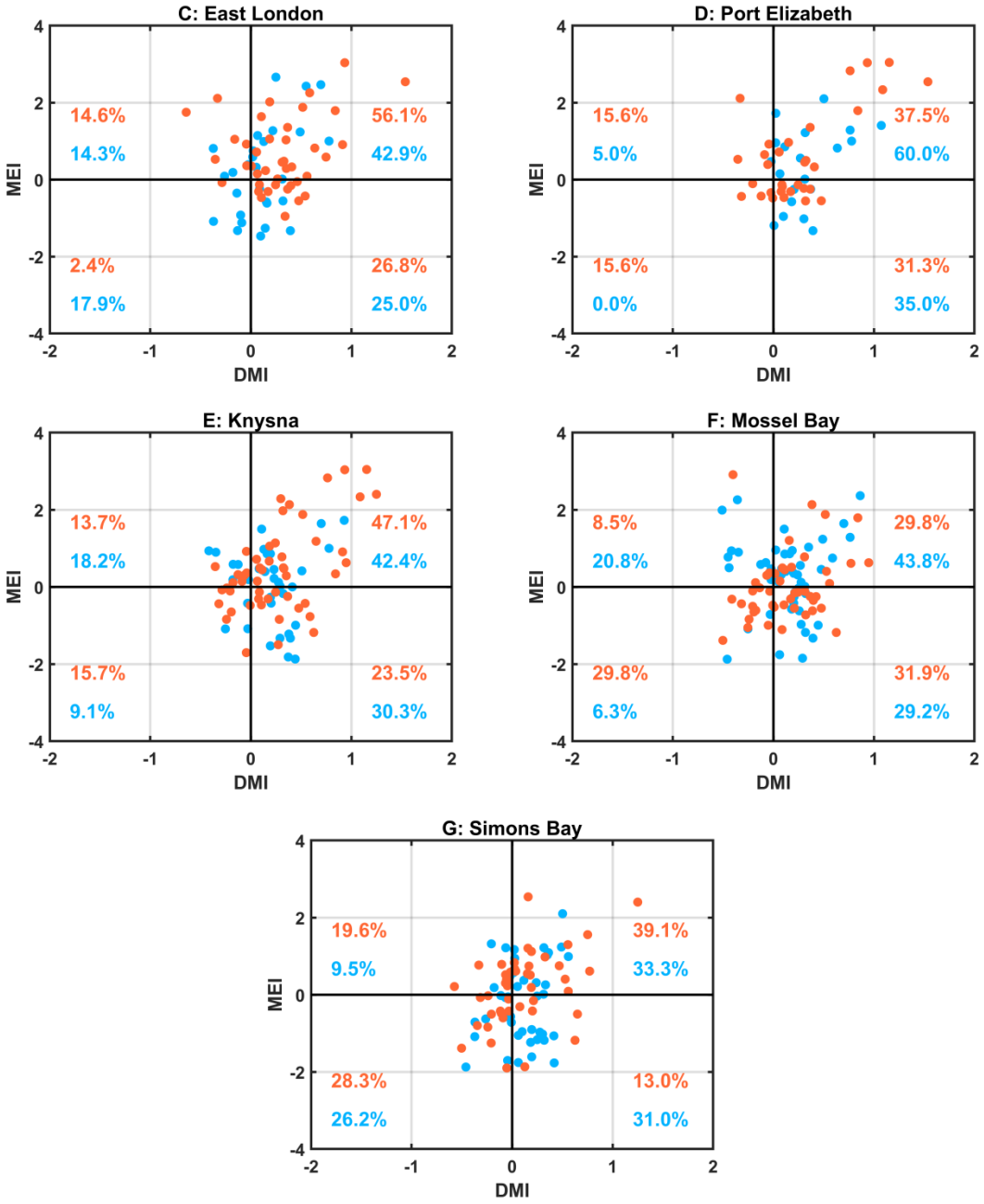

C.1: The MEI/DMI combinations in months with higher/lower (in red/blue) sea level than 1.5 standard deviations above/below mean sea level at (A) Richards Bay, (B) Durban, (C) East London, (D) Port Elizabeth, (E) Knysna, (F) Mossel Bay and (G) Simons Bay, respectively. The percentages indicate the number of months within a quadrant divided by the total number of the recorded SL months of the paired interactions.

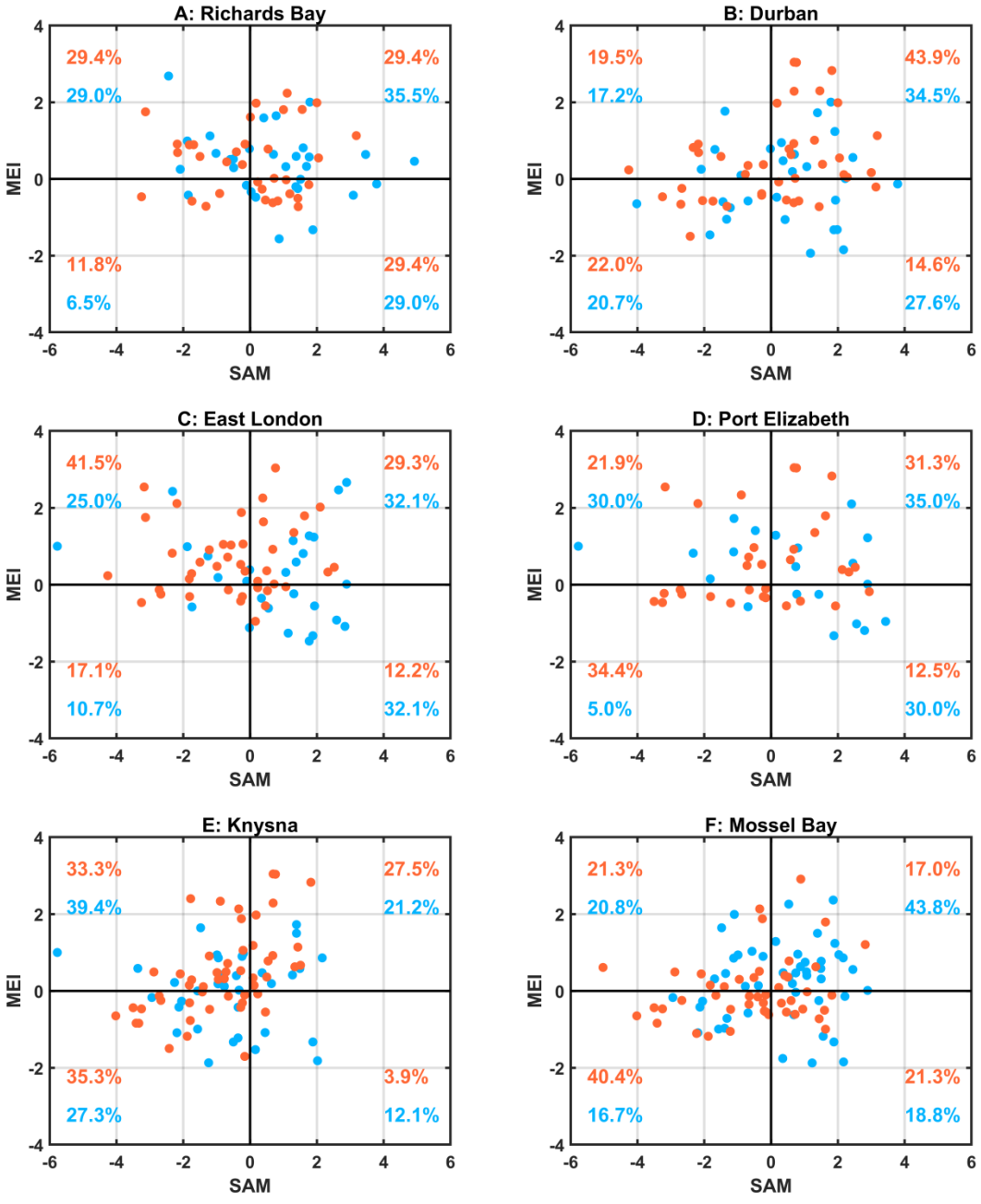
A: Richards Bay
29.4%
29.4%
29.0%
35.5%
11.8%
29.4%
6.5%
29.0%
B: Durban
19.5%
43.9%
17.2%
34.5%
22.0%
14.6%
20.7%
27.6%
C: East London
41.5%
29.3%
25.0%
32.1%
17.1%
12.2%
10.7%
32.1%
D: Port Elizabeth
21.9%
31.3%
30.0%
35.0%
34.4%
12.5%
5.0%
30.0%
E: Knysna
33.3%
27.5%
39.4%
21.2%
35.3%
3.9%
27.3%
12.1%
F: Mossel Bay
21.3%
17.0%
20.8%
43.8%
40.4%
21.3%
16.7%
18.8%
MEI
SAM

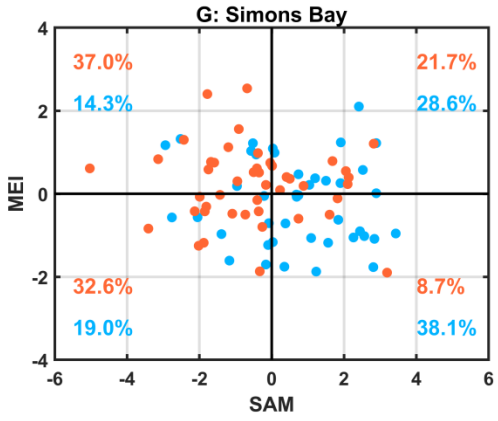

C.2: The MEI/SAM combinations in months with higher/lower (in red/blue) sea level than 1.5 standard deviations above/below mean sea level at (A) Richards Bay, (B) Durban, (C) East London, (D) Port Elizabeth, (E) Knysna, (F) Mossel Bay and (G) Simons Bay, respectively. The percentages indicate the number of SL months within a quadrant divided by the total number of the recorded SL months of the paired interactions.

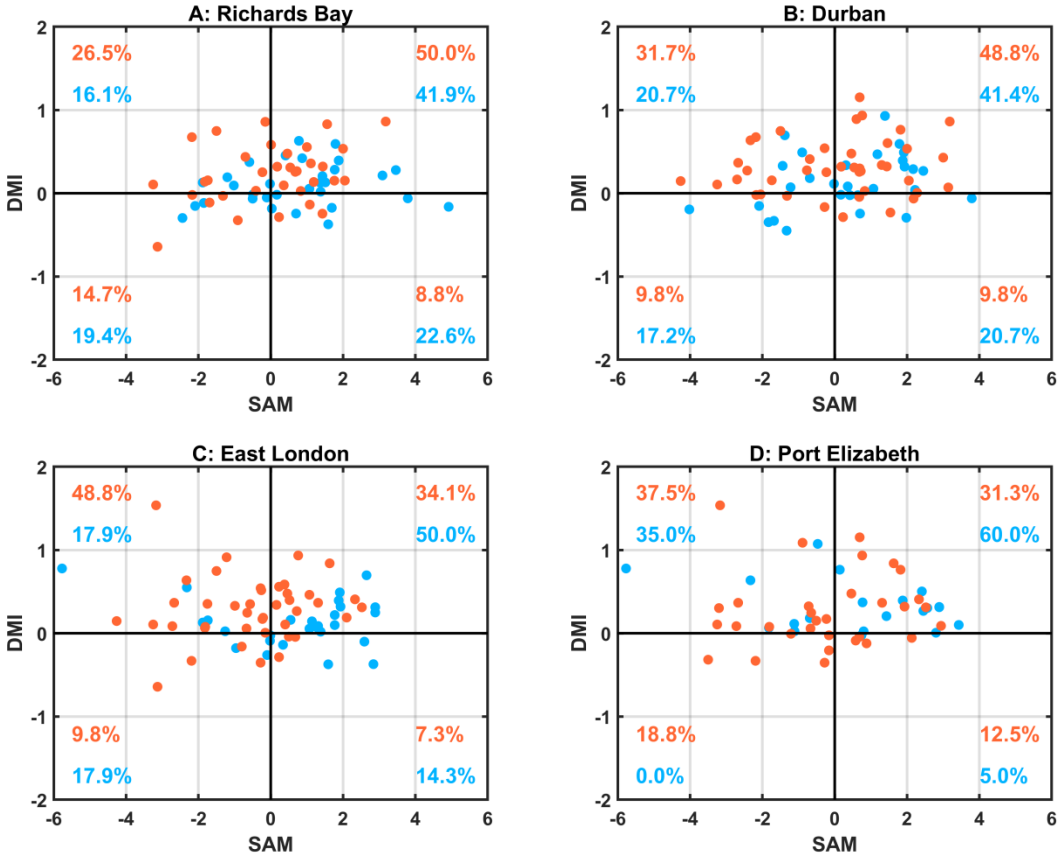

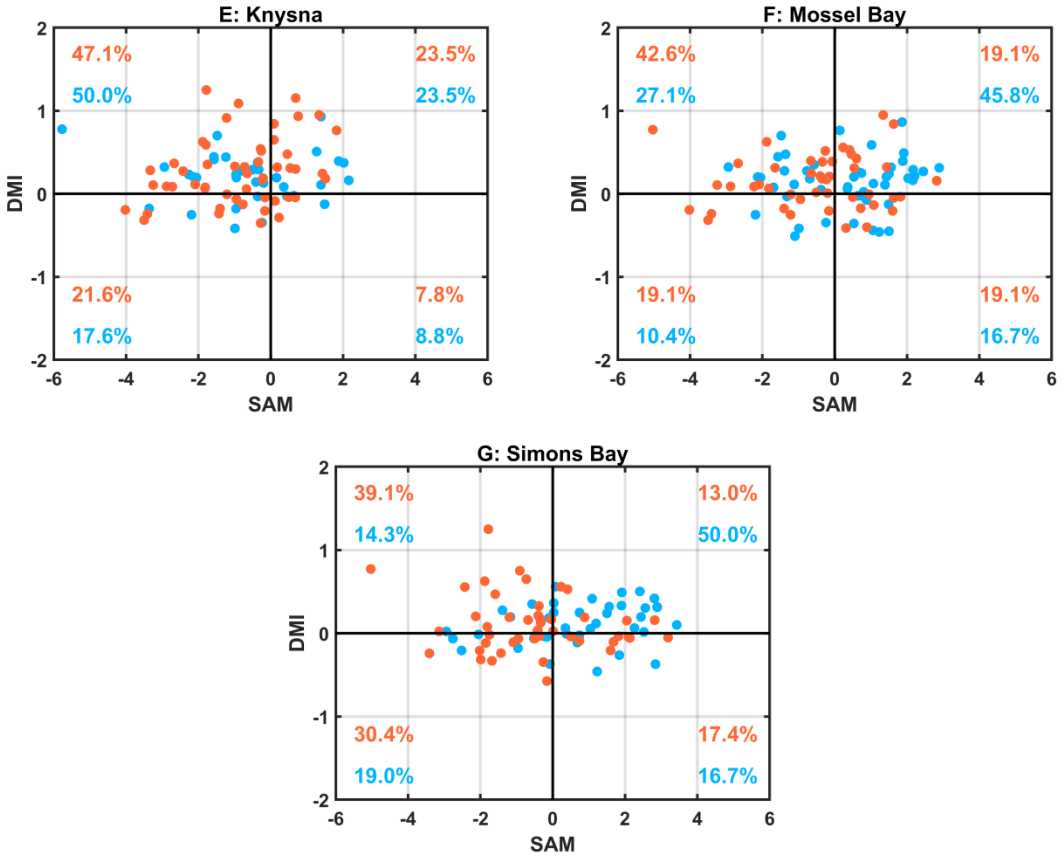

C.3: The DMI/SAM combinations in months with higher/lower (in red/blue) sea level than 1.5 standard deviations above/below mean sea level at (A) Richards Bay, (B) Durban, (C) East London, (D) Port Elizabeth, (E) Knysna, (F) Mossel Bay and (G) Simons Bay, respectively. The percentages indicate the number of SL months within a quadrant divided by the total number of the recorded SL months of the paired interactions.